Lecture Notes

Physical Chemistry IV: Magnetic Resonance

HS 2020

Laboratorium für Physikalische Chemie, ETH Zürich, Vladimir-Prelog-Weg 2,
8093 Zürich, Switzerland

PD Dr. Thomas Wiegand, Office: HCI D 217, Email: towi@nmr.phys.chem.ethz.ch
Prof. Gunnar Jeschke, Office: HCI F 227, Email: gjeschke@ethz.ch
Prof. Matthias Ernst, Office: HCI D 227, Email: maer@ethz.ch

Table of Content

1 Magnetic Properties

Practically all materials interact with magnetic fields. Below, a frog levitating in a high-field magnet is shown:

Figure 1.1: Levitating Frog
Picture of a frog levitating in the bore of a 16 T magnet (http://www.ru.nl/hfml/research/levitation/diamagnetic/) and M.V. Berry and A.K. Geim, Eur. J. Phys. **18**, 307-313 (1997)). This paper is available in electronic form at the URL mentioned above.

1.1 Definitions of Magnetostatics

1.1.1 Magnetic Field and Magnetic Induction

The magnetic field $\vec{H}$ that levitates the frog of Fig. 1.1 is produced by an (constant) electrical current flowing through a solenoid coil. According to A.M. Ampère (1775-1836), a current described by its position-dependent *current density*[1] $\vec{j}(\vec{r})$:

$$\vec{j}(\vec{r}) = \lim_{\Delta c \to 0} \frac{\Delta I}{\Delta c} \qquad [1.1]$$

creates a magnetic field:

[1] Deutsch: Stromdichte

Box I: Aide memoire:

Nabla Operator: $\nabla = \left(\frac{\partial}{\partial x}, \frac{\partial}{\partial y}, \frac{\partial}{\partial z}\right)$

$$\text{rot}\ \vec{v} = \nabla \times \vec{v} = \left(\frac{\partial v_3}{\partial y} - \frac{\partial v_2}{\partial z}, \frac{\partial v_1}{\partial z} - \frac{\partial v_3}{\partial x}, \frac{\partial v_2}{\partial x} - \frac{\partial v_1}{\partial y}\right) = \text{vector}$$

$$\text{div}\ \vec{v} = \nabla \bullet \vec{v} = \frac{\partial v_1}{\partial x} + \frac{\partial v_2}{\partial y} + \frac{\partial v_3}{\partial z} = \text{scalar}$$

$$\text{grad}\ f = \nabla f = \left(\frac{\partial f}{\partial x}, \frac{\partial f}{\partial y}, \frac{\partial f}{\partial z}\right) = \text{vector}$$

$$\text{grad}\ \vec{v} = \nabla \otimes \vec{v} = \begin{bmatrix} \frac{\partial v_1}{\partial x} & \frac{\partial v_2}{\partial x} & \frac{\partial v_3}{\partial x} \\ \frac{\partial v_1}{\partial y} & \frac{\partial v_2}{\partial y} & \frac{\partial v_3}{\partial y} \\ \frac{\partial v_1}{\partial z} & \frac{\partial v_2}{\partial z} & \frac{\partial v_3}{\partial z} \end{bmatrix} = \text{tensor (dyade)}$$

$$\text{rot}\ \vec{H}(\vec{r}) = \vec{j}(\vec{r})\ . \qquad [1.2]$$

$\vec{j}(\vec{r})$ is the current ΔI per cross-section element Δc and the direction of $\vec{j}(\vec{r})$ is perpendicular to the element Δc.

The *magnetic field*[1] $\vec{H}$ is a vector quantity and describes the field generated by the current. The dimension of $\vec{j}(\vec{r})$ is $\frac{A}{m^2}$, accordingly the dimension of the magnetic field strength $H = \left|\vec{H}\right|$ is

$$[H] = \frac{A}{m}. \qquad [1.3]$$

[1] Deutsch: Magnetfeld

For a solenoid coil (N turns and length a) which is much longer than wide, the field inside the coil, obtained by evaluating [1.2] is given by

$$H = N\frac{I}{a} . \qquad [1.4]$$

Furthermore, we define the *magnetic induction*[1] $\vec{B}$. In vacuum, $\vec{H}$ and $\vec{B}_0 = \vec{B}(\text{vacuum})$ are parallel and proportional:

$$\vec{B}_0 = \mu_0 \vec{H} \qquad [1.5]$$

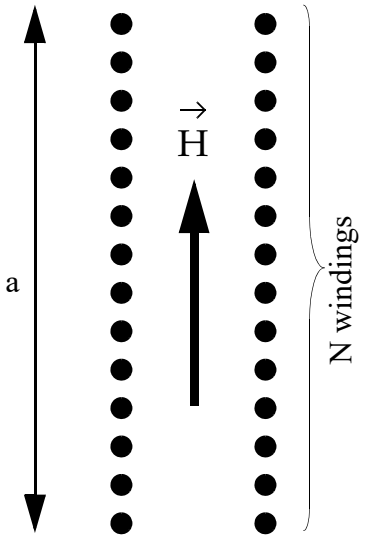

Figure 1.2: Solenoid Coil

They differ in numerical value and also in units. The proportionality constant $\mu_0 = 4\pi \cdot 10^{-7} \frac{Vs}{Am}$ is the so called *permeability*[2] of the vacuum. The unit of the magnetic induction B (often also called the magnetic field!!!) is:

$$[B] = \text{Tesla} = \frac{Vs}{m^2} = T. \qquad [1.6]$$

The strength of the earth magnetic induction ("magnetic field", magnetic flux density) is between 60 μT at the poles and 30 μT at the equator. Permanent magnets can reach about 2 T, superconducting magnets about 25 T and special high-field magnets (Bitter magnets) 60 T. The older literature also uses the unit Gauss (G) with 1 G = 100 μT = 10^{-4} T.

1.1.2 Magnetic Susceptibility and Magnetization

In a medium, the relationship between $\vec{H}$ and $\vec{B}$ is modified by the *magnetic susceptibility*[3] χ of the medium

$$\vec{B} = \mu_0(1 + \underset{\sim}{\chi})\vec{H} \qquad [1.7]$$

[1] Deutsch: magnetische Induktion

[2] Deutsch: Permeabilität

[3] Deutsch: magnetische Suszeptibilität

In isotropic media, $\underset{\sim}{\chi}$ is a dimensionless scalar, written as χ. In anisotropic media $\vec{B}$ is, in general, not parallel to $\vec{H}$ and $\underset{\sim}{\chi}$ it is a tensor that can be described by a 3x3 matrix. In vacuum, χ is always 0.

If $\chi > 0$, the magnetic field is enhanced by the material which is then called *paramagnetic*. If $\chi < 0$, the magnetic field is decreased by the material which is then called *diamagnetic*. Electrons can give rise to both paramagnetism (for systems with unpaired electrons) and diamagnetism. The nuclear effects are always paramagnetic but usually much smaller than the electronic effects. For water, we have $\chi_{\text{electrons}} = -8.8 \cdot 10^{-6}$ and $\chi_{\text{nuclei}} = +2.0 \cdot 10^{-9}$. Equation [1.7] can be rewritten as

$$\vec{B} = \mu_0(1 + \underset{\sim}{\chi})\vec{H} = \mu_0\left(\vec{H} + \vec{M}\right) = \vec{B}_0 + \mu_0\vec{M} \qquad [1.8]$$

with

$$\vec{M} = \underset{\sim}{\chi}\vec{H}. \qquad [1.9]$$

We call $\vec{M}$ the *magnetization*[1] and it can be interpreted as the magnetic field induced in the medium by the external field $\vec{H}$:

$$[M] = \frac{A}{m} \qquad [1.10]$$

1.1.3 An Atomistic Picture for the Magnetization

In the previous chapter, we have described the "medium" as structureless. In an atomistic picture, the magnetization can be described by elementary magnetic dipoles $\vec{\mu}$ (e.g. of nuclei, electrons) that get aligned by $\vec{H}$:

$$\vec{M} = \frac{1}{V}\vec{m} = \frac{1}{V}\sum_{\text{sample}}\vec{\mu} \qquad [1.11]$$

[1] Deutsch: Magnetisierung

Here $\vec{m}$ is the *magnetic dipole moment*[1] ($[\vec{m}] = [\vec{\mu}] = A \cdot m^2$) and V the volume of the sample considered. Note that the magnetic dipole moment is an *extensive* property, i.e., it depends on the sample size and is additive so that the property of the entire sample is the sum of its constituents while the magnetic field and the magnetization are *intensive* properties which need no specification of the sample size[2].

Note that there are no magnetic monopoles, in contrast to electric phenomena where monopoles (charges) as well as dipoles (and quadrupoles) exist and are important.

1.1.4 A Magnetic Dipole in a Homogeneous or Inhomogeneous Magnetic Field

From a compass needle, we know that a magnetic dipole moment tends to align with an external magnetic field. It experiences a mechanical torque[3]:

$$\vec{T} = \vec{m} \times \vec{B} \qquad [1.12]$$

Here $\vec{m}$ denotes magnetic dipole moment of the needle. The corresponding potential energy is

$$E_{pot} = -\vec{m} \cdot \vec{B} = -|\vec{m}||\vec{B}|\cos\theta\,. \qquad [1.13]$$

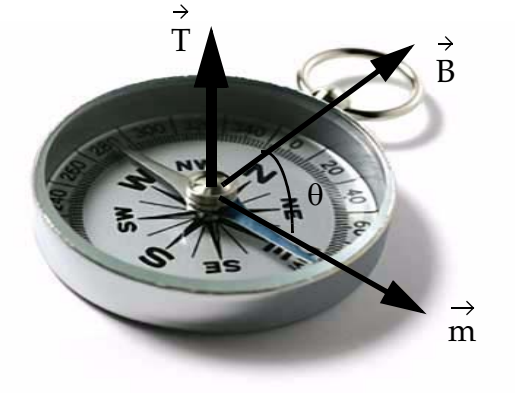

Figure 1.3: Torque on Magnetic Dipole

Table 1.1: Energy of a magnetic dipole in an static magnetic field:

parallel orientation	minimum energy (negative)

[1] Deutsch: magnetisches Dipolmoment

[2] Simple examples for extensive and intensive properties are mass and specific weight, respectively.

[3] Deutsch: Drehmoment

Table 1.1: Energy of a magnetic dipole in an static magnetic field:

antiparallel orientation	maximum energy (positive)
perpendicular orientation	zero point for energy (arbitrarily defined)

In inhomogeneous magnetic fields a dipole experiences, in addition to the torque, a force[1] $\vec{F}$ proportional to the field gradient

$$\vec{F}_m = \mathrm{grad}\left(\vec{B}\right) \cdot \vec{m} \qquad [1.14]$$

Note that $\mathrm{grad}\left(\vec{B}\right)$ is a tensor. For $\vec{B} = (0, 0, B(z))$ and $\vec{m} = (0, 0, m_z)$ Eq. [1.14] simplifies to:

$$F_m(z) = \frac{dB}{dz} m_z \; . \qquad [1.15]$$

1.1.5 The Levitation of the Frog

A necessary condition for the frog to levitate at a position z is, that the magnetic force acting on the induced magnetization, $F_m(z)$, counterbalances the gravitational force F_g:

$$F_m(z) = -F_g . \qquad [1.16]$$

The gravitational force is always negative and is given by

$$F_g = -Mg = -\rho V g \; . \qquad [1.17]$$

Here M is the mass, ρ is the density, V the volume and g the gravitational constant.

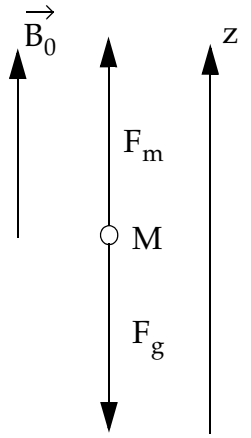

Figure 1.4: Force Balance

For levitation, the force acting at $F_m(z+\delta)$ with δ positive must be smaller than the force at $F_m(z)$, the force acting at $F_m(z-\delta)$ must be larger. In other words, the energy at the position z must be at a minimum. Here, we consider only a one-

[1] Deutsch: Kraft

dimensional problem. In three dimensions we must request, in addition, that there is an energy minimum also with respect to the x and y coordinates.

The magnetic force of Eq. [1.15] can be rewritten, using Eqs. [1.9] and [1.11] and using $B = \mu_0 H$ as:

$$F_m(z) = \frac{\chi}{\mu_0} V B(z) \frac{d}{dz} B(z) \qquad [1.18]$$

Levitation is obtained for $F_m(z) = -F_g$ or

$$B(z) \frac{d}{dz} B(z) = \frac{\mu_0 \rho g}{\chi}. \qquad [1.19]$$

The frog consists mainly of water. Therefore, we are going to use the susceptibility and density of water, $\chi_{water} = -8.8 \cdot 10^{-6}$, $\rho = 1000\ \mathrm{kg/m^3}$ and obtain the condition:

$$B(z) \frac{d}{dz} B(z) = -1400\ \frac{\mathrm{T}^2}{\mathrm{m}}. \qquad [1.20]$$

$B(z)$ is always positive and, therefore, $\frac{d}{dz} B(z)$ must be negative. This condition is fulfilled if the frog is positioned above the center of the magnet where the field decreases with increasing z. The quantitative relationship between the magnetic field strength B and the gradient $\frac{d}{dz} B(z)$ depends on the construction details of the magnet, in the experiments of Fig. 1.1 a magnet with $\frac{d}{dz} B(z) = -8.13 \cdot B_0$ T/m was used and for fields larger than 13.1 T, levitation (in one dimension) could be achieved. A detailed analysis shows that in three dimensions only a limited range of B_0 leads to minima in all three dimensions and, therefore, to levitation[1]. For paramagnetic samples, the samples would hang below the center of the magnet because χ is positive. However, no stable solutions in three dimensions can be found and the sample escapes in the x/y plane.

[1] For details see the literature cited in the caption of Fig. 1.1.

1.2 The Gyromagnetic Equation

In Eq. [1.11], we have tentatively assigned the origin of the macroscopic magnetization to microscopic magnetic moments. The *microscopic magnetic moments*[1] of electrons and nuclei are always connected to a *general angular momentum*[2] $\vec{L}$:

$$\vec{\mu} = \gamma \vec{L} \; . \qquad [1.21]$$

Here, γ is the *gyromagnetic ratio*[3]**.** For nuclei, γ is a constant which is characteristic for each isotope.

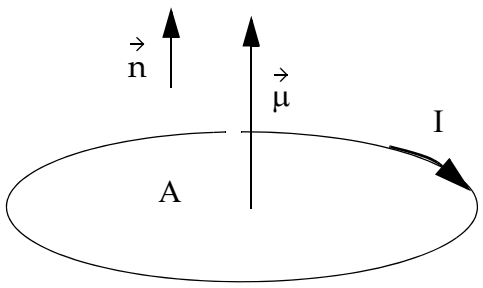

Figure 1.5: Orbital Angular Momentum

We will not prove [1.21] but only illustrate it by the magnetic moment and *orbital angular momentum*[4] of an electron. For an electron moving around a nucleus, we can use the picture of Ampere according to which the magnetic dipole moment $\vec{\mu}$ caused by the electric current I flowing in a loop around a area A (see Fig. 1.5) is given by:

$$\vec{\mu} = IA\vec{n} \qquad [1.22]$$

This result is a consequence of Eq. [1.2]. In this simple picture, the magnetic moment becomes connected to an angular momentum $\vec{L}$ as the current is caused by an electron moving on a circle:

$$I = \frac{-e}{\tau} \qquad [1.23]$$

τ is the time needed for the electron to complete a circle, e the electron charge. We can easily compare the magnetic moment

---

1 Deutsch: magnetisches Moment

2 Deutsch: Drehimpuls (Drall)

3 Deutsch: gyromagnetisches Verhältnis

4 Deutsch: Bahndrehimpuls

$$\vec{\mu} = \frac{-eA}{\tau}\vec{n} \qquad [1.24]$$

where $\vec{n}$ is a unit vector normal to the loop with the angular momentum of the electron:

$$\vec{L} = \vec{r} \times \vec{p}, \qquad [1.25]$$

Here $\vec{r}$ is the radius of the circle and $\vec{p} = m_e\vec{v}$ is the *(linear) momentum*[1] of the electron (m_e: electron mass). The velocity $\vec{v}$ can be expressed by the radius r and the cycle time τ as $|\vec{v}| = \frac{2\pi|\vec{r}|}{\tau}$ and we obtain:

$$\vec{L} = \frac{2m_eA}{\tau}\vec{n}. \qquad [1.26]$$

By comparison of Eqs. [1.24] and [1.26] we find the gyromagnetic equation:

$$\vec{\mu} = \gamma\vec{L} \qquad [1.27]$$

with the gyromagnetic ratio:

$$\gamma_L = -\frac{e}{2m_e} \qquad [1.28]$$

It will turn out that the electron has in addition to the orbital angular momentum also a quantum-mechanical *spin angular momentum*[2] which has no classical counterpart. Nevertheless, a gyromagnetic equation of the form of Eq. [1.21] is still valid. The gyromagnetic ratio, however, is different from the one given in Eq. [1.28] and the angular momentum $\vec{L}$ has no classical counterpart anymore.

In EPR (electron paramagnetic resonance), one often uses the Bohr magneton defined by

$$\beta_e = \hbar\gamma_L \qquad [1.29]$$

instead of γ_L. The gyromagnetic Eq. [1.21] is then written as

---

1 Deutsch: Impuls

2 Deutsch: Spindrehimpuls

$$\vec{\mu} = -g\beta_e \frac{\vec{L}}{\hbar} \qquad [1.30]$$

where the so called g-factor has been introduced. We have $\frac{-g\beta_e}{\hbar} = \gamma$. For the free electron, g has a value of about 2.0023.

1.3 Dynamic Effects in Homogeneous Fields: The Bloch Equations

Equation [1.12] describes the mechanical torque on a magnetic object. For a compass needle which has a macroscopic magnetic moment but no angular momentum, this means that the needle tries to align with the magnetic field. For an initial condition which is not aligned with the field, the needle will experience a torque $\vec{T} = \vec{m} \times \vec{B}$ (see Eq. [1.12]) which tries to align it with the field. This will lead to an oszillatory motion and, in the presence of damping, to an alignement of $\vec{m}$ and $\vec{B}$. A compass needle is overdamped and no oscillations are seen.

For a system which has, in addition to a magnetic moment, also an angular momentum we have a different situation. According to the Newton laws of mechanics the torque and the change in angular momentum must be equal:

$$\frac{d}{dt}\vec{L} = \vec{T} \qquad [1.31]$$

Using the gyromagnetic equation $\vec{L} = \frac{1}{\gamma}\vec{\mu}$ and $\vec{T} = \vec{\mu} \times \vec{B}$, we obtain[1], after summation in the unit volume, the equation of the motion for the magnetization vector ($\vec{M} = \frac{1}{V} \sum_{sample} \vec{\mu}$).

$$\frac{d}{dt}\vec{M} = \gamma \vec{M} \times \vec{B} \qquad [1.32]$$

We are free to assume that the magnetic field vector is along the z axis and we write $\vec{B} = (0, 0, B_0)$.

[1] Note that we have used $\vec{\mu}$ because we refer to the sum over microscopic moments (nuclear spins) whereas we had used $\vec{m}$ for the macroscopic system of a compass needle. In a classical description, both systems follow the same laws.

Note that we have replaced the magnetic induction $\vec{B}$ by the vacuum induction $\vec{B}_0$ (the "external field"). This is justified by the small size of the susceptibility χ,(see Chapter 1.1.4). The coupled system of differential equations of Eq. [1.32] has the form

$$\begin{aligned}\frac{d}{dt}M_x(t) &= \gamma M_y(t)B_0 \\ \frac{d}{dt}M_y(t) &= -\gamma M_x(t)B_0 \\ \frac{d}{dt}M_z(t) &= 0\end{aligned} \qquad [1.33]$$

and the solution is easily found to be

$$\begin{aligned}M_x(t) &= M_x(0)\cos\omega_0 t - M_y(0)\sin\omega_0 t \\ M_y(t) &= M_x(0)\sin\omega_0 t + M_y(0)\cos\omega_0 t \\ M_z(t) &= M_z(0)\end{aligned} \qquad [1.34]$$

with the initial condition $\vec{M}(0) = (M_x(0), M_y(0), M_z(0))$ and the abbreviation $\omega_0 = -\gamma B_0$. One can easily verify the solution Eq. [1.34] by inserting it into the differential equations of Eq. [1.33].

In vector form we can write the solution of Eq. [1.34] in the compact form

$$\vec{M}(t) = R_z(\omega_0 t)\vec{M}(0) \qquad [1.35]$$

where $R_z(\varphi)$ is the rotation matrix that performs a (right-handed) rotation of the initial magnetization $\vec{M}(0)$ vector around the z-axis:

$$R_z(\omega_0 t) = \begin{bmatrix}\cos(\omega_0 t) & -\sin(\omega_0 t) & 0 \\ \sin(\omega_0 t) & \cos(\omega_0 t) & 0 \\ 0 & 0 & 1\end{bmatrix}. \qquad [1.36]$$

The frequency ω_0 is called the Larmor (angular) frequency[1] and is defined by:

[1] Note that some textbooks use a different sign convention and define ω_0 with the same sign as γ. However, the sense of rotation for a proton (γ positive) is always $x \to -y \to -x \to y$ for a magnetic field along the z-axis of a right-handed coordinate system. Electrons have a negative γ and rotate anti-clockwise.

$$\omega_0 = -\gamma B_0 \qquad [1.37]$$

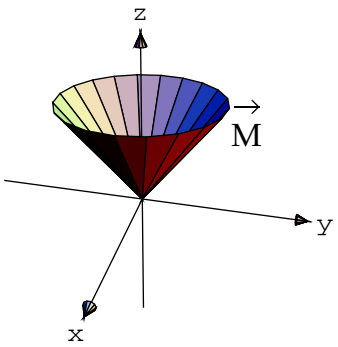

Figure 1.6: Larmor Precession
Precession of the magnetization vector around the z-axis for a nucleus with positive gyromagnetic ratio.

Note that we have attached a sign to the frequency: a positive frequency describes a right-handed rotation around the positive z-axis, a negative frequency a left-handed rotation. For a positive gyromagnetic ratio γ, (e.g for protons) the Larmor frequency is negative and a left-handed (clockwise rotation) arises: $x \rightarrow -y \rightarrow -x \rightarrow y$.

For electrons and nuclei with a negative gyromagnetic ratio (e.g. ^{15}N) a right-handed (anti-clockwise) rotation arises: $x \rightarrow y \rightarrow -x \rightarrow -y$

Often, the free precession frequencies are given in frequencies instead of angular frequencies and are then denoted by ν_0 with $\nu_0 = \omega_0/2\pi$. Examples for precession frequencies of the electron ($\gamma/2\pi = -28.02 \cdot 10^9 Hz/T$) and the proton ($\gamma/2\pi = 42.58 \cdot 10^6 Hz/T$) in practically important magnetic fields are given in the Table 1.2:

Table 1.2: Resonance frequencies and magnetic field strengths.

B_0	υ_0 (proton)	υ_0 (electron)
0.34 T		9.4 GHz (X-Band)
1 T		28.0 GHz (K-Band)
4.7 T	-200 MHz	132 GHz
14.1 T	-600 MHz	
18.8 T	-800 MHz	

The precession motion of the magnetization vector around a magnetic field vector is in full analogy to the precession of a (mechanical) spinning top[1] around the

[1] Deutsch: Kreisel

gravitational force field. The equation of the motion for the mechanical gyroscope is given by (see e.g. Kneubühl, Kapitel 3.4.4):

$$\frac{d}{dt}\vec{L} = T = \vec{r} \times \vec{F} \qquad [1.38]$$

using $\vec{r} = \frac{|\vec{r}|}{|\vec{L}|}\vec{L}$, we obtain

$$\frac{d}{dt}\vec{L} = \vec{T} = \frac{|\vec{r}|}{|\vec{L}|}\vec{L} \times \vec{F} \qquad [1.39]$$

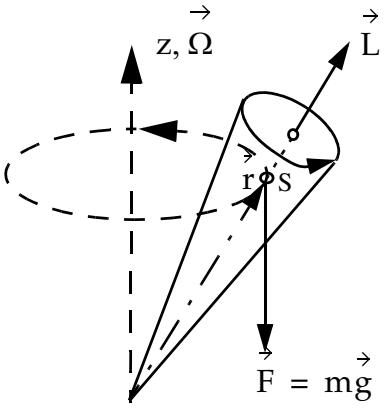

Figure 1.7: Mechanical Precession

which has the same form as Eq. [1.32] and we can make the following identification:

magnetic gyroscope	mechanical gyroscope
$\vec{M}$	$\vec{L}$
γ	$\lvert\vec{r}\rvert / \lvert\vec{L}\rvert$
$\vec{B}$	$\vec{F}$
$\vec{\omega} = -\gamma\vec{B}$	$\vec{\omega} = -\left(\lvert\vec{r}\rvert / \lvert\vec{L}\rvert\right)\vec{F}$

The top moves always perpendicular to the applied force $\vec{F}$.

1.3.1 Phenomenological Introduction of Relaxation Processes

It is not very plausible to assume that the (macroscopic) magnetization vector precesses forever around the magnetic field. In reality, there are damping mechanisms that return the magnetization vector to its energetically most favorable orientation parallel to $\vec{B}_0$ and to its equilibrium length. We denote the equilibrium magnetization by $\vec{M}_0$. Note that the equilibrium position is always parallel to $\vec{B}_0$ (and never antiparallel) independent of the sign of γ because the nuclei are all paramagnetic $\chi \geq 0$.

1.3.1.1 Longitudinal Relaxation

We call the magnetization component along the z-direction (the magnetic field direction) the longitudinal component M_z. Its magnitude and orientation determine the potential energy of the system according to Eq. [1.13]:

$$E_{pot} = -\vec{m} \cdot \vec{B} = -V\vec{M}\vec{B} = -VM_zB_0 \qquad [1.40]$$

A change in M_z involves energy-exchange with the environment. This process returns a non-equilibrium magnetization towards the equilibrium value $\vec{M}_0$. Assuming a first order kinetics, we write

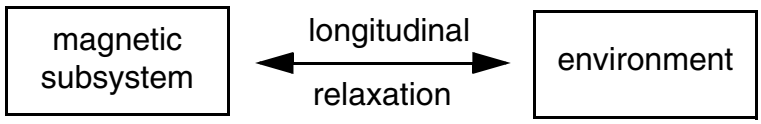

Figure 1.8: Coupling of Spin System and Environment

$$\frac{dM_z}{dt} = -\frac{1}{T_1}(M_z - M_0) \qquad [1.41]$$

with the time constant T_1, the *longitudinal relaxation*[1] time, also called the *spin-lattice relaxation*[2] time

1.3.1.2 Transverse Relaxation

Because the equilibrium magnetization has no transverse components, it must decay to zero. We assume again a first order kinetics. Due to the axial symmetry of our problem, we assume that both transverse components decay to zero with the same rate constant $1/T_2$ and write

$$\frac{d}{dt}M_x(t) = -\frac{1}{T_2}M_x$$
$$\frac{d}{dt}M_y(t) = -\frac{1}{T_2}M_y \qquad [1.42]$$

[1] Deutsch: Longitudinale Relaxationszeit

[2] Deutsch: Spin-Gitter Relaxationszeit

T_2 is the *transverse relaxation*[1] time, also called the *spin-spin relaxation*[2] time.

1.3.2 The Bloch Equations

Combining the relaxation terms of Eqs. [1.41] and [1.42] with the differential equations for the precession (Eq. [1.33]) we arrive at a set of differential equations known as the Bloch equations[3]:

$$\begin{aligned}\frac{d}{dt}M_x(t) &= \gamma M_y B_0 - \frac{M_x}{T_2}\\ \frac{d}{dt}M_y(t) &= -\gamma M_x B_0 - \frac{M_y}{T_2}\\ \frac{d}{dt}M_z(t) &= -\frac{M_z - M_0}{T_1}\end{aligned} \quad . \qquad [1.43]$$

or, in vector form

$$\frac{d}{dt}\vec{M} = \gamma\left(\vec{M}\times\vec{B}\right) - \Re\left\{\vec{M} - \vec{M}_0\right\} \qquad [1.44]$$

where $\Re$ is the relaxation matrix:

$$\Re = \begin{bmatrix} 1/T_2 & 0 & 0\\ 0 & 1/T_2 & 0\\ 0 & 0 & 1/T_1\end{bmatrix} \qquad [1.45]$$

The solution of Eq. [1.44] is given by:

$$\begin{aligned}M_x(t) &= [M_x(0)\cos\omega_0 t - M_y(0)\sin\omega_0 t]\exp(-t/T_2)\\ M_y(t) &= [M_x(0)\sin\omega_0 t + M_y(0)\cos\omega_0 t]\exp(-t/T_2)\\ M_z(t) &= M_0 + (M_z(0) - M_0)\exp(-t/T_1)\end{aligned} \qquad [1.46]$$

or in a matrix notation

---

1 Deutsch: Transversale Relaxationszeit

2 Deutsch: Spin-Spin Relaxationszeit

3 F. Bloch, Phys.Rev. 70, 260 (1946).

$$\vec{M}(t) = R_z(\omega_0 t) \cdot e^{-\Re t}\left(\vec{M}(0) - \vec{M}_0\right) + \vec{M}_0 \qquad [1.47]$$

where $R_z(\varphi)$ is the rotation matrix of Eq. [1.36] and $\vec{M}(0) = (M_x(0), M_y(0), M_z(0))$ is the initial magnetization at time t=0. $\vec{M}_0$ is of the form $(0, 0, M_0)$. For $\vec{M}(0)$=(0,M(0),0), the motion shown in Fig. 1.9 is obtained (for positive γ).

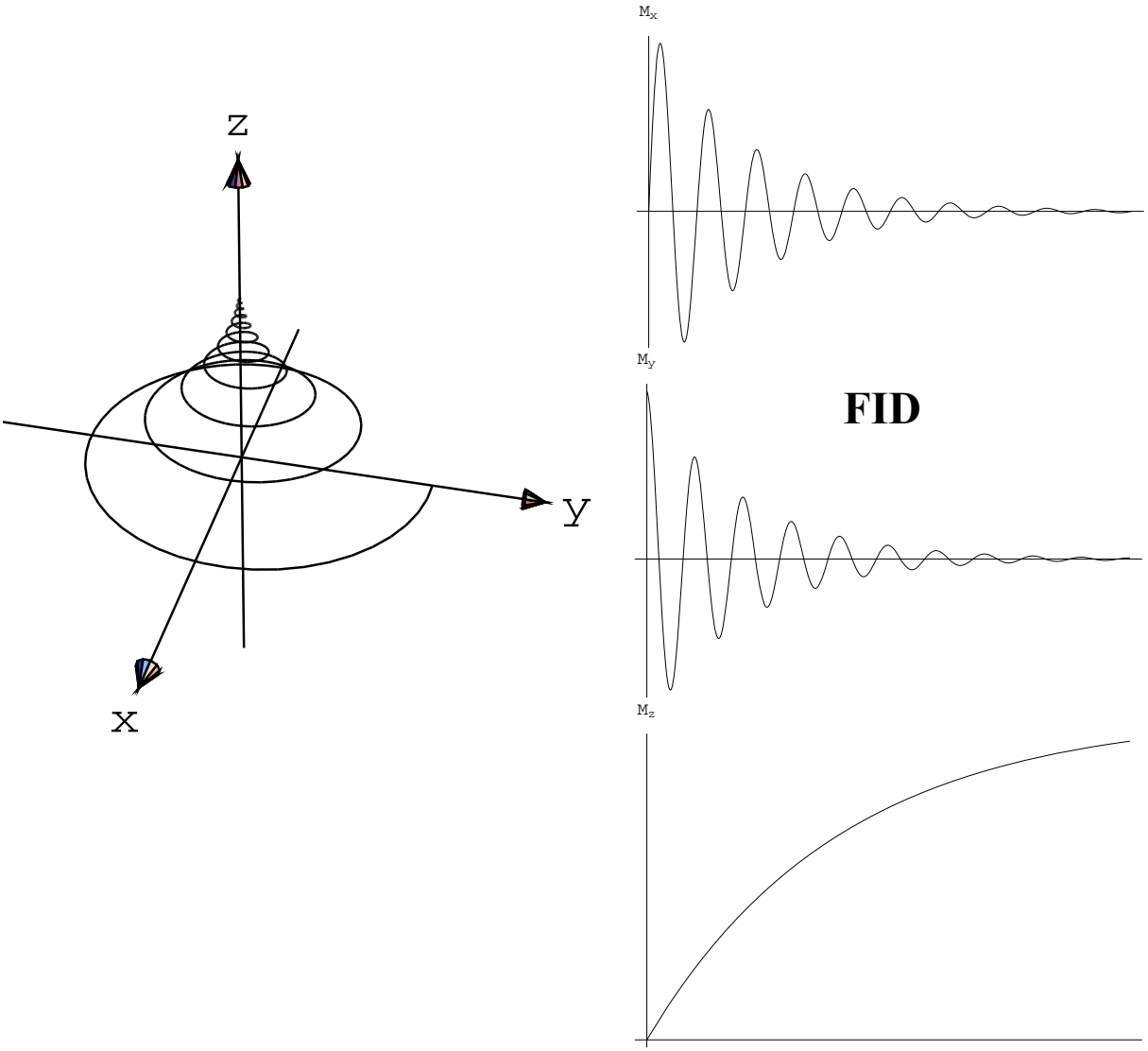

Figure 1.9: Bloch Equations
Time evolution of the magnetization vector starting from y magnetization,(0,1,0), as described by the Bloch equations (for positive γ).

2 A Classical Description of NMR Spectroscopy

2.1 The NMR Spectrum and its Fine Structure

The NMR experiment detects one of the transverse components of the magnetization (here we define it to be $M_y(t)$). The longitudinal magnetization gives no signal in conventional NMR. Therefore, the equilibrium magnetization $\vec{M}_0$ must be perturbed in the experiment.

In a *pulsed experiment*, a short but intense radio-frequency (rf) pulse is used to create a non-equilibrium magnetization $\vec{M}(0)$, e.g., $(0, M_0, 0)$. This initial excitation process ($\vec{M}_0$ -> $\vec{M}(0)$) will be discussed below. Afterwards, the magnetization $M_y(t)$ can be observed in the absence of further rf irradiation ("free induction decay", FID). For an ensemble of non-interacting spins, the FID is described by the Bloch equations. For $\vec{M}(0) = (0, M_0, 0)$, the solution of the Bloch equations is displayed in Fig. 1.9. Included in the Figure is $M_y(t)$, which induces the FID. Usually, we do not plot the FID, but its Fourier transform, the NMR spectrum $S(\omega)$.

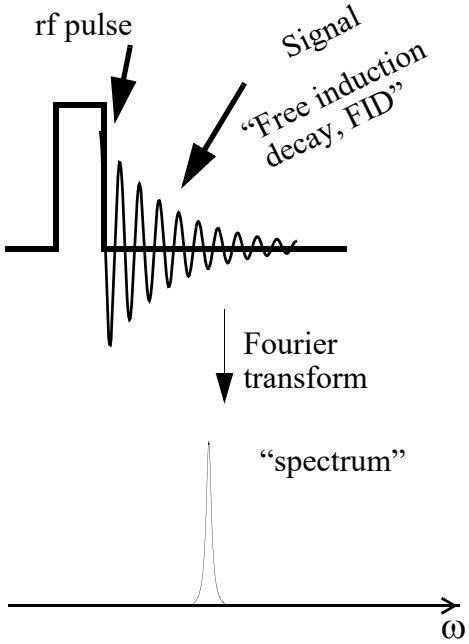

Figure 2.1: Schematic NMR Experiment

For isolated nuclei, the gyromagnetic ratio is a material constant for each isotope. For ethanol, CH_3-CH_2-OH, we would therefore expect a strong proton resonance signal at the proton resonance frequency and a much weaker signal from the carbons because only about 1% of the carbon nuclei (the isotope ^{13}C), are NMR active. The most common carbon isotope ^{12}C is not NMR active. The exact resonance

frequency depends on the susceptibility of the medium (see Eq. [1.7]), e.g., on the solvent for the nuclei in a dissolved molecule.

In addition, it also depends on the local interactions within the molecule. The electrons in the molecule will locally modify the field, similar to the susceptibility on a macroscopic level. We call this effect the *chemical shift*. Its magnitude is on the scale of parts per million (ppm) of the applied field and it leads to the slight modification of the Larmor frequency that is experimentally observed. We will denote the modified Larmor frequency by ω_0* The proton spectrum of ethanol, reproduced in Fig. 2.2, consist of three groups of resonances with different values for ω_0* . The fine structure within each proton line comes from the interaction between neighboring protons ("J-coupling"). The interaction with the rare ^{13}C spins is not seen here. A detailed discussion of these effects will be given later.

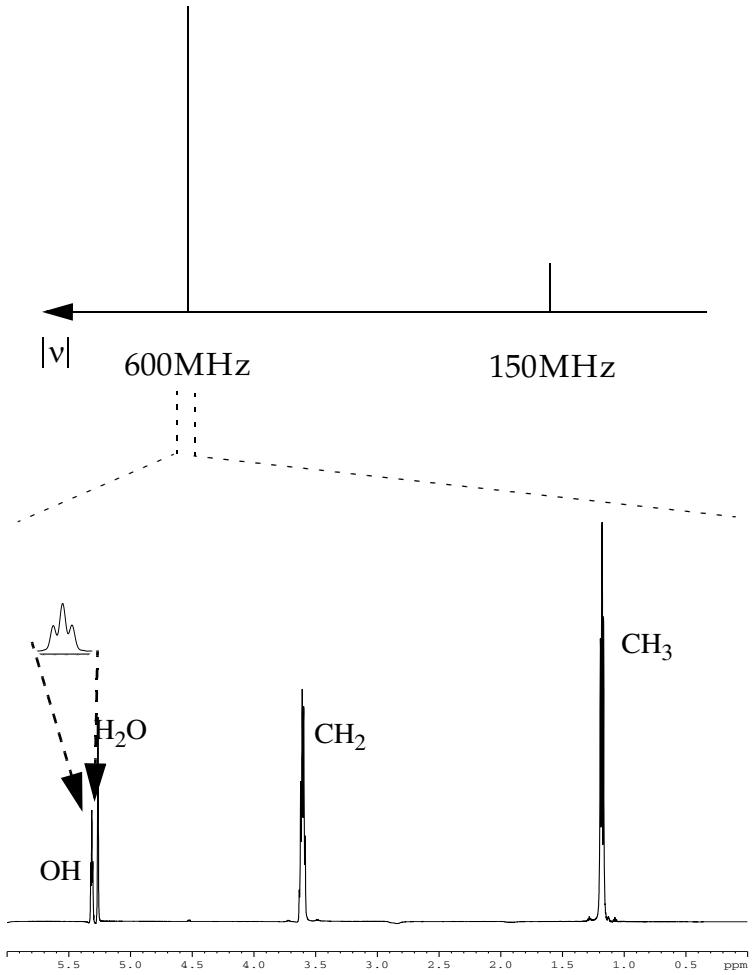

Figure 2.2: NMR Resonance Frequencies
NMR spectrum of ethanol measured at 14.1 Tesla field strength. The frequency axis in the proton spectrum is given in ppm and frequencies are given with respect to a reference substance (TMS: Tetramethylsilane).

Because of the linearity of the Bloch equations, we can describe a system with N non-interacting resonance lines just as the superposition of N systems each with a different resonance frequency ω_0* .

2.2 Generating Non-Equilibrium Magnetization

According to the Bloch equations (Eq. [1.43]), the initial magnetization will be aligned with the field vector $\vec{B}_0$ in a time-constant magnetic field. This process happens in a time in the order of T_2 (typically μs to s) and will reach its equilibrium magnitude after a time in the order of T_1 (typically μs to hours). To observe a precession, we first have to prepare a state with the magnetization vector tilted away from the equilibrium z-direction.

To prepare such a state, the application of time-dependent magnetic fields $B(t)$ is mandatory. A conceptually simple way to obtain an initial state along the y-axis, would be to suddenly change the magnetic field B_0 to point along the x-axis. Then one would wait until the magnetization has precessed around the x-axis by $\pi/2$. Then one would switch the field direction suddenly back to the z -axis. The precession time should be fast compared to the relaxation times, the field switching is assumed to be infinitely fast.

In practice, such a procedure is impossible for high-field spectroscopy and the magnetic field direction must remain fixed. However, exactly the same effect can be obtained by the (additional) application of a time-dependent field $B_1(t)$ in the x-y plane:

$$\vec{B}(t) = \vec{B}_0 + \vec{B}_1(t) \qquad [2.1]$$

with the time-dependent part given by

$$\vec{B}_1(t) = B_1(\cos\omega_{rf}t \cdot \vec{e}_x + \sin\omega_{rf}t \cdot \vec{e}_y) \qquad [2.2]$$

Because the range of typical frequencies ω_{rf} is in the radio-frequency region (10-1000 MHz) of the electromagnetic spectrum, $\vec{B}_1(t)$ is usually called the *radio-frequency (rf) field*. Here, we have chosen to use a time-dependent rf-field that rotates in the x/y plane with the frequency ω_{rf}. Such a field is called *circularly polarized*[1].

[1] Deutsch: zirkularpolarisiert

2.3 Rf Irradiation and the Rotating Coordinate Frame

The solution of the equation of motion of the magnetization vector in the presence of a (time-dependent) rf-field is difficult. We can, however, apply a trick and describe our problem in a coordinate system that rotates relative to the laboratory frame around the z-axis with the frequency ω_{rf}. A vector in the "new" (the rotating) coordinate system is obtained from the vector in the "old" (the laboratory) coordinate system by the following transformation:

$$\vec{v}^{r} = T\vec{v} \qquad [2.3]$$

with[1]

$$T(\phi) = \begin{bmatrix} \cos\phi & \sin\phi & 0 \\ -\sin\phi & \cos\phi & 0 \\ 0 & 0 & 1 \end{bmatrix}. \qquad [2.4]$$

where $\phi = \omega_{rf}t$.

The magnetic field in the rotating frame is time-independent

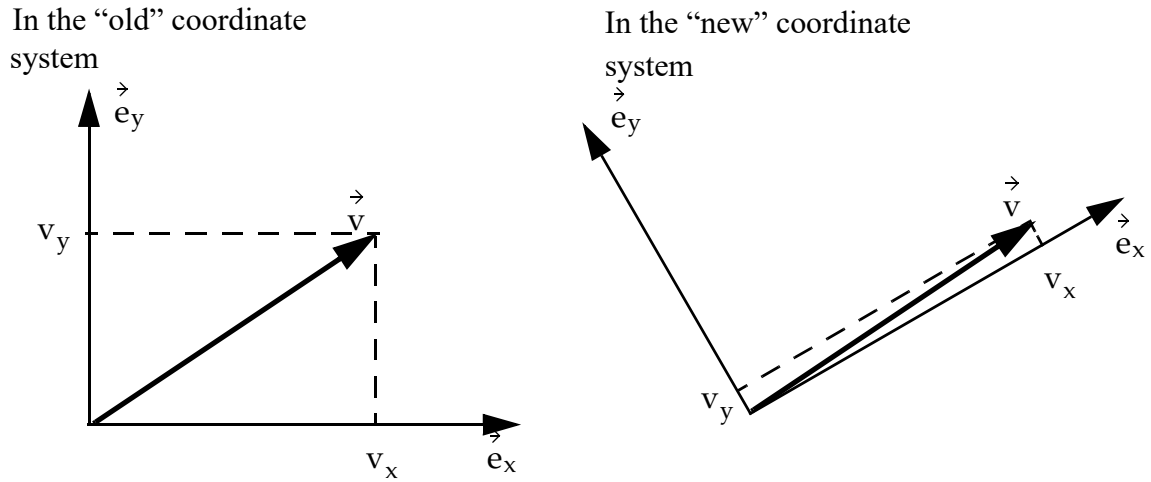

Figure 2.3: Coordinate Transformations: One and the Same Vector

[1] Note that the sine terms in the transformation matrix have the opposite sign from the respective term in Eq. [1.36] because, here, we describe the same object (vector) in a rotated coordinate system, while Eq. [1.36] describes the rotation of a (vector) object in a fixed coordinate system.

$$\vec{B}^{r} = B_0\vec{e}_z + T(\omega_{rf}t)\vec{B}_1 = B_0\vec{e}_z + B_1\vec{e}_x^{r}. \qquad [2.5]$$

and *we have replaced the time-dependent problem by a time-independent one*.

Next, we want to know the equivalent of the Bloch equations, $\frac{d}{dt}\vec{M} = \gamma\left(\vec{M}\times\vec{B}\right) - \Re\left\{\vec{M} - \vec{M}_0\right\}$, in the rotating frame. Multiplying on both sides with T leads to:

$$\begin{aligned} T\frac{d}{dt}\vec{M} &= \gamma\left(\vec{M}^{r}\times\vec{B}^{r}\right) - T\Re\left\{\vec{M} - \vec{M}_0\right\} \\ &= \gamma\left(\vec{M}^{r}\times\vec{B}^{r}\right) - \Re\left\{\vec{M}^{r} - \vec{M}_0\right\} \end{aligned} \qquad [2.6]$$

How do we transform the derivative of a vector, $T\left(\frac{d}{dt}\vec{v}\right)$ into the rotating frame?

We look at a time-dependent vector $\vec{v}$ in the lab frame. The change of the vector which occurs in a (infinitesimal) time interval dt is denoted by $d\vec{v}$. The corresponding change in the rotating frame is denoted by $d\vec{v}^{r}$. The simple-minded solution of just transforming $d\vec{v}$ like an ordinary vector is wrong: $d\vec{v}^{r} \neq Td\vec{v}$. This is easily seen: a time-independent vector in the lab frame ($d\vec{v} = \vec{0}$) must be time-dependent if seen from a rotating frame ($d\vec{v}^{r} \neq 0$) while $Td\vec{v} = \vec{0}$.

In dt, the rotating frame has rotated with respect to lab frame by the infinitesimal angle $d\phi$. The rotation matrix $T(d\phi)$ for an infinitesimal rotation can be written as $T(d\phi) = 1 + \varepsilon$ with

$$\varepsilon = \begin{bmatrix} 0 & d\phi & 0 \\ -d\phi & 0 & 0 \\ 0 & 0 & 0 \end{bmatrix}. \qquad [2.7]$$

1 denotes the 3x3 unity matrix. Note that we have replaced $\sin d\phi$ by $d\phi$ and $\cos d\phi$ by 1.

In the more general case of a three-dimensional rotation, we obtain in full analogy to the one-dimensional case:

$$\varepsilon = \begin{bmatrix} 0 & d\phi_3 & -d\phi_2 \\ -d\phi_3 & 0 & d\phi_1 \\ d\phi_2 & -d\phi_1 & 0 \end{bmatrix} \qquad [2.8]$$

We look first at a vector that is constant in the lab frame. The change in the rotating-frame vector components by the infinitesimal rotation of the coordinate system is given by $\delta\vec{v}^{r} = T\vec{v}^{r} - \vec{v}^{r} = \varepsilon\vec{v}^{r}$ or:

$$\begin{aligned} \delta v_1{}^{r} &= v_2^r d\phi_3 - v_3^r d\phi_2 \\ \delta v_2{}^{r} &= v_3^r d\phi_1 - v_1^r d\phi_3 \\ \delta v_3{}^{3} &= v_1^r d\phi_2 - v_2^r d\phi_1 \end{aligned} \qquad [2.9]$$

If we define a vector of angular changes, $\overrightarrow{d\phi} = (d\phi_1, d\phi_2, d\phi_3)$, we can rewrite this set of equations in vector form as:

$$\delta\vec{v}^{r} = \vec{v}^{r} \times \overrightarrow{d\phi} \qquad [2.10]$$

Equation [2.10] describes the differential change of a vector that is constant in the lab frame due to description from a rotating frame.

We can now calculate the total change in the rotating frame of a general vector that has a change of $\overrightarrow{dv}$ already in the lab frame. It is the sum of the change $\overrightarrow{dv}$ (transformed to the rotating frame) and the change $\delta\vec{v}^{r}$:

$$d\vec{v}^{r} = Td\vec{v} + \delta\vec{v}^{r} \qquad [2.11]$$

Using Eq. [2.10] and dividing by dt leads to

$$\frac{d\vec{v}^{r}}{dt} = T\frac{d\vec{v}}{dt} + \vec{v}^{r} \times \frac{\overrightarrow{d\phi}}{dt} \qquad [2.12]$$

The last term is the angular velocity of the frame and, in our case, is given by a rotation around the z-axis with a constant angular velocity ω_{rf}: $\vec{\omega}_{rf} = \omega_{rf}\vec{e}_z$. Therefore we write

$$T\frac{d\vec{v}}{dt} = \frac{d\vec{v}^{r}}{dt} - \vec{v}^{r} \times \vec{\omega}_{rf} \qquad [2.13]$$

By inserting Eq. [2.13] into Eq. [2.6] with $\vec{v} \to \vec{M}$ we can rewrite the Bloch equation completely in terms of rotating-frame quantities:

$$\frac{d\vec{M}^{r}}{dt} - \vec{M}^{r} \times \vec{\omega}_{rf} = \gamma\left(\vec{M}^{r} \times \vec{B}^{r}\right) - \Re\left\{\vec{M}^{r} - \vec{M}_0\right\} \qquad [2.14]$$

and

$$\frac{d}{dt}\vec{M}^{r} = \gamma\left(\vec{M}^{r} \times \vec{B}_{eff}^{r}\right) - \Re\left\{\vec{M}^{r} - \vec{M}_0\right\} \qquad [2.15]$$

with the effective field in the rotating frame given by:

$$\vec{B}_{eff}^{r} = \vec{B}^{r} + \frac{\omega_{rf}}{\gamma}\vec{e}_z = \vec{B}_0^{r} + \frac{\omega_{rf}}{\gamma}\vec{e}_z + \vec{B}_1^{r} = \Delta\vec{B}^{r} + \vec{B}_1^{r}. \qquad [2.16]$$

In the rotating frame, the corrected field

$$\Delta\vec{B}^{r} = \vec{B}_o + \frac{\omega_{rf}}{\gamma}\vec{e}_z \qquad [2.17]$$

takes the role of the applied field $\vec{B}_o$ in the laboratory frame!

The equilibrium magnetization, $\vec{M}_0$, is not influenced by the rotating-frame transformation because it is parallel to the rotation axis. In the special case of a vanishing rf field ($B_1 = 0$) the effective field is then given by:

$$\vec{B}_{eff}^{r} = \Delta\vec{B}^{r} = -\frac{\Omega}{\gamma}\vec{e}_z \qquad [2.18]$$

And the Larmor precession frequency in the rotating frame amounts to:

$$\Omega = \omega_0 - \omega_{rf} = -\gamma\Delta\vec{B}^{r}. \qquad [2.19]$$

or, considering the chemical shift,

$$\Omega = \omega_0^{*} - \omega_{rf} \qquad [2.20]$$

With these definitions the FID in the rotating frame is given by

$$\vec{M}^{r}(t) = R_z(\Omega t) \cdot e^{-\Re t}\left(\vec{M}^{r}(0) - \vec{M}_0\right) + \vec{M}_0 \qquad [2.21]$$

Close to resonance when $\omega_{rf} \approx \omega_0$ and $\Omega \approx 0$, the field along the z-axis, $\Delta\vec{B}^{\vec{r}}$ becomes very small and vanishes altogether at exact resonance. Then, the only effects seen are the ones of relaxation: $\vec{M}^{\vec{r}}(t) = e^{-\Re t}\left(\vec{M}^{\vec{r}}(0) - \vec{M}_0\right) + \vec{M}_0$.

2.4 Intense Radio-Frequency Pulses

To prepare a certain initial magnetization vector short intense rf pulses can be applied. In practice the circularly-polarized fields $\vec{B}_1(t) = B_1(\cos\omega_{rf}t \cdot \vec{e}_x + \sin\omega_{rf}t \cdot \vec{e}_y)$ introduced in Eq. [2.2] are rarely used. Instead, linearly polarized pulses of the form:

$$\vec{B}_1(t) = 2B_1 \cos\omega_{rf}t \cdot \vec{e}_x \qquad [2.22]$$

are applied.

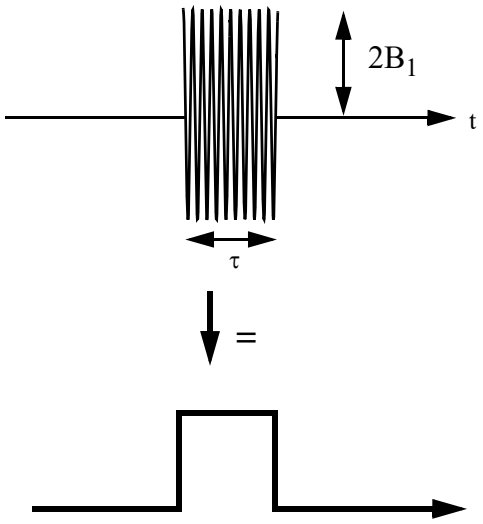

Figure 2.4: Schematic Representatic of rf Pulses

Linearly polarized pulses can be looked at as the superposition of two circularly polarized fields of opposite polarization:

$$\vec{B}_1(t) = B_1(\cos\omega_{rf}t \cdot \vec{e}_x + \sin\omega_{rf}t \cdot \vec{e}_y) + B_1(\cos\omega_{rf}t \cdot \vec{e}_x - \sin\omega_{rf}t \cdot \vec{e}_y) \qquad [2.23]$$

The component that rotates in the opposite way as the magnetization under the static field has only a negligible effect on the magnetization[1]. That the counter-rotating component alone has no effect on the magnetization can be seen by assuming a circularly polarized field with the wrong rotation direction and transforming it into the rotating frame with the "correct" rotation direction rotating at $\omega_{rf} = -\omega_0$. Then the term $\Delta\vec{B}^{\vec{r}} = \vec{2B_o}$ in the rotating frame is much larger than $\vec{B}_1^{\vec{r}}$ and the latter has almost no influence on the time evolution of the magnetization vector.

Usually, the duration of the pulses can, in NMR, be chosen to be much shorter than the relaxation times, $\tau \ll T_1, T_2$ and relaxation during the pulses can be

[1] see F. Bloch and A. Siegert, Phys.Rev. 57, 522 (1940)

neglected. Typical pulse lengths for excitation of the magnetization from the equilibrium position are in the range of 1-20 μs.

2.4.1 On-Resonance Pulses

If the pulse is applied exactly *on resonance*, i.e., $\omega_{rf} = \omega_0$, the Bloch equations are of the form

$$\frac{d}{dt}\vec{M}^{r} = \gamma\left(\vec{M}^{r} \times B_1\vec{e}_x^{r}\right) . \qquad [2.24]$$

This corresponds to a rotation around the x-axis of the coordinate system. The time evolution of the magnetization for the initial condition in equilibrium $\vec{M}(0) = \vec{M_0} = M_0\vec{e}_z$ is:

$$\vec{M}(t) = M_0(0, -\sin\beta, \cos\beta) \quad \text{with} \quad \beta = -\gamma B_1 t \qquad [2.25]$$

The angle β is called the *flip angle* of the pulse.

- A *90° pulse* ($\beta = -\gamma B_1 t = \pi/2$) flips the magnetization into the x-y plane and generates the largest initial FID.
- A *180° pulse* ($\beta = -\gamma B_1 t = \pi$) inverts the magnetization vector and does not generate any detectable transverse magnetization.

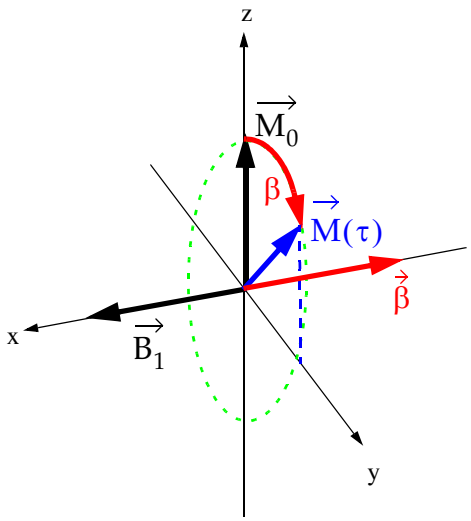

Figure 2.5: A β_{-x} On-Resonance Pulse

Formally, we can write the flip angle as a vector,

$$\vec{\beta} = -\gamma t\vec{B_1} \qquad [2.26]$$

whose magnitude is the flip angle and whose direction is either parallel or anti-parallel to the direction of the irradiation field, depending on the sign of γ. For positive gyromagnetic ratios γ, $\vec{\beta}$ and $\vec{B_1}$ are antiparallel, for negative γ parallel. For

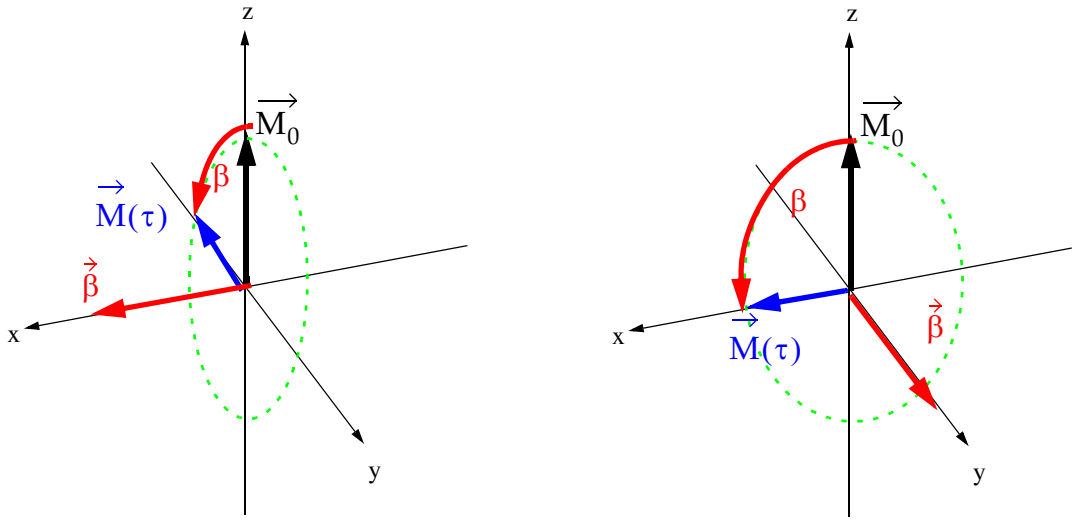

$\left(\frac{\pi}{2}\right)_x$ pulse: $z \rightarrow -y \rightarrow -z \rightarrow y \rightarrow z$

$\left(\frac{\pi}{2}\right)_y$ pulse: $z \rightarrow x \rightarrow -z \rightarrow -x \rightarrow z$

Figure 2.6: Rf Pulses: Rotation Convention

all systems, the rotation of the magnetization around the $\vec{\beta}$ vector is always right-handed. For pulses along the x or y axes of the rotating frame, the direction of the β vector is usually denoted by a subscript, e.g. 90^0_x or $\left(\frac{\pi}{2}\right)_x$.

2.4.2 Off-Resonance Pulses

If the frequency of the applied rf pulse ω_{rf} is not equal to the Larmor frequency ω_0, i.e., $\Omega = \omega_0 - \omega_{rf} \neq 0$, we talk of *off-resonance* irradiation. The Bloch equation is given by

$$\frac{d}{dt}\vec{M}^r = \gamma\left(\vec{M}^r \times (B_1\vec{e}_x^r + \Delta B\vec{e}_z^r)\right) \quad [2.27]$$

and describes a rotation around the effective field $\vec{B}_{eff}$. The effective field is larger than the applied B_1 field:

$$B_{eff} = \sqrt{B_1^2 + \Delta B^2}\ . \quad [2.28]$$

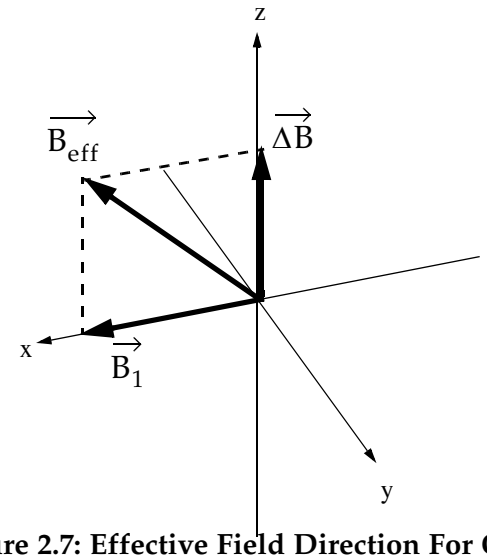

Figure 2.7: Effective Field Direction For Off--Resonance Pulses

Therefore, the flip-angle β is larger than for on-resonance irradiation with the same B_1 field. The cone on which the magnetization precesses, on the other hand, becomes narrower due to the smaller angle between the effective field and the initial magnetization. For very short pulses, the trajectory of the magnetization becomes independent of the offset.

Obviously, the off-resonance effects become smaller as the pulse becomes more intense (larger B_1). For hard pulses that should have the same effect on all resonance lines in a spectrum irrespective of their chemical shift, it is necessary that

$$|\gamma B_1| \gg \Omega_{max} \; . \qquad [2.29]$$

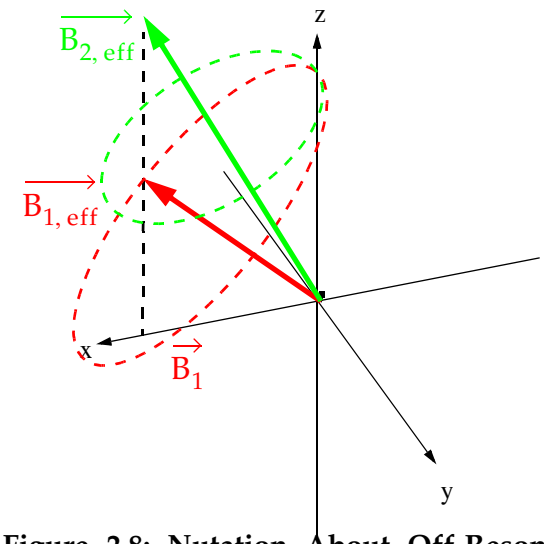

Figure 2.8: Nutation About Off-Resonance Pulses

In NMR, the technically achievable field strengths characterized by the nutation frequency $\omega_1 = -\gamma B_1$ are typically in the order of 10 to 200 kHz which is in fact larger than the spread, e.g., in a proton spectrum which is in the order of 8 kHz (in a 800 MHz magnet). On the other hand, some nuclei have a much larger chemical-shift range (^{13}C has about 40 kHz spread on a 800 MHz magnet) and the hard-pulse condition might not always be fulfilled.

2.4.3 Spin Lock

As we have seen, the component of the magnetization which is perpendicular to the effective field (in the rotating frame) oscillates around that field with a frequency of $\omega_{eff} = -\gamma B_{eff}$. The component along the effective field direction $\overrightarrow{B_{eff}}$ remains (in the absence of relaxation) unchanged. The following pulse sequence first rotates the magnetization along the x axis and then spin locks it. In the absence of relaxation, the magnetization stays locked to the x-direction of the rotating frame at all times. This is also true, if we irradiate slightly off resonance, but have an rf field strong enough to dominate the off-resonance term: $B_1 \gg |\Delta B|$. Then, the 90^0 pulse

rotates all spins (irrespective of the chemical shift) to the x-axis and, instead of precessing at their rotating-frame frequency $-\gamma\Delta B$, all spins stay along the x-axis of the rotating frame at all times. Taking into account relaxation, the spin-locked component is given by:

$$M_x(\tau) = M_x(0)e^{-\tau/T_{SL}} \qquad [2.30]$$

From the steady-state solution of the Bloch equations when $\frac{dM_x}{dt} = \frac{dM_y}{dt} = 0$, it can be shown that these components also vanish for long times, given that the irradiation field is strong enough to fulfill:

$$\omega_1^2 T_1 T_2 \gg 1. \qquad [2.31]$$

Then the magnetization approaches a vanishing value at equilibrium $\overrightarrow{M_0} = (0, 0, 0)$. We call this effect *saturation*.

2.4.4 Adiabatic Fast Passage

In this experiment the rf-frequency of the applied pulse is changed as a function of time $\omega_{rf} = \omega_{rf}(t)$. Therefore, the z component of the magnetic field in the rotating frame $\Delta B(t) = \vec{B}_o + (\omega_{rf}(t))/\gamma$ is also time dependent. For an initial condition of $\omega_{rf}(t) \ll \omega_0$, the effective field is approximately aligned with the static field and the z axis. On approaching the resonance condition, $\omega_0 = \omega_{rf}$, it rotates in

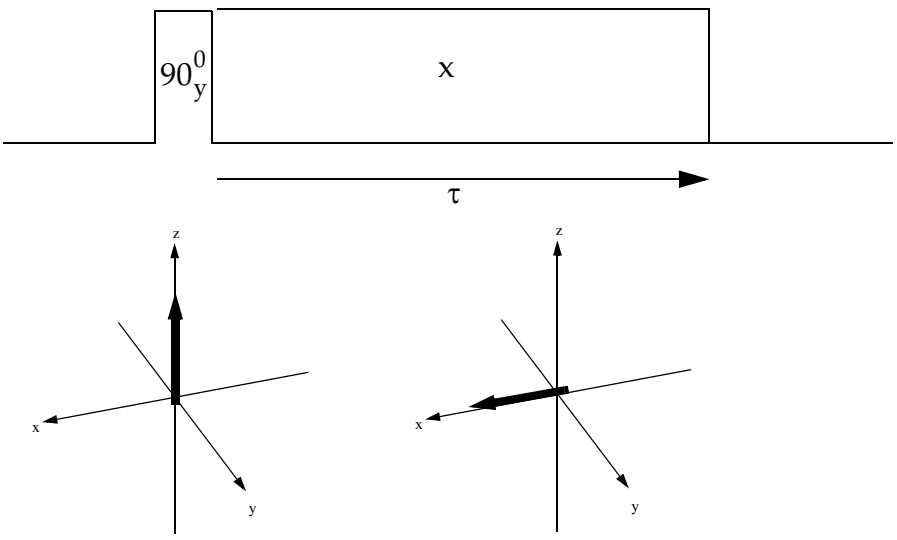

Figure 2.9: Spin Lock

the x-z plane and is parallel with the x axis of the rotating frame at exact resonance. A further increase of ω_{rf} continues the rotation until the effective field ends up to be antiparallel to the z axis.

In the course of this motion of the effective field axis, the magnetization tries to rotate around the effective field direction with the frequency $\omega_{eff}(t) = -\gamma B_{eff}(t)$. If the adiabatic condition is fulfilled:

$$\left|\frac{d}{dt}\theta\right| \ll |\omega_{eff}| \qquad [2.32]$$

the magnetization stays spin-locked at all times and is "dragged along" by the effective-field vector.

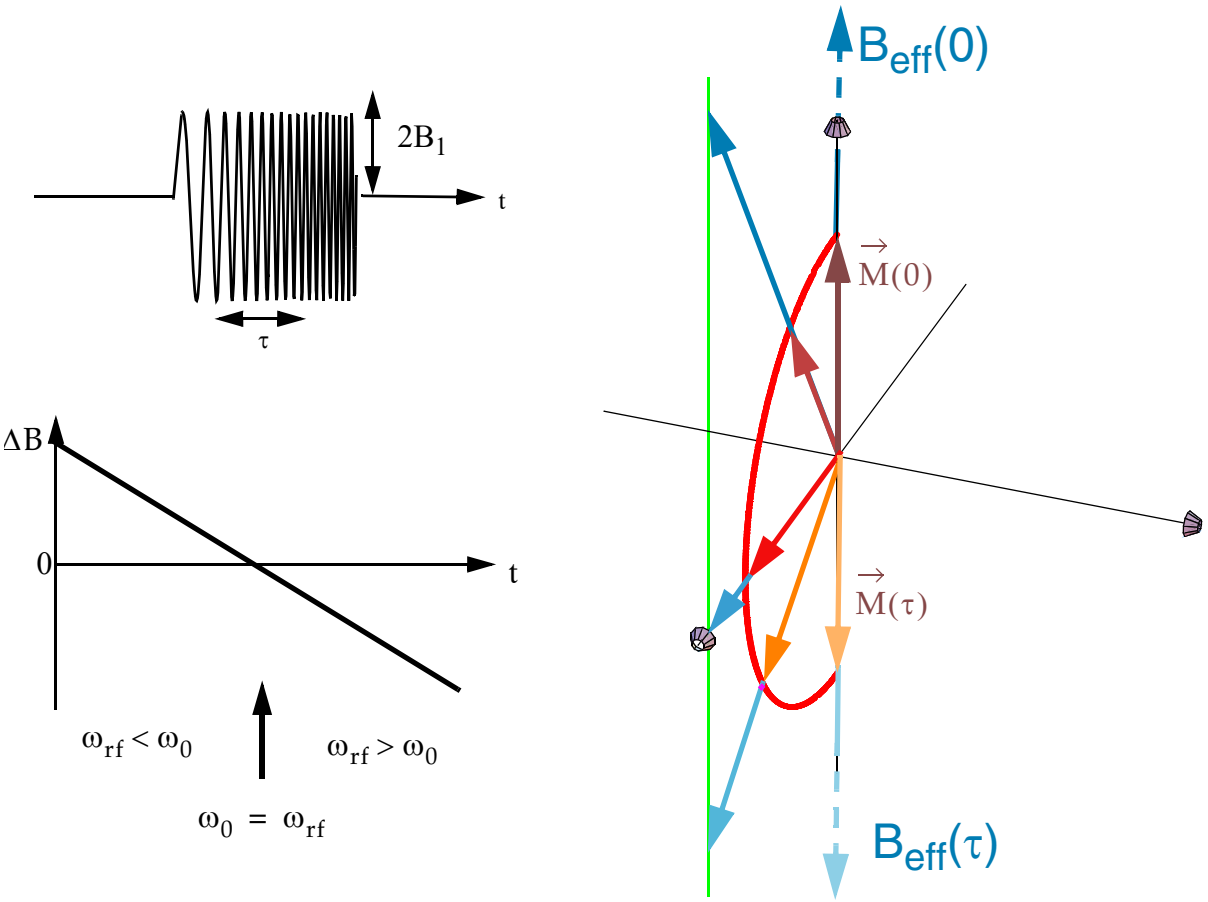

Figure 2.10: Adiabatic Pulses

2.5 Detecting the Magnetization in the Time Domain

As discussed earlier, the nuclear precession is induced by applying a current to a coil which produces a magnetic field. A precessing magnetic moment produces, in return, a time-dependent magnetic field which induces a current into the coil. A simple one-pulse NMR experiment is shown in Figure 2.11. Because excitation and detection of the resulting signal occur in two different time periods, the same coil can be used for both processes. The basic block diagram of a NMR spectrometer is shown in Fig. 2.12.

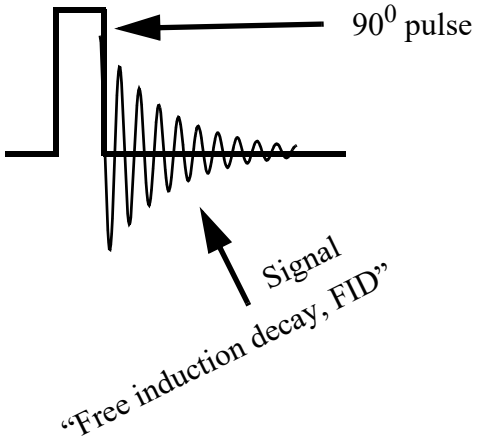

Figure 2.11: Schematic NMR Experiment

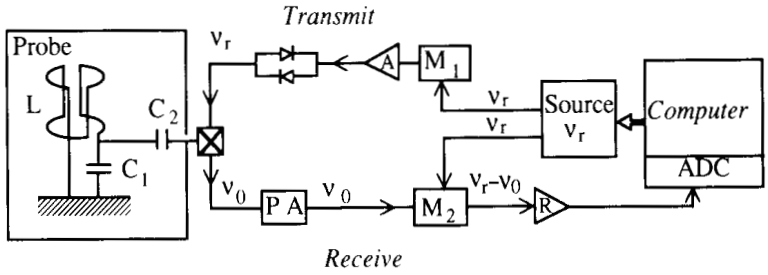

Block diagram of a pulse NMR spectrometer. The source (frequency synthesizer) provides a sine wave whose frequency ν_r is close to the nuclear resonance frequency ν_0. This r.f. wave is shaped into pulsed form by means of the mixer M_1 and subsequently amplified (power amplifier A delivering several tens or hundreds of watts) and applied to the probe, which essentially comprises a resonant circuit LC_1 (with the tuning condition $4\pi^2\nu_r^2LC_1 \approx 1$); the capacity C_2 is used for matching the whole circuit (LC_1, C_2) to a pure resistive impedance of 50 Ω. L is the self-induction coefficient of the coil surrounding the sample, which is generally of the saddle type, for a vertical cryomagnet and a vertical sample tube (when other configurations are used, a solenoid is preferable). The purpose of the crossed diodes in the transmitter circuit is to isolate the latter during signal reception. The NMR signal is detected through the same circuit LC_1C_2. The cross is a symbol for diode-based circuitry aimed at commuting and protecting the preamplifier (PA). The NMR signal, at frequency ν_0, is demodulated with respect to ν_r (by means of the mixer M_2) and thus shifted to a low frequency signal $\nu_r - \nu_0$, which is amplified (amplifier R), digitized in an analog-to-digital-converter (ADC) and processed by a computer

Figure 2.12: Block Diagram of a NMR Spectrometer
From D. Canet: Nuclear Magnetic Resonance, Wiley.

The NMR signal as detected by the coil oscillates at the Larmor frequency. It is circularly polarized but we only detect one component in the laboratory frame leading to a linearly polarized signal, e.g.,

$$M_x(t) = M_x^r(t)\cos(\omega_{rf}t) - M_y^r(t)\sin(\omega_{rf}t) \ . \qquad [2.33]$$

The analysis (e.g. the digitization) of a signal at a few 100 MHz with an accuracy of a few mHz is difficult and, therefore, the signal is often demodulated with respect to ω_{rf}, the carrier frequency. Then it looks like we would have detected the magnetization in the rotating frame. *Note, that the physical detection process always happens in the laboratory frame.* Of course, we are able to calculate the two components, $M_x^r(t)$ and $M_y^r(t)$, at the same time. This is referred to as *quadrature detection* (Fig. 2.13). It allows us to distinguish positive from negative rotating-frame frequencies Ω and the carrier frequency ω_{rf} can be set into the center of the spectrum to be detected. Single channel demodulation (e.g. $M_x^r(t)$ only) leads to spectra that are symmetric around $\Omega = 0$ and the carrier frequency must be set to a value outside the interesting spectral area.

It is convenient to combine the magnetization components $M_x^r(t)$ and $M_y^r(t)$ to the complex signal function:

$$s(t) = M_+ = M_x^r(t) + iM_y^r(t) \qquad [2.34]$$

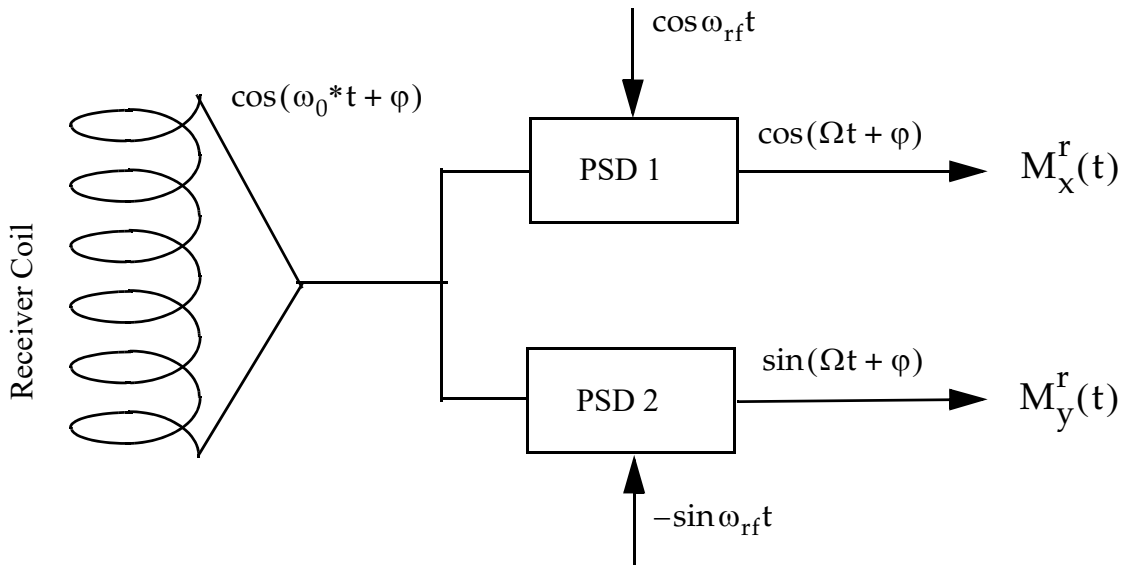

Figure 2.13: Schematic of a PSD Receiver

2.6 The Spectrum in the Frequency Domain

The NMR spectrum, $S(\omega)$, is the Fourier transform of the time-domain signal $s(t)$:

$$S(\omega) = \int_{-\infty}^{\infty} s(t) e^{-i\omega t} dt. \qquad [2.35]$$

For the solution of the Bloch equations in the rotating frame with $M_0 = (M_0, 0, 0)$,

$$\begin{aligned} M_x^r(t) &= M_0 \cos(\Omega t) e^{-\frac{t}{T_2}} \\ M_y^r(t) &= M_0 \sin(\Omega t) e^{-\frac{t}{T_2}} \end{aligned} \qquad [2.36]$$

we obtain the complex signal function

$$s(t) = M_x^r(t) + iM_y^r(t) = M_0 e^{i\Omega t} e^{-\frac{t}{T_2}} \qquad [2.37]$$

and the associated complex spectrum

$$S(\omega) = M_0 \int_0^{\infty} e^{i(\Omega - \omega)t} e^{-t/T_2} dt \qquad [2.38]$$

(note, that $s(t) = 0$ for $t < 0$) which amounts to

$$S(\omega) = M_0 \frac{1}{1/T_2 - i(\Omega - \omega)} \qquad [2.39]$$

The real and imaginary part of the spectrum are denoted as *absorption* and *dispersion* signals, $A(\omega)$ and $D(\omega)$, respectively: $S(\omega) = A(\omega) + iD(\omega)$ and have the form:

$$\begin{aligned} A(\omega) &= M_0 \frac{1/T_2}{1/T_2^2 + (\Omega - \omega)^2} \\ D(\omega) &= M_0 \frac{\Omega - \omega}{1/T_2^2 + (\Omega - \omega)^2} \end{aligned}. \qquad [2.40]$$

The absorptive part, $A(\omega)$, is a Lorentzian line (Fig. 2.14a) centered at the rotating-frame resonance frequency Ω. The full width at half height (FWHH) of the line is $2/T_2$. Note that the frequency axis is given in angular frequencies $\omega = 2\pi\nu$. The FWHH expressed in Hertz is $(2/T_2)/(2\pi) = 1/(\pi T_2)$ (see Fig. 2.14b). Therefore, T_2 must be 0.32 s to yield a line-width of 1 Hz since NMR spectra are almost always plotted in Hertz and not angular frequencies.

The Dispersion signal is of the form shown in Fig. 2.14c with a distance between the maximum and minimum equal to $2/T_2$.

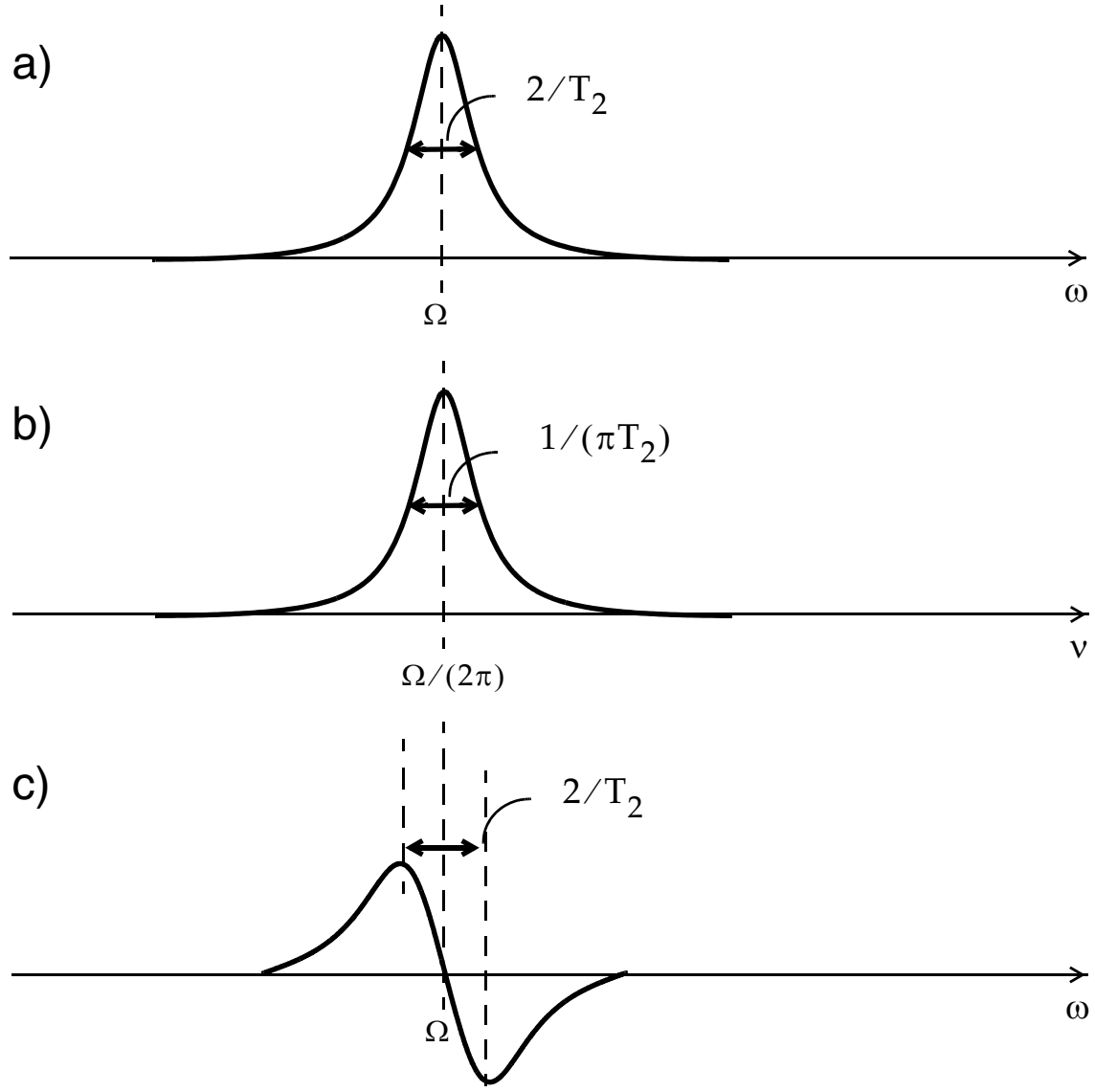

Figure 2.14: Lineshape of a Lorentzian Line
a) Absorptive part of a Lorentzian line in angular frequencies. b) Absorptive part of the Lorentzian in line with a frequency axis in Hertz. c) Dispersive part of a Lorentzian line.

The measurement of the absorption signal is more advantageous, because it decays, in the wings, with $1/(\Omega - \omega)^2$ while the dispersion signal decays only linearly with $1/(\Omega - \omega)$. Therefore, the resolution in an absorption spectrum containing several lines is better.

2.7 Continuous-Wave Spectroscopy: Steady-State Solutions

In continuous-wave (cw) spectroscopy we irradiate the spin system with a constant B_1 field and not with pulses as in Fourier spectroscopy which we discussed in the previous Chapters. The rf frequency or the static magnetic field are slowly changed in the course of the experiment and the steady-state response of the signal is measured as a function of field or frequency. Continuous-wave spectroscopy is nowadays mostly used in EPR spectroscopy and very rarely in NMR spectroscopy.

The spin system is irradiated at a frequency ω_{rf} with a constant radio-frequency field along the x direction. This leads to a magnetic-field vector in the rotating frame given by:

$$\vec{B}_{eff}^{r} = (B_1, 0, \Delta B_0) \ . \qquad [2.41]$$

We reach a steady-state of the system after the initial transient response of the system is damped out by the relaxation processes. The steady-state solution of the Bloch equations (Eq. [2.15]) is given by

$$\frac{d}{dt}\vec{M}^{r} = 0 = \gamma\left(\vec{M}^{r} \times \vec{B}_{eff}^{r}\right) - \Re\left\{\vec{M}^{r} - \vec{M}_0\right\} \qquad [2.42]$$

and leads to the three equations:

$$
\begin{aligned}
0 &= \gamma \Delta B_0 M_y^r - \frac{M_x^r}{T_2} \\
0 &= -\gamma \Delta B_0 M_x^r + \gamma B_1 M_z^r - \frac{M_y^r}{T_2} \\
0 &= -\gamma B_1 M_y^r - \frac{(M_z^r - M_0)}{T_1}
\end{aligned}
\qquad [2.43]
$$

with the solution:

$$
\begin{aligned}
M_x^r &= \gamma B_1 M_0 \frac{\gamma \Delta B_0}{(1 + (\gamma B_1)^2 T_1 T_2)/T_2^2 + (\gamma \Delta B_0)^2} \\
M_y^r &= \gamma B_1 M_0 \frac{1/T_2}{(1 + (\gamma B_1)^2 T_1 T_2)/T_2^2 + (\gamma \Delta B_0)^2} \\
M_z^r &= M_0 \frac{1/T_2^2 + (\gamma \Delta B_0)^2}{(1 + (\gamma B_1)^2 T_1 T_2)/T_2^2 + (\gamma \Delta B_0)^2}
\end{aligned}
\quad . \qquad [2.44]
$$

2.7.1 Weak rf Irradiation

If the cw irradiation is weak in the sense that

$$
S = (\gamma B_1)^2 T_1 T_2 \ll 1 \qquad [2.45]
$$

we can simplify the solution for the steady state and obtain

$$
\begin{aligned}
M_x^r &= \gamma B_1 M_0 \frac{\gamma \Delta B_0}{(1/T_2)^2 + (\gamma \Delta B_0)^2} \\
M_y^r &= \gamma B_1 M_0 \frac{1/T_2}{(1/T_2)^2 + (\gamma \Delta B_0)^2} \\
M_z^r &= M_0
\end{aligned}
\quad . \qquad [2.46]
$$

In this case, we have a linear system with respect to the rf-field amplitude γB_1 and the transverse components are given by a Lorentzian line (Eq. [2.40]) where M_x^r is the dispersive part and M_y^r is the absorptive part of the line. In this approximation the longitudinal component is the equilibrium magnetization.

The integral over the absorption line

$$I = \int_{-\infty}^{\infty} M_y^r(\Delta B_0)d\Delta B_0 = (\gamma B_1 M_0)\int_{-\infty}^{\infty} \frac{1/T_2}{(1/T_2)^2 + (\gamma\Delta B_0)^2}d\Delta B_0 = B_1 M_0 \pi \qquad [2.47]$$

is independent of the relaxation times T_1 and T_2 and proportional to the equilibrium magnetization M_0. Therefore, the integral of the absorption signal is in the limit of weak rf fields a measure for the number of spins.

2.7.2 Strong rf Irradiation: Saturation Effects

If the cw irradiation is not in the weak field limit of Eq. [2.45] then we obtain a broadened Lorentzian line. Setting the line width to

$$\frac{1}{T_2'} = \sqrt{1+S}\frac{1}{T_2} = \sqrt{1+(\gamma B_1)^2 T_1 T_2}\frac{1}{T_2} \qquad [2.48]$$

we obtain the solution

$$\begin{aligned} M_x^r &= \gamma B_1 M_0 \frac{\gamma\Delta B_0}{(1/T_2')^2 + (\gamma\Delta B_0)^2} \\ M_y^r &= \frac{\gamma B_1 M_0}{\sqrt{1+S}} \frac{1/T_2'}{(1/T_2')^2 + (\gamma\Delta B_0)^2} \\ M_z^r &= M_0 \frac{(1/T_2)^2 + (\gamma\Delta B_0)^2}{(1/T_2')^2 + (\gamma\Delta B_0)^2} \end{aligned} \qquad [2.49]$$

where the absorption part (M_y^r) of the Lorentzian line is scaled by $1/(\sqrt{1+S})$.

The maximum intensity of the absorption line at $\Delta B_0 = 0$ is given by

$$M_y^r(\Delta B_0 = 0) = \frac{\gamma B_1 M_0 T_2}{1+S} \qquad [2.50]$$

which reaches a maximum for $S = 1$ or $\gamma B_1 = 1/\sqrt{T_1 T_2}$ leading to a maximum absorption signal intensity of

$$M_y^r(\Delta B_0 = 0) = \frac{1}{2} M_0 \sqrt{\frac{T_2}{T_1}} \,. \qquad [2.51]$$

The dependence of the peak intensity on the rf-field amplitude γB_1 is shown in Fig. 2.15a.

The maximum of the dispersive part of the signal $M_x^r(\max)$ at $\gamma \Delta B_0 = \pm 1/T_2'$ behaves differently under saturation and reaches asymptotically a value of

$$\lim_{\gamma B_1 \to \infty} (M_x^r(\max)) = \frac{1}{2} M_0 \sqrt{\frac{T_2}{T_1}} \qquad [2.52]$$

as shown in Fig. 2.15b.

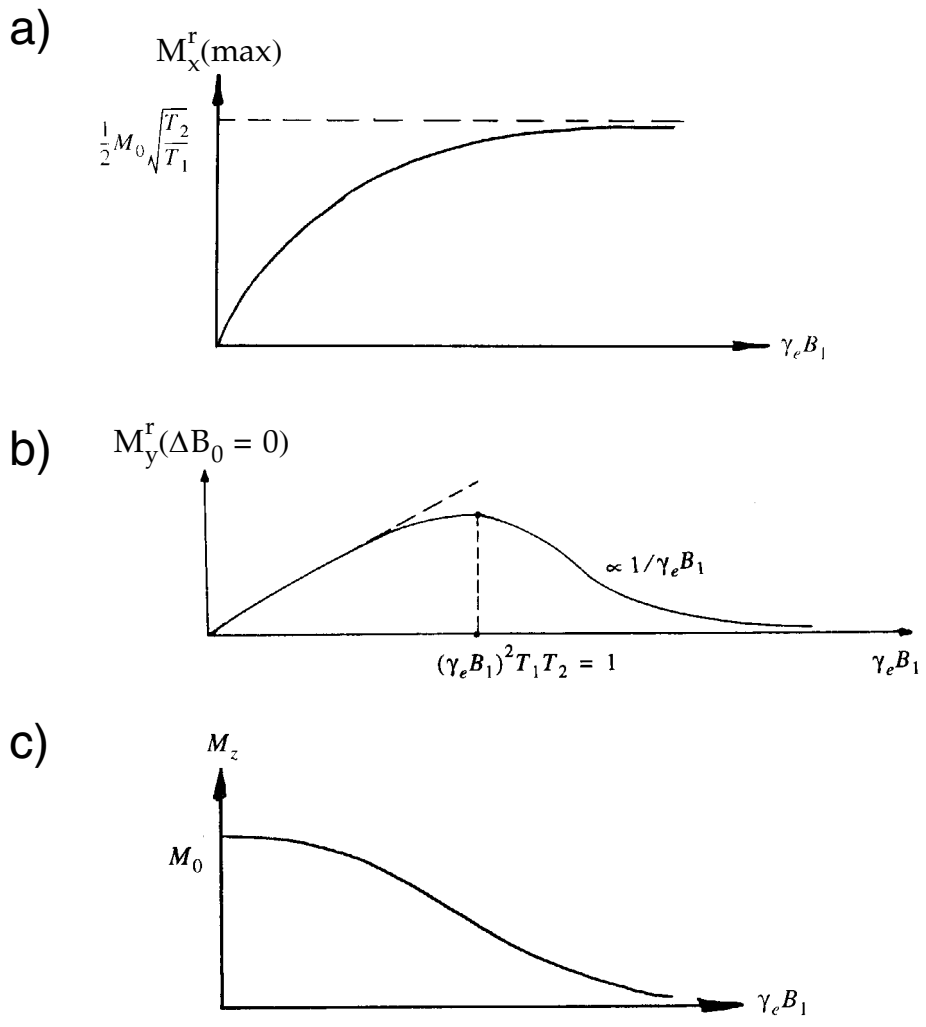

Figure 2.15: Saturation Behavior Under CW Irradiation

The longitudinal component is given by

$$M_z^r(\Delta B_0 = 0) = \frac{M_0}{(1+S)} = \frac{M_0}{1+(\gamma B_1)^2 T_1 T_2} \qquad [2.53]$$

goes also towards zero for large rf-field amplitudes γB_1 as shown in Fig. 2.15c.

2.8 Pulse Trickery Part I

2.8.1 Spin Echoes

After a 90° Pulse, the magnetization in the x-y plane (the NMR signal) for an ensemble of spins decays due to several mechanisms:

- T_2 Relaxation
- Dephasing of the individual signal due to an inhomogeneous applied external magnetic field $B_0 = B_0(\vec{r})$.
- Dephasing due to a distribution of chemical shifts. If there is only a small number of chemical shifts, the absolute value total magnetization $|s_{tot}(t)| = \left|\sum_i s_i(t)\right|$ will increase and decrease do to the constructive and destructive interference of the two signal oscillating at different rotating-frame frequencies. For a distribution of chemical shifts (for example in an inhomogeneous material like a polymer), the signal will decay monotonously and not recover: $|s_{tot}(t_1)| > |s_{tot}(t_2)|$ for $t_1 < t_2$.

The last two mechanisms can be "un-done" by a 180° refocusing pulse (Fig. 2.16): At time $t = \tau$, the full signal is restored $\vec{s}(\tau) = \vec{s}(0)$ if we neglect true relaxation ($T_2 \to \infty$). This is called a *spin echo*. The effect was first observed (for a slightly different pulse sequence, namely 90^0-τ-90^0) by Erwin Hahn[1], and is also known as the *Hahn echo*.

[1] E.L Hahn, Phys.Rev. **80**, 580 (1950).

2.8.2 Composite Pulses

In the preceding chapter, we have assumed that we are able to apply rf pulses with well-defined rotation axis and flip angles. In a real experimental setup, the rf-field strength B_1 is always inhomogeneous ($B_1 = B_1(\vec{r})$) and we will not be able to obtain a well-defined flip angle for all nuclei in the sample. In addition, experimentally we might not set the pulse length to the correct values. These errors of a few degrees only in a good experiment can sometimes be avoided by adiabatic methods (see Chapter 2.4.4). Alternatively, we may use *composite pulses* instead of a single pulse. For example, we can replace a $(\pi)_x$ pulse by a composite pulse $(\pi/2)_x(\pi)_y(\pi/2)_x$. For exact pulses, the two lead obviously to the same result, namely an inversion of the magnetization. If all pulses are too short (or too long) by a certain percentage, the composite pulse will lead to a resulting magnetization that is closer to an inversion than the single pulse.

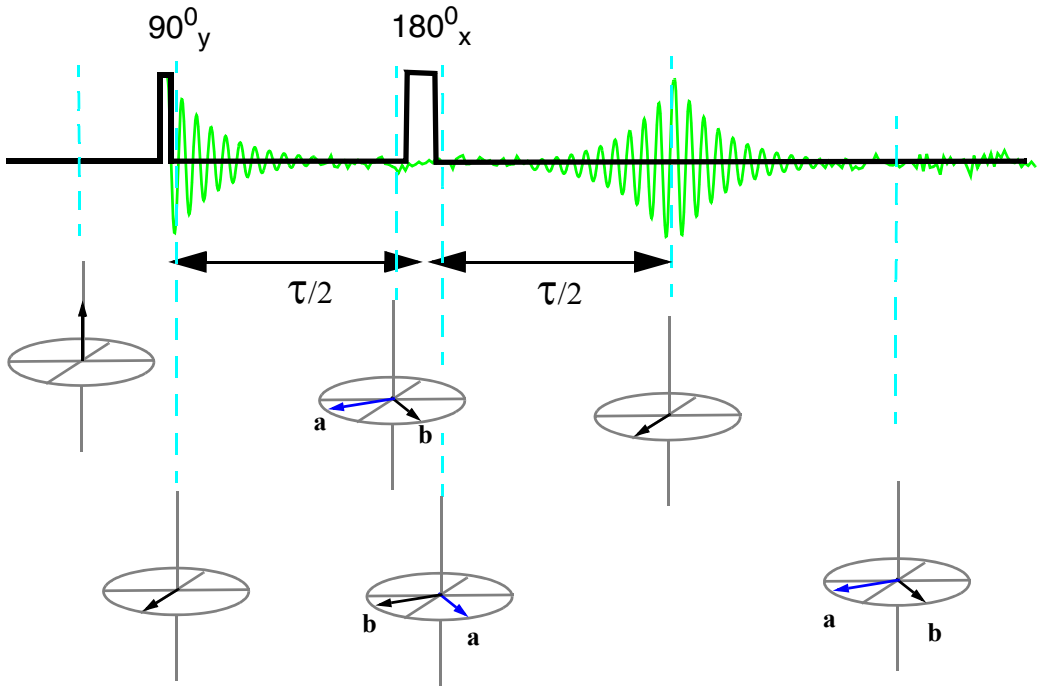

Figure 2.16: Spin Echo

2.9 Relaxation Measurements

2.9.1 Longitudinal Relaxation

One way to measure the longitudinal relaxation time T_1 is the inversion-recovery experiment. The time evolution of the (undetectable) z-component of the magnetization is indirectly monitored by measuring $M_x^r(t=0)$ for a whole series of values τ. $M_z(\tau)$ is initially inverted and returns to the equilibrium position with the exponential law:

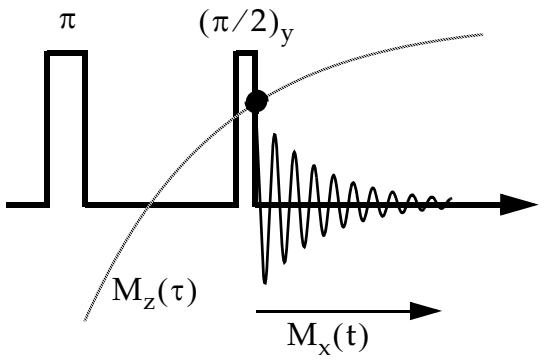

Figure 2.18: Inversion-Recovery Pulse Sequence

$$M_z(\tau) = M_x^r(t=0;\tau) = M_0(1-2e^{-\tau/T_1}) \qquad [2.54]$$

Instead of measuring only one point in the FID, it is (experimentally) more accurate to measure the entire (complex) FID for each value of τ: $s(t;\tau)$. According to

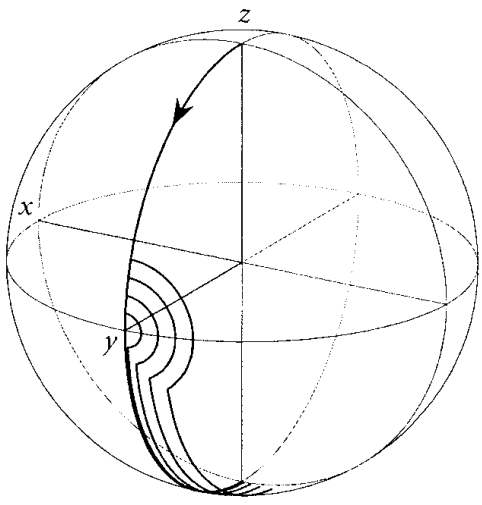

Family of magnetization trajectories for the composite $(\pi/2)_x$ $(\pi)_y$ $(\pi/2)_x$ pulse with pulse lengths 80%, 85%, 90%, 95% and 100% of the nominal value. The shortfall of the first pulse is compensated by an equal shortfall of the third pulse through the action of the $(\pi)_y$ pulse.

Figure 2.17: Composite Pulse

the basic theorems of the Fourier transform (see lecture PC VI), the integral over the resonance line $\int_{-\infty}^{\infty} A(\omega)d\omega$ is equal to the desired value $M_x(t=0)$. This procedure also allows us to separately determine the T_1 times of different resonance lines if the lines are separated in the spectrum.

As an example for the information content of the T_1 relaxation time, a few empirical rules for ^{13}C relaxation are given here. ^{13}C nuclei are usually relaxed by the interaction with close-by protons:

- T_1 is proportional to the 6'th power of the distance to the nearest protons.
- T_1 is inversely proportional to the number of nearest protons.
- T_1 depends on the correlation time τ_c of the random process that modulates the ^{13}C-^{1}H magnetic interaction, in liquids usually the (inverse) molecular tumbling rate.

2.9.2 Transverse Relaxation

According to the Bloch equations, the decay of the transverse magnetization can be used to determine T_2. However, as mentioned in Chapter 2.8.1, there are other effects (e.g. magnetic field inhomogeneities) that lead to a decay of the FID. The apparent decay is often also exponential and can, phenomenologically be described by an effective relaxation time T_2^*. Obviously $T_2^* \leq T_2$ must always be true.

To determine T_2, we can use the echo experiment of Fig. 2.16 and measure the echo amplitude as a function of τ. Like for the T_1 experiment, this requires one experiment per τ value to be performed. We can also extend the experiment of Fig. 2.16 and produce a multiple echo train ("Carr-Purcell pulse train") which allows us to determine T_2 in a single experiment where all echo-maxima are sampled.

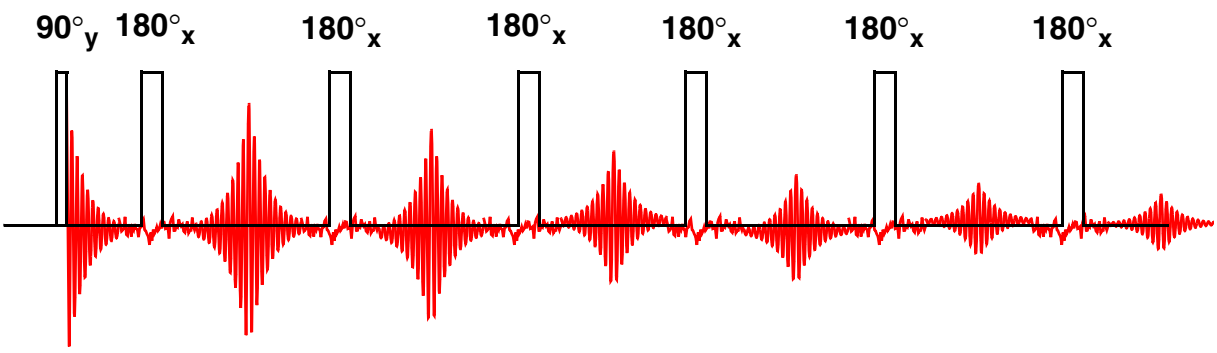

Figure 2.19: Carr-Purcell Sequence

3 Chemical-Exchange Phenomena

NMR can detect and characterize dynamic processes, e.g. chemical reactions or conformational changes, in a number of time regimes (Fig. 3.1a). It is a particular property of NMR spectroscopy that dynamic chemical equilibria can be characterized. There is no need to first create a non-equilibrium state.

In this chapter, we will use a simple two-site exchange model (Fig. 3.1b) to discuss the basic properties.

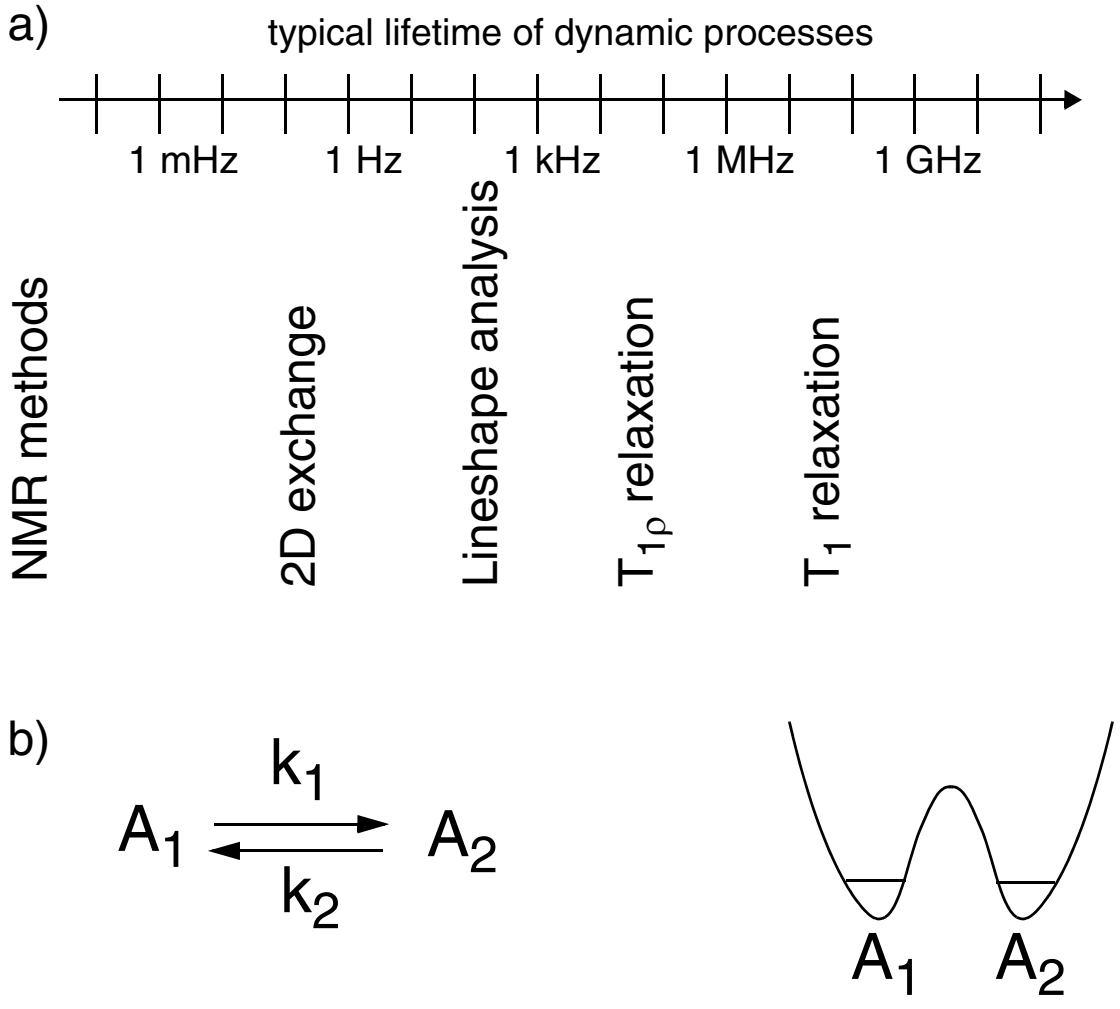

Figure 3.1: Chemical Exchange
a) Time scales and methods. b) Simple two-site exchange model.

3.1 The McConnell Equations

In the absence of exchange, the Bloch equations (we will use the rotating-frame version but leave away the superscripts r) are valid for each of the sites separately (see Eq. [2.15]):

$$\frac{d}{dt}\overrightarrow{M_1} = \gamma\left(\overrightarrow{M_1} \times \vec{B}_{eff,\,1}\right) - \Re_1\left\{\overrightarrow{M_1} - \overrightarrow{M}_{0,\,1}\right\}$$
$$\frac{d}{dt}\overrightarrow{M_2} = \gamma\left(\overrightarrow{M_2} \times \vec{B}_{eff,\,2}\right) - \Re_2\left\{\overrightarrow{M_2} - \overrightarrow{M}_{0,\,2}\right\} \qquad [3.1]$$

We assume now the presence of a molecular exchange mechanism of first order that interchanges the chemical species A_1 and A_2. The reaction is assumed to be so fast that the magnetization of the nuclei does not change during the conversion. Each component of the magnetization of species 1 changes not only due to the precession, but there is an additional influx of magnetization from species 2 and a loss of magnetization to species 2:

$$\left(\frac{d}{dt}\overrightarrow{M_1}\right)_{exchange} = k_2\overrightarrow{M_2} - k_1\overrightarrow{M_1} \qquad [3.2]$$

and

$$\left(\frac{d}{dt}\overrightarrow{M_2}\right)_{exchange} = k_1\overrightarrow{M_1} - k_2\overrightarrow{M_2} \qquad [3.3]$$

The combination of these two equations with the Bloch equations (eq. [3.1]) leads to the ***McConnell Equations:***

$$\frac{d}{dt}\overrightarrow{M_1} = \gamma\left(\overrightarrow{M_1} \times \vec{B}_{eff,\,1}\right) - R_1\left\{\overrightarrow{M_1} - \overrightarrow{M}_{0,\,1}\right\} + k_2\overrightarrow{M_2} - k_1\overrightarrow{M_1}$$
$$\frac{d}{dt}\overrightarrow{M_2} = \gamma\left(\overrightarrow{M_2} \times \vec{B}_{eff,\,2}\right) - R_2\left\{\overrightarrow{M_2} - \overrightarrow{M}_{0,\,2}\right\} + k_1\overrightarrow{M_1} - k_2\overrightarrow{M_2} \qquad [3.4]$$

This is a set of six coupled differential equations. In the absence of rf irradiation, the set can be split into a set of 4 coupled equations for the transverse components and a set of 2 coupled equations for the longitudinal components.

3.2 Line-Shape Analysis

The four coupled equations for the transverse components of the magnetization are given by:

$$\begin{aligned}
\frac{d}{dt}M_{1x} &= -\Omega_1 M_{1y} - \frac{1}{T_2^{(1)}}M_{1x} + k_2 M_{2x} - k_1 M_{1x} \\
\frac{d}{dt}M_{1y} &= \Omega_1 M_{1x} - \frac{1}{T_2^{(1)}}M_{1y} + k_2 M_{2y} - k_1 M_{1y} \\
\frac{d}{dt}M_{2x} &= -\Omega_2 M_{2y} - \frac{1}{T_2^{(2)}}M_{2x} + k_1 M_{1x} - k_2 M_{2x} \\
\frac{d}{dt}M_{2y} &= \Omega_2 M_{2x} - \frac{1}{T_2^{(2)}}M_{2y} + k_1 M_{1y} - k_2 M_{2y}
\end{aligned} \qquad [3.5]$$

Using the complex magnetization $G = M_x + iM_y$ introduced in Eq. [2.34], we can simplify the system of four equations to two coupled equations for the complex magnetization:

$$\begin{aligned}
\frac{d}{dt}G_1 &= i\Omega_1 G_1 - \frac{1}{T_2^{(1)}}G_1 + k_2 G_2 - k_1 G_1 \\
\frac{d}{dt}G_2 &= i\Omega_2 G_2 - \frac{1}{T_2^{(2)}}G_2 + k_1 G_1 - k_2 G_2
\end{aligned} \qquad [3.6]$$

or in vector form:

$$\frac{d}{dt}\vec{G} = \underset{\sim}{S}\vec{G} \qquad [3.7]$$

with

$$\vec{G} = \begin{pmatrix} G_1 \\ G_2 \end{pmatrix}, \qquad \underset{\sim}{S} = i\underset{\sim}{\Omega} + \underset{\sim}{R} + \underset{\sim}{K},$$

$$\underset{\sim}{\Omega} = \begin{bmatrix} \Omega_1 & 0 \\ 0 & \Omega_2 \end{bmatrix}, \qquad \underset{\sim}{R} = -\begin{bmatrix} \frac{1}{T_2^{(1)}} & 0 \\ 0 & \frac{1}{T_2^{(2)}} \end{bmatrix}, \qquad \underset{\sim}{K} = \begin{bmatrix} -k_1 & k_2 \\ k_1 & -k_2 \end{bmatrix} \qquad [3.8]$$

$\underset{\sim}{S}$ is called the spectral matrix. It contains all the information about the spin system. $\underset{\sim}{R}$ is the relaxation matrix and $\underset{\sim}{K}$ the usual kinetic matrix.

The formal solution of [3.7] is given by

$$\vec{G}(t) = e^{\underset{\sim}{S}t}\left(\vec{G}(0)\right) \qquad [3.9]$$

and the observed NMR signal, s(t), is just given by the sum of the two components, $s(t) = G_1(t) + G_2(t)$, or in vector notation as the product of the unity vector $\vec{e} = (1, 1)$ with $\vec{G}(t)$:

$$s(t) = \vec{e} \cdot \vec{G}(t) \qquad [3.10]$$

In [3.9] we are faced with the problem to calculate the exponent of a matrix, e^M. For diagonal matrixes, it can easily be shown that:

$$\exp\begin{bmatrix} \Lambda_{11} & 0 & 0 \\ 0 & \Lambda_{22} & 0 \\ 0 & 0 & .... \end{bmatrix} = \begin{bmatrix} e^{\Lambda_{11}} & 0 & 0 \\ 0 & e^{\Lambda_{22}} & 0 \\ 0 & 0 & .... \end{bmatrix} \qquad [3.11]$$

Using the rule:

$$e^M = T^{-1} e^{TMT^{-1}} T \qquad [3.12]$$

where T is chosen such that $TMT^{-1} = \Lambda$ is diagonal, we can, therefore, easily calculate e^M numerically. Analytical solutions are only possible if the eigenvalues and the eigenvectors of $\underset{\sim}{M}$, which are identical to the diagonal elements of $\underset{\sim}{\Lambda}$, can be evaluated.

For the symmetric exchange: $k_1 = k_2 = k$, and in the absence of relaxation the eigenvalues of the matrix $\underset{\sim}{S}$ are given by:

$$\Lambda_{1,2} = \frac{i}{2}(\Omega_1 + \Omega_2) - k \mp \sqrt{k^2 - \frac{1}{4}(\Omega_1 - \Omega_2)^2} \qquad [3.13]$$

and the signal function $s(t) = \vec{e} \cdot \vec{G}(t)$ is of the form

$$s(t) = \left(1 - \frac{k}{\sqrt{k^2 - \frac{1}{4}(\Omega_1 - \Omega_2)^2}}\right) e^{\Lambda_1 t} + \left(1 + \frac{k}{\sqrt{k^2 - \frac{1}{4}(\Omega_1 - \Omega_2)^2}}\right) e^{\Lambda_2 t} \qquad [3.14]$$

The solutions given in Eqs. [3.13] and [3.14] can easily be obtained using a computer-algebra program like Mathematica or of course, by manual determination of the eigenvalues and eigenvectors of the (complex) 2x2 matrix. The initial magnetization $\vec{G}(0)$ is assumed to be along the x-axis and the two lines have the same intensity $\vec{G}(0) = (1, 1)$.

We see from [3.14] that the spectrum consists of two lines with intensities $c_1 = 1 - k/\sqrt{k^2 - \frac{1}{4}(\Omega_1 - \Omega_2)^2}$ and $c_2 = 1 + k/\sqrt{k^2 - \frac{1}{4}(\Omega_1 - \Omega_2)^2}$ and frequencies Λ_1 and Λ_2, respectively.

The specification of $\vec{c}$ and $\vec{\Lambda}$ is a very compact way to describe the spectrum and it can easily be expanded to more than two resonance lines in the spectrum. For n lines, the length of the two vectors will simply become n. The FID is always described by:

$$s(t) = \vec{c} \cdot \exp\left(\vec{\Lambda} \cdot t\right). \qquad [3.15]$$

Here the exponential of the vector is taken element-wise and the dot denotes the usual scalar product of two vectors. It should be noted that c_i and Λ_i are both complex numbers.

Because of the identity $e^{\Lambda_i t} = e^{iIm\{\Lambda_i\}t} e^{Re\{\Lambda_i\}t}$, the imaginary part of the Eigenvalues $Im\{\Lambda_i\}$ characterizes the frequency of the Lorentzian resonance line while the real part describes the linewidth: $-Re\{\Lambda_i\} = 1/T_2^{(i)}$.

Because the intensity c_i is complex, the resonance has not only an absorption component (of intensity $\mathrm{Re}\{c_i\}$) but also a dispersion component of intensity $-\mathrm{Im}\{c_i\}$ (Fig. 3.2).

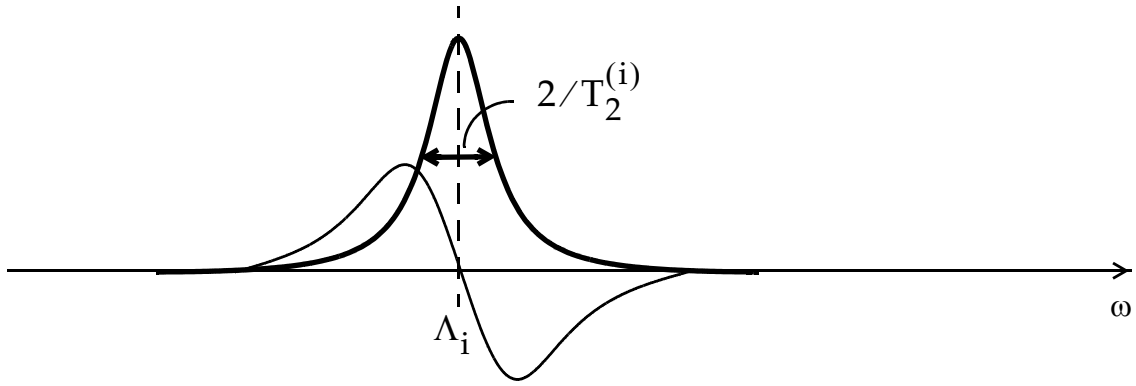

Figure 3.2: Lorentzian Line

The real and imaginary part of the two eigenvalues $\Lambda_{1,2}$ as given in Eq. [3.13] are plotted in Fig. 3.3 as a function of the ratio $r = k/(\Omega_1 - \Omega_2)$. For $r < 1/2$, there are two different imaginary parts and, therefore, two resonance lines centered at different frequencies. The linewidth, i.e., the negative of the real part of $\Lambda_{1,2}$ is identical for both resonances and increases with increasing k. For $r > 1/2$, the imaginary parts become degenerate but there are still two individual components of the line. The two components differ now in linewidth but they are centered at the same resonance frequency.

The intensities of the two lines (see Eq. [3.14]) are plotted in Fig. 3.4. For $r < 1/2$, the absorption component (the integral of the absorption part) stays constant,

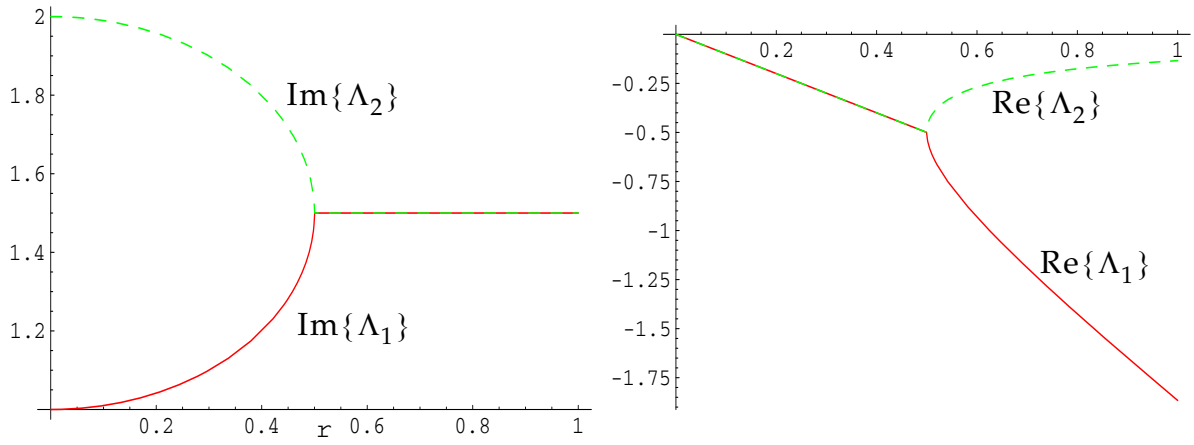

Figure 3.3: Eigenvalues for a Two-Site Exchange Model

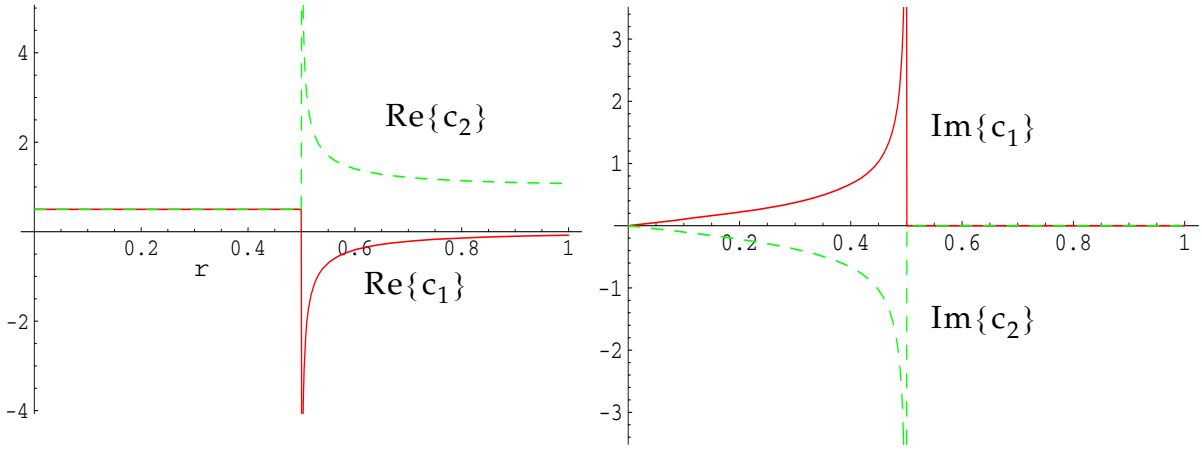

Figure 3.4: Intensities for a Two-Site Exchange Model

while two dispersive parts with opposite sign develop for $r > 0$. For $r > 1/2$, the dispersive parts vanish altogether. The intensity of the narrower line approaches (for $r \to \infty$ the sum of the two lines at $r = 0$, while the intensity of the broad component vanishes at larger r values. The total lineshape with its four components at $r = 0.3$ is given in Fig. 3.5.

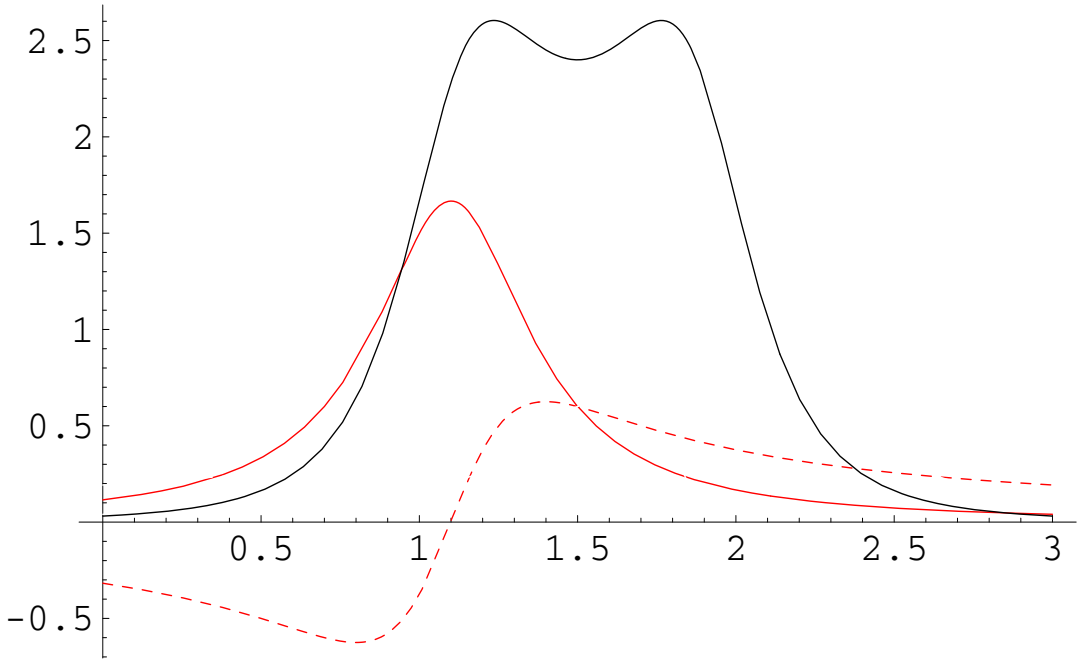

Figure 3.5: Lineshape For an Exchange Problem With r = 0.3
Lineshape for an exchanging two-spin system (r=0.3). For one of the two resonances, the absorption part (solid line) and the dispersion part (dashed line) are displayed. The individual contribution from the other resonance are the mirror image of the components given.

The total lineshape of the symmetric two-site exchange as a function of r is given in Fig. 3.6. For $r < 0.25$ two separated lines appear. At $r = 0$, they are of course centered at their original resonance frequencies Ω_1 and Ω_2. With increasing r (increasing k or increasing temperature), they broaden and move closer together. At coalescence

$$r_{coaleszence} = \frac{1}{2\sqrt{2}} \approx 0.35 \qquad [3.16]$$

the two lines merge into a single signal. Note, that there are still two different eigenfrequencies involved and the line is composed of two Lorentzian components centered at different frequencies. Due to the linewidth they do, however, merge into one signal. With increasing temperature, the signal sharpens up and at $r \gg 1$, a single sharp signal emerges.

The resulting spectra for an asymmetric two-site exchange $k_1 \neq k_2$ are shown in Fig. 3.7.

3.2.1 The Limit of Slow Exchange

In the limit of slow exchange $k \ll |\Omega_1 - \Omega_2|$, the intensity vector $\vec{c}$ and the spectral vector simplify to

$$\begin{aligned} \vec{c} &= (1, 1) \\ \vec{\Lambda} &= (i\Omega_2 - k, i\Omega_1 - k) \end{aligned} \qquad [3.17]$$

The spectrum consists in this limit of two well-separated absorptive Lorentzian lines. The exchange rate k is encoded in the linewidth as shown in Fig. 3.8 with the full width at half height equal to $2k$. The natural line width due to relaxation processes gives a lower limit for the rate constant of the exchange processes that can be measured with this experiment.

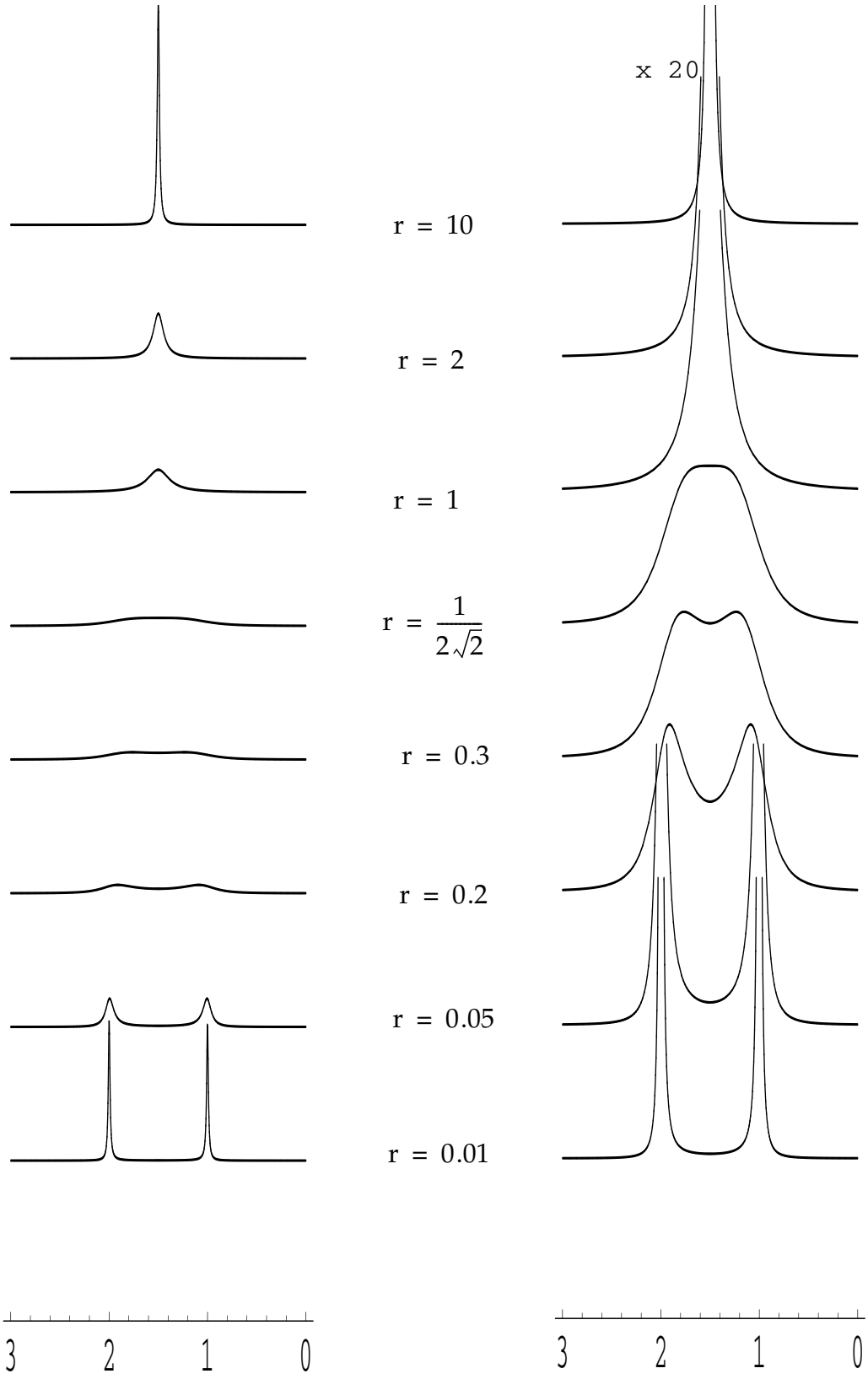

Figure 3.6: Chemical-Exchange Lineshapes
for a symmetric two-site exchange problem as a function of the normalized rate constant r.

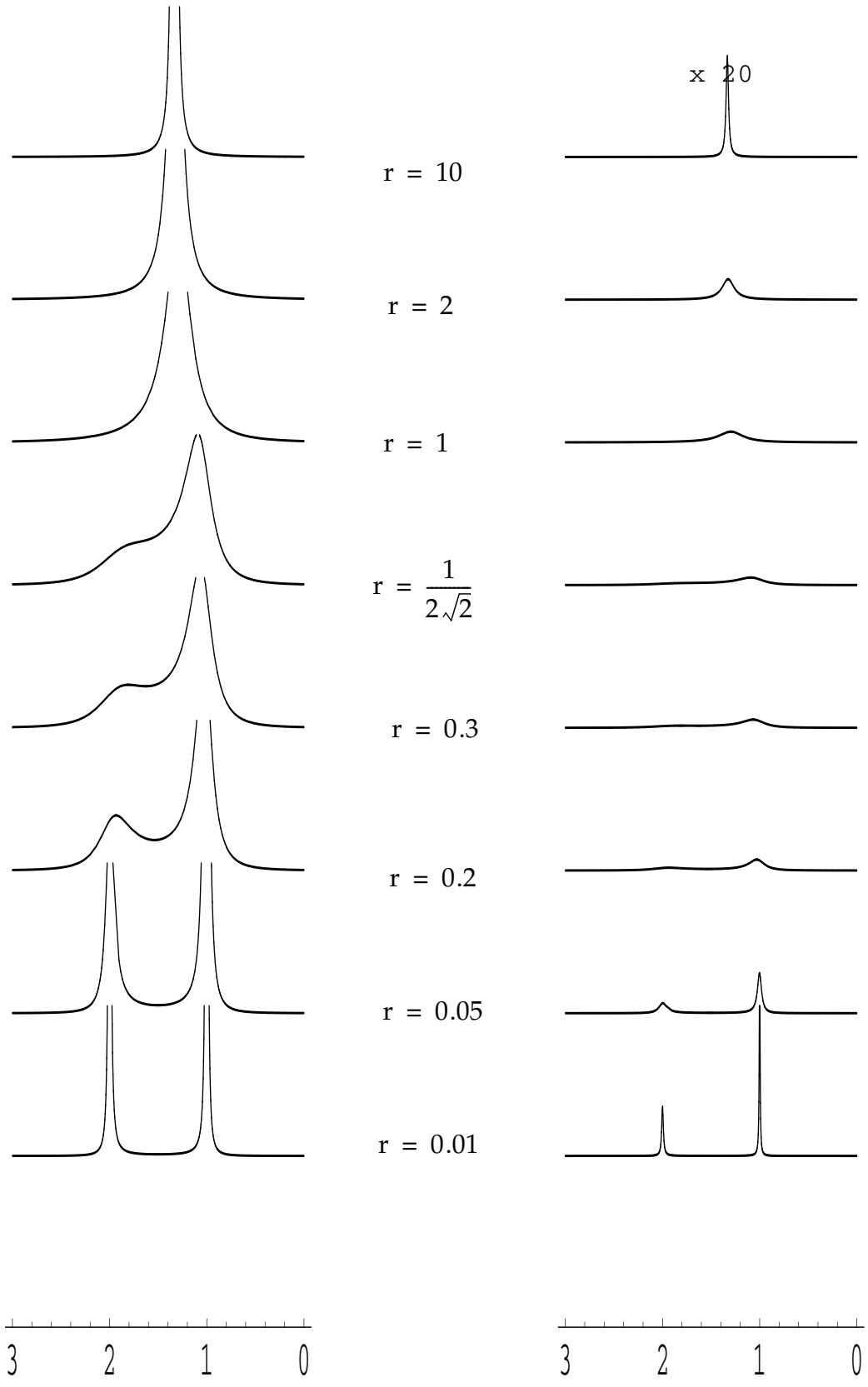

Figure 3.7: Chemical-Exchange Lineshapes
for an asymmetric two-site exchange (K=3) as a function of the normalized rate constant r.

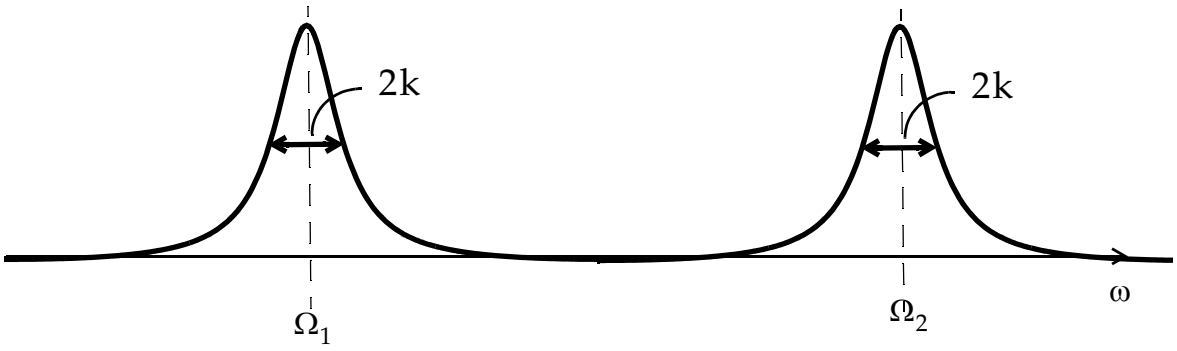

Figure 3.8: Slow Exchange
The line width is a measure for the rate constant of the exchange process.

3.2.2 The Limit of Fast Exchange

For $k \gg |\Omega_1 - \Omega_2|$, the eigenvalues can be simplified in the following way:

$$\begin{aligned}
\Lambda_{1,2} &= \frac{i}{2}(\Omega_1 + \Omega_2) - k \mp \sqrt{k^2 - \frac{1}{4}(\Omega_1 - \Omega_2)^2} \\
&\approx \frac{i}{2}(\Omega_1 + \Omega_2) - k \mp k\left[1 - \frac{(\Omega_1 - \Omega_2)^2}{8k^2}\right] \\
\Lambda_1 &= i\frac{(\Omega_1 + \Omega_2)}{2} - 2k + \frac{(\Omega_1 - \Omega_2)^2}{8k} \\
\Lambda_2 &= i\frac{(\Omega_1 + \Omega_2)}{2} - \frac{(\Omega_1 - \Omega_2)^2}{8k}
\end{aligned} \qquad [3.18]$$

and the intensity vector becomes:

$$c_1 = 0 \qquad c_2 = 2 \qquad [3.19]$$

The spectrum consists of a single line at the mean position $\bar{\Omega} = (\Omega_1 + \Omega_2)/2$ with a linewidth (FWHH) of $(\Omega_1 - \Omega_2)^2/(4k)$ as plotted in Fig. 3.9.

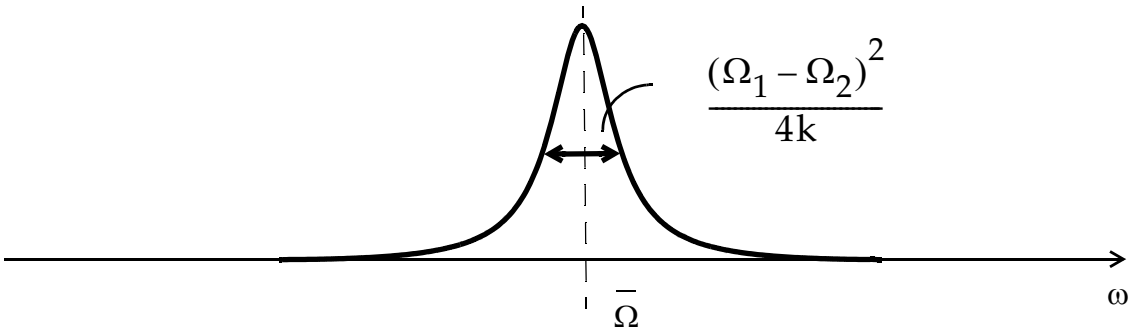

Figure 3.9: Fast Exchange
The line width is a measure for the rate constant of the exchange process.

3.3 2D Exchange Spectroscopy

The line-shape methods are, for the detection of slow processes, limited to cases where the exchange broadening exceeds the natural linewidth $1/T_2$. In this chapter, we will discuss methods that work with longitudinal magnetization components instead of transverse magnetization as in the case of the line-shape methods. With longitudinal magnetization, we are limited only by T_1 instead of T_2. Because T_1 can be much longer than T_2 (up to several orders of magnitude), this allows us to characterize processes that would be too slow to cause any visible line-shape effects. For simplicity, we restrict the discussion again to the symmetric two-site exchange. The longitudinal components of the magnetization follow the differential equations (see Eq. [3.4])

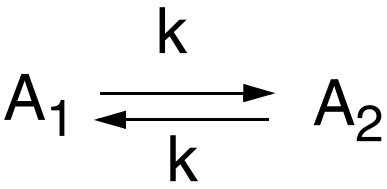

Figure 3.10: Two-Site Exchange

$$\frac{d}{dt}M_{1z} = -\frac{M_{1z} - M_{0,1}}{T_1^{(1)}} + k(M_{2z} - M_{1z})$$

$$\frac{d}{dt}M_{2z} = -\frac{M_{2z} - M_{0,2}}{T_1^{(2)}} + k(M_{1z} - M_{2z}) \qquad [3.20]$$

or, in the absence of relaxation

$$\frac{d}{dt}\begin{pmatrix} M_{1z} \\ M_{2z} \end{pmatrix} = \begin{pmatrix} -k & k \\ k & -k \end{pmatrix}\begin{pmatrix} M_{1z} \\ M_{2z} \end{pmatrix} . \qquad [3.21]$$

Instead of solving this matrix equation in a similar manner as for the transverse components, we can in this special case directly find the "eigenmodes" of the magnetization by a linear combination of M_{1z} and M_{2z}:

$$\frac{d}{dt}\begin{pmatrix} M_{1z} + M_{2z} \\ M_{1z} - M_{2z} \end{pmatrix} = \begin{pmatrix} 0 & 0 \\ 0 & -2k \end{pmatrix}\begin{pmatrix} M_{1z} + M_{2z} \\ M_{1z} - M_{2z} \end{pmatrix} . \qquad [3.22]$$

Equation [3.22] can easily be solved, because the matrix exponential is now trivial due to the diagonal K matrix:

$$\begin{pmatrix} M_{1z} + M_{2z} \\ M_{1z} - M_{2z} \end{pmatrix}(\tau) = \begin{pmatrix} 1 & 0 \\ 0 & e^{-2k\tau} \end{pmatrix}\begin{pmatrix} M_{1z} + M_{2z} \\ M_{1z} - M_{2z} \end{pmatrix}(0) . \qquad [3.23]$$

The sum magnetization stays constant while the difference magnetization decays exponentially with a time constant of $\tau_c = 1/(2k)$. To obtain the time-evolution of M_{1z} and M_{2z}, we can write:

$$\begin{aligned} M_{1z}(\tau) &= \frac{1}{2}[M_{1z} + M_{2z}](0) + \frac{1}{2}[M_{1z} - M_{2z}](0)e^{-2k\tau} \\ M_{2z}(\tau) &= \frac{1}{2}[M_{1z} + M_{2z}](0) - \frac{1}{2}[M_{1z} - M_{2z}](0)e^{-2k\tau} \end{aligned} \qquad [3.24]$$

To measure k, we must prepare the spin system in a non-equilibrium state $[M_{1z} - M_{2z}](0) \neq 0$. The large magnetization difference is obtained after a selective π pulse on one of the two resonances. As in the T_1-relaxation experiments, the magnetization-difference at time τ is measured with a $\frac{\pi}{2}$ readout pulse applied at time τ, just before detection as shown in Fig. 3.11.For more than two exchanging spins, a series of experiments with different selective inversion at the beginning must be performed.

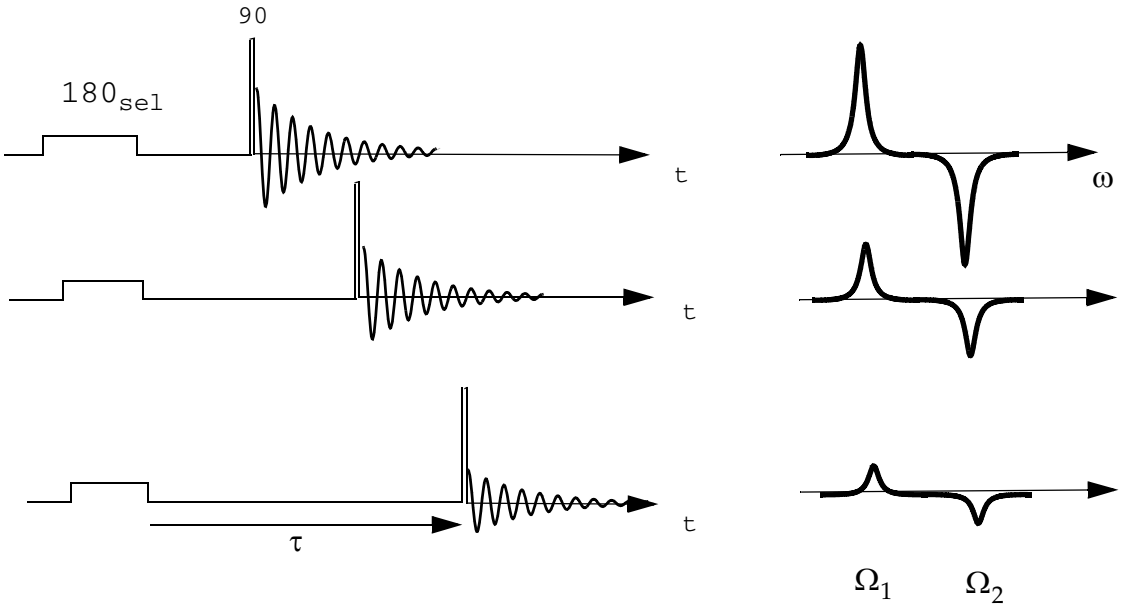

Figure 3.11: 1D Longitudinal Exchange Experiment

Alternatively, it is also possible, to observe all exchange processes in a single, ***two-dimensional experiment***. In this experiment, we replace the selective π pulse by a pair of nonselective $\pi/2$ pulses with a separation of t_1. This leads to the pulse scheme shown in Fig. 3.12.

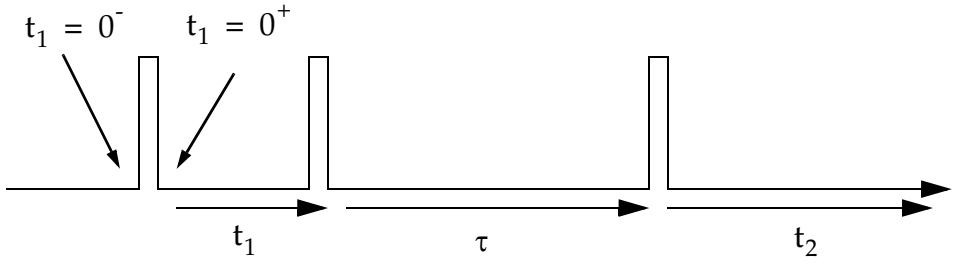

Figure 3.12: 2D Longitudinal Exchange Experiment

We assume that t_1 and t_2 are short enough, such that the exchange process can be neglected during these periods. Then, we obtain

$$\begin{aligned}\overrightarrow{M_1}(t_1=0^-) &= M_0\overrightarrow{e_z}\\ \overrightarrow{M_1}(t_1=0^+) &= M_0\overrightarrow{e_x}\\ \overrightarrow{M_1}(t_1,\tau=0^-) &= M_0(\cos(\Omega_1 t_1)\overrightarrow{e_x} + \sin(\Omega_1 t_1)\overrightarrow{e_y})\end{aligned} \qquad [3.25]$$

at the end of the t_1 period the x-component of the magnetization is flipped along -z by a 90 degree pulse:

$$\overrightarrow{M_1}(t_1, \tau=0^+) = -M_0(\cos(\Omega_1 t_1)\vec{e}_z - \sin(\Omega_1 t_1)\vec{e}_y) \qquad [3.26]$$

and analogously:

$$\overrightarrow{M_2}(t_1, \tau=0^+) = -M_0(\cos(\Omega_2 t_1)\vec{e}_z - \sin(\Omega_2 t_1)\vec{e}_y) \; . \qquad [3.27]$$

If we choose the mixing time τ to be longer than T_2 (or if we apply field-gradient pulses or phase-cycling schemes) the transverse magnetization component in Eqs. [3.26] and [3.27] decay (or are cancelled out) and we can assume that at the beginning of the mixing period the magnetization is along the z-direction and the size of the magnetization depends on the resonance frequencies during t_1:

$$\overrightarrow{M_1}(t_1, \tau=0^+) = -M_0\cos(\Omega_1 t_1)\vec{e}_z \qquad [3.28]$$

and analogously:

$$\overrightarrow{M_2}(t_1, \tau=0^+) = -M_0\cos(\Omega_2 t_1)\vec{e}_z \; . \qquad [3.29]$$

In the mixing time, the two magnetization components mix according to Eq. [3.24]. The resulting components $M_{1z}(t_1, \tau, t_2=0^-) = M_{1z}(t_1, \tau)$ and $M_{2z}(t, \tau)$ are rotated (by the third pulse) to the x-axis:

$$\overrightarrow{M_1}(t_1, \tau, t_2=0^+) = M_{1z}(t_1, \tau)\vec{e}_x \qquad [3.30]$$

and detected in the course of t_2. Here, we only detect the real part M_x:

$$s(t_1, \tau, t_2) = M_{1z}(t_1, \tau)\cos(\Omega_1 t_2) + M_{2z}(t_1, \tau)\cos(\Omega_2 t_2) \qquad [3.31]$$

By inserting the solution of Eq. [3.24] into [3.31] we obtain

$$\begin{aligned} s(t_1, \tau, t_2) = -M_0(&a_{11}(\tau)\cos(\Omega_1 t_1)\cos(\Omega_1 t_2) \\ &+ a_{22}(\tau)\cos(\Omega_2 t_1)\cos(\Omega_2 t_2) \\ &+ a_{12}(\tau)\cos(\Omega_1 t_1)\cos(\Omega_2 t_2) \\ &+ a_{21}(\tau)\cos(\Omega_2 t_1)\cos(\Omega_1 t_2)) \end{aligned} \qquad [3.32]$$

with

$$a_{11}(\tau) = a_{22}(\tau) = \frac{1 + e^{-2k\tau}}{2}$$
$$a_{12}(\tau) = a_{21}(\tau) = \frac{1 - e^{-2k\tau}}{2} \qquad [3.33]$$

The NMR signal $s(t_1, \tau, t_2)$ consists of four signals with (normalized) intensities a_{ij} and with frequencies Ω_i and Ω_j in the first and second time dimension of the experiment, respectively.

The Fourier transformation in two dimensions can proceed step wise: first we transfer with respect to the time variable t_2

$$s(t_1, \tau, \omega_2) = \int_0^\infty s(t_1, \tau, t_2) e^{-i\omega_2 t_2} dt_2 \qquad [3.34]$$

and then with respect to t_1:

$$S(\omega_1, \tau, \omega_2) = \int_0^\infty s(t_1, \tau, \omega_2) e^{-i\omega_1 t_1} dt_1 \qquad [3.35]$$

$S(\omega_1, \tau, \omega_2)$ is the two-dimensional frequency domain spectrum shown schematically in Figure 3.13.

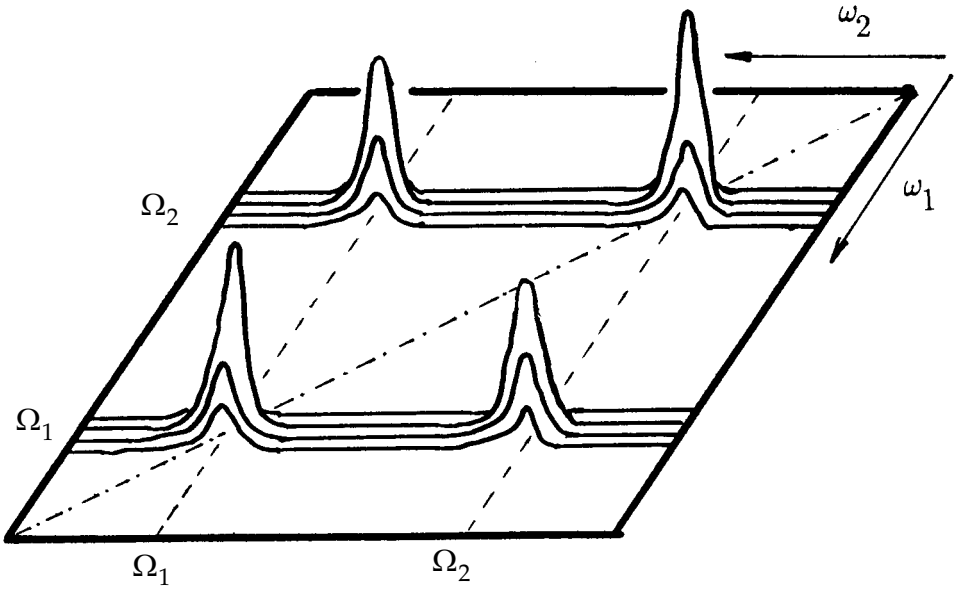

Figure 3.13: Two-Dimensional Exchange Spectrum

The diagonal peaks with intensity a_{11} and a_{22} represent magnetization located in the same chemical form in both time periods, a_{12} and a_{21} represent magnetization that has been transported between the two chemical forms by the chemical-exchange process during the mixing time τ.

The intensity of diagonal and cross peaks in the presence of a uniform relaxation with the same time constant T_1 for both sites is

$$a_{11}(\tau) = a_{22}(\tau) = \frac{1 + e^{-2k\tau}}{2} e^{-\tau/T_1}$$
$$a_{12}(\tau) = a_{21}(\tau) = \frac{1 - e^{-2k\tau}}{2} e^{-\tau/T_1} \qquad [3.36]$$

and the cross-peak intensity goes through a maximum (growth due to chemical exchange, decay due to relaxation). The time dependence of the peaks with and without relaxation is plotted in Fig. 3.14.

3.3.1 Examples of 2D Exchange Spectra (EXSY)

3.3.1.1 Exchange Between $SNCl_4$ and $SnBr_4$

In a 1:1 mixture of $SnCl_4$ and $SnBr_4$, the following chemical processes take place:

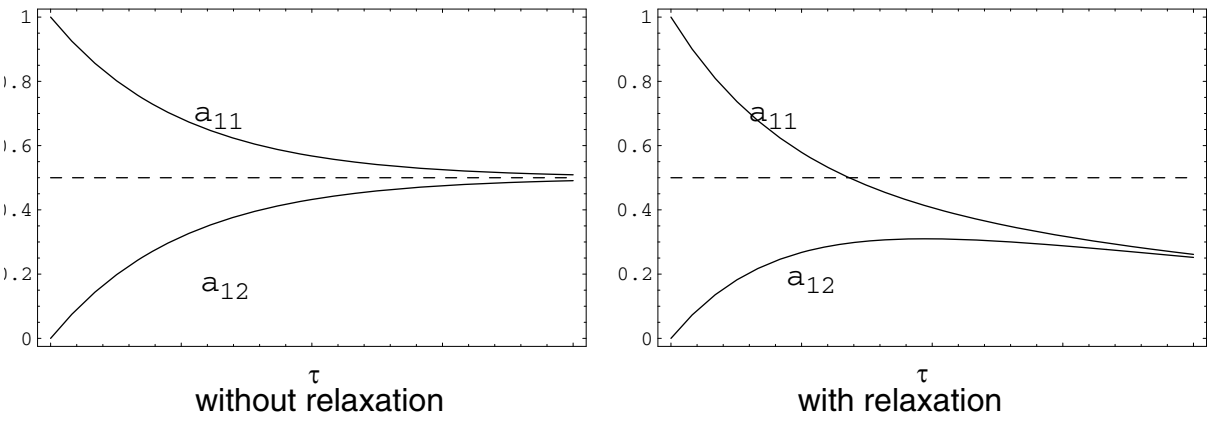

Figure 3.14: Intensity in a 2D Exchange Spectrum
cross peaks (a_{12}) and diagonal peaks (a_{11}) as a function of the mixing time τ.

$$
\begin{aligned}
SnCl_4 + SnBr_4 &\rightleftharpoons SnCl_3Br + SnClBr_3 \\
SnCl_3Br + SnBr_4 &\rightleftharpoons SnCl_2Br_2 + SnClBr_3 \\
SnCl_2Br_2 + SnBr_4 &\rightleftharpoons SnClBr_3 + SnClBr_3 \\
SnClBr_3 + SnBr_4 &\rightleftharpoons SnBr_4 + SnClBr_3
\end{aligned}
\qquad [3.37]
$$

^{119}Sn is a spin 1/2 nucleus (like protons and carbon) with a natural abundance of 8.6% and a gyromagnetic ratio in-between carbon and hydrogen. It occurs, in the mixture given above, in five different environments with 0,1,2,3,4 Br in the molecule. Therefore, the Sn spectrum consists of five lines. The chemical exchange processes are represented in the 2D EXSY spectra shown in Fig. 3.15.

3.3.1.2 Methyl-Exchange in the Heptamethylbenzenonium Ion.

From the EXSY spectrum in heptamethylbenzenonium ion, it can be seen that the 2D spectrum is not only useful to obtain the exchange rate constant but that it can also trace out the exchange mechanism. For methyl exchange in

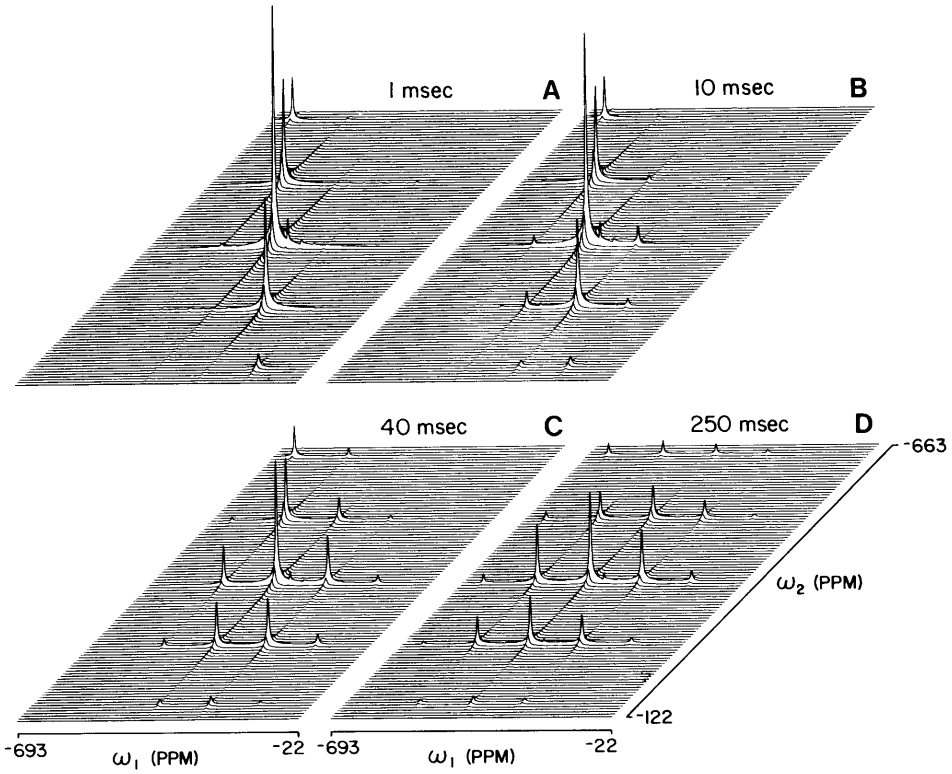

Figure 3.15: Two-Dimension Exchange Example
From R. Ramachandran et.al., J.Magn.Reson. **65**, 136 (1985).

heptamethylbenzenonium ion, two mechanisms are conceivable: (A) a 1-2 shift (the CH_3 group always jumps to one of the neighbors (left or right)) or (B) a π transition state where the CH_3 group first moves to the top of the ring (making a π complex) and then falls, randomly, into one of the six positions. It is clearly seen from the spectrum of Fig. 3.16 that the 1-2 shift mechanism is the correct one. For a random shift, cross peaks between all diagonal signals would be expected.

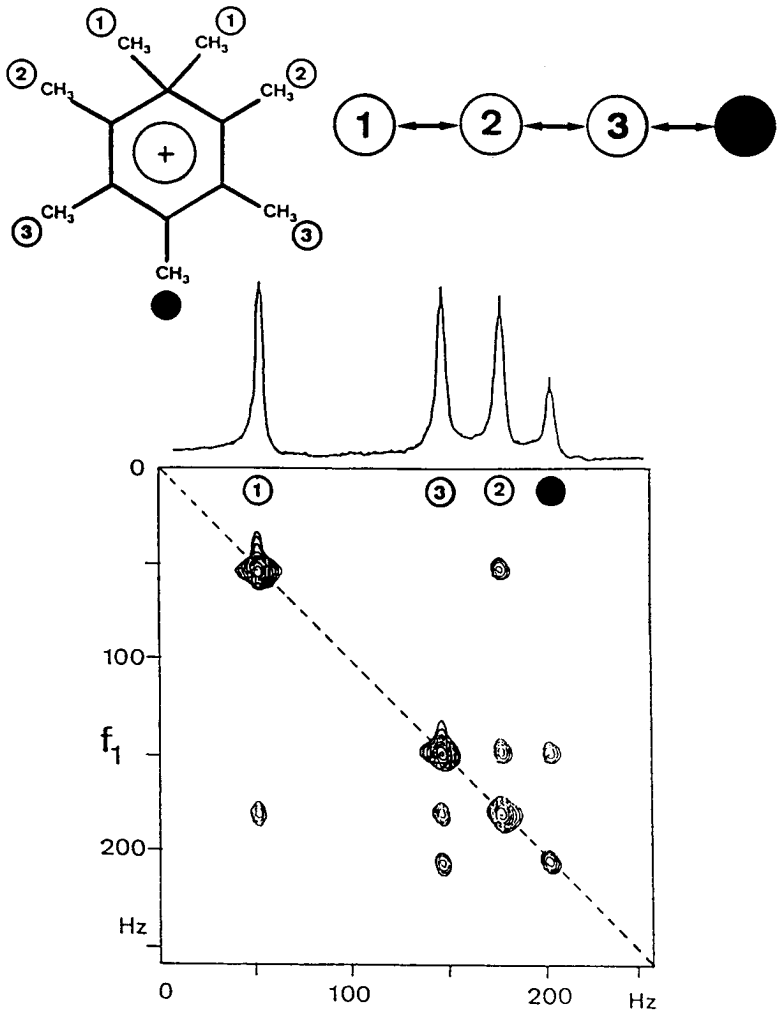

Figure 3.16: Two-Dimension Exchange Example
From. B.H. Meier and R.R. Ernst, J. Am. Chem. Soc. **101**, 6441 (1979)

4 Quantum Description of Spin Systems

In the classical description, the time evolution of the observable (the magnetization $\vec{M}$) was described by a system of differential equations in $\vec{M}$ (see Eq. [1.31]).

In the quantum description we distinguish between the *state* of the quantum system and the *observable*, the physical quantity we choose to measure:

State of the system:	State function $\|\psi(\vec{q}, \vec{Q}, s_e, s_n, t)\rangle$
Observable:	Operator $\hat{A}$

4.1 The State Function

The state-function $|\psi(\vec{q}, \vec{Q}, s_e, s_n, t)\rangle$ (where $\vec{q}$ and s_e denote the space variables (position and momentum) and spin variables of electrons; $\vec{Q}$ and s_n, the space and spin variables of the nuclei can be described by a vector in an N-dimensional vector space:

$$|\psi(t)\rangle = \sum_{i=1}^{N} c_i(t)|\phi_i\rangle \qquad [4.1]$$

Here, the $|\phi_i\rangle$ are (orthogonal) basis-functions that span the space in the same way as unit-vectors along the x, y and z-axis span the normal three-dimensional space. If the wave function $|\psi(t)\rangle$ is time dependent, this will be reflected in a time dependence of the expansion coefficients $c_i(t)$. An example for N=2 is shown in Fig. 4.1.

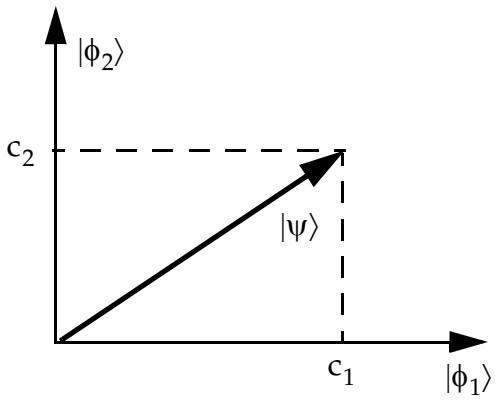

Figure 4.1: Vectors and Basis Functions

This N-dimensional space (where N can be infinite in the general case) is called a *Hilbert space*. Its properties are listed in

Box II. We can represent an abstract state function $|\psi(t)\rangle$ by a (complex) vector $\vec{\psi}(t) = (c_1(t), c_2(t), ..., c_N(t))$. Obviously, the actual value of the vector elements depends on the choice of the basis set. (See Eq. [4.1]). There is an infinite number of possible basis sets and, therefore, an infinite number of vector representations of any given state function . The relation between $|\psi(t)\rangle$ and $\vec{\psi}(t)$ is an isomorphism:

$$|\psi(t)\rangle \quad \longleftrightarrow \quad \vec{\psi}(t) \qquad \text{isomorphous} \qquad . \qquad [4.2]$$

Both representations contain the same information about the state and can be mapped unambigiously onto each other.

4.2 Operators

An operator $\hat{A}$ transforms the state function $|\psi(t)\rangle$ into another state function in the same Hilbert space

$$|\psi'(t)\rangle = \hat{A}|\psi(t)\rangle \; . \qquad [4.3]$$

This is illustrated in Fig. 4.2. If we represent the state function by a vector, the operator $\hat{A}$ has the form of a matrix A. The relationship is again an isomorphism. The matrix elements of $\tilde{A}$ in the basis spanned by the set of basis functions $|\phi_i\rangle$ are obtained through

$$A_{ij} = \langle\phi_i|\hat{A}|\phi_j\rangle \; . \qquad [4.4]$$

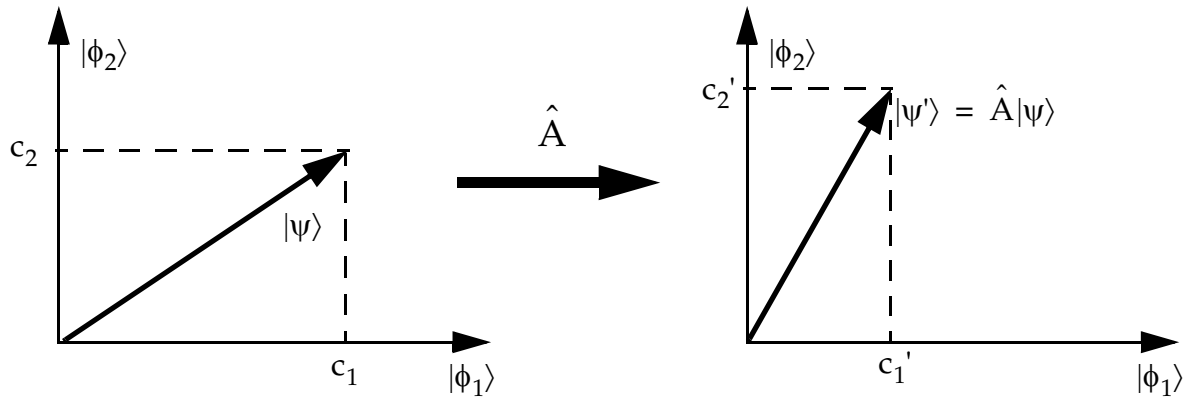

Figure 4.2: Transformation of a State Function By An Operator

Box II: Hilbert Space

A **Hilbert space** is a special ("complete") complex **vector space** with a **scalar product**. The abstract definition of a **vector space** (often also called a linear space) is as follows: A vector space is a space of elements $x, y, z, \ldots$ (called vectors) on which a sum $x + y$ and a multiplication with a scalar, λ, are defined. The following conditions (the "axioms" of a vector space) must be fulfilled:

(A1) $(x + y) + z = x + (y + z)$

(A2) $x + y = y + x$

(A3) There is a zero element 0 for which $0 + x = x$

(A4) For each x there is its inverse $-x$: $x + (-x) = 0$.

(A5) $(\lambda\mu)x = \lambda(\mu x)$

(A6) $1x = x$

(A7) $\lambda(x + y) = \lambda x + \lambda y$

(A8) $(\lambda + \mu)x = \lambda x + \mu x$.

For NMR, the most important example of a vector space is the space of ordered "N-tupels" $\vec{x} = (x_1, \ldots, x_N)$ of complex numbers together with the sum $\vec{x} + \vec{y} = (x_1 + y_1, \ldots, x_N + y_N)$ and the multiplication with a complex scalar $\lambda\vec{x} = (\lambda x_1, \ldots, \lambda x_N)$. This space is called $\mathbb{C}^N$. *However, there are many more examples of vector spaces, e.g., with polynomials or mappings as elements).*

A **scalar product** (often called "inner" product) $\langle x|y\rangle$ has the following axioms:

(B1) $\langle x + y|z\rangle = \langle x|z\rangle + \langle y|z\rangle$

(B2) $\langle y|x\rangle = \langle x|y\rangle^*$, where * denotes the complex conjugate

(B3) $\langle \lambda x|\mu y\rangle = \lambda^* \cdot \mu\langle x|y\rangle$

(B4) $\langle x|x\rangle \geq 0$ for all x

(B5) $\langle x|x\rangle = 0$ if and only if $x = 0$.

For the example of $\mathbb{C}^N$, the scalar product is defined by $\langle\vec{x}|\vec{y}\rangle = \sum_{i=1}^{N} x_i^* y_i$. For most situations encountered in NMR, the relevant Hilbert space can be mapped "one-to-one" to the well-known space $\mathbb{C}^N$ with some finite dimension N. In other cases, however, the Hilbert space can be infinite-dimensional. The most important example is given by the state functions $|\psi\rangle$ of a particle, which depend on a continuous space variable $\vec{r} = (r_1, r_2, r_3)$ and forms an infinite-dimensional Hilbert space. In this case the scalar product has the form $\langle\psi|\phi\rangle = \iiint \psi^*(\vec{r})\phi(\vec{r})dr_1dr_2dr_3$.

4.3 Time Evolution of a State Function: The Equation of Motion

The time evolution of a closed quantum system is described by the time-dependent *Schrödinger equation* (Schrödinger 1926)

$$i\hbar\frac{\partial}{\partial t}|\psi(t)\rangle = \hat{H}|\psi(t)\rangle \qquad [4.5]$$

where $\hat{H}$ is the *Hamiltonian*. It can easily be shown, that the particular solutions (stationary states)

$$|\psi_k(t)\rangle = |\tilde{\psi}_k\rangle \exp(-itE_k/\hbar) \qquad [4.6]$$

are all solutions of Eq. [4.5] where $|\tilde{\psi}_k\rangle$ is a solution of the *time-independent* Schrödinger equation:

$$\hat{H}|\tilde{\psi}_k\rangle = E_k|\tilde{\psi}_k\rangle \ . \qquad [4.7]$$

The N values E_k are called the *eigenvalues* or *principal values* of the Hamiltonian. They have the dimension of an energy.

4.4 The Result of a Quantum Measurement

Quantum measurements do not always lead to a reproducible result because quantum theory allows only probabilistic predictions. The quantity A to be measured is represented by an operator $\hat{A}$. The *expectation value* of an observable, denoted by $\langle\hat{A}\rangle$, is defined by:

$$\langle\hat{A}\rangle(t) = \frac{\langle\psi(t)|\hat{A}|\psi(t)\rangle}{\langle\psi(t)|\psi(t)\rangle} \qquad [4.8]$$

where $\langle\hat{A}\rangle$ can be interpreted as the arithmetic mean of the results of a large number of measurements of the observable $\hat{A}$ on a quantum system characterized by the state function $|\psi(t)\rangle$.

Given that we know the initial state of a quantum system $|\psi(t=0)\rangle$, its Hamiltonian as well as the operator that describes our measurement we can, with the

help of Eq. [4.8], predict the probability distribution result of a measurement at any point in time given that we are able to solve the equation of the motion (Eq. [4.5]).

4.5 The Hamiltonian I

The question to be answered next is therefore: "How do we know the Hamiltonian of a given system?"

The recipe to be followed is called the correspondence principle. First we formulate the classical energy function in the Hamilton form and then we replace the classical quantities by operators.

Step 1: Reformulation of the Newton mechanics in Hamilton form: In the Newton form, we describe a system of point masses with mass m_1, m_2, m_3, ..., m_n by n position vectors $\vec{q}_1, ...,\vec{q}_n$ and n velocity vectors $\vec{v}_1, ..., \vec{v}_n$. In the absence of magnetic interactions, the energy is given by:

$$E = \frac{1}{2}\sum_{i=1}^{N} m_i v_i^2 + V(\vec{q}_1, ...\vec{q}_n) \qquad [4.9]$$

where $V(\vec{q}_1, \ldots\vec{q}_n)$ is the potential energy of the system.

In The Hamilton form, we describe the system in terms of n position vectors $\vec{q}_1, \ldots\vec{q}_n$ and n momentum vectors $\vec{p}_1, ..., \vec{p}_n$. In the absence of magnetic interactions, we have $\vec{p}_i = m_i\vec{v}_i$ and the Hamilton function is given by:

$$H(\vec{p}_1, ..., \vec{p}_n, \vec{q}_1, \ldots\vec{q}_n) = \frac{1}{2}\sum_{i=1}^{N} \frac{p_i^2}{m_i} + V(\vec{q}_1, \ldots\vec{q}_n). \qquad [4.10]$$

Step 2: Correspondence principle. Make the following replacements:

$$\begin{aligned} \vec{p}_i &\rightarrow \hat{\vec{p}}_i \\ \vec{q}_i &\rightarrow \hat{\vec{q}}_i \end{aligned} \qquad [4.11]$$

The vector operators $\hat{\vec{p}}_i$ and $\hat{\vec{q}}_i$ do not commute but fulfil the Heisenberg relation:

$$[\hat{q}_\nu, \hat{p}_\mu] \equiv \hat{q}_\nu \hat{p}_\mu - \hat{p}_\mu \hat{q}_\nu = i\hbar\delta_{\nu\mu} \qquad , \qquad \nu, \mu = x, y, z \qquad [4.12]$$

4.6 Angular Momentum and Spin

A classical angular momentum $\vec{L} = \vec{q} \times \vec{p}$ translates, according to the correspondence principle, to a quantum-mechanical momentum (vector)-operator:

$$\hat{\vec{l}} = \hat{\vec{q}} \times \hat{\vec{p}} \qquad [4.13]$$

Using the Heisenberg commutation rules for $\hat{\vec{q}}$ and $\hat{\vec{p}}$, we find the commutation rules for the dimensionless angular momentum operator $\hat{\vec{L}} = \frac{1}{\hbar}\hat{\vec{l}}$:

$$\begin{aligned} [\hat{L}_x, \hat{L}_y] &= i\hat{L}_z \\ [\hat{L}_y, \hat{L}_z] &= i\hat{L}_x \\ [\hat{L}_z, \hat{L}_x] &= i\hat{L}_y \end{aligned} \qquad [4.14]$$

The isotropy of space requires that the angular momentum is preserved in a closed system.

The total angular-momentum operator $\hat{\vec{j}}$ consists of two components, namely the orbital angular momentum, $\hat{\vec{l}}$, that is obtained via the correspondence principle and the so-called *spin angular momentum* $\hat{\vec{s}}$:

$$\hat{\vec{j}} = \hat{\vec{l}} + \hat{\vec{s}} \qquad [4.15]$$

The expectation value of the total angular momentum $\hat{\vec{j}}$ is a preserved quantity required by the isotropic property of free space.

The dimensionless quantity $\hat{\vec{S}} = \frac{1}{\hbar}\hat{\vec{s}}$ fulfills the same commutation relationships as $\hat{\vec{L}}$:

$$\begin{aligned} [\hat{S}_x, \hat{S}_y] &= i\hat{S}_z \\ [\hat{S}_y, \hat{S}_z] &= i\hat{S}_x \\ [\hat{S}_z, \hat{S}_x] &= i\hat{S}_y \end{aligned} \qquad [4.16]$$

We interpret the spin angular momentum as the non-classical part of the total angular momentum. It cannot be derived through the correspondence principle and is an inherently quantum-mechanical property. It is, therefore, not possible to find a classical analogy for the spin!

4.7 Matrix Representation of Spin Operators

The general recipe to obtain an explicit matrix representation of a quantum mechanical operator is given in Eq. [4.4]:

$$A_{ij} = \langle \phi_i | \hat{A} | \phi_j \rangle \qquad [4.17]$$

The dimension needed to represent the operator $\hat{A}$ depends on the type of operator. All operators obtained from classical counterparts through the principle of correspondence have infinite dimensions. This is easily seen from the Heisenberg commutation rules of Eq. [4.12]. For a matrix representation with NxN matrices we would obtain by taking the trace on each side of the equal sign

$$\mathrm{Tr}\{qp - pq\} = \mathrm{Tr}\{qp\} - \mathrm{Tr}\{pq\} = 0 = i\hbar N \qquad [4.18]$$

This equation is obvious wrong, except for the classical limit $\hbar \to 0$. Therefore, no finite-dimensional matrix representations for $\hat{p}$ and $\hat{q}$ exist. The well-known representation by multiplication and differential operators is given in

Box III: Schrödinger Representation for Position and Momentum

The representation of the position operator $\hat{q}$ and the momentum operator $\hat{p}$ by the multiplication operator

$$\hat{q}_\nu = q_\nu \qquad [4.19]$$

and the differentiation operator

$$\hat{p}_\nu = \frac{\hbar}{i}\frac{\partial}{\partial q_\nu} \qquad [4.20]$$

fulfils the Heisenberg relations.

Spin operators, however, have finite-dimensional matrix representations. They can be represented in Hilbert spaces of dimension

$$D = 2I + 1 \qquad [4.21]$$

where I is the *spin-quantum number* which is a "material constant" for each nuclear isotope and for the electron. It can be half-integer or integer: I= 0, 1/2, 1, 3/2, 2, ...

Table 4.1: Spin Quantum Numbers of Some Important Nuclei

nucleus	^{1}H	^{2}H	^{3}H	^{3}He	^{12}C	^{13}C	^{14}N	^{15}N
I	1/2	1	1/2	1/2	0	1/2	1	1/2
nucleus	^{17}O	^{19}F	^{23}Na	^{27}Al	^{31}P	^{129}Xe	^{131}Xe	^{195}Pt
I	5/2	1/2	3/2	5/2	1/2	1/2	3/2	1/2

The electron and a number of practically important spins (^{1}H, ^{13}C, ^{15}N, ^{19}F, ...) have a spin-quantum number I = 1/2 and can be represented by 2x2 matrices. A complete set of orthogonal 2x2 matrices are the so called Pauli matrices together with the unity matrix:

$$E = \begin{bmatrix} 1 & 0 \\ 0 & 1 \end{bmatrix} \qquad I_x = \begin{bmatrix} 0 & \frac{1}{2} \\ \frac{1}{2} & 0 \end{bmatrix} \qquad I_y = \begin{bmatrix} 0 & \frac{-i}{2} \\ \frac{i}{2} & 0 \end{bmatrix} \qquad I_z = \begin{bmatrix} \frac{1}{2} & 0 \\ 0 & \frac{-1}{2} \end{bmatrix} \qquad [4.22]$$

They fulfill the commutation relationship of Eq. [4.16] which can easily be seen by inserting and calculating the matrix products. Therefore, they are a valid representation of an angular momentum operator. The matrix I_z is diagonal and the basis function $|\phi_m\rangle$ are the eigenfunctions of the operator $\hat{I}_z$:

$$\hat{I}_z|\phi_m\rangle = m|\phi_m\rangle \qquad [4.23]$$

where m is the *magnetic quantum number* and can take values from the range:

$$m = -I, -I+1, ..., 0, ..., I-1, I. \qquad [4.24]$$

For spin-1/2 nuclei, we denote the two basis functions by:

$$\begin{aligned} \phi_{1/2} &= \alpha \\ \phi_{-1/2} &= \beta \end{aligned} \qquad [4.25]$$

An alternative orthogonal set of matrices for spin-1/2 nuclei is formed by I_z, $I^+ = I_x + iI_y$ and $I^- = I_x - iI_y$:

$$E = \begin{bmatrix} 1 & 0 \\ 0 & 1 \end{bmatrix} \qquad I^+ = \begin{bmatrix} 0 & 1 \\ 0 & 0 \end{bmatrix} \qquad I^- = \begin{bmatrix} 0 & 0 \\ 1 & 0 \end{bmatrix} \qquad I_z = \begin{bmatrix} \frac{1}{2} & 0 \\ 0 & \frac{-1}{2} \end{bmatrix} \qquad [4.26]$$

$\hat{I}^+$ and $\hat{I}^-$ are called raising and lowering operators, respectively. By applying the matrix representations to the basis vectors $(1, 0)$ and $(0, 1)$, we obtain:

$$\begin{aligned} \hat{I}^+|\alpha\rangle &= 0 & \hat{I}^-|\alpha\rangle &= |\beta\rangle \\ \hat{I}^+|\beta\rangle &= |\alpha\rangle & \hat{I}^-|\beta\rangle &= 0 \end{aligned} \qquad [4.27]$$

The equivalent expression for a general spin quantum number I is:

$$\begin{aligned} \hat{I}^+|\phi_m\rangle &= \sqrt{I(I+1) - m(m+1)}|\phi_{m+1}\rangle \\ \hat{I}^-|\phi_m\rangle &= \sqrt{I(I+1) - m(m-1)}|\phi_{m-1}\rangle \end{aligned} \qquad [4.28]$$

A third, almost equivalent alternative set of spin operators are the spherical-tensor operators denoted by T_{lm}. Here l is the rank of the Tensor and m denotes one of the components m: -l, -l+1, ..., 0, ..., +l-1, +l. For a spin-1/2 system, we only need spherical-tensor operators with $l = 1$:

$$\begin{aligned} \hat{T}_{00}^{(1)} &= \hat{E} \\ \hat{T}_{10}^{(1)} &= \hat{I}_z \\ \hat{T}_{11}^{(1)} &= \frac{-1}{\sqrt{2}}\hat{I}^+ \\ \hat{T}_{1,-1}^{(1)} &= \frac{1}{\sqrt{2}}\hat{I}^- \end{aligned} \qquad [4.29]$$

and in matrix representation:

$$T^{(1)}_{00} = \begin{bmatrix} 1 & 0 \\ 0 & 1 \end{bmatrix} \qquad T^{(1)}_{10} = \begin{bmatrix} \frac{1}{2} & 0 \\ 0 & \frac{-1}{2} \end{bmatrix} \qquad T^{(1)}_{11} = \begin{bmatrix} 0 & \frac{-1}{\sqrt{2}} \\ 0 & 0 \end{bmatrix} \qquad T^{(1)}_{1,-1} = \begin{bmatrix} 0 & 0 \\ \frac{1}{\sqrt{2}} & 0 \end{bmatrix} . \quad [4.30]$$

For a spin 1/2 one can easily verify the following expectation values for the α state:

$$\begin{aligned} \langle \hat{I}_z \rangle &= \langle \alpha | \hat{I}_z | \alpha \rangle = \frac{1}{2} \\ \langle \hat{I}_x \rangle &= \langle \alpha | \hat{I}_x | \alpha \rangle = 0 \\ \langle \hat{I}_y \rangle &= \langle \alpha | \hat{I}_y | \alpha \rangle = 0 \\ \langle \hat{I}^2 \rangle &= \langle \hat{I}_x^2 \rangle + \langle \hat{I}_y^2 \rangle + \langle \hat{I}_z^2 \rangle = I(I+1) = \frac{3}{4} . \end{aligned} \quad [4.31]$$

For the evaluation with matrices, it is important to note that the so called "bra" state $\langle \alpha |$ has expansion coefficients that are the complex conjugate of the ones of the "ket" state $|\alpha\rangle$.

$$\begin{aligned} |\psi\rangle &= c_1 |\alpha\rangle + c_2 |\beta\rangle & \vec{\psi} &= \begin{pmatrix} c_1 \\ c_2 \end{pmatrix} \\ \langle \psi | &= c_1^* \langle \alpha | + c_2^* \langle \beta | & \vec{\psi}' &= \begin{pmatrix} c_1 & c_2 \end{pmatrix} \end{aligned} \quad [4.32]$$

From Eq. [4.31], we note that only the z-component of the angular momentum has a non-vanishing expectation value. However, it is not correct to say that the angular momentum can be represented by a vector along the z-direction because the length of the vector $\sqrt{\langle \hat{I}^2 \rangle} = \sqrt{3}/2$ is longer than its z-component $\langle \hat{I}_z \rangle = 1/2$. This is, of course, in accordance with the uncertainty principle: because the operators

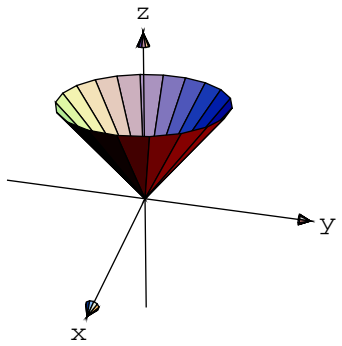

Figure 4.3: Angular Momentum

$\hat{I}_j$ do not commute, they cannot have simultaneously well-defined expectation values. Because the states α and β are chosen such that they yield a well-defined value for $\langle \hat{I}_z \rangle$, they do not contain any information about the x and y components any more. Pictorially, we can represent the possible states as vectors on a cone as shown in Fig. 4.3.

4.8 The Density Operator

All experimentally observable quantum-mechanical quantities are expectation values of operators. If we insert the expansion of Eq. [4.1]

$$|\psi(t)\rangle = \sum_{i=1}^{N} c_i(t)|\phi_i\rangle \qquad [4.33]$$

into the definition of for an expectation value (Eq. [4.6]) we obtain:

$$\langle \hat{A} \rangle = \sum_i \sum_j c_i(t)^* c_j(t) \langle \phi_i | \hat{A} | \phi_j \rangle \qquad [4.34]$$

Here we have adopted the convention that the state function is normalized: $\langle \psi(t)|\psi(t)\rangle = 1$.

We see from Eq. [4.34] that the information we need to characterize a system and to calculate the expectation value of an observable is contained in the product $c_i(t)^* c_j(t)$ of the expansion coefficients. This suggests the construction of an operator $\hat{\rho}(t)$ that contains these products as the elements of its matrix representation:

$$\langle \phi_k | \hat{\rho}(t) | \phi_l \rangle = c_k c_l^* \qquad [4.35]$$

We call this operator the *density operator* and the matrix the *density matrix*. Formally we can write

$$\hat{\rho}(t) = |\psi(t)\rangle\langle\psi(t)| = \sum_i \sum_j c_i(t) c_j^*(t) |\phi_i\rangle\langle\phi_j| \qquad [4.36]$$

and in a matrix representation using $\rho_{ij} = \langle \phi_i | \hat{\rho}(t) | \phi_j \rangle = c_i(t) c_j^*$:

$$\rho = \begin{bmatrix} c_1c_1^* & c_1c_2^* & .... & c_1c_{N-1}^* & c_1c_N^* \\ c_2c_1^* & c_2c_2^* & .... & c_2c_{N-1}^* & c_2c_N^* \\ .... & .... & .... & .... & .... \\ c_{N-1}c_1^* & c_{N-1}c_2^* & .... & c_{N-1}c_{N-1}^* & c_{N-1}c_N^* \\ c_Nc_1^* & c_Nc_2^* & .... & c_Nc_{N-1}^* & c_Nc_N^* \end{bmatrix} \qquad [4.37]$$

For a single spin or a *pure state* where all the members of the spin ensemble are in the same state, the density operator contains exactly the same information as the state function. By inserting Eq. [4.36] into the expression of the expectation value (Eq. [4.34]), we find:

$$\begin{aligned} \langle A \rangle &= \sum_i \sum_j c_i(t)^* c_j(t) \langle \phi_i | A | \phi_j \rangle \\ &= \sum_i \sum_j \langle \phi_j | \hat{\rho}(t) | \phi_i \rangle \langle \phi_i | \hat{A} | \phi_j \rangle \\ &= \sum_j \langle \phi_j | \hat{\rho}(t) \hat{A} | \phi_j \rangle \\ &= tr\{ \hat{\rho}(t) \hat{A} \} \quad . \end{aligned} \qquad [4.38]$$

This trace can be conveniently evaluated as the product of the matrix representations of the observable and the density operator:

$$\langle \hat{A} \rangle = tr\{ \hat{\rho}(t) \cdot \hat{A} \} \; . \qquad [4.39]$$

Normally we investigate quantum systems that are in a *mixed state*, e.g., for an ensemble of spins in thermal equilibrium. In such a system, the different systems in the ensemble are in different states and the system cannot be described by a single wave function but a set of wave functions $|\psi_k(t)\rangle$ and their probabilities P_k. Nevertheless, according to equation Eq. [4.38], the system can still be described by a single density operator that we define as

$$\begin{aligned} \hat{\rho}(t) &= \sum_k P_k |\psi_k(t)\rangle\langle\psi_k(t)| = \sum_k P_k \sum_i \sum_j c_i^{(k)}(t) c_j^{(k)*}(t) |\phi_i\rangle\langle\phi_j| \\ &= \sum_i \sum_j \overline{c_i(t) c_j^*(t)} |\phi_i\rangle\langle\phi_j| \end{aligned} \qquad [4.40]$$

where the overbar denotes the ensemble average. In all practically important cases, we refer to this second definition if we write the symbol $\hat{\rho}(t)$. Still, Eq. [4.39] is valid for the new definition of the density operator.

Because we use normalized state functions, the trace of the density operator is always equal to unity:

$$\mathrm{tr}\{\hat{\rho}(t)\} = 1 \; . \qquad [4.41]$$

For pure states, we find $\mathrm{tr}\{\hat{\rho}^2\} = 1$, for mixed states, in contrast, we find that $\mathrm{tr}\{\hat{\rho}^2\} < 1$.

4.9 The Liouville-von Neumann Equation and its Solution

Because the density operator is a function of the state function, we must be able to formulate a differential equation for it that is the equivalent to the time-dependent Schrödinger equation (Eq. [4.5]). By inserting the expansion of Eq. [4.1], $|\psi(t)\rangle = \sum_i c_i(t)|\phi_i\rangle$, into the Schrödinger equation, we obtain

$$\begin{aligned} \frac{d}{dt}\left(\sum_i c_i(t)|\phi_i\rangle\right) &= \frac{-i}{\hbar}\hat{H}\left(\sum_i c_i(t)|\phi_i\rangle\right) \\ \sum_i \frac{d}{dt}c_i(t)|\phi_i\rangle &= \frac{-i}{\hbar}\hat{H}\left(\sum_i c_i(t)|\phi_i\rangle\right) \end{aligned} \qquad [4.42]$$

multiplying both sides with $\langle\phi_k|$ leads to

$$\dot{c}_k(t) = -\frac{i}{\hbar}\sum_i c_i(t)\langle\phi_k|\hat{H}|\phi_i\rangle \qquad [4.43]$$

and

$$\dot{c}_k^*(t) = \frac{i}{\hbar}\sum_i c_i^*(t)\langle\phi_i|\hat{H}|\phi_k\rangle \qquad [4.44]$$

With this result, we obtain for the time-derivative of the density operator in matrix form

$$\frac{d}{dt}\rho_{kl} = \frac{d}{dt}\langle\phi_k|\hat{\rho}(t)|\phi_l\rangle = \frac{d}{dt}(c_k(t)c_l^*(t)) = \dot{c}_k c_l^* + c_k \dot{c}_l^* \qquad [4.45]$$

Inserting Eqs. [4.43] and [4.44] leads to

$$\dot{\rho}_{kl} = -\frac{i}{\hbar}\sum_j H_{kj}c_j c_l^* + \frac{i}{\hbar}\sum_j H_{jl}c_k c_j^* = -\frac{i}{\hbar}\left(\sum_j H_{kj}\rho_{jl} - \sum_j \rho_{kj}H_{jl}\right) \qquad [4.46]$$

In operator form, the Liouville-von Neumann equation reads as

$$\frac{d}{dt}\hat{\rho} = -\frac{i}{\hbar}[\hat{H}, \hat{\rho}(t)] \qquad [4.47]$$

Its solution is, for time-independent Hamiltonians, easily found to be

$$\hat{\rho}(t) = e^{-\frac{i}{\hbar}\hat{H}t}\hat{\rho}(0)e^{\frac{i}{\hbar}\hat{H}t} . \qquad [4.48]$$

Homework: Confirm the validity of this solution by calculating the derivative of $\hat{\rho}(t)$.

With this result, we can formulate the general result for the expectation value of any time-independent operator as

$$\langle\hat{A}\rangle = tr\{\hat{\rho}(t)\hat{A}\} = tr\left\{e^{-\frac{i}{\hbar}\hat{H}t}\hat{\rho}(0)e^{\frac{i}{\hbar}\hat{H}t}\hat{A}\right\} \qquad [4.49]$$

For the explicit evaluation this expression is usually expressed in a matrix representation. As a basis set, it is most convenient to use the eigenbasis of the Hamiltonian, i.e., the basis in which the Hamiltonian $\hat{H}$ is diagonal. In this basis, the exponential is easily evaluated as:

$$H = \begin{bmatrix} H_{11} & 0 & 0 \\ 0 & H_{22} & 0 \\ 0 & 0 & .... \end{bmatrix} \qquad e^{-\frac{i}{\hbar}Ht} = \begin{bmatrix} e^{-\frac{i}{\hbar}H_{11}t} & 0 & 0 \\ 0 & e^{-\frac{i}{\hbar}H_{22}t} & 0 \\ 0 & 0 & .... \end{bmatrix} \qquad [4.50]$$

and by inserting into Eq. [4.49] we obtain:

$$\langle\hat{A}\rangle(t) = \sum_k\sum_l \rho_{kl}(0)A_{lk}\exp\left(-\frac{i}{\hbar}(H_{kk} - H_{ll})t\right) \qquad [4.51]$$

Here, the $(H_{kk} - H_{ll})/\hbar = \omega_{kl}$ denote the transition frequencies and the coefficients $\rho_{kl}(0)A_{lk}$ the intensities of the transitions. We can arrange them again into an intensity vector $\vec{c}$ and a frequency vector $\vec{\Lambda}$. The time-domain signal is given by (see Eq. [3.15]:

$$s(t) = \langle \hat{I}_x \rangle(t) = \vec{c} \cdot \exp\left(\vec{\Lambda} t\right) \qquad [4.52]$$

4.10 The Initial Density Operator

To solve the Liouville-von Neumann equation, we need to know the initial state of the spin system, described by $\hat{\rho}(0)$. Usually, an experiment starts at *thermal equilibrium* ($\hat{\rho}_0$), where the spin system is in equilibrium with its environment:

$$\hat{\rho}_0 = \frac{e^{-\hat{H}/k_B T}}{Tr\left\{e^{-\hat{H}/k_B T}\right\}} \qquad [4.53]$$

This is the so called *Boltzmann distribution* or *canonical distribution*. Here, k_B is the Boltzmann constant ($1.3806\ 10^{-23}$ J/K).

In the Eigenbasis of the Hamiltonian, the matrix elements of the density operator are, therefore, given by:

$$(\hat{\rho}_0)_{kl} = \frac{\delta_{kl} e^{-E_k/k_B T}}{\sum_l e^{-E_l/k_B T}} \qquad [4.54]$$

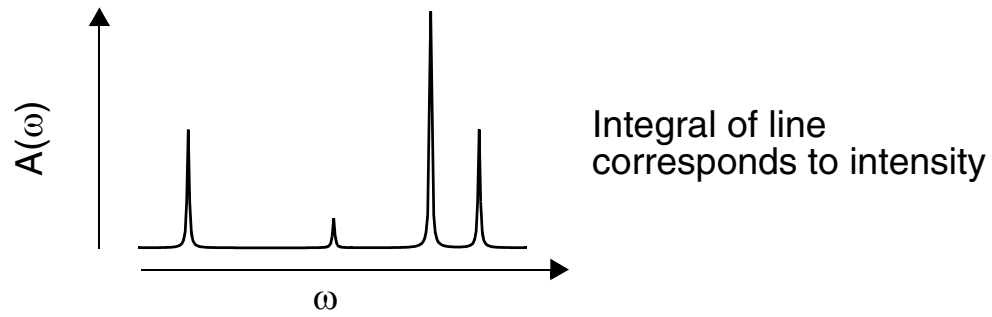

Figure 4.4: Transition Frequencies and Intensities

and the density operator in matrix form is:

$$\rho_0 = \begin{bmatrix} p_1 & 0 & 0 \\ 0 & p_2 & 0 \\ 0 & 0 & .... \end{bmatrix} \qquad [4.55]$$

The p_i are called the population of the states i and are sometimes represented in energy-level diagrams as shown in Fig. 4.5.

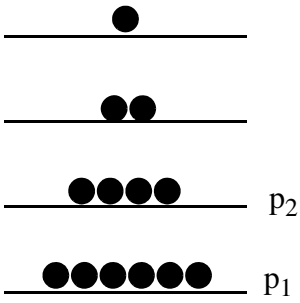

Figure 4.5: Boltzmann Distribution

4.11 The Observable Operator in NMR

NMR experiments measure the magnetization $\langle \hat{M}_x \rangle$ or $\langle \hat{M}_y \rangle$ in the laboratory frame of reference:

$$\hat{M}_x = \sum_k \gamma_k \hat{I}_{kx}. \qquad [4.56]$$

As mentioned in Chapter 2.5, this observable signal is demodulated with the rf carrier frequency and the demodulated signal is identical to a hypothetical detection of $\hat{M}^+ = \hat{M}_x + i\hat{M}_y$ in a rotating frame of reference.

4.12 The Hamiltonian II

We consider a system with

- K nuclei with position $\vec{Q_a}$ mass M_a, momentum $\vec{P_a}$ electrical quadrupole moment Q_a, charge $Z_a e_0$ and spin angular momentum $\gamma_a \hbar \hat{\vec{I}}_a$
- M electrons with position $\vec{q_k}$ mass m_0, momentum $\vec{p_k}$, charge $-e_0$ orbital angular momentum $-\beta \hat{\vec{L}}_k$ and the spin angular momentum $-g\beta \hat{\vec{S}}_k$.
- An external magnetic field $\vec{B_0}$ which we will treat as a classical entity.
- An external electric field $\vec{E}$, also treated classically.

All these quantities interact with each other according to the schematic drawing of Figure 4.6.

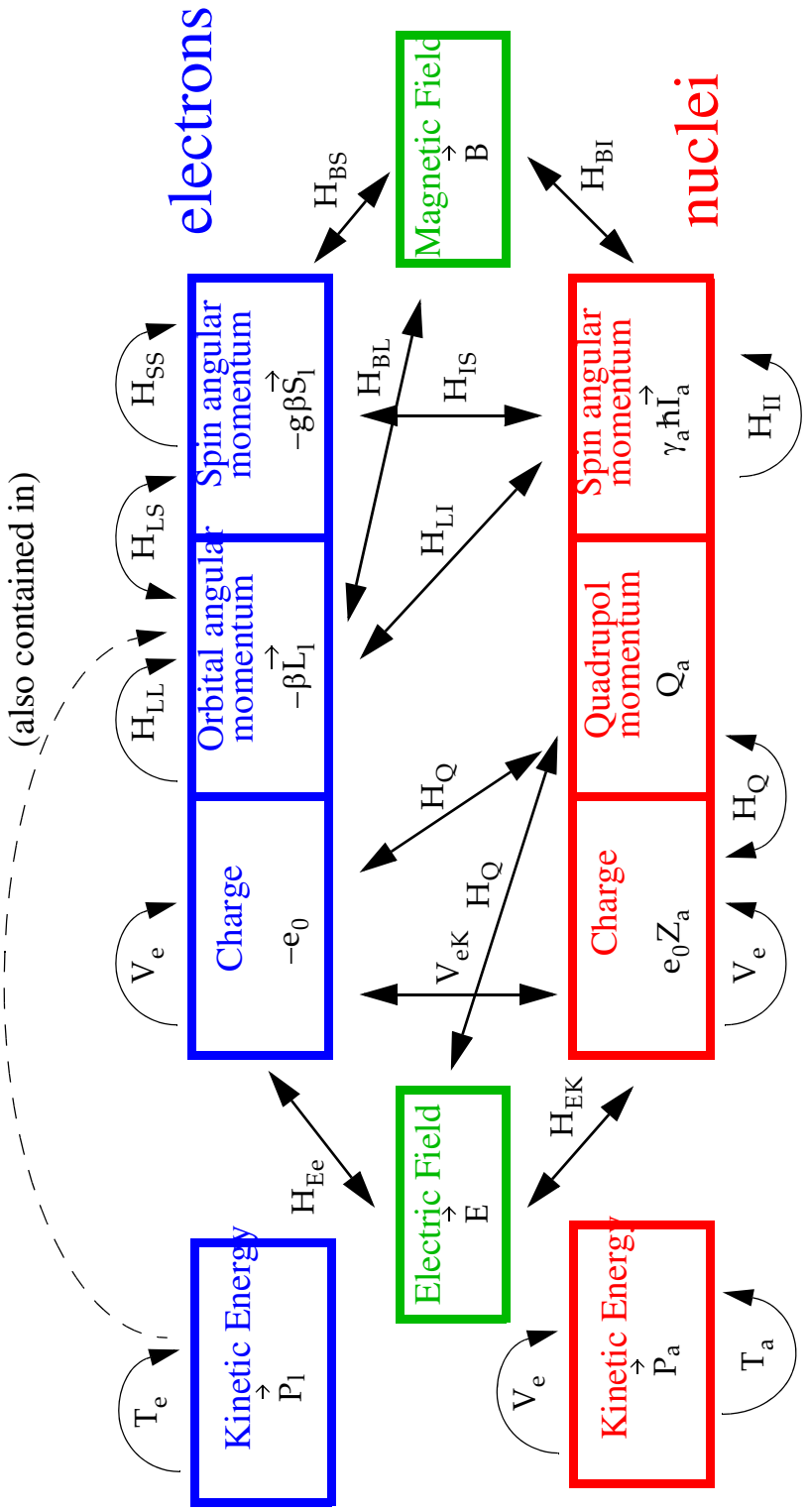

Figure 4.6: Interaction Between Different Quantities

This leads to a rather complicated Hamiltonian

$$\hat{H} = \hat{T}_k + \hat{T}_e + \hat{V}_k + \hat{V}_e + \hat{V}_{ek} + \hat{H}_Q + \hat{H}_{LL} + ... \quad [4.57]$$

that, even for very simple molecules, cannot be solved analytically. As a first step of simplification, the Born-Oppenheimer-Approximation is usually applied. The kinetic energy of the nuclei $\hat{T}_k$ is neglected and the position operators $\hat{\vec{Q}}_a$ become parameters with a fixed value instead of being free variables. The resulting Hamiltonian is still complex and we proceed with a further approximation that leads us to the spin Hamiltonian.

4.13 The Spin Hamiltonian

The spin energies (and the orbital energies of the unpaired electrons) are the smallest energies in the Hamiltonian considered in the preceding chapter. Consequently, they lead to the lowest characteristic frequencies in the entire Hamiltonian. Typical frequencies for nuclear magnetic resonance spectroscopy are in the range of 1 to 1000 MHz. The motion of the electrons proceed on a much faster time scale and for the calculation of the "slow" NMR interactions, we may average over the "fast" electron motion. This averaged Hamiltonian is called the spin Hamiltonian:

$$\hat{H}^s = \langle \psi(\vec{q}, s_e, s_k) | \hat{H} | \psi(\vec{q}, s_e, s_k) \rangle^{\varnothing} \quad [4.58]$$

where $\varnothing$ indicates that we have integrated over the space coordinates of all electrons and over the spin coordinates of the paired electrons.For diamagnetic systems without unpaired electrons, we are, therefore, left with a Hamiltonian that contains only nuclear spin operators and (constant) numbers:

$$\hat{H}^s(s_k) = \hat{H}_{BI} + \hat{H}_{II} + \hat{H}_Q . \quad [4.59]$$

Here $\hat{H}_{BI}$ denotes the interaction between the nuclear spin and the magnetic field $\vec{B}$, $\hat{H}_{II}$ describes the spin-spin interactions and $\hat{H}_Q$ the quadrupole interactions (see also Fig. 4.6). For paramagnetic systems, the spatial coordinates of the unpaired electrons remain:

$$\hat{H}^{s}(\vec{q}_{up}, s_e, s_k) = \hat{H}_{BS}(s_e) + \hat{H}_{BL}(\vec{q}_{up}) + \hat{H}_{SS}(s_e) + \hat{H}_{LL}(\vec{q}_{up}) + \hat{H}_{LS}(\vec{q}_{up}, s_e) + \hat{H}_{IS}(s_k, s_e) + \hat{H}_{LI}(\vec{q}_{up}, s_k) + H^{(s)}(s_k) \quad [4.60]$$

For the identification of the interactions see Fig. 4.6.

In the simplified Hamiltonian of Eq. [4.59], the information about molecular quantities (e.g. structure) is found in numerical constant. Explicitly treated are only the spin coordinates. Therefore, the resulting Hamiltonian is of finite dimension and usually relatively easy to manipulate.

In the following, we will only be concerned with spin Hamiltonians. To simplify the notation, the superscript(s) will be omitted and, for convenience, we will express the Hamiltonian in angular frequency units:

$$\hat{\mathcal{H}} = \frac{1}{\hbar}\hat{H}^{s} \quad [4.61]$$

4.14 The Spin-Density Operator

We have obtained the spin Hamiltonian from the full Hamiltonian by eliminating all other degrees of freedom by an integration. The same procedure must be applied to obtain the density operator in spin space, which we denote by $\hat{\sigma}$, from the full density operator $\hat{\rho}$.

For the spin interactions we can work in the high-temperature approximation:

$$E_k \ll k_B T \qquad \begin{array}{ll} \text{Nuclear spin:} & E_k/k_B \approx 1\text{mK} \\ \text{Electron spin:} & E_k/k_B \approx 1\text{K} \end{array} \quad [4.62]$$

Then we can expand the exponential of [4.53] in a power series. Keeping terms to first order only, we obtain the following simplified expression for the equilibrium spin density operator:

$$\sigma_0 \cong \frac{\hat{1} - \hbar\hat{\mathcal{H}}/k_B T}{Tr\{\hat{1} - \hbar\hat{\mathcal{H}}/k_B T\}} \cong \frac{\hat{1}}{Tr\{\hat{1}\}} - \frac{\hbar\hat{\mathcal{H}}}{k_B T \cdot Tr\{\hat{1}\}} \quad [4.63]$$

The largest term in Eq. [4.63] is the unity operator $\hat{1}$. This term is irrelevant because not observable. For NMR experiments, we may, therefore, calculate with an initial "density operator" of

$$\hat{\sigma}'_0 \cong \frac{-\hbar}{k_B T \cdot \mathrm{Tr}\{\hat{1}\}} \hat{\mathcal{H}} \qquad [4.64]$$

In practice, the dash is usually left away and we write $\hat{\sigma}_0$ instead of $\hat{\sigma}'_0$. This sloppy notation is often convenient but can also be dangerous. $\hat{\sigma}'_0$ is traceless and, strictly speaking, not a density operator. Its elements do not represent the populations but the difference populations from an even distribution over all energy levels which corresponds to a the equilibrium state at infinite temperature.

We have now set the stage to quantum-mechanically calculate the magnetic-resonance signal $s(t)$ of a spin system in the time domain. The spectrum $S(\omega)$ is obtained from $s(t)$ by a Fourier transformation. The necessary steps are summarized in Box IV.

Box IV: General Recipe to Calculate an NMR Spectrum

I) Get the spin Hamiltonian(s). Many experiments consist of several time periods with different Hamiltonians. The general principles how to obtain the Hamiltonian of a given system are mentioned in Chapters 4.5, 4.6, and 4.13. More detailed and practically applicable recipe will be given in the following section.

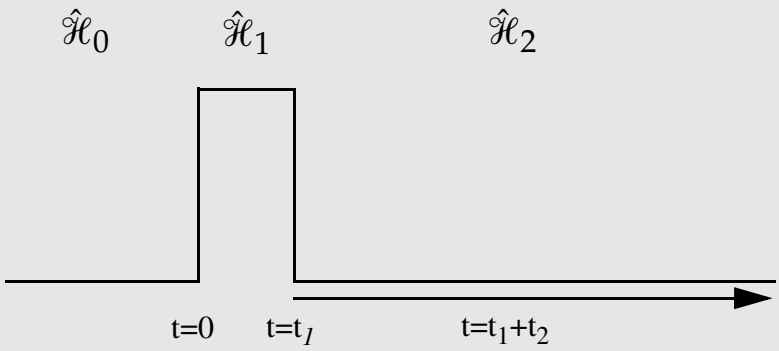

[4.65]

II) Determine the initial density operator (the unity part is dropped) according to Eq. [4.64]:

$$\hat{\sigma}(t=0) = \hat{\sigma}_0 = \frac{-\hbar}{k_B T \cdot \mathrm{Tr}\{\hat{1}\}} \hat{\mathcal{H}}_0 . \qquad [4.66]$$

III) Evaluate $\hat{\sigma}(t=t_1)$ using the equation of motion, the Liouville-von Neumann equation (Eq. [4.48])

IV) Determine the density operator as a function of t_2 applying the Liouville-von Neumann equation again.

V) Determine $\langle \hat{M}_x \rangle(t_2)$ by evaluating the trace of Eq. [4.38]. The detection operator is taken from Eq. [4.56]:

$$s(t_2) = \langle \hat{M}_x \rangle(t_2) = \mathrm{tr}\{\hat{\sigma}(t_1 + t_2)\hat{M}_x\} \qquad [4.67]$$

or (often more easily) by applying Eq. [4.51]:

$$\langle \hat{M}_x \rangle(t_2) = \sum_k \sum_l \sigma_{kl}(t_1, t_2=0)(M_x)_{lk} \exp(-i(H_{kk} - H_{ll})t_2) \qquad [4.68]$$

5 The Nuclear Spin Hamiltonian: Information Content of NMR Spectra

5.1 Interaction With an External Field B_0

The interaction of a spin with the external magnetic field, that is always described classically, is called the *Zeeman interaction* and is of the form:

$$\hat{\mathcal{H}}_z = -\sum_i \gamma_i \hat{\vec{I}}_i \cdot \vec{B_0} \qquad [5.1]$$

or, assuming $\vec{B_0} = (0, 0, B_0)$

$$\hat{\mathcal{H}}_z = \sum_i \omega_{0i} \hat{I}_{iz} \ . \qquad [5.2]$$

Equation [5.1] can easily be derived from the classical energy of a magnetic dipole $\vec{\mu}$ in a magnetic field ($E_{pot} = -\vec{\mu} \cdot \vec{B}$, see Eq. [1.13]) and the gyromagnetic equation [1.16] ($\vec{\mu} = \gamma \vec{L}$) using the principle of correspondence.

There is a usually small difference between $\hat{\mathcal{H}}_{BI}$ (Chapter 4.12) and $\hat{\mathcal{H}}_z$. $\hat{\mathcal{H}}_z$ is the interaction with the applied external field B_0 only. The magnetic field at the site of the nuclei k, $\vec{B_k}$ is modified through the electronic environment. This effect, the chemical shift, is excluded from the Zeeman Hamiltonian.

5.2 Interaction With an rf-Field B_1

The interaction with either a *linearly polarized* rf field:

$$\vec{B_1}(t) = B_1(\cos[\omega_{rf} t + \varphi(t)], 0, 0) \qquad [5.3]$$

or a *circularly polarized* rf field:

$$\vec{B_1}(t) = B_1(\cos[\omega_{rf} t + \varphi(t)], \sin[\omega_{rf} t + \varphi(t)], 0) \qquad [5.4]$$

is described, in complete analogy to the Zeeman Hamiltonian (Eq. [5.1]), as

$$\hat{\mathcal{H}}_{rf}(t) = -\sum_i \gamma_i \hat{\vec{I}}_i \cdot \vec{B_1}(t) \qquad [5.5]$$

In multiple-resonance experiments, $\vec{B_1}$ consists of a sum of individual fields.

5.3 Interaction-Frame Representation

An interaction-frame representation is a concept that generalizes the rotating-frame representation that we have discussed earlier. We describe the spin system in an interaction frame with respect to the interaction $\hat{\mathcal{H}}_0 = \sum_i \omega_{rf,i} \hat{I}_{iz}$. Here, $\omega_{rf,i}$ will be chosen close to $\omega_{0,i}$ and $\hat{\mathcal{H}}_0 \approx \hat{\mathcal{H}}_z$. An operator $\hat{A}'$ in the interaction frame of reference is related to the original operator $\hat{A}$ by:

$$\hat{A}' = \hat{R}(t)\hat{A}\hat{R}^{-1}(t) \; . \qquad [5.6]$$

We choose the rotation matrix as

$$\hat{R}(t) = e^{i\hat{\mathcal{H}}_0 t} \qquad [5.7]$$

For the case where only one type of nuclei is considered, we have

$$\hat{\mathcal{H}}_0 = \sum_l \omega_{rf,l} \hat{I}_{lz} = \omega_{rf} \hat{F}_z \qquad [5.8]$$

with the *total spin operator* $\hat{F}_z = \sum_l \hat{I}_{lz}$.

To evaluate the time dependence of the density operator in the rotating frame $\hat{\sigma}'$, we need to know the equivalent of the Liouville-von Neumann equation in the interaction frame. The procedure followed is reminiscent of the transformation to the rotating frame in the classical description. The relationship between $\hat{\sigma}$ and $\hat{\sigma}'$ is given by Eq. [5.6]:

$$\begin{aligned} \hat{\sigma}' &= \hat{R}(t)\hat{\sigma}\hat{R}^{-1}(t) \\ \hat{\sigma} &= \hat{R}^{-1}(t)\hat{\sigma}'\hat{R}(t) \end{aligned} \qquad [5.9]$$

$$\frac{d}{dt}(\hat{R}^{-1}\hat{\sigma}'\hat{R}) = -i[\hat{\mathcal{H}}\hat{R}^{-1}\hat{\sigma}'\hat{R} - \hat{R}^{-1}\hat{\sigma}'\hat{R}\hat{\mathcal{H}}]$$

$$-i\omega_{rf}\hat{F}_z\hat{R}^{-1}\hat{\sigma}'\hat{R} + \hat{R}^{-1}\frac{d}{dt}\hat{\sigma}'\hat{R} + \hat{R}^{-1}\hat{\sigma}'i\omega_{rf}\hat{F}_z\hat{R} = -i[\hat{\mathcal{H}}\hat{R}^{-1}\hat{\sigma}'\hat{R} - \hat{R}^{-1}\hat{\sigma}'\hat{R}\hat{\mathcal{H}}]$$

$$\hat{R}^{-1}\frac{d}{dt}\hat{\sigma}'\hat{R} = -i[\hat{\mathcal{H}}\hat{R}^{-1}\hat{\sigma}'\hat{R} - \hat{R}^{-1}\hat{\sigma}'\hat{R}\hat{\mathcal{H}} - \omega_{rf}(\hat{F}_z\hat{R}^{-1}\hat{\sigma}'\hat{R} - \hat{R}^{-1}\hat{\sigma}'\hat{F}_z\hat{R})]$$

$$\frac{d}{dt}\hat{\sigma}' = -i[\hat{R}\hat{\mathcal{H}}\hat{R}^{-1}\hat{\sigma}' - (\hat{\sigma}'\hat{R}\hat{\mathcal{H}}\hat{R}^{-1} - \omega_{rf}(\hat{F}_z\hat{\sigma}' - \hat{\sigma}'\hat{F}_z))]$$

$$\frac{d}{dt}\hat{\sigma}' = -i[\hat{\mathcal{H}}' - \omega_{rf}\hat{F}_z, \hat{\sigma}'] \qquad [5.10]$$

Here $\hat{\mathcal{H}}' = \hat{R}\hat{\mathcal{H}}\hat{R}^{-1}$ is the transformed Hamiltonian. In going from line 3 to line 4, we have multiplied, from the left with $\hat{R}$ and from the right with $\hat{R}^{-1}$. We have used that $\hat{F}_z$ commutes with $\hat{R}$ because of Eq. [5.8]. Note that the last line in Eq. [5.10] is **not** just equal to the Liouville-van Neumann equation for the dashed operators but that:

$$\frac{d}{dt}\hat{\sigma}' = -i[\hat{\mathcal{H}}' - \hat{\mathcal{H}}_0, \hat{\sigma}'] \qquad [5.11]$$

A new term $-\hat{\mathcal{H}}_0$ appears which represents the fact that the new coordinate system is accelerated with respect to the original coordinate system. Eq. [5.11] is valid irrespective of the choice of $\hat{\mathcal{H}}_0$. Often, the identification $\hat{\mathcal{H}}'' = \hat{\mathcal{H}}' - \hat{\mathcal{H}}_0$ is made and $\hat{\mathcal{H}}''$ is then called the interaction-frame Hamiltonian. Then, we recover the standard Liouville-van Neumann equation:

$$\frac{d}{dt}\hat{\sigma}' = -i[\hat{\mathcal{H}}'', \hat{\sigma}'] \qquad [5.12]$$

Care has to be exercised not to mix up $\hat{\mathcal{H}}'$ and $\hat{\mathcal{H}}''$. By going into the interaction frame, we have not only changed the active Hamiltonian $\hat{\mathcal{H}}''$ but we have also manipulated the time dependence of the Hamiltonian which is described by the Liouville-von Neumann equation.

For the operators $\hat{I}_x$, $\hat{I}_y$ and $\hat{I}_z$, we find:

$$\begin{aligned}\hat{I}'_x &= \hat{I}_x\cos(\omega_{rf}t) + \hat{I}_y\sin(\omega_{rf}t)\\ \hat{I}'_y &= \hat{I}_y\cos(\omega_{rf}t) - \hat{I}_x\sin(\omega_{rf}t)\\ \hat{I}'_z &= \hat{I}_z\end{aligned} \qquad [5.13]$$

If we compare Eq. [5.13] with the expression for the transformation of a classical vector to the rotating frame (Eq. [2.2]) we find that they are fully equivalent.

The rf-Hamiltonian in the interaction frame is given by (for simplicity, we set $\varphi(t) = 0$):

$$\hat{\mathcal{H}}'_{rf} = -\sum_i \gamma_i B_1 \hat{I}'_{ix} \qquad [5.14]$$

For arbitrary values of $\varphi(t)$, we have:

$$\begin{aligned}\hat{\mathcal{H}}'_{rf} &= -\sum_i \gamma_i B_1 (\hat{I}'_x\cos\varphi(t) + \hat{I}'_y\sin\varphi(t))\\ &= \sum_i \omega_{1i} (\hat{I}'_x\cos\varphi(t) + \hat{I}'_y\sin\varphi(t))\end{aligned} \qquad [5.15]$$

Often, the dash in, e.g., $\hat{I}'_x$ is left away. The interaction-frame Hamiltonian $\hat{\mathcal{H}}''$ for a spin system with a lab-frame Hamiltonian of $\hat{\mathcal{H}} = \hat{\mathcal{H}}_z + \hat{\mathcal{H}}_{rf}$ is given by:

$$\hat{\mathcal{H}}'' = \hat{\mathcal{H}}'_{rf} + \Omega\hat{F}_z \qquad [5.16]$$

where $\Omega = \omega_0 - \omega_{rf}$ and for $\Omega = 0$ by

$$\hat{\mathcal{H}}'' = \hat{\mathcal{H}}'_{rf}. \qquad [5.17]$$

Box V: Rotating Frame

By transforming into the rotating frame, we have:

- Changed the Hamiltonian, i.e., for $\omega_{rf} = \omega_0$, we have removed the Zeeman term.
- Removed the time-dependence from the rf Hamiltonian.
- Usually, the remaining time-dependent terms are neglected. This approximation is called the secular approximation and must be justified on a case-by-case basis.

5.4 The Chemical-Shift or Chemical-Shielding Hamiltonian

The magnetic field at the site of different nuclei k, $\vec{B}_k$ differs from the applied magnetic field, due to the interaction with the surrounding electrons. It is *shielded* by the electrons and leads to a *shift* of the resonance line in the NMR spectrum. We express the field at the position of the nucleus as

$$\vec{B}_k = \vec{B}_0 + \vec{B}_S \qquad [5.18]$$

The correction field $\vec{B}_S$ is proportional to the static field $\vec{B}_0$ and we can write:

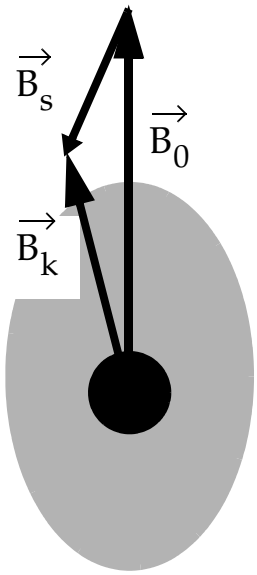

Figure 5.1: Local B Field

$$\begin{bmatrix} B_{S,x} \\ B_{S,y} \\ B_{S,z} \end{bmatrix} = -\begin{bmatrix} \sigma_{xx}^{(k)} & \sigma_{xy}^{(k)} & \sigma_{xz}^{(k)} \\ \sigma_{yx}^{(k)} & \sigma_{yy}^{(k)} & \sigma_{yz}^{(k)} \\ \sigma_{zx}^{(k)} & \sigma_{zy}^{(k)} & \sigma_{zz}^{(k)} \end{bmatrix} \begin{bmatrix} 0 \\ 0 \\ B_0 \end{bmatrix} \qquad [5.19]$$

The Hamiltonian that describes the interaction with the correction field is, therefore, given by

$$\hat{\mathcal{H}}_S = \sum_k \gamma_k (\hat{I}_{kx}, \hat{I}_{ky}, \hat{I}_{kz}) \begin{bmatrix} \sigma_{xx}^{(k)} & \sigma_{xy}^{(k)} & \sigma_{xz}^{(k)} \\ \sigma_{yx}^{(k)} & \sigma_{yy}^{(k)} & \sigma_{yz}^{(k)} \\ \sigma_{zx}^{(k)} & \sigma_{zy}^{(k)} & \sigma_{zz}^{(k)} \end{bmatrix} \begin{bmatrix} 0 \\ 0 \\ B_0 \end{bmatrix} \qquad [5.20]$$

or, in compact form:

$$\hat{\mathcal{H}}_S = \sum_k \gamma_k \vec{\hat{I}}_k \cdot \underline{\sigma}^{(k)} \cdot \vec{B}_0 \qquad [5.21]$$

The resulting Hamiltonian is a scalar operator. The quantity $\underline{\sigma}$ is the anisotropic chemical-shielding tensor (*CSA*).

In the interaction frame (high-field approximation), the transverse terms $\hat{I}'_x$ and $\hat{I}'_y$ are time-dependent with the Larmor frequency with an average value of zero. They can, therefore, be neglected as "non-secular" terms in a good approximation. In the interaction frame, the chemical-shielding Hamiltonian simplifies to:

$$\hat{\mathcal{H}}'_s = \sum_k \gamma_k \sigma_{zz}^{(k)} B_0 \hat{I}_{kz} \qquad [5.22]$$

The transition frequency in the Hamiltonian is given by $\omega_{12} = -\sigma_{zz}^{(k)}\omega_0$ and the spectrum consists of a single line at position ω_{12} (if given in angular frequencies) or at $-\sigma_{zz}^{(k)}$ if given in ppm. If the three principal values of $\underline{\sigma}^{(k)}$ are identical, we can replace them by a scalar quantity, the so-called isotropic chemical shift, σ_{iso}, times a unity matrix.

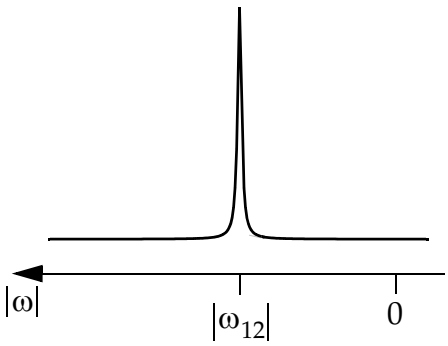

Figure 5.2: Chemical Shift

The isotropic chemical shielding is given by:

$$\sigma_{iso} = \frac{1}{3}(\sigma_{xx} + \sigma_{yy} + \sigma_{zz}) \qquad [5.23]$$

Such an isotropic interaction is also obtained in liquid phase where the tumbling of the molecules leads to an averaged chemical shielding. Here, σ_{iso} takes then the role of $\sigma_{zz}^{(k)}$ in Eq. [5.22].

The isotropic chemical shielding is zero for a bare nucleus. Nuclei in molecules are almost always more shielded than the bare nucleus. They have positive values of the chemical shielding and, therefore, lower resonance frequencies (because $\omega_0 = -\gamma B_0$). Often *chemical shifts* denoted by δ are used instead of the *chemical shielding* σ:

$$\delta = \frac{\sigma_{reference} - \sigma}{1 - \sigma_{reference}} \approx \sigma_{reference} - \sigma \qquad [5.24]$$

The second relationship is usually a very good approximation because shieldings are in the order of some parts per million (ppm). For proton and carbon spectroscopy TMS (tetramethylsilan) is often taken as the reference compound. Protons as well as

carbons are well shielded in this compound and the chemical shifts of most compounds on this scale is positive. It should be noted that NMR spectra of nuclei with a positive γ are conventionally drawn with the frequency axis going from right to left (see Box VI). This is quite natural because the frequencies are negative. Often

Box VI: : Conventions for the Representation of an NMR Spectrum

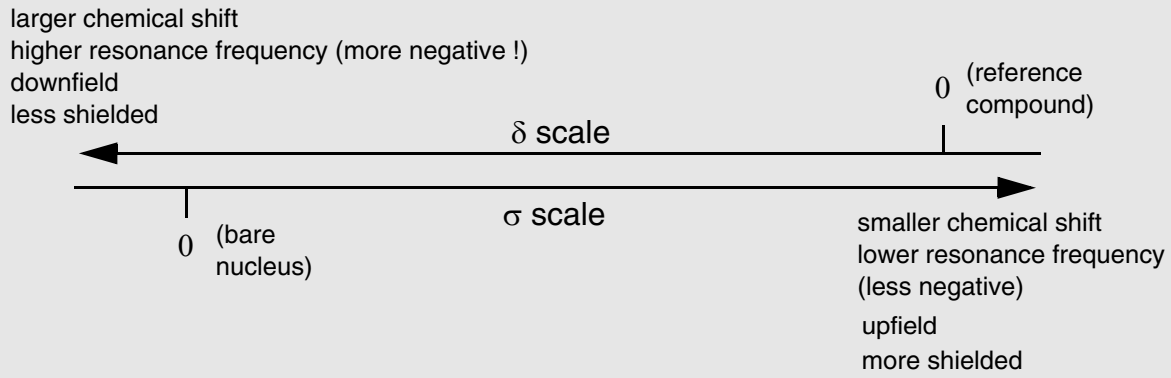

the sign of the frequency is, however, dropped and then it looks like the frequency axis would increase from right to left. Typical values for ^{13}C are given in Box VII.

Box VII: : Typical Chemical-Shift Values For Carbons (Isotropic Values)

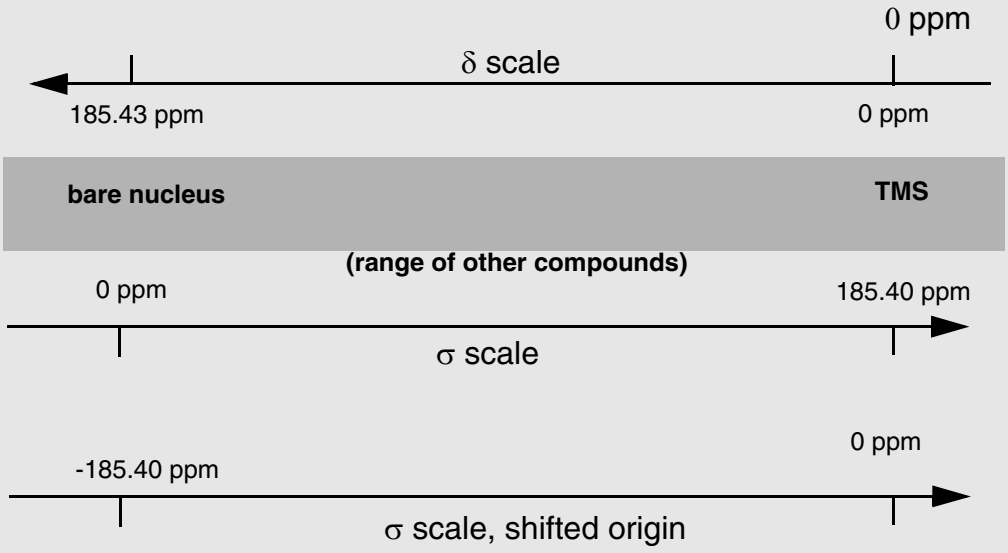

5.4.1 Origin of the Chemical Shielding

The numerical values for the tensor elements of $\underline{\sigma}$ can be calculated by quantum-chemical methods for isolated molecules which are not too large (density-functional methods). We can distinguish four important effects that contribute to the chemical shielding. There are diamagnetic and paramagnetic effects.

5.4.1.1 Diamagnetic Effect

In a magnetic field $\vec{B_0}$ the electron cloud precesses and generates a reaction field $\vec{B_d}$ that counteracts $\vec{B_0}$. This effect is called the *Lamb-Shift*.

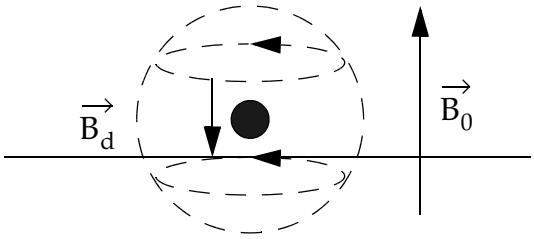

Figure 5.3: Lamb Shift

An elementary calculation using the Biot-Savart law leads to:

$$\sigma_{iso} = \frac{\mu_0 e^2}{3m_e} \int_0^\infty r\rho(\vec{r})dr \qquad [5.25]$$

Note the increasing weight of the electron density $\rho(\vec{r})$ at larger distances r. Differences in the diamagnetic Lamb shift are the dominant effect for observed proton shifts but are less important for the heavier nuclei.

5.4.1.2 Paramagnetic Effect

The paramagnetic effect is caused by a (partial) excitation of the *electrons* (by the magnetic field) into a paramagnetic state. This leads to a amplification of the applied field. Low-lying electronic states

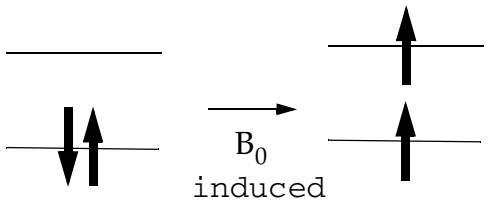

Figure 5.4: Paramagnetic Shift

cause a stronger paramagnetic effect. For the understanding of the isotropic carbon shifts the paramagnetic shift is an important contribution.

	excited states	paramagn. ^{13}C shift	^{13}C shift (TMS)
alkanes	high lying	small	10-50 ppm
alkenes	medium	medium	110-150 ppm
aromatics	medium	medium	110-140 ppm
ketones	low	high	170-230 ppm

5.4.1.3 Ring-Current Effects

A magnetic field can induce a ring-current within a π system. The effect is similar to the Lamb shift except that the current flows through several bonds. The current produces a field of the form shown in the figure. Inside the ring, a diamagnetic effect is observed, outside the ring a paramagnetic effect. The effect is anisotropic and depends on the direction of the field $\vec{B}_0$ with respect to the ring plane.

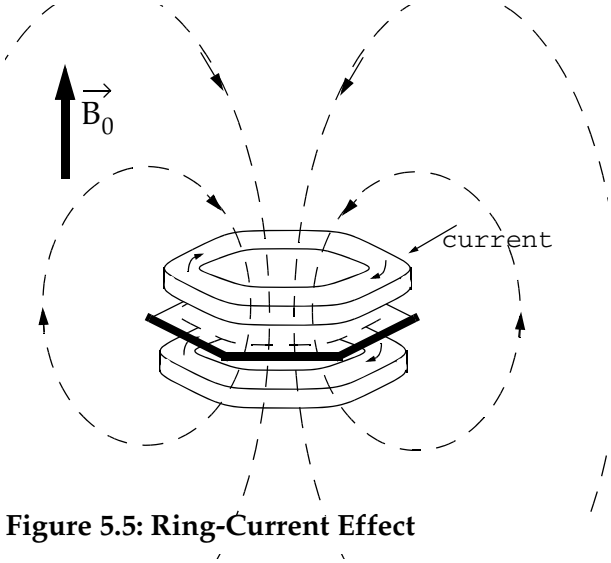

Figure 5.5: Ring-Current Effect

Figure 5.6a shows an example for strong ring-current effects in 15,16-Dihydro,15,16-dimethylpyren on the isotropic chemical shifts. The chemical shifts of protons of the CH_3 groups on top of the rings are shifted upfield to -4.23 ppm while the protons outside the ring are shifted downfield to +8.6 ppm. The proton chemical-shift effects close to a benzene ring as a function of the position are graphically shown in Fig. 5.6b.

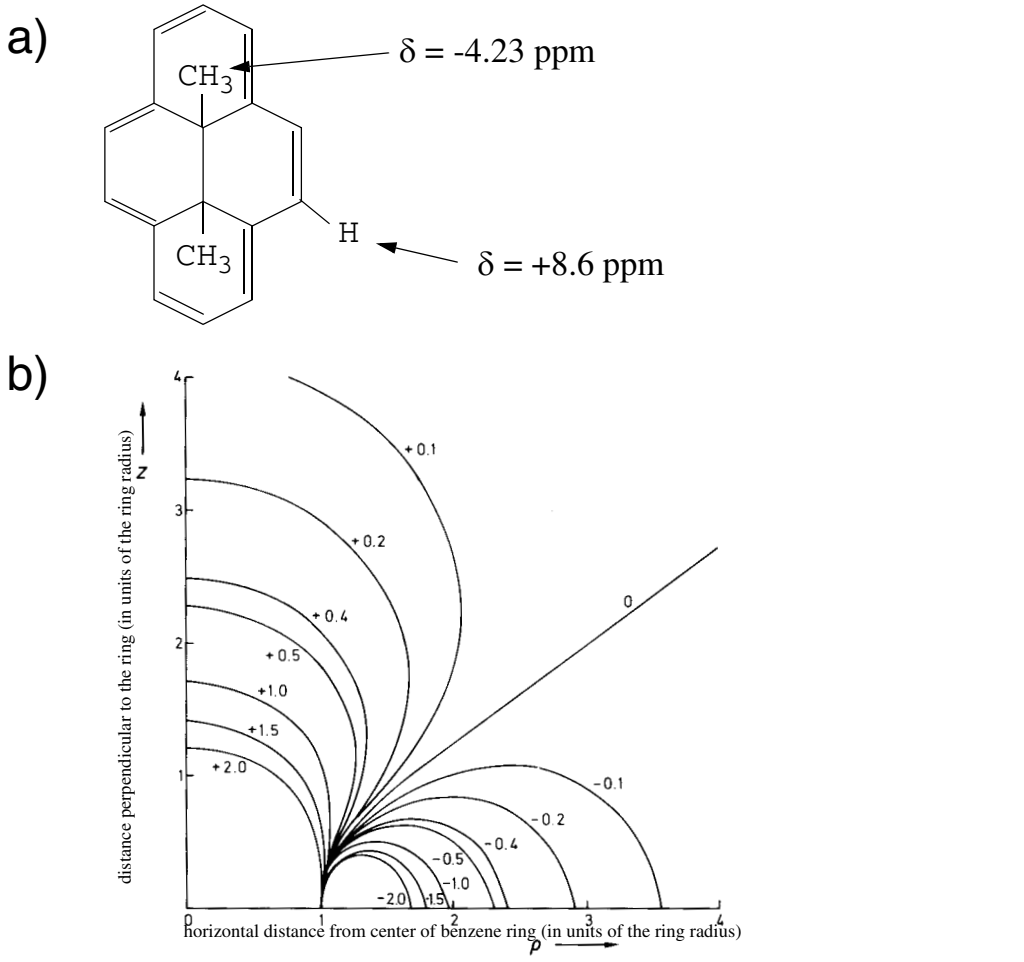

Graphic representation of the influence of the magnetic anisotropy of the benzene ring on proton resonance frequencies (after Ref. 1)
From: H. Günter: "NMR Spectroscopy", Wiley.

Figure 5.6: Ring-Current Effects

5.4.1.4 Anisotropic Neighbor Effect

The electron density centered at a neighboring nucleus polarizes the electron density and leads to an induced dipolar moment $\vec{\mu}_{ind}$. The field of this induced moment at the position of spin S leads to an additional field. If the induced moment has a magnitude which is independent of the direction of $\vec{B}_0$, the effect vanishes in the isotropic average and is only observed in oriented phases, if $|\vec{\mu}_{ind}|$ depends on the direction of the external field, an isotropic contribution arises.

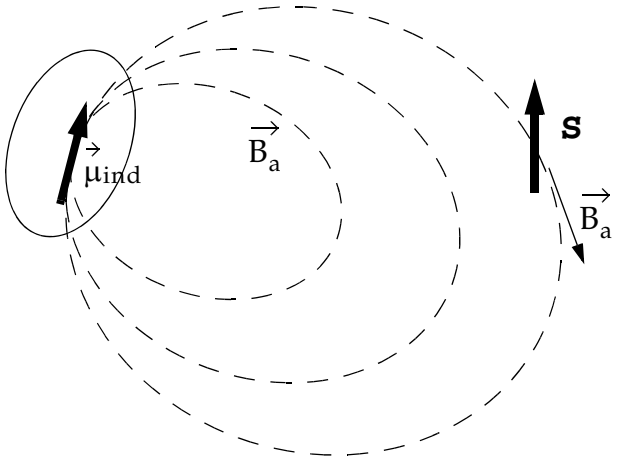

Figure 5.7: Anisotropic Neighbor Effects

Figure 5.8 shows as an example the molecule acetylene. If the axis of the molecule is parallel to the field, a large $\vec{\mu}_{ind}$ is induced leading to a diamagnetic shielding, if the axis is perpendicular, a weak paramagnetic shielding is obtained.

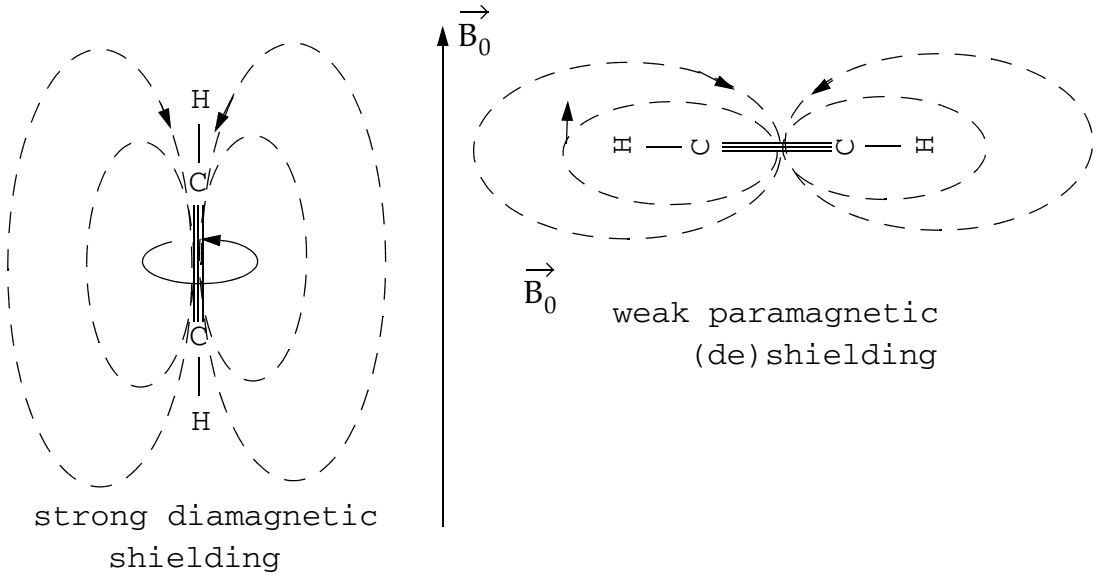

Figure 5.8: Anisotropic Neighbor Effects

5.4.2 Some Examples for Isotropic Chemical-Shift Values

The typical proton chemical-shift range lies between 0 and 11 ppm. For carbons, a range between 0 and 180 ppm is most commonly found. Figure 5.9 shows the typical chemical-shift ranges for protons and carbons found for characteristic groups in organic molecules.

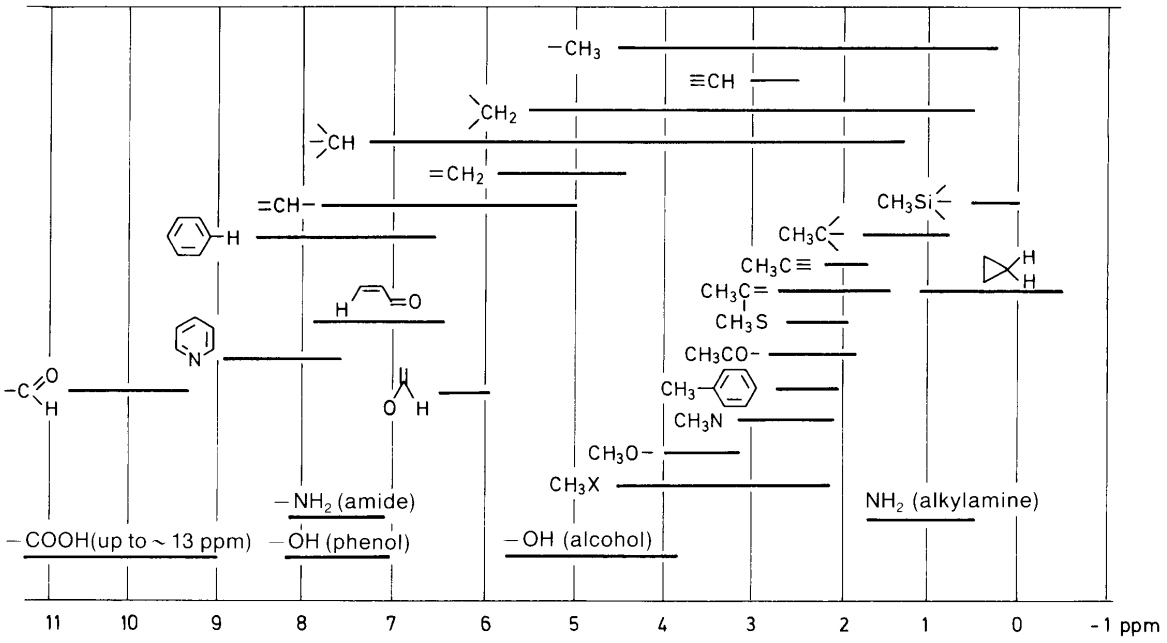

Figure 2.6 δ-Scale of chemical shifts of proton resonances in organic compounds

From: H. Günter: "NMR Spectroscopy", Wiley.

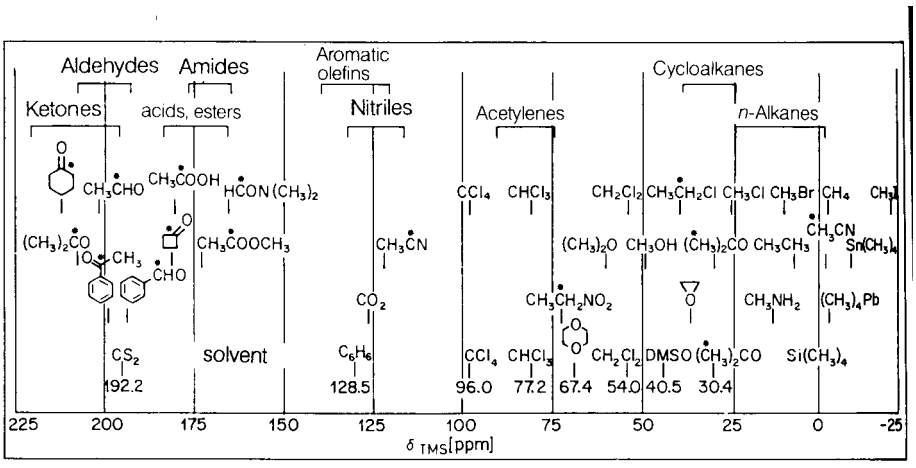

Figure 12.3 ^{13}C chemical shift diagram (Ref. 40)

From: H. Günter: "NMR Spectroscopy", Wiley.

Figure 5.9: Typical Chemical Shifts for protons and Carbons

5.4.3 Single-Crystal Spectra

The resonance frequency is proportional to the zz-element of the shielding tensor in the laboratory frame. Because the chemical shielding tensor is defined with respect to a molecule-fixed coordinate system we must first transform it into the laboratory frame to obtain the resonance frequency by:

$$\underline{\sigma}^{(k)} = R\underline{\sigma}^{(k)}_{MF}R^{-1} \qquad [5.26]$$

A particular molecular fixed coordinate system is the principal axis system (*PAS*), where $\underline{\sigma}$ is diagonal:

$$\underline{\sigma} = \begin{bmatrix} \sigma^{(k)}_{11} & 0 & 0 \\ 0 & \sigma^{(k)}_{22} & 0 \\ 0 & 0 & \sigma^{(k)}_{33} \end{bmatrix} \qquad [5.27]$$

The diagonal values of this matrix are called the *principal values* of the chemical-shielding tensor, the direction of the axis system, *the principal directions*. The ordering of the principal values is chosen such that:

- $\sigma^{(k)}_{11}$ is the least shielded component (see Box VI),
- $\sigma^{(k)}_{33}$ is the most shielded component,
- $\sigma^{(k)}_{22}$ lies in between.

The rotation matrices R that transform from one coordinate system to the other are usually expressed in term of the three Euler angles α, β, γ. The rotation matrix $R(\alpha, \beta, \gamma)$ is constructed from three successive rotations:

$$R(\alpha, \beta, \gamma) = R_{z''}(\gamma) \cdot R_{y'}(\beta) \cdot R_z(\alpha) \qquad [5.28]$$

This convention implies three rotations of the coordinate system:

- first by α around the original z-axis
- second by β around the new y′-axis
- last by γ around the new z″-axis

The original axes (x,y,z) are rotated to the new axis (x″,y″,z″)

The inverse rotation $R(\alpha, \beta, \gamma)^{-1}$ is given by:

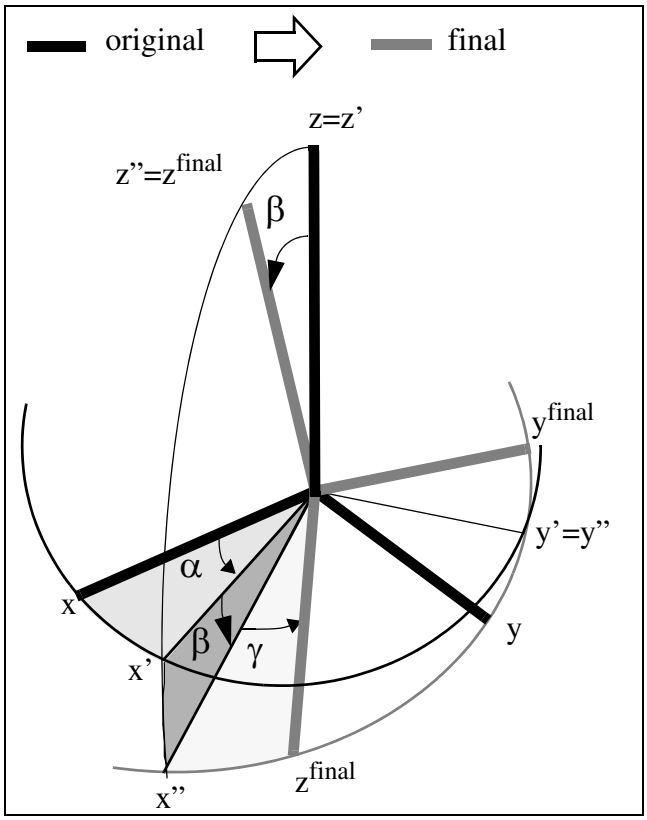

Figure 5.10: Euler-Angle Rotations

$$(R(\alpha, \beta, \gamma))^{-1} = R(-\gamma,-\beta,-\alpha) = R_{z''}(-\alpha) \cdot R_{y'}(-\beta) \cdot R_z(-\gamma) \qquad [5.29]$$

If we transform from the PAS (original) to the Lab (final) system (Fig. 5.11), we call the Euler angles (α, β, γ), if we transform from the Lab (original) to the PAS (final), we call them (φ, θ, χ). They fulfill the relationship:

$$\alpha = -\chi \qquad \beta = -\theta \qquad \gamma = -\varphi \qquad [5.30]$$

$$R(\alpha, \beta, \gamma) = (R(\varphi, \theta, \chi))^{-1}: \qquad [5.31]$$

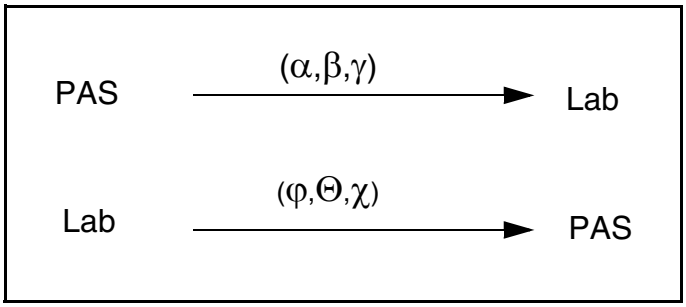

Figure 5.11: Coordinate Transformations

Since the definition of the Euler angles allows only for rotations about the y and z axis, rotations around other axis have to be constructed from these using the sequence:

- Rotation by θ around z-axis: R(0, 0, θ)
- Rotation by θ around y-axis: R(0, θ, 0)
- Rotation by θ around x-axis: R($-\pi/2$, θ, $\pi/2$)

The cartesian matrix representation of R is, for the rotation around the z axis:

$$R_z = \begin{bmatrix} \cos\psi & \sin\psi & 0 \\ -\sin\psi & \cos\psi & 0 \\ 0 & 0 & 1 \end{bmatrix} \qquad [5.32]$$

and around the y-axis:

$$R_y = \begin{bmatrix} \cos\psi & 0 & -\sin\psi \\ 0 & 1 & 0 \\ \sin\psi & 0 & \cos\psi \end{bmatrix} \qquad [5.33]$$

and, therefore, for the combination of the three Euler rotations:

$$R(\alpha, \beta, \gamma) = \begin{bmatrix} \cos\alpha\cos\beta\cos\gamma - \sin\alpha\sin\gamma & \sin\alpha\cos\beta\cos\gamma + \cos\alpha\sin\gamma & -\sin\beta\cos\gamma \\ -\sin\alpha\cos\gamma - \cos\alpha\cos\beta\sin\gamma & -\sin\alpha\cos\beta\sin\gamma + \cos\alpha\cos\gamma & \sin\beta\sin\gamma \\ \cos\alpha\sin\beta & \sin\alpha\sin\beta & \cos\beta \end{bmatrix} \qquad [5.34]$$

5.4.4 Determination of Principal Axes and Principal Values in a Single Crystal

In a single crystal the principal value and the principal directions of the CSA tensor with respect to a crystal-fixed coordinate system can be determined by measuring at least six different, non-degenerate orientations (α, β, γ) of the single crystal with respect to the external field.

In practice, the orientation dependence is measured by rotating the single crystal around an axis perpendicular to the magnetic field and measuring the

spectrum as a function of the rotation angle (e.g. β). An example for such a rotation pattern is given in Fig. 5.12. Usually, 3 rotations around orthogonal axes are performed, in principle, two around non-orthogonal axes are sufficient. The diagram of the resonance frequency as a function of each of the rotation angles is called the *rotation plot* and from these data, the six parameters ($\alpha, \beta, \gamma, \sigma_{11}, \sigma_{22}, \sigma_{33}$) that define the chemical-shielding tensor can be determined.

If the orientation of the molecule with respect to the crystal axis system is known, i.e., if the X-ray or neutron structure is known, the orientation of the CSA in

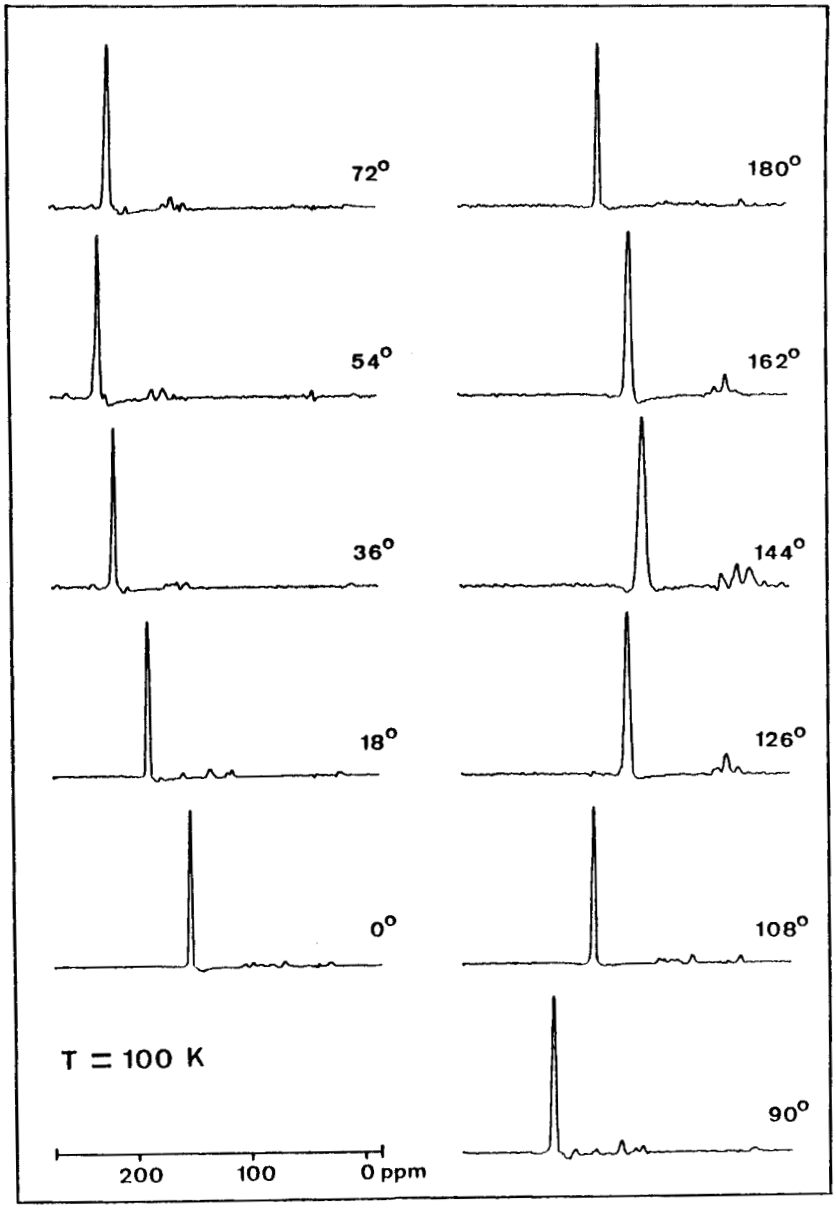

Figure 5.12: ^{13}C spectrum of a benzoic acid single crystal
^{13}C enriched at the carboxylic position, as a function of the rotation angle.

the molecular coordinate system can be calculated. If the orientation of the CSA with respect to the molecular axes is known (see below), the orientation of the molecule in the crystal axes system can be determined.

5.4.5 The Spectrum of a Powder Sample

For a powder sample, the FID (and the spectrum) is the weighted superposition of the possible crystallite orientations:

$$s(t) = \frac{1}{8\pi^2}\int_0^{2\pi}\int_0^{\pi}\int_0^{2\pi} s(\alpha, \beta, \gamma, t)\delta\alpha \sin\beta\delta\beta\delta\gamma \qquad [5.35]$$

Because of the axial symmetry around the direction of the applied field, the last rotation γ which is around the direction of $\vec{B}_0$ does not influence the NMR signal and can be evaluated immediately in the above integral, leading to:

$$s(t) = \frac{1}{4\pi}\int_0^{2\pi}\int_0^{\pi} s(\alpha, \beta, t)\delta\alpha \sin\beta\delta\beta\,. \qquad [5.36]$$

The spectrum of a powdered sample (Fourier transform of Eq. [5.36]) is shown in Fig. 5.13.

From the edges of the powder pattern, the principal values of the CSA tensor can immediately be determined. If two of the principal values are identical, the tensor is called *axially symmetric*.

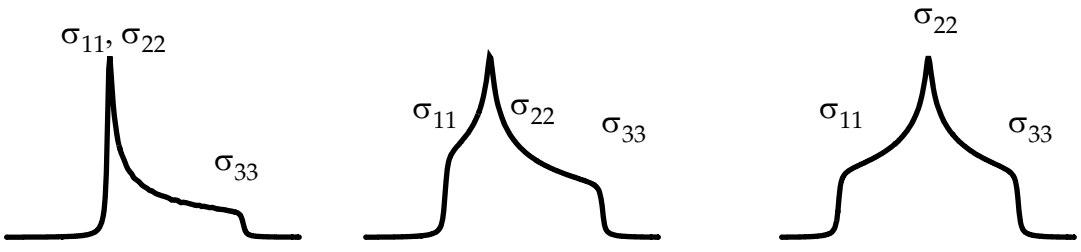

Figure 5.13: Powder patterns observed in solid phase.

Instead of $\sigma_{11}, \sigma_{22}, \sigma_{33}$ one sometimes uses the isotropic value σ_{iso}, the anisotropy δ and the asymmetry η to characterize a tensor:

$$\sigma_{iso} = \frac{1}{3}tr\{\underset{\sim}{\sigma}\} = \frac{1}{3}(\sigma_{xx} + \sigma_{yy} + \sigma_{zz}) \qquad \delta = \sigma_{zz} - \sigma_{iso} \qquad \eta = \frac{\sigma_{yy} - \sigma_{xx}}{\delta} \qquad [5.37]$$

$\sigma_{xx}, \sigma_{yy}, \sigma_{zz}$ are the same as the $\sigma_{11}, \sigma_{22}, \sigma_{33}$ except of the ordering which is done using the convention:

$$|\sigma_{zz} - \sigma_{iso}| \geq |\sigma_{xx} - \sigma_{iso}| \geq |\sigma_{yy} - \sigma_{iso}| \qquad [5.38]$$

Here, $\eta = 0$ denotes an axially symmetric tensor and η varies between 0 and 1. The shape of the tensor is only determined by η while δ gives the width of the pattern and a negative δ leads to the mirror image of the tensor.

The orientation of the principal axes of the CSA tensor with respect to a molecular frame of reference, however, cannot be determined from powder spectra. It is sometimes fixed by symmetry constraints but in general it must either be calculated or estimated using the empirical rules given in Box VIII. The width of the tensors is often in the same order of magnitude as the entire isotropic chemical shift range (examples for ^{13}C see Fig. 5.14)

A partially ordered sample will lead to a different pattern as illustrated in Fig. 5.15.

Box VIII: Empirical rules for the orientation of the ^{13}C tensor principal axis with respect to a molecular coordinate system:

1) Methyl carbons have almost axially symmetric tensor with the unique axis along the local threefold symmetry axis.

The tensor is averaged due to classical or tunnelling motion around the C_3 axis.

2) Ring carbons possess three distinct tensor elements with

- the most shielded axis perpendicular to the plane and
- the least shielded axis bisecting the C-C-C angle of the ring carbons

3) The most shielded direction is

- perpendicular to the ring in aromatic carbons,
- along the C_3 axis for methyl carbons, and
- perpendicular to the sp^2 plane for carbonyl and carboxylic carbons

4) The least shielded direction is

- in the ring plane for carbon rings, bisecting the C-C-C angle,
- perpendicular to the C_3 axis for methyl carbons and perpendicular to a plane of symmetry in which the methyl group is connected
- in the sp^2 plane for carbonyl and carboxyl carbons

5) The intermediately shielded direction is

- tangential to the ring for aromatic carbons,
- for non-averaged methyl groups perpendicular to the C_3 axis in the plane of symmetry,
- in the sp^2 plane and perpendicular to the C-C bond for carboxyl carbons

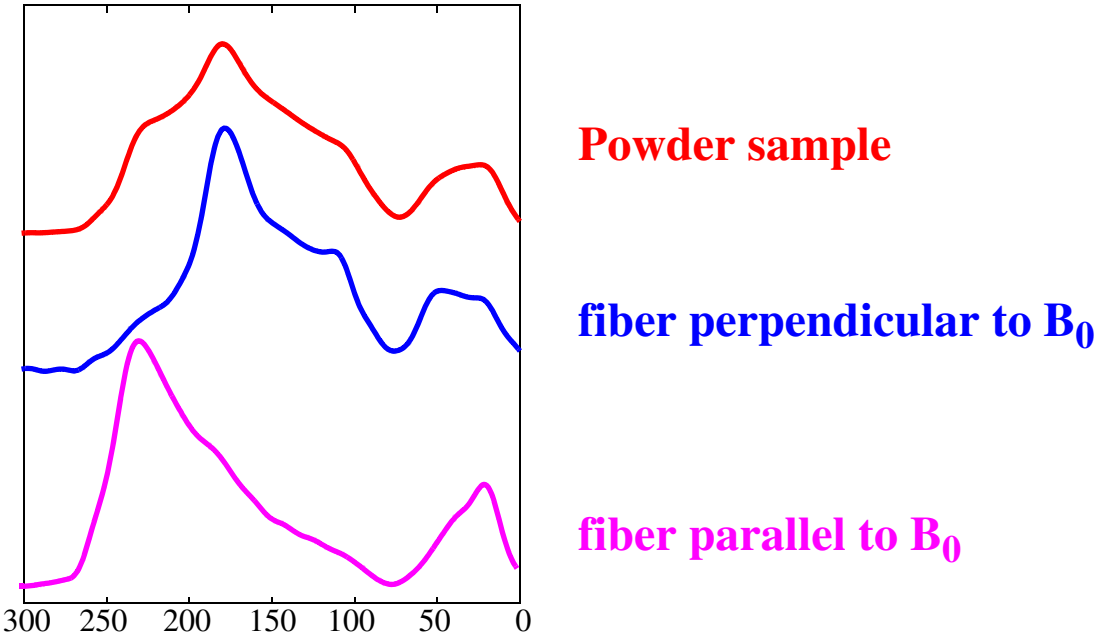

Figure 5.15: ^{13}C Spectra of powdered and uniaxially oriented samples of spider silk (Nephila edulis) (^{13}C enriched at the alanine carboxylic position)

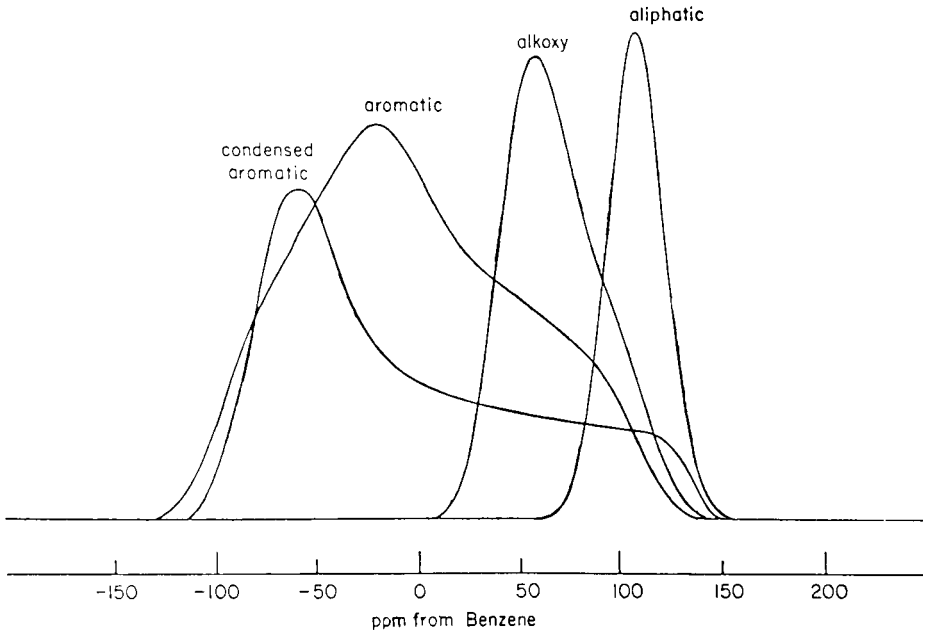

Figure 5.14: Typical ^{13}C Chemical-Shift Tensors

5.5 The Indirect Spin-Spin Coupling (J-Coupling)

Here we consider the coupling between two nuclei which is mediated through the electrons. An exact description is, as in the case of the chemical shielding, a formidable task involving the quantum description of the electrons. If we restrict ourselves to the isotropic coupling, we can write the J-coupling Hamiltonian between two spins in the general form

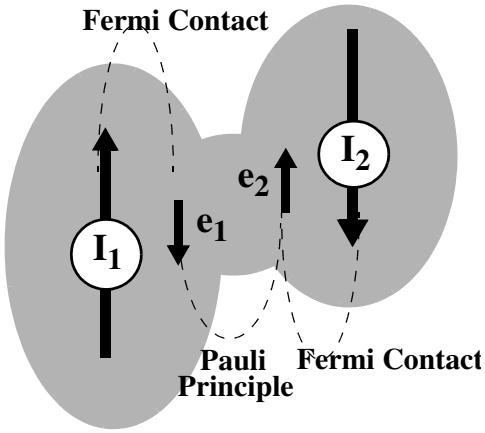

Figure 5.16: J Coupling

$$\hat{\mathcal{H}}_J = 2\pi J_{12} \hat{\vec{I}}_1 \hat{\vec{I}}_2 \qquad [5.39]$$

The coupling constant J_{12} can be obtained by quantum-chemical methods similar to the chemical shieldings. In general, the J coupling will be anisotropic, but the anisotropy is seldom of practical significance and we neglect it here.

Note that the J-coupling Hamiltonian is the same in the laboratory frame and in the rotating frame

$$\hat{\mathcal{H}}'_J = \hat{\mathcal{H}}_J \qquad [5.40]$$

for homonuclear spins because the scalar product of two vectors is independent of the coordinate system the two individual vectors are described in. For heteronuclear spins, the rotating-frame Hamiltonian is given by

$$\hat{\mathcal{H}}'_J = 2\pi J_{12} \hat{I}_{1z} \hat{I}_{2z} \; . \qquad [5.41]$$

One contribution to the indirect spin-spin coupling is the Fermi contact interaction between electrons and nuclei. This interaction is proportional to the probability density of the electron at the nuclear position:

$$J = \frac{3\mu_0}{4\pi} \beta\gamma\delta(\vec{r_e} - \vec{r_N}) \; . \qquad [5.42]$$

The Fermi-contact interaction favors an antiparallel orientation of a nuclear spin. Through the correlation of the spins of two electrons in the same bonding orbital (Pauli principle), this leads to an (opposite) polarization of the other electron. As a consequence, the energy of a system with two spins that share an electron pair depends on the relative orientation of the two spins. An antiparallel arrangement is favored. Note that the Fermi-contact interaction is isotropic: it does not depend on the orientation of the molecules in the magnetic field.

For a multi-spin system, the J Hamiltonian is just the sum of the individual two-spin interactions

$$\hat{\mathcal{H}}_J = 2\pi \sum_{i<j} J_{ij} \hat{\vec{I}}_i \hat{\vec{I}}_i \quad . \qquad [5.43]$$

No term with more than two spin operators appears! This is a general property of NMR Hamiltonians, only *one-particle interactions* (e.g. chemical shift) and *two-particle interactions* (e.g. J coupling) must be taken into account.

For a one-bond coupling between two like spins, J is usually positive (see Fig. 5.16) leading to antiparallel spins in the ground state, for a two-bond coupling, J is often negative because the exchange integral of overlapping orbitals favors parallel electron spins.

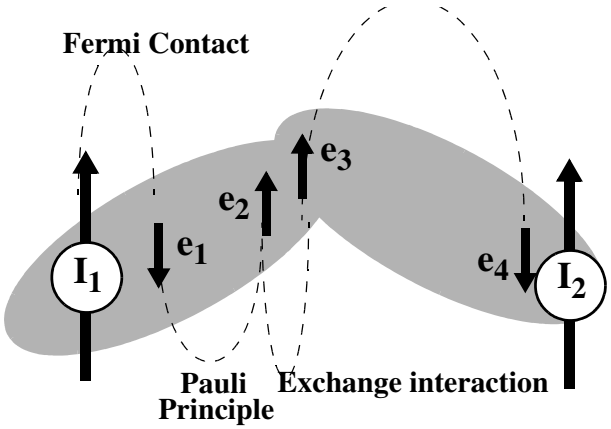

Figure 5.17: J Coupling

These rule are, however, only valid, if the Fermi contact interaction is the dominant source for the indirect coupling, e.g. for proton-proton couplings but not for fluorine-fluorine couplings. There is another source for J-coupling interactions: a dipolar interaction between the nuclear and electron spins, combined again with the Pauli principle. This mechanism provides a source for anisotropic J interactions. The anisotropy plays, however, no

important role except for very heavy nuclei. Typical values for isotropic J couplings are:

spins involved	J
H-H	280 Hz
H-C-**H** (“geminal”)	8-12 Hz
H-C-C-**H** (“vicinal”)	0-10 Hz
H-C-**F**	40-80 Hz
F-C-**F**	150-270 Hz
H-^{13}**C**	100-250 Hz
H-C-^{13}**C**	0-60 Hz
^{13}**C**-^{13}**C**	30-80 Hz
^{15}**N**-^{13}**C**	2-20 Hz
^{1}**H**-^{15}**N**	70-110 Hz

Multi-bond couplings are usually dependent on the conformation of the molecule and are an important source for structural information. For vicinal protons (3-bond coupling), the *Karplus relation* for the dihedral angle ϑ holds:

$$J_{iso}^{vic} = A\cos^2\varphi + B\cos\varphi + C \qquad [5.44]$$

where, for two carbons in between the protons one possible parametrisation is A = 9, B = -0.5 C = -0.28.

5.6 Spectrum of a Two-Spin System in Liquid Phase

In isotropic liquid phase, the isotropic chemical shift and the J coupling are the only interactions necessary to describe the spin system. The Hamiltonian in the laboratory frame of reference is given by the Zeeman term (Eq. [5.2]) the chemical-shielding term (Eq. [5.21]) and the J coupling (Eq. [5.43]).

$$\begin{aligned}\hat{\mathcal{H}} &= \hat{\mathcal{H}}_Z + \hat{\mathcal{H}}_S + \hat{\mathcal{H}}_J \\ &= \omega_0(\hat{I}_{1z} + \hat{I}_{2z}) - \omega_0(\sigma_{iso}^{(1)} \cdot \hat{I}_{1z} + \sigma_{iso}^{(2)} \cdot \hat{I}_{2z}) + 2\pi J_{12}\vec{\hat{I}}_1\vec{\hat{I}}_2\end{aligned} \qquad [5.45]$$

In the rotating frame, we have

$$\hat{\mathcal{H}}'' = \Omega_1 \cdot \hat{I}_{1z} + \Omega_2 \cdot \hat{I}_{2z} + 2\pi J_{12}\vec{\hat{I}}_1\vec{\hat{I}}_2 \qquad [5.46]$$

where Ω_1 and Ω_2 are the rotating frame frequencies of the two nuclei $\Omega_i = (1 - \sigma_{iso}^{(i)})\omega_0 - \omega_{rf}$. The Ω_i can be interpreted as the chemical shifts of the nuclei (in angular frequencies, not in ppm) measured with respect to the rf irradiation frequency.

We now calculate the spectrum after a $(\pi/2)_y$ pulse following the steps outlined in Box IV for the schematic pulse sequence shown in Fig. 5.18

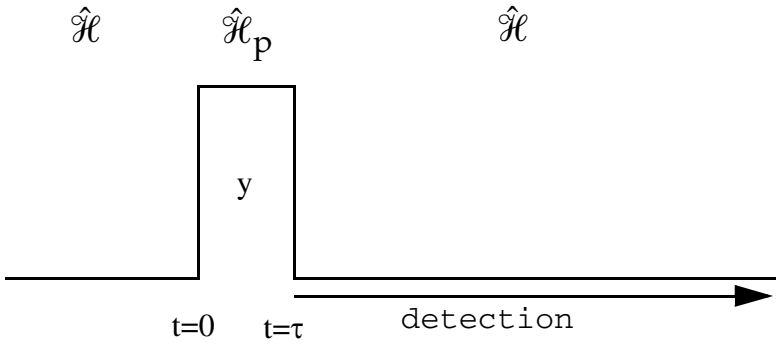

Figure 5.18: Simple 1D Pulse Sequence

I) The Hamiltonian before and after the pulse is given by $\hat{\mathcal{H}}$ of Eqs. [5.45] and [5.46] in the laboratory or rotating frame, respectively. During the pulse, the Hamiltonian is given in the rotating frame by

$$\hat{\mathcal{H}}_p'' = \Omega_1 \cdot \hat{I}_{1z} + \Omega_2 \cdot \hat{I}_{2z} + 2\pi J_{12}\vec{\hat{I}}_1\vec{\hat{I}}_2 + \omega_1(\hat{I}_{1y} + \hat{I}_{2y}) \approx \omega_1(\hat{I}_{1y} + \hat{I}_{2y}) \qquad [5.47]$$

if we assume that the rf-field amplitudes are much stronger than all the internal interactions.

II) The initial density operator is given by $\hat{\sigma}_0 = c \cdot \hat{\mathcal{H}}$ (see Eq. [4.64]). $\hat{\mathcal{H}}$ is the laboratory-frame Hamiltonian and in a good approximation we only need to consider the dominant Zeeman term:

$$\hat{\sigma}_0 = c \cdot (\hat{I}_{1z} + \hat{I}_{2z}) \qquad [5.48]$$

Here, c is a proportionality factor and the part of the density operator proportional to the unity operator has been omitted as discussed in Chapter 4.14.

Note that the initial density operator $\hat{\sigma}_0' = \hat{\sigma}_0$ and the rotating-frame Hamiltonian $\hat{\mathcal{H}}_p''$ only consist of one-spin terms. We can, therefore, evaluate the evolution during the pulse for each of the spins separately.
The initial density operator in matrix representation is:

$$\hat{\sigma}'_0 = c\begin{bmatrix} 1/2 & 0 \\ 0 & -1/2 \end{bmatrix} \qquad [5.49]$$

while the Hamiltonian during the pulse is given by:

$$\mathcal{H}''_p = \omega_1\begin{bmatrix} 0 & -i/2 \\ i/2 & 0 \end{bmatrix} . \qquad [5.50]$$

We can now calculate $\hat{\sigma}'(\tau)$ by application of the Liouville van Neumann equation:

$$\begin{aligned} \hat{\sigma}'(\tau) &= \exp(-i\hat{\mathcal{H}}''_p\tau)\hat{\sigma}'_0\exp(i\hat{\mathcal{H}}''_p\tau) \\ &= c \cdot \exp\left(-i\omega_1\tau\begin{bmatrix} 0 & -i/2 \\ i/2 & 0 \end{bmatrix}\right)\begin{bmatrix} 1/2 & 0 \\ 0 & -1/2 \end{bmatrix}\exp\left(i\omega_1\tau\begin{bmatrix} 0 & -i/2 \\ i/2 & 0 \end{bmatrix}\right) . \end{aligned} \qquad [5.51]$$

We calculate e^M according to

$$e^M = R^{-1}e^{RMR^{-1}}R \qquad [5.52]$$

where $RMR^{-1} = \Lambda$ is the transformation into the eigenbase of M where Λ is a diagonal matrix. For diagonal matrices, we know that:

$$\exp\begin{bmatrix} \Lambda_{11} & 0 \\ 0 & \Lambda_{22} \end{bmatrix} = \begin{bmatrix} e^{\Lambda_{11}} & 0 \\ 0 & e^{\Lambda_{22}} \end{bmatrix} . \qquad [5.53]$$

Therefore, we need to diagonalize the matrix

$$\begin{bmatrix} 0 & -i/2 \\ i/2 & 0 \end{bmatrix}. \qquad [5.54]$$

The eigenvalues are obtained as solutions of

$$E^2 - \left(-\frac{i}{2}\right) \cdot \frac{i}{2} = E^2 - \frac{1}{4} = 0 \quad ; \qquad E = \pm\frac{1}{2} \qquad [5.55]$$

and the transformation is found (by determining the eigenvectors) as:

$$\frac{1}{\sqrt{2}}\begin{bmatrix} i & 1 \\ -i & 1 \end{bmatrix}\begin{bmatrix} 0 & -i/2 \\ i/2 & 0 \end{bmatrix}\begin{bmatrix} -i & i \\ 1 & 1 \end{bmatrix}\frac{1}{\sqrt{2}} = \begin{bmatrix} 1/2 & 0 \\ 0 & -1/2 \end{bmatrix} \qquad [5.56]$$

Now we can determine $e^{-i\omega_1\tau\hat{I}_y}$ as:

$$\frac{1}{2}\begin{bmatrix} -i & i \\ 1 & 1 \end{bmatrix}\begin{bmatrix} e^{-\frac{i\omega_1\tau}{2}} & 0 \\ 0 & e^{\frac{i\omega_1\tau}{2}} \end{bmatrix}\begin{bmatrix} i & 1 \\ -i & 1 \end{bmatrix} = \begin{bmatrix} \cos\frac{\omega_1\tau}{2} & -\sin\frac{\omega_1\tau}{2} \\ \sin\frac{\omega_1\tau}{2} & \cos\frac{\omega_1\tau}{2} \end{bmatrix} \qquad [5.57]$$

and the density operator after the pulse is given by

$$\hat{\sigma}'(\tau) = c\begin{bmatrix} \cos\frac{\omega_1\tau}{2} & -\sin\frac{\omega_1\tau}{2} \\ \sin\frac{\omega_1\tau}{2} & \cos\frac{\omega_1\tau}{2} \end{bmatrix}\begin{bmatrix} \frac{1}{2} & 0 \\ 0 & -\frac{1}{2} \end{bmatrix}\begin{bmatrix} \cos\frac{\omega_1\tau}{2} & \sin\frac{\omega_1\tau}{2} \\ -\sin\frac{\omega_1\tau}{2} & \cos\frac{\omega_1\tau}{2} \end{bmatrix} = \frac{c}{2}\begin{bmatrix} \cos\omega_1\tau & \sin\omega_1\tau \\ \sin\omega_1\tau & -\cos\omega_1\tau \end{bmatrix}. \qquad [5.58]$$

We call $\beta = \omega_1\tau$ the flip angle of the pulse which we chose to be $\beta = \omega_1\tau = \pi/2$. Then we obtain for the density operator after the $\frac{\pi}{2}$ pulse

$$\hat{\sigma}'(\tau) = c\begin{bmatrix} 0 & 1/2 \\ 1/2 & 0 \end{bmatrix} = c\hat{I}_x \qquad [5.59]$$

To evaluate the NMR signal during detection, we need the two-spin Hamiltonian $\mathcal{H}'' = \Omega_1 \cdot \hat{I}_{1z} + \Omega_2 \cdot \hat{I}_{2z} + 2\pi J_{12}\hat{\vec{I}}_1\hat{\vec{I}}_2$. To calculate the matrix representation of this two-spin Hamiltonian, we need to know how to calculate the matrix representation of products and sums of spin operators. These rules are summarized in Box IX.

Box IX: Direct Product and Direct Sum of Spin Operators

- Let $\hat{A}$ and $\hat{B}$ be operators that act on the same spin.
- The matrix product is defined as $(A \cdot B) = (A) \cdot (B)$, normal matrix product.
- The matrix sum $(A + B) = (A) + (B)$, normal element-wise matrix sum. Note, both matrices have to be expressed in the same basis system.
- Let $\hat{A}$ and $\hat{B}$ be operators that act on different spins. The spin space where $\hat{A}$ is defined (e.g. spin 1) has dimension N, the one of $\hat{B}$ dimension M.
- The matrix product is defined as $(A \cdot B) = (A) \otimes (B)$, the direct matrix product:

$$(A \cdot C) = \begin{bmatrix} a_{11}(C) & .... & a_{1N}(C) \\ .... & .... & .... \\ a_{N1}(C) & .... & a_{NN}(C) \end{bmatrix} = \begin{bmatrix} \begin{bmatrix} a_{11}c_{11} & .... & a_{11}c_{1M} \\ .... & .... & .... \\ a_{11}c_{M1} & .... & a_{11}c_{MM} \end{bmatrix} & .... & \begin{bmatrix} a_{1N}c_{11} & .... & a_{1N}c_{1M} \\ .... & .... & .... \\ a_{1N}c_{M1} & .... & a_{1N}c_{MM} \end{bmatrix} \\ .... & .... & .... \\ \begin{bmatrix} a_{N1}c_{11} & .... & a_{N1}c_{1M} \\ .... & .... & .... \\ a_{N1}c_{M1} & .... & a_{N1}c_{MM} \end{bmatrix} & .... & \begin{bmatrix} a_{NN}c_{11} & .... & a_{NN}c_{1M} \\ .... & .... & .... \\ a_{NN}c_{M1} & .... & a_{NN}c_{MM} \end{bmatrix} \end{bmatrix} \quad [5.60]$$

- The matrix sum is defined as $(A + B) = (A) \otimes (E_2) + (E_1) \otimes (B)$ where (E_1) and (E_2) are identity matrices of dimension N and M respectively.

The matrix representation of the density operator

$$\hat{\sigma}(\tau) = c((\hat{I}_{1x}) \otimes (E_2) + (E_1) \otimes (\hat{I}_{2x})) \quad [5.61]$$

in the combined two-spin Hilbert space of both spins (of dimension $2x2 = 4$) is given by

$$\sigma'(\tau) = c \begin{bmatrix} 0 & 1/2 & 1/2 & 0 \\ 1/2 & 0 & 0 & 1/2 \\ 1/2 & 0 & 0 & 1/2 \\ 0 & 1/2 & 1/2 & 0 \end{bmatrix}. \quad [5.62]$$

The basis functions of the combined Hilbert space of two spin 1/2 are $|\alpha_1\alpha_2\rangle$, $|\alpha_1\beta_2\rangle$, $|\beta_1\alpha_2\rangle$ and $|\beta_1\beta_2\rangle$.

The Hamiltonian is given by:

$$\mathcal{H}'' = \Omega_1((\hat{I}_{1z}) \otimes (E_2)) + \Omega_2((E_1) \otimes (\hat{I}_{2z})) + 2\pi J((\hat{I}_{1x}) \otimes (\hat{I}_{2x}) + (\hat{I}_{1y}) \otimes (\hat{I}_{2y}) + (\hat{I}_{1z}) \otimes (\hat{I}_{2z})) \quad [5.63]$$

or, in matrix representation:

$$\mathcal{H}'' = \Omega_1 \begin{bmatrix} 1/2 & 0 & 0 & 0 \\ 0 & 1/2 & 0 & 0 \\ 0 & 0 & -1/2 & 0 \\ 0 & 0 & 0 & -1/2 \end{bmatrix} + \Omega_2 \begin{bmatrix} 1/2 & 0 & 0 & 0 \\ 0 & -1/2 & 0 & 0 \\ 0 & 0 & 1/2 & 0 \\ 0 & 0 & 0 & -1/2 \end{bmatrix} + 2\pi J \begin{bmatrix} 1/4 & 0 & 0 & 0 \\ 0 & -1/4 & 1/2 & 0 \\ 0 & 1/2 & -1/4 & 0 \\ 0 & 0 & 0 & 1/4 \end{bmatrix}$$

$$= \begin{bmatrix} \frac{\Omega_1 + \Omega_2}{2} + \frac{\pi J}{2} & 0 & 0 & 0 \\ 0 & \frac{\Omega_1 - \Omega_2}{2} - \frac{\pi J}{2} & \pi J & 0 \\ 0 & \pi J & \frac{\Omega_2 - \Omega_1}{2} - \frac{\pi J}{2} & 0 \\ 0 & 0 & 0 & \frac{-(\Omega_1 + \Omega_2)}{2} + \frac{\pi J}{2} \end{bmatrix} \quad [5.64]$$

The detection operator is given by $\hat{M}_x = \gamma(\hat{I}_{1x} + \hat{I}_{2x}) = \gamma\hat{F}_x$ (see Eq. [4.56]) which has a matrix representation of

$$(\hat{F}_x) = \begin{bmatrix} 0 & 1/2 & 1/2 & 0 \\ 1/2 & 0 & 0 & 1/2 \\ 1/2 & 0 & 0 & 1/2 \\ 0 & 1/2 & 1/2 & 0 \end{bmatrix}. \quad [5.65]$$

If all matrices were in the eigenbase of the Hamiltonian, the NMR signal could easily be evaluated by:

$$\langle \hat{M}_x \rangle(t) = \gamma \sum_k \sum_l \sigma'_{kl}(\tau)(F_x)_{lk} \exp(-i\omega_{kl}t) \quad [5.66]$$

with the four transition frequencies $\omega_{kl} = (\mathcal{H}'')_{kk} - (\mathcal{H}'')_{ll}$ and the intensities $\gamma\sigma'_{kl}(\tau)(F_x)_{lk}$ which, in our specific experiment, evaluate to $c\gamma(F_x)^2_{lk}$ because $\hat{\sigma}(\tau) = \hat{F}_x$. To diagonalize the Hamiltonian

$$\begin{bmatrix} \frac{\Omega_1+\Omega_2}{2}+\frac{\pi J}{2} & 0 & 0 & 0 \\ 0 & \frac{\Omega_1-\Omega_2}{2}-\frac{\pi J}{2} & \pi J & 0 \\ 0 & \pi J & \frac{\Omega_2-\Omega_1}{2}-\frac{\pi J}{2} & 0 \\ 0 & 0 & 0 & \frac{-(\Omega_1+\Omega_2)}{2}+\frac{\pi J}{2} \end{bmatrix} \qquad [5.67]$$

we only need to diagonalize the center 2x2 block.Using the general relation for 2x2 matrices:

$$\begin{bmatrix} \cos\alpha & \sin\alpha \\ -\sin\alpha & \cos\alpha \end{bmatrix} \begin{bmatrix} a & b \\ b & c \end{bmatrix} \begin{bmatrix} \cos\alpha & -\sin\alpha \\ \sin\alpha & \cos\alpha \end{bmatrix} = \begin{bmatrix} E_2 & 0 \\ 0 & E_3 \end{bmatrix} \qquad 2\alpha = \operatorname{atan}\left(\frac{2b}{a-c}\right) \qquad [5.68]$$

where α is given by $2\alpha = \operatorname{atan}\left(\frac{2\pi J}{\Omega_1-\Omega_2}\right)$ we obtain

$$\mathcal{H}'' = \begin{bmatrix} \frac{\Omega_1+\Omega_2}{2}+\frac{\pi J}{2} & 0 & 0 & 0 \\ 0 & -\frac{\pi J}{2}+S & 0 & 0 \\ 0 & 0 & -\frac{\pi J}{2}-S & 0 \\ 0 & 0 & 0 & \frac{-(\Omega_1+\Omega_2)}{2}+\frac{\pi J}{2} \end{bmatrix} \qquad [5.69]$$

with

$$S = \sqrt{\left(\frac{\Omega_1-\Omega_2}{2}\right)^2+(\pi J)^2}\ . \qquad [5.70]$$

Transforming the detection operator into the eigenbase of the Hamiltonian using the 4x4 transformation matrix

$$U = \begin{bmatrix} 1 & 0 & 0 & 0 \\ 0 & \cos\alpha & \sin\alpha & 0 \\ 0 & -\sin\alpha & \cos\alpha & 0 \\ 0 & 0 & 0 & 1 \end{bmatrix} \qquad [5.71]$$

leads to

$$\hat{U}\hat{F}_x\hat{U}^{-1} = \begin{bmatrix} 0 & \frac{\cos\alpha+\sin\alpha}{2} & \frac{\cos\alpha-\sin\alpha}{2} & 0 \\ \frac{\cos\alpha+\sin\alpha}{2} & 0 & 0 & \frac{\cos\alpha+\sin\alpha}{2} \\ \frac{\cos\alpha-\sin\alpha}{2} & 0 & 0 & \frac{\cos\alpha-\sin\alpha}{2} \\ 0 & \frac{\cos\alpha+\sin\alpha}{2} & \frac{\cos\alpha-\sin\alpha}{2} & 0 \end{bmatrix} \qquad [5.72]$$

and we obtain the intensities of the four "allowed" single-quantum transitions:

frequency	intensity
$\omega_{12} = \frac{\Omega_1+\Omega_2}{2} + \pi J - \sqrt{\left(\frac{\Omega_2-\Omega_1}{2}\right)^2 + (\pi J)^2}$	$I_{12} = \left(\frac{\cos\alpha+\sin\alpha}{2}\right)^2 = \frac{1+\sin 2\alpha}{4}$
$\omega_{13} = \frac{\Omega_1+\Omega_2}{2} + \pi J + \sqrt{\left(\frac{\Omega_2-\Omega_1}{2}\right)^2 + (\pi J)^2}$	$I_{13} = \left(\frac{\cos\alpha-\sin\alpha}{2}\right)^2 = \frac{1-\sin 2\alpha}{4}$
$\omega_{24} = \frac{\Omega_1+\Omega_2}{2} - \pi J + \sqrt{\left(\frac{\Omega_2-\Omega_1}{2}\right)^2 + (\pi J)^2}$	$I_{24} = \left(\frac{\cos\alpha+\sin\alpha}{2}\right)^2 = \frac{1+\sin 2\alpha}{4}$
$\omega_{34} = \frac{\Omega_1+\Omega_2}{2} - \pi J - \sqrt{\left(\frac{\Omega_2-\Omega_1}{2}\right)^2 + (\pi J)^2}$	$I_{34} = \left(\frac{\cos\alpha-\sin\alpha}{2}\right)^2 = \frac{1-\sin 2\alpha}{4}$

For the particular solution we have assumed that α is positive. In principle one should distinguish according to the sign of J.

The basis functions that span the eigenbase of the Hamiltonian are

$$\begin{gathered} |\alpha_1\alpha_2\rangle \\ \cos\alpha|\alpha_1\beta_2\rangle + \sin\alpha|\beta_1\alpha_2\rangle \\ -\sin\alpha|\alpha_1\beta_2\rangle + \cos\alpha|\beta_1\alpha_2\rangle \\ |\beta_1\beta_2\rangle \end{gathered} \quad . \qquad [5.73]$$

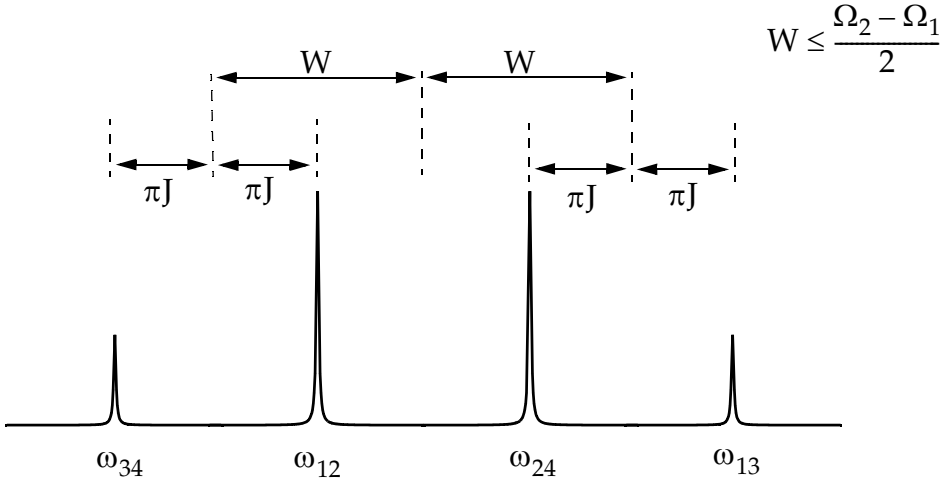

Figure 5.19: Spectrum of a J-Coupled Two-Spin System

The resulting spectrum is shown in Fig. 5.19. The appearance of the spectrum as a function of the ratio $k = |(\Omega_2 - \Omega_1)/(2\pi J)|$ is displayed in Fig. 5.20.

5.7 Allowed and Forbidden Transitions

In the example presented above, we have seen that only the transitions (12), (13), (24), and (34) out of the six possible ones lead to a non-zero intensity in the spectrum. They are called allowed transitions. Such transitions can only appear where the detection operator has nonzero elements. The detection operator is always a linear combination of $\hat{F}^+$ and $\hat{F}^-$. This operator has only matrix-elements between states with a difference in the total magnetic quantum number of 1.

$$M_\ell = \sum_k m_{\ell k} \qquad [5.74]$$

Here, the $m_{\ell k}$ denote the magnetic quantum numbers of the individual nuclei contained in the spin system considered (in this example, there are only two spins). This is the selection rule for magnetic resonance:

$$M_k - M_j = \pm 1 \qquad [5.75]$$

only *one-quantum transitions* are allowed. The *zero-quantum transition* (23) and the *double-quantum transition* (14) are forbidden.

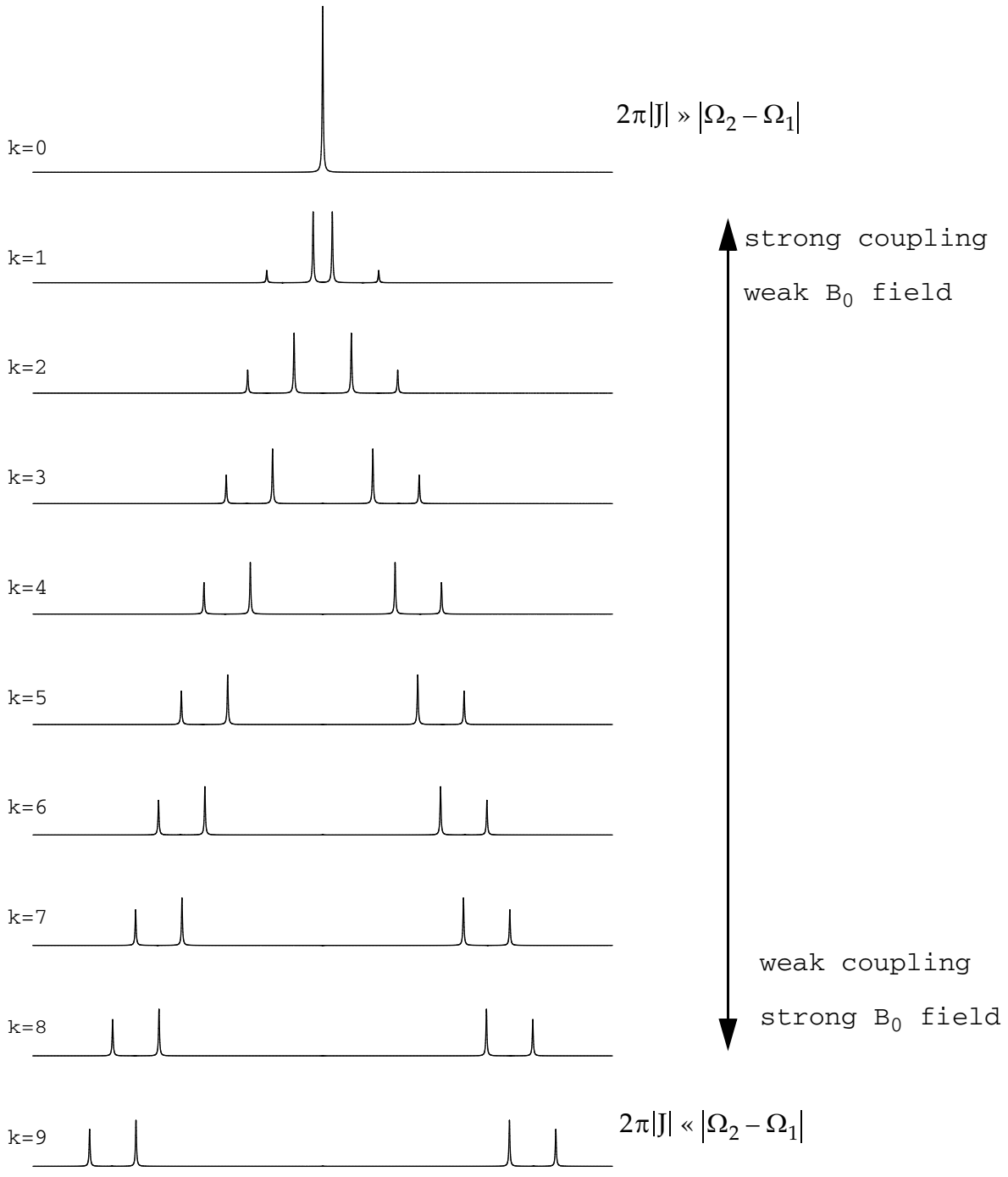

Figure 5.20: J-Coupled Spectra of a Two-Spin System
for a constant J as a function of the difference in resonance frequency $|\Omega_2 - \Omega_1|$. The parameter k is defined as $k = |(\Omega_2 - \Omega_1)/(2\pi J)|$.

5.8 The Magnetic Dipole Interaction

The magnetic dipole-dipole interaction has a classical analogy, the interaction between two magnetic (dipole) moments $\vec{\mu_1}$ and $\vec{\mu_2}$. The classical interaction energy of two magnetic moments located at positions connected by the vector $\vec{r_{12}}$ is given by:

$$E = \frac{\mu_0}{4\pi}\frac{1}{r_{12}^3}\left(\vec{\mu_1}\cdot\vec{\mu_2} - \frac{3}{r_{12}^2}(\vec{\mu_1}\cdot\vec{r_{12}})(\vec{\mu_2}\cdot\vec{r_{12}})\right) \quad [5.76]$$

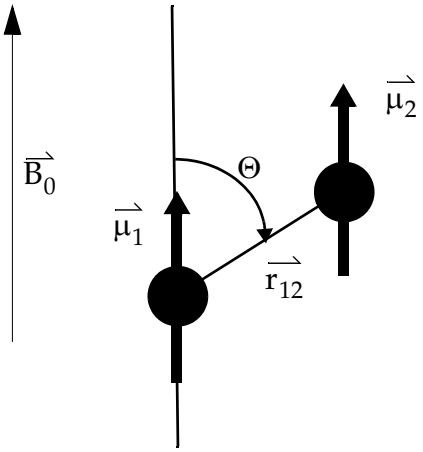

Figure 5.21: Dipole Moment

For the special case where the two magnetic moments are aligned with the z-axis ($\vec{B_0}$), the classical energy function reduces to:

$$E = \frac{\mu_0}{4\pi}\frac{1}{r_{12}^3}\mu_1\mu_2(1-3\cos\theta^2) \quad [5.77]$$

The quantum-mechanical spin Hamiltonian is obtained from Eq. [5.76] as:

$$\begin{aligned}\hat{\mathcal{H}}_D &= \frac{\mu_0}{4\pi}\frac{\gamma_1\gamma_2\hbar}{r_{12}^3}\left(\hat{\vec{I}}_1\cdot\hat{\vec{I}}_2 - \frac{3}{r_{12}^2}\left(\hat{\vec{I}}_1\cdot\vec{r_{12}}\right)\left(\hat{\vec{I}}_2\vec{r_{12}}\right)\right) \\ &= \hat{\vec{I}}_1\underline{D}\hat{\vec{I}}_2\end{aligned} \quad [5.78]$$

$\tilde{D}$ is a 3x3 matrix with the elements:

$$(D)_{\alpha\beta} = \frac{\mu_0}{4\pi}\frac{\gamma_1\gamma_2\hbar}{r_{12}^3}(\delta_{\alpha\beta} - 3e_\alpha e_\beta) \qquad \alpha, \beta = x, y, z \quad [5.79]$$

where the e_α are the components of a unit vector parallel to $\vec{r_{12}}$. For $\vec{r_{12}} = (0, 0, r_{12})$, we have

$$D = \frac{\mu_0}{4\pi}\frac{\gamma_1\gamma_2\hbar}{r_{12}^3}\begin{bmatrix}1 & 0 & 0\\ 0 & 1 & 0\\ 0 & 0 & -2\end{bmatrix} \quad [5.80]$$

Using spherical coordinates for $\overrightarrow{r_{12}}$:

$$\begin{aligned} r_x &= r\sin\theta\cos\varphi \\ r_y &= r\sin\theta\sin\varphi \\ r_z &= r\cos\theta \end{aligned}$$

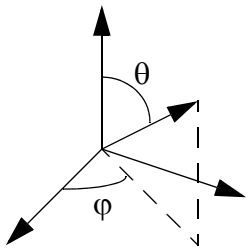

and the shift operators, the dipolar interaction can be rewritten in the so-called dipolar alphabet:

$$\hat{\mathcal{H}}_D = \frac{\mu_0}{4\pi}\frac{\gamma_1\gamma_2\hbar}{r_{12}^3}[\hat{A}+\hat{B}+\hat{C}+\hat{D}+\hat{E}+\hat{F}] \qquad [5.81]$$

with:

$$\begin{aligned} \hat{A} &= \hat{I}_{1z}\hat{I}_{2z}(1-3\cos\theta^2) \\ \hat{B} &= (\hat{I}_1^+\hat{I}_2^- + \hat{I}_1^-\hat{I}_2^+)\frac{3\cos\theta^2-1}{4} \\ \hat{C} &= (\hat{I}_1^+\hat{I}_{2z} + \hat{I}_{1z}\hat{I}_2^+)\frac{-3\sin\theta\cos\theta e^{-i\varphi}}{2} \\ \hat{D} &= (\hat{I}_1^-\hat{I}_{2z} + \hat{I}_{1z}\hat{I}_2^-)\frac{-3\sin\theta\cos\theta e^{i\varphi}}{2} \\ \hat{E} &= \hat{I}_1^+\hat{I}_2^+\frac{-3\sin\theta^2 e^{-2i\varphi}}{4} \\ \hat{F} &= \hat{I}_1^-\hat{I}_2^-\frac{-3\sin\theta^2 e^{2i\varphi}}{4} \end{aligned} \qquad [5.82]$$

In the presence of a strong Zeeman interaction, one transforms into the rotating frame. The operators $\hat{I}^+$ and $\hat{I}^-$ become time dependent and the terms $\hat{C}$ to $\hat{F}$ can be neglected as non-secular terms leading to

$$\hat{\mathcal{H}}_D' = \frac{\mu_0}{4\pi}\frac{\gamma_1\gamma_2\hbar}{r_{12}^3}(\hat{A}+\hat{B}). \qquad [5.83]$$

The term $\hat{A}$ remains obviously always invariant when going into the rotating frame since it contains only $\hat{I}_z$ operators. For the term $\hat{B}$, two situations must be distinguished:

- *Homonuclear case* (both nuclei have the same Zeeman-frequency and the same rotating frame transformation applies): Here $\hat{I}_1^+\hat{I}_2^- + \hat{I}_1^-\hat{I}_2^+$ is time-independent and must be taken into account.
- *Heteronuclear case*: Here we need two different rotating frames for the two spins rotating at their specific Larmor frequencies. In the rotating frame, the term $\hat{I}_1^+\hat{I}_2^- + \hat{I}_1^-\hat{I}_2^+$ is time-dependent with a frequency equal to the difference of the two Larmor frequencies. Therefore, it can be neglected as non secular in excellent approximation.

The simplified secular rotating-frame dipolar-coupling Hamiltonian is of the form

- for a homonuclear spin pair:

$$\hat{\mathcal{H}}'_D = \frac{-\mu_0}{4\pi}\frac{\gamma_1\gamma_2\hbar}{r_{12}^3}\frac{(3\cos\theta^2-1)}{2}\left[2\hat{I}_{1z}\hat{I}_{2z} - \frac{1}{2}(\hat{I}_1^+\hat{I}_2^- + \hat{I}_1^-\hat{I}_2^+)\right] \qquad [5.84]$$

- for a heteronuclear spin pair:

$$\hat{\mathcal{H}}'_D = \frac{-\mu_0}{4\pi}\frac{\gamma_1\gamma_2\hbar}{r_{12}^3}\frac{(3\cos\theta^2-1)}{2}2\hat{I}_{1z}\hat{I}_{2z} \qquad [5.85]$$

The constant

$$d = \frac{-\mu_0}{4\pi}\frac{\gamma_1\gamma_2\hbar}{r_{12}^3}\frac{(3\cos\theta^2-1)}{2} \qquad [5.86]$$

is often called the dipolar coupling constant. Due to the dependence on the angle θ, the dipolar coupling constant changes mangnitude and sign for different orientations.

5.8.1 Spectrum of a Heteronuclear Dipolar-Coupled Spin Pair

Assuming that the rotating-frame Hamiltonian consists only of the dipolar interaction, it has the form:

$$\hat{\mathcal{H}}'' = \hat{\mathcal{H}}'_D = 2d\hat{I}_{1z}\hat{I}_{2z} \qquad [5.87]$$

with the matrix representation

$$(\mathcal{H}'') = 2d\begin{bmatrix} 1/4 & 0 & 0 & 0 \\ 0 & -1/4 & 0 & 0 \\ 0 & 0 & -1/4 & 0 \\ 0 & 0 & 0 & 1/4 \end{bmatrix} \qquad [5.88]$$

This leads to the transition frequencies for the allowed transitions of:

$$\begin{aligned} \omega_1 &= (\mathcal{H}'')_{11} - (\mathcal{H}'')_{22} = d \\ \omega_2 &= (\mathcal{H}'')_{33} - (\mathcal{H}'')_{44} = -d \end{aligned} \qquad [5.89]$$

and a spectrum with two lines with a splitting of 2d as shown in Fig. 5.22.

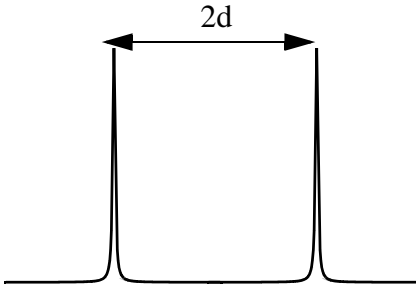

Figure 5.22: Dipolar Splitting for a Single Crystal Orientation

5.8.2 Spectrum of a Homonuclear Dipolar-Coupled Spin Pair

Here the term $\hat{B}$ must also be taken into account. In this case $\hat{\mathcal{H}}$ has permutation symmetry with respect to an exchange of the two nuclei:

$$\hat{P}(12)\hat{\mathcal{H}} = \hat{\mathcal{H}} \qquad [5.90]$$

As a consequence, the eigenfunctions transform according to the irreducible representations A and B of the permutation group of two elements. From this argument we obtain immediately the Eigenfunctions:

- Symmetric representation A:

$$\begin{aligned} \phi_1 &= \alpha\alpha \\ \phi_2 &= \frac{1}{\sqrt{2}}(\alpha\beta + \beta\alpha) \\ \phi_3 &= \beta\beta \end{aligned} \qquad [5.91]$$

- Anti-symmetric representation B:

$$\phi_4 = \frac{1}{\sqrt{2}}(\alpha\beta - \beta\alpha) \qquad [5.92]$$

We can now calculate the diagonal elements of $\mathcal{H}_D'$ in this basis and obtain

$$\begin{aligned} E_1 &= \langle\phi_1|\mathcal{H}|\phi_1\rangle = \frac{d}{2} \\ E_2 &= \langle\phi_2|\mathcal{H}|\phi_2\rangle = -d \\ E_3 &= \langle\phi_3|\mathcal{H}|\phi_3\rangle = \frac{d}{2} \\ E_4 &= \langle\phi_4|\mathcal{H}|\phi_4\rangle = 0 \end{aligned} \qquad [5.93]$$

The transition frequencies for the allowed transitions are

$$\begin{aligned} \omega_1 &= (E_1 - E_2) = \frac{3d}{2} \\ \omega_2 &= (E_2 - E_3) = \frac{-3d}{2} \end{aligned} \qquad [5.94]$$

and the spectrum has two lines with a splitting of 3d as shown in Fig. 5.23

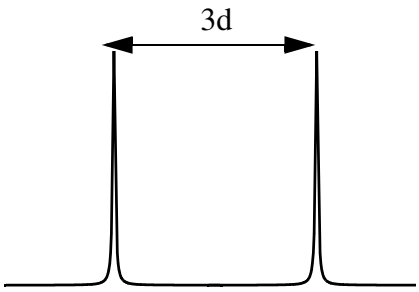

Figure 5.23: Dipolar Splitting for a Single Crystal orientation

Exercise: Show that the allowed transitions in this case are indeed the 1-2 and 2-3 transitions.

5.8.3 Intermediate Cases

The spectrum of two dipolar-coupled nuclei can be calculated in almost complete analogy to the one of two J-coupled nuclei. The matrix representation of the Hamiltonian is given by (compare to Eq. [5.67]!):

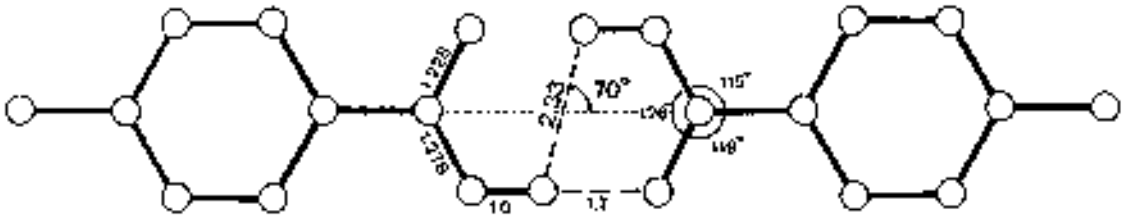

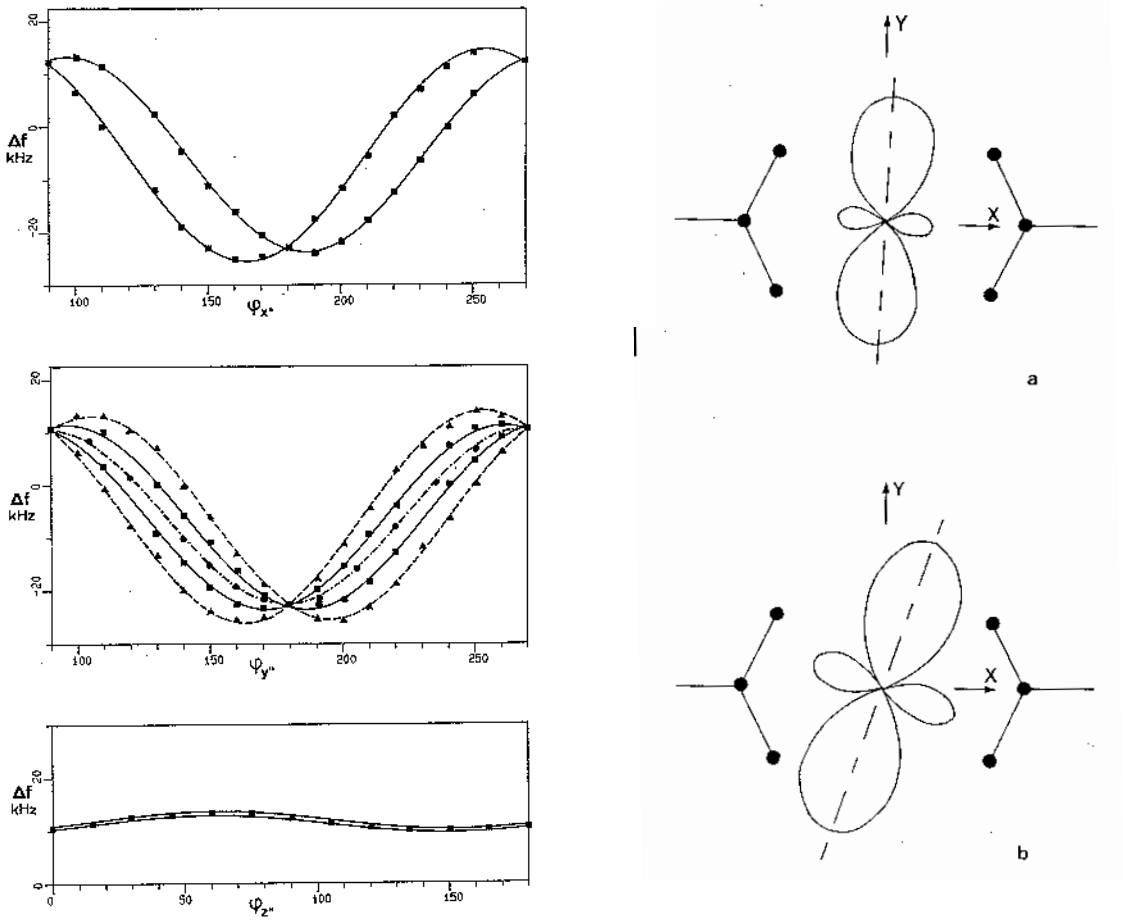

Figure 5.24: Measured Dipolar Splitting
between the two protons in p-toluoic acid at room temperature and at 10 K. The experiment manifests the proton tautometrism.

$$(\mathcal{H}_D) = \begin{bmatrix} \frac{\Omega_1+\Omega_2}{2}+\frac{d}{2} & 0 & 0 & 0 \\ 0 & \frac{\Omega_1-\Omega_2}{2}-\frac{d}{2} & -\frac{d}{2} & 0 \\ 0 & -\frac{d}{2} & \frac{\Omega_2-\Omega_1}{2}-\frac{d}{2} & 0 \\ 0 & 0 & 0 & \frac{-(\Omega_1+\Omega_2)}{2}+\frac{d}{2} \end{bmatrix} \quad [5.95]$$

Note that the off-diagonal matrix elements have the same size as the diagonal matrix elements while, in the case of the J-coupling Hamiltonian, they were a factor two larger!

With $2\alpha = \operatorname{atan}\left(\frac{-d}{\Omega_1-\Omega_2}\right)$ we obtain again four "allowed" transitions with the following frequencies and intensities:

frequency	intensity
$\omega_{12} = \frac{\Omega_1+\Omega_2}{2} + d - \sqrt{\left(\frac{\Omega_2-\Omega_1}{2}\right)^2+\left(\frac{d}{2}\right)^2}$	$I_{12} = \left(\frac{\cos\alpha+\sin\alpha}{2}\right)^2 = \frac{1+\sin 2\alpha}{4}$
$\omega_{13} = \frac{\Omega_1+\Omega_2}{2} + d + \sqrt{\left(\frac{\Omega_2-\Omega_1}{2}\right)^2+\left(\frac{d}{2}\right)^2}$	$I_{13} = \left(\frac{\cos\alpha-\sin\alpha}{2}\right)^2 = \frac{1-\sin 2\alpha}{4}$
$\omega_{24} = \frac{\Omega_1+\Omega_2}{2} - d + \sqrt{\left(\frac{\Omega_2-\Omega_1}{2}\right)^2+\left(\frac{d}{2}\right)^2}$	$I_{24} = \left(\frac{\cos\alpha+\sin\alpha}{2}\right)^2 = \frac{1+\sin 2\alpha}{4}$
$\omega_{34} = \frac{\Omega_1+\Omega_2}{2} - d - \sqrt{\left(\frac{\Omega_2-\Omega_1}{2}\right)^2+\left(\frac{d}{2}\right)^2}$	$I_{34} = \left(\frac{\cos\alpha-\sin\alpha}{2}\right)^2 = \frac{1-\sin 2\alpha}{4}$

The resulting spectra are plotted in Fig. 5.25.

5.8.4 Powder Spectra of Dipolar Couplings

In the case of powders, we obtain again a powder pattern which is the superposition of the splittings weighted by their probabillity. Since the dipolar-

coupling tensor is always axially symmetric ($\eta = 0$), the dipolar powder pattern (also called Pake pattern) can be described by the superposoition of two axially symmetric

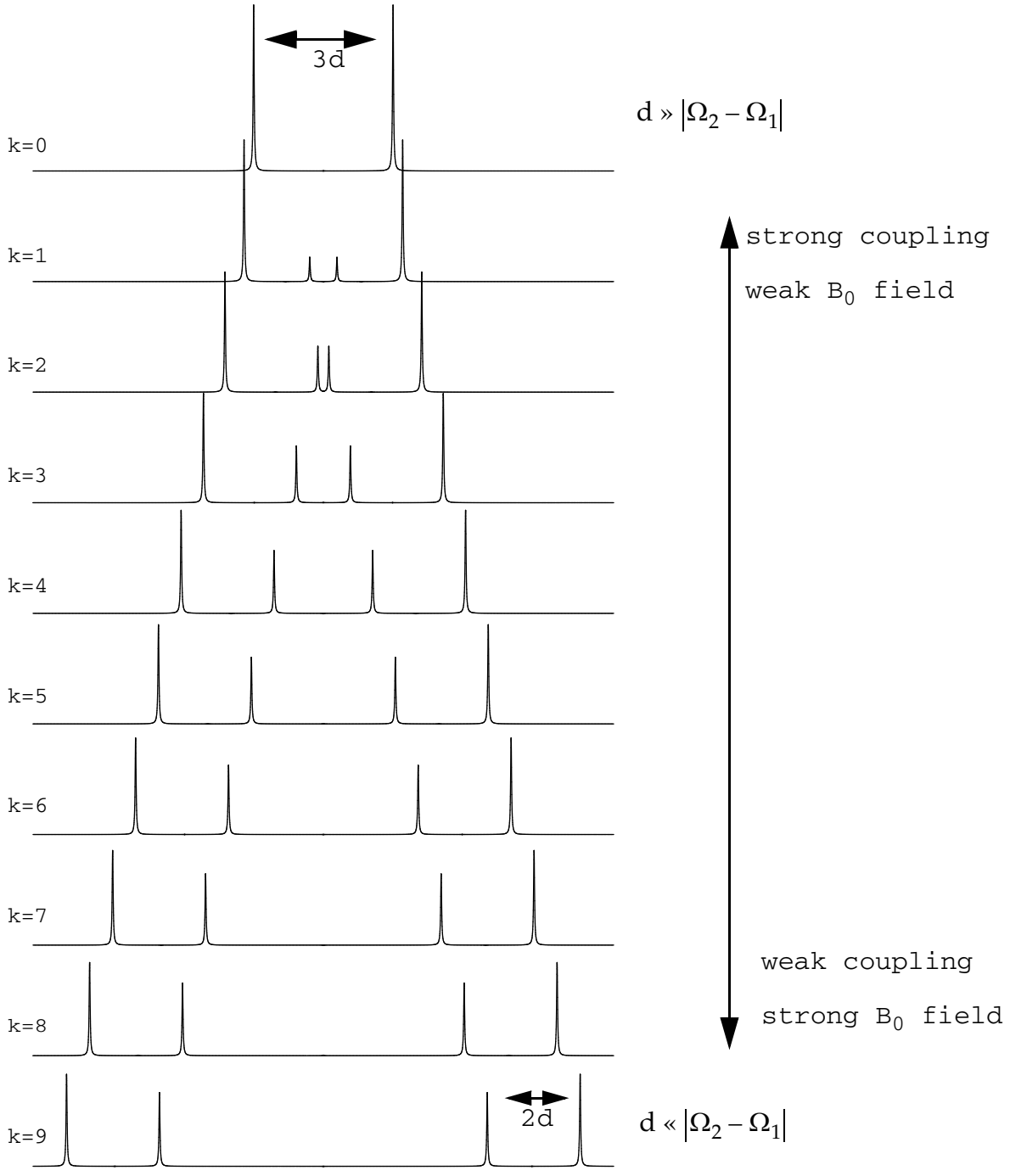

Figure 5.25: D-Coupled Spectra of a Two-Spin System
for constant D as a function of the difference in resonance frequency $|\Omega_2 - \Omega_1|$ .The parameter k is defined as $k = |(\Omega_2 - \Omega_1)/d|$.

second-rank tensor powder patterns (Fig. 5.26). The distance of the two horns is equal to $\delta_D/2$ for the heteronuclear case and to $3\delta_D/4$ for the homonuclear case.

5.9 The Nuclear Quadrupole Interaction

For nuclei with a non-spherically symmetric charge distribution, the energy depends on the orientation of the nucleus with respect to the electric field gradient. Only spins with a spin quantum number $I \geq 1$ have a non-symmetric charge distribution. The classical potential energy of a nucleus with a charge density of $\rho(\vec{r})$ in an electrostatic potential $V(\vec{r})$ caused by electrons and other nuclei is given by:

$$E = \int \rho(\vec{r}) V(\vec{r}) dv \qquad [5.96]$$

where the integral covers the entire space.

We can expand this energy in a Taylor expansion centered at $\vec{r} = 0$. With $\alpha, \beta = 1, 2, 3$, we obtain

$$E = V(0)\int \rho(\vec{r})dv + \sum_{\alpha} V_\alpha(0)\int x_\alpha \rho(\vec{r})dv + \frac{1}{2!}\sum_{\alpha,\beta} V_{\alpha\beta}\int x_\alpha x_\beta \rho(\vec{r})dv + \ldots \qquad [5.97]$$

with

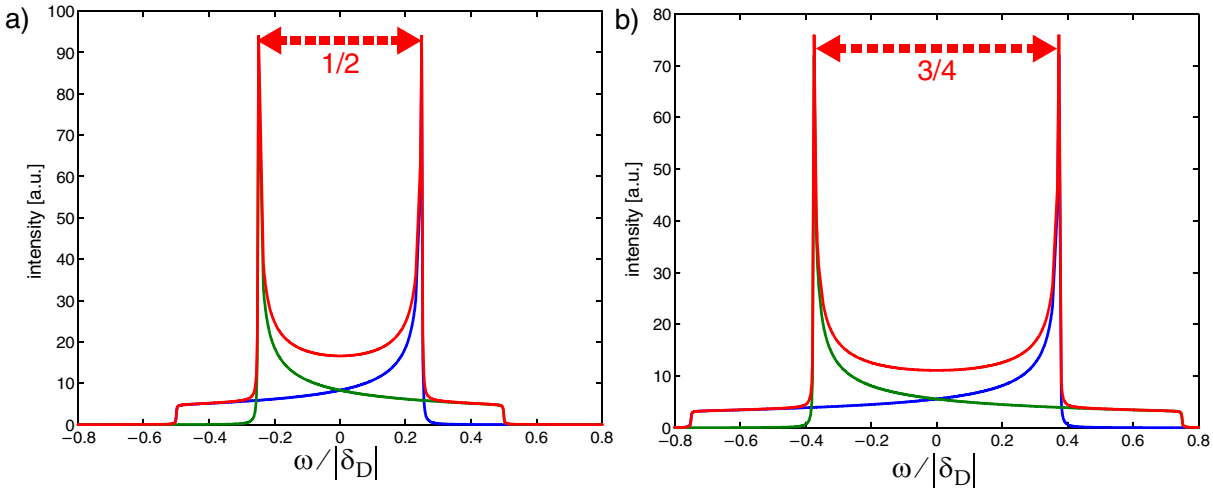

Figure 5.26: Dipolar Powder Patterns (Pake Pattern)
a) for a heteronuclear spin system (weak-coupling limit) and b) for a homonuclear spin system (strong-coupling limit).

$$V_\alpha = \left.\frac{\partial V}{\partial x_\alpha}\right|_{\vec{r}=0} \qquad V_{\alpha\beta} = \left.\frac{\partial}{\partial x_\alpha}\frac{\partial V}{\partial x_\beta}\right|_{\vec{r}=0} \qquad [5.98]$$

The first term is the electrostatic energy: $V(0)\int\rho(\vec{r})dv = V(0)eZ$, the second term is the energy of the electric dipole moment in the electric field. It can be shown that the electric dipole moment of any nucleus vanishes based on symmetry considerations. The third term is the classical electric quadrupole energy. It is convenient to use the quantities $Q_{\alpha\beta}$ defined by

$$Q_{\alpha\beta} = \int[3x_\alpha x_b - \delta_{\alpha\beta}r^2]\rho(\vec{r})dv \qquad [5.99]$$

which we call the components of the electric quadrupole tensor. For the quadrupole energy, we obtain (in the absence of electrical charges):

$$E = \frac{1}{6}\sum_{\alpha,\,\beta} V_{\alpha\beta}Q_{\alpha\beta} \qquad [5.100]$$

To obtain the quadrupole Hamiltonian from the classical form Eq. [5.100] demands a rather lengthy derivation. The interested reader is refereed to C.P. Slichters book "Principles of Magnetic Resonance", 3rd edition, Chapter 10). The result is:

nucleus	I	Q[10^{-24} cm^2]
^{2}H	1	$2.77 \cdot 10^{-3}$
^{14}N	1	$1.6 \cdot 10^{-2}$
^{17}O	5/2	$-2.6 \cdot 10^{-2}$

$$\hat{\mathcal{H}}_Q = e\frac{Q}{6I(2I-1)}\sum_{\alpha,\,\beta} V_{\alpha\beta}\left[\frac{3}{2}(\hat{I}_\alpha\hat{I}_\beta + \hat{I}_\beta\hat{I}_\alpha) - \delta_{\alpha\beta}\hat{I}^2\right] \qquad [5.101]$$

Here, e is the electron charge, I the spin-quantum number ($I > \frac{1}{2}$) and Q is the quadrupole moment of the nucleus.

In the eigenbase of the field-gradient tensor $\tilde{V}$, the Hamiltonian takes the particularly simple form

$$\hat{\mathcal{H}}_Q = \frac{e^2qQ}{4I(2I-1)}[(3\hat{I}_z^2 - \hat{I}^2) - \eta(\hat{I}_x^2 - \hat{I}_y^2)] \qquad [5.102]$$

with the abbreviations:

$$V_{zz} = eq = \text{electric field gradient}$$
$$\frac{V_{xx} - V_{yy}}{V_{zz}} = \eta = \text{asymmetry parameter} \qquad [5.103]$$

The quadrupole interaction leads to observable signals even in the absence of a magnetic field.

6 Product-Operator Formalism

Instead of performing the calculations in an explicit matrix representation for the density operator and the Hamiltonian as done in Chapter 5.6, it is for simple Hamiltonians often more convenient to use a symbolic notation with spin operators.

6.1 One Spin I=1/2

As discussed earlier the evolution of a one-spin system during a strong pulse or the free evolution under the chemical shift is described by the Liouville-von Neumann equation as $\hat{\sigma}(t) = e^{-i\beta\hat{I}_p}\hat{\sigma}(0)e^{i\beta\hat{I}_p}$, where p is x or y and $\beta = \omega_1 t$ for an rf pulse and $p = z$ and $\beta = \Omega t$ for a free precession period. The density operator can always be expanded in terms of the complete set of base operators $\hat{E}, \hat{I}_x, \hat{I}_y, \hat{I}_z$. As usual, we neglect the part proportional to unity and write:

$$\hat{\sigma}(t) = c_x(t)\hat{I}_x + c_y(t)\hat{I}_y + c_z(t)\hat{I}_z . \qquad [6.1]$$

For the special case where $\hat{\sigma}(0) = \hat{I}_z$ and $p = y$, we have found that $\hat{\sigma}(t) = \hat{I}_z\cos(\beta) + \hat{I}_x\sin(\beta)$ and we symbolically write:

$$\hat{I}_z \xrightarrow{\hat{I}_y(\beta)} \hat{I}_z\cos(\beta) + \hat{I}_x\sin(\beta) \qquad [6.2]$$

This can be understood as a rotation of $\hat{I}_z$ around the $\hat{I}_y$ axis by an angle β and is fully analogous to the classical description (see Fig. 2.5). Equivalently, we obtain:

$$\hat{I}_x \xrightarrow{\hat{I}_z(\beta)} \hat{I}_x\cos(\beta) + \hat{I}_y\sin(\beta) \qquad [6.3]$$

Generalizing Eqs. [6.2] and [6.3] we can write:

$$\hat{I}_q \xrightarrow{\hat{I}_p(\beta)} \begin{cases} \hat{I}_q & \text{if } [\hat{I}_q, \hat{I}_p] = 0 \\ \hat{I}_q\cos(\beta) + i[\hat{I}_q, \hat{I}_p]\sin(\beta) & \text{else} \end{cases} \qquad [6.4]$$

with $p, q = x, y, z$. Note that this relation only holds for spin 1/2! For multiple-pulse experiments, the notation of Eq. [6.4] can lead to long formulas with many sine and cosine terms. If one is only interested in what terms can be generated (without knowing their time-dependent weights) one can use the so-called *branch diagram*:

$$\hat{I}_q \xrightarrow{\hat{I}_p(\beta)} \begin{cases} \hat{I}_q \\ i[\hat{I}_q, \hat{I}_p] \end{cases} \qquad [6.5]$$

as a short-hand notation.

6.2 Two Spins I=1/2

For systems of two spins with I = 1/2, the 16-dimensional space as used in Chapter 5.6 can be spanned by basis operators that are products of the cartesian single-spin operators:

$$\begin{aligned} Q = 0 \quad & \frac{1}{2}\hat{E} \\ Q = 1 \quad & \hat{I}_{1x}, \hat{I}_{1y}, \hat{I}_{1z}, \hat{I}_{2x}, \hat{I}_{2y}, \hat{I}_{2z} \\ Q = 2 \quad & 2\hat{I}_{1x}\hat{I}_{2x}, 2\hat{I}_{1x}\hat{I}_{2y}, 2\hat{I}_{1x}\hat{I}_{2z} \\ & 2\hat{I}_{1y}\hat{I}_{2x}, 2\hat{I}_{1y}\hat{I}_{2y}, 2\hat{I}_{1y}\hat{I}_{2z} \\ & 2\hat{I}_{1z}\hat{I}_{2x}, 2\hat{I}_{1z}\hat{I}_{2y}, 2\hat{I}_{1z}\hat{I}_{2z} \end{aligned} \qquad [6.6]$$

It can be shown (e.g. by matrix calculation) that these operators all fulfill a generalization of the set of rules given in Eq. [6.4]:

$$\hat{C}_q \xrightarrow{\hat{C}_p(\beta)} \begin{cases} \hat{C}_q & \text{if } [\hat{C}_q, \hat{C}_p] = 0 \\ \hat{C}_q \cos(\beta) + i[\hat{C}_q, \hat{C}_p]\sin(\beta) & \text{else} \end{cases} \qquad [6.7]$$

where $\hat{C}_q$ can be any operator out of Eq. [6.6]. Note that Eq. [6.7] holds for any number of spin 1/2, not only for a two-spin system.

To evaluate the commutators $[\hat{C}_q, \hat{C}_p]$, the following rules are useful:

$$
\begin{aligned}
[\hat{I}_{1p}, \hat{I}_{2q}] &= 0 && \text{for all } p, q \\
[2\hat{I}_{1p}\hat{I}_{2q}, \hat{I}_{1r}] &= 2[\hat{I}_{1p}, \hat{I}_{1r}]\hat{I}_{2q} \\
[2\hat{I}_{1p}\hat{I}_{2q}, \hat{I}_{2r}] &= 2\hat{I}_{1p}[\hat{I}_{2q}, \hat{I}_{2r}] \\
[2\hat{I}_{1p}\hat{I}_{2q}, 2\hat{I}_{1r}\hat{I}_{2s}] &= \begin{cases} 0 & \text{if } p \neq r \text{ and } q \neq s \\ [\hat{I}_{2q}, \hat{I}_{2s}] & \text{if } p = r \\ [\hat{I}_{1p}, \hat{I}_{1r}] & \text{if } q = s \\ 0 & \text{if } p = r \text{ and } q = s \end{cases}
\end{aligned}
\qquad [6.8]
$$

A table of commutators for two-spin systems is given in Fig. 6.1. The one- and two-spin operators in Eq. [6.6] are denoted as follows:

Operator	Name
$\hat{E}$	unity
$\hat{I}_{kz}$	polarization, longitudinal spin order
$2\hat{I}_{kz}\hat{I}_{lz}$	longitudinal two-spin order
$\hat{I}_{kx}$	single-quantum coherence (of spin k), in-phase coherence
$2\hat{I}_{kx}\hat{I}_{lz}$	anti-phase coherence (of spin k)
$2\hat{I}_{kx}\hat{I}_{lx}$	multiple-quantum coherence (mixture of zero- and double-quantum coherence)

Cohe-	Commutator with							
rence	E	I_z	S_z	I_zS_z	I_x	I_y	I_xS_z	I_yS_z
E	0	0	0	0	0	0	0	0
I_z	0	0	0	0	I_y	$-I_x$	I_yS_z	$-I_xS_z$
S_z	0	0	0	0	0	0	0	0
I_zS_z	0	0	0	0	I_yS_z	$-I_xS_z$	I_y	$-I_x$
I_x	0	$-I_y$	0	$-I_yS_z$	0	I_z	0	I_zS_z
I_y	0	I_x	0	I_xS_z	$-I_z$	0	$-I_zS_z$	0
I_xS_z	0	$-I_yS_z$	0	$-I_y$	0	I_zS_z	0	I_z
I_yS_z	0	I_xS_z	0	I_x	$-I_zS_z$	0	$-I_z$	0
S_x	0	0	$-S_y$	$-I_zS_y$	0	0	$-I_xS_y$	$-I_yS_y$
S_y	0	0	S_x	I_zS_x	0	0	I_xS_x	I_yS_x
I_zS_x	0	0	$-I_zS_y$	$-S_y$	I_yS_x	$-I_xS_x$	0	0
I_zS_y	0	0	I_zS_x	S_x	I_yS_y	$-I_xS_y$	0	0
I_xS_x	0	$-I_yS_x$	$-I_xS_y$	0	0	I_zS_x	$-S_y$	0
I_yS_y	0	I_xS_y	I_yS_x	0	$-I_zS_y$	0	0	S_x
I_xS_y	0	$-I_yS_y$	I_xS_x	0	0	I_zS_y	S_x	0
I_yS_x	0	I_xS_x	$-I_yS_y$	0	$-I_zS_x$	0	0	$-S_y$

cohe-	Commutator with							
rence	S_x	S_y	I_zS_x	I_zS_y	I_xS_x	I_yS_y	I_xS_y	I_yS_x
E	0	0	0	0	0	0	0	0
I_z	0	0	0	0	I_yS_x	$-I_xS_y$	I_yS_y	$-I_xS_x$
S_z	S_y	$-S_x$	I_zS_y	$-I_zS_x$	I_xS_y	$-I_yS_x$	$-I_xS_x$	I_yS_y
I_zS_z	I_zS_y	$-I_zS_x$	S_y	$-S_x$	0	0	0	0
I_x	0	0	$-I_yS_x$	$-I_yS_y$	0	I_zS_y	0	I_zS_x
I_y	0	0	I_xS_x	I_xS_y	$-I_zS_x$	0	$-I_zS_y$	0
I_xS_z	I_xS_y	$-I_xS_x$	0	0	S_y	0	$-S_x$	0
I_yS_z	I_yS_y	$-I_yS_x$	0	0	0	$-S_x$	0	S_y
S_x	0	S_z	0	I_zS_z	0	I_yS_z	I_xS_z	0
S_y	$-S_z$	0	$-I_zS_z$	0	$-I_xS_z$	0	0	$-I_yS_z$
I_zS_x	0	I_zS_z	0	S_z	I_y	0	0	$-I_x$
I_zS_y	$-I_zS_z$	0	$-S_z$	0	0	$-I_x$	I_y	0
I_xS_x	0	I_xS_z	$-I_y$	0	0	0	S_z	I_z
I_yS_y	$-I_yS_z$	0	0	I_x	0	0	$-I_z$	$-S_z$
I_xS_y	$-I_xS_z$	0	0	$-I_y$	$-S_z$	I_z	0	0
I_yS_x	0	I_yS_z	I_x	0	$-I_z$	S_z	0	0

Figure 6.1: Commutators.
All commutators should be multiplied by i and all products of two spin operators should be multiplied by 2. These constants were left away for brevity. Example: I_yS_z stands for $i \cdot 2I_yS_z$

The different types of coherences can be related to the elements of the density operator in the matrix representation for a two spin system. The shading of the elements shows which type of operators contribute to which elements of the density operator.

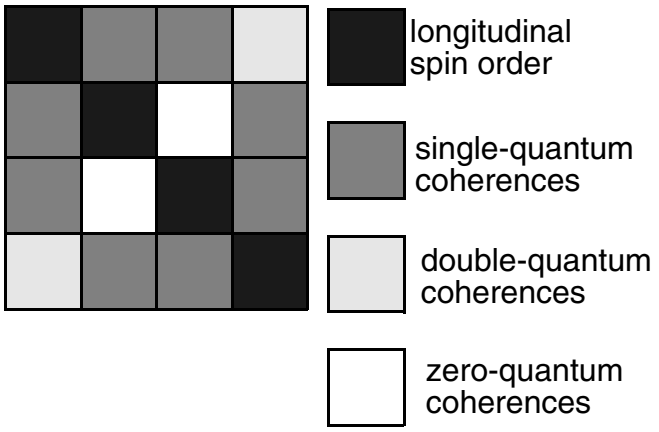

A longitudinal two-spin order operator which describes the scalar or dipolar coupling in the "weak coupling" situation (see below) acts on one-spin coherence as:

$$\hat{I}_{kx} \xrightarrow{2\hat{I}_{kz}\hat{I}_{lz}(\pi J_{kl}t)} \hat{I}_{kx}\cos(\pi J_{kl}t) + 2\hat{I}_{ky}\hat{I}_{lz}\sin(\pi J_{kl}t) \qquad [6.9]$$

Note the close analogy to the evolution under $\hat{I}_z(\beta)$ of Eq. [6.3]:

$$\hat{I}_x \xrightarrow{\hat{I}_z(\beta)} \hat{I}_x\cos(\beta) + \hat{I}_y\sin(\beta) \qquad [6.10]$$

The rotation of Eq. [6.9] can be described in a 3-dimensional subspace. This is actually true for any rotation around a product operator as illustrated for a few examples in Fig. 6.2.

6.3 The Spectrum of a Weakly-Coupled Two-Spin System in Liquids

The use of the product-operator formalism is particularly useful in liquid-state NMR in the "weak-coupling" situation where $|(\Omega_2 - \Omega_1)/(2\pi J)| \gg 1$. Then, the Hamiltonian of Eq. [5.46]

$$\mathcal{H}'' = \Omega_1 \cdot \hat{I}_{1z} + \Omega_2 \cdot \hat{I}_{2z} + 2\pi J_{12}\vec{\hat{I}}_1\vec{\hat{I}}_2 \qquad [6.11]$$

simplifies to

$$\mathcal{H}'' = \Omega_1 \cdot \hat{I}_{1z} + \Omega_2 \cdot \hat{I}_{2z} + 2\pi J_{12} \hat{I}_{1z} \hat{I}_{2z} \ . \qquad [6.12]$$

Heteronuclear J couplings are always in the "weak coupling" limit because the transverse components are non secular in the rotating frame as discussed in Chapter 5.8 for the dipolar coupling Hamiltonian.

Such a Hamiltonian is particularly simple because all its terms commute with each other and we are able to evaluate their action on the density operator sequentially. For a general N-spin system in the "weak-coupling" limit, we have

$$\hat{\sigma}(t) = \prod_k \exp(-i\Omega_k t \hat{I}_{kz}) \prod_{k<l} \exp(-i\pi J_{kl} t 2\hat{I}_{kz}\hat{I}_{lz}) \sigma(0)$$
$$\times \prod_k \exp(i\Omega_k t \hat{I}_{kz}) \prod_{k<l} \exp(i\pi J_{kl} t 2\hat{I}_{kz}\hat{I}_{lz}) \qquad [6.13]$$

We now describe the same experiment as in Chapter 5.6 with the Hamiltonian

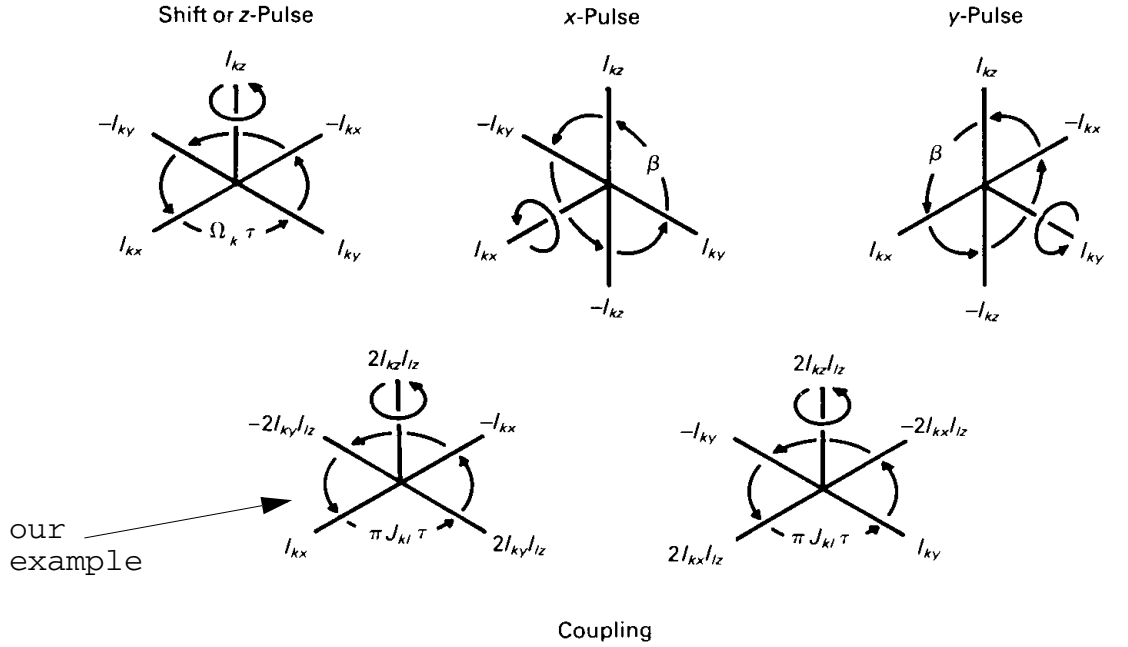

Rotations in subspaces spanned by products of Cartesian spin operators, corresponding to chemical shifts (rotation about I_{kz}), r.f. pulses (rotations about I_{kx} and I_{ky}), and weak scalar couplings (rotations about $2\,I_{kz}I_{lz}$). Note that we consistently use positive rotations (frequencies and angles) in the right-handed sense (clockwise when looking along the rotation vector). (Reproduced from Ref. 2.13.)

Figure 6.2: Rotations in a Three-Dimensional Subspace
From: Ernst, Bodenhausen, Wokaun: Principles of Nuclear Magnetic Resonance in One and Two Dimensions, Oxford.

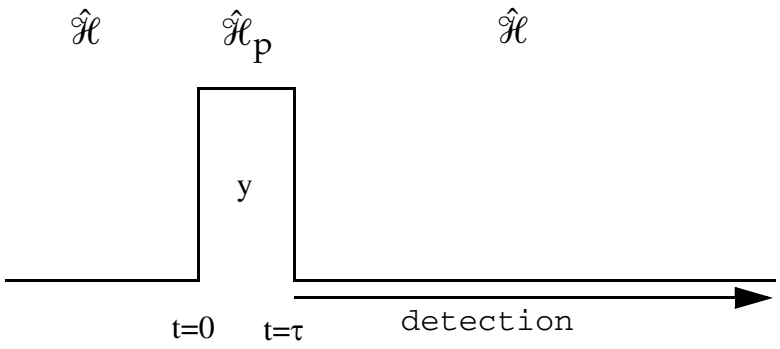

Figure 6.3: Simple 1D Pulse Sequence

$$\hat{\mathcal{H}}_p'' = \omega_1(\hat{I}_{1y} + \hat{I}_{2y}) \ . \qquad [6.14]$$

The initial density operator is of the form $\hat{\sigma}_0 = \frac{1}{2} \cdot (\hat{I}_{1z} + \hat{I}_{2z})$. The term $\hat{I}_{1z}$ evolves according to the branch diagram:

$$\hat{I}_{1z} \xrightarrow{\hat{I}_{1y}\left(\frac{\pi}{2}\right)} \hat{I}_{1x} \xrightarrow{\hat{I}_{2y}\left(\frac{\pi}{2}\right)} \hat{I}_{1x} \xrightarrow{\hat{I}_{1z}(\Omega_1 t)} \begin{cases} \hat{I}_{1x} \xrightarrow{\hat{I}_{2z}(\Omega_2 t)} \hat{I}_{1x} \xrightarrow{2\hat{I}_{1z}\hat{I}_{2z}(\pi J t)} \begin{cases} \hat{I}_{1x} \\ 2\hat{I}_{1y}\hat{I}_{2z} \end{cases} \\ \hat{I}_{1y} \xrightarrow{\hat{I}_{2z}(\Omega_2 t)} \hat{I}_{1y} \xrightarrow{2\hat{I}_{1z}\hat{I}_{2z}(\pi J t)} \begin{cases} \hat{I}_{1y} \\ 2\hat{I}_{1x}\hat{I}_{2z} \end{cases} \end{cases} \qquad [6.15]$$

and $\hat{I}_{2z}$ according to:

$$\hat{I}_{2z} \xrightarrow{\hat{I}_{1y}\left(\frac{\pi}{2}\right)} \hat{I}_{2z} \xrightarrow{\hat{I}_{2y}\left(\frac{\pi}{2}\right)} \hat{I}_{2x} \xrightarrow{\hat{I}_{1z}(\Omega_1 t)} \hat{I}_{2x} \xrightarrow{\hat{I}_{2z}(\Omega_1 t)} \begin{cases} \hat{I}_{2x} \xrightarrow{2\hat{I}_{1z}\hat{I}_{2z}(\pi J t)} \begin{cases} \hat{I}_{2x} \\ 2\hat{I}_{1z}\hat{I}_{2y} \end{cases} \\ \hat{I}_{2y} \xrightarrow{2\hat{I}_{1z}\hat{I}_{2z}(\pi J t)} \begin{cases} \hat{I}_{2y} \\ 2\hat{I}_{1z}\hat{I}_{2x} \end{cases} \end{cases} \qquad [6.16]$$

For a detection operator of $\hat{M}_x = \gamma(\hat{I}_{1x} + \hat{I}_{2x})$, we only have to evaluate a single term in each branch diagram, namely $\hat{I}_{1x}$ and $\hat{I}_{2x}$ which have the weight

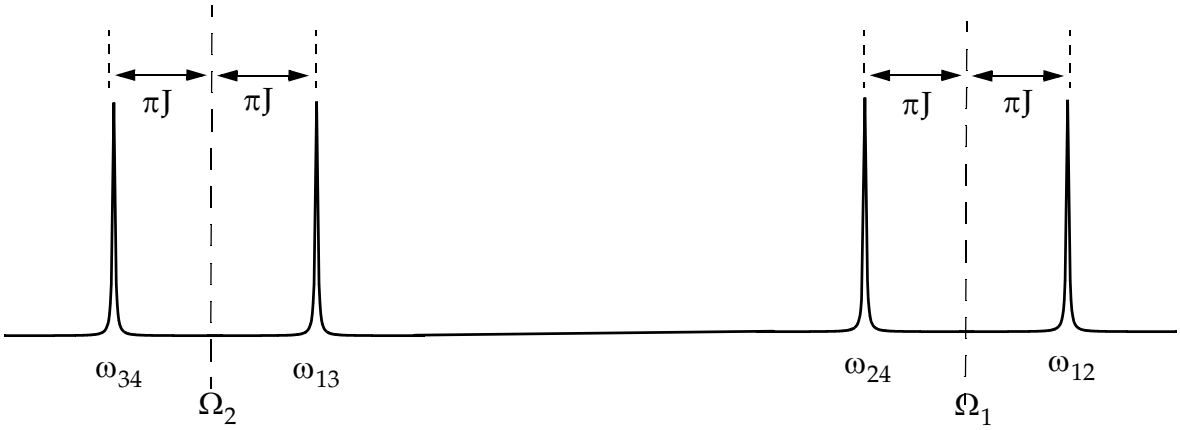

Figure 6.4: Schematic Spectrum of a Weakly-Coupled Two-Spin System

$\frac{1}{2}\cos(\Omega_1 t)\cos(\pi J t)$ and $\frac{1}{2}\cos(\Omega_2 t)\cos(\pi J t)$, respectively. Therefore, the NMR signal is given by:

$$s(t) = \frac{1}{4}(\cos((\Omega_1 + \pi J)t) + \cos((\Omega_1 - \pi J)t) + \cos((\Omega_2 + \pi J)t) + \cos((\Omega_2 - \pi J)t)) \quad [6.17]$$

and consist of four lines of equal intensity:

frequency	intensity
$\omega_{12} = \Omega_1 + \pi J$	$I_{12} = \frac{1}{4}$
$\omega_{13} = \Omega_2 + \pi J$	$I_{13} = \frac{1}{4}$
$\omega_{24} = \Omega_1 - \pi J$	$I_{24} = \frac{1}{4}$
$\omega_{34} = \Omega_2 - \pi J$	$I_{34} = \frac{1}{4}$

A schematic drawing of such a spectrum is given in Fig. 6.4.

6.4 More Than Two Spins I=1/2

The product-operator basis can easily be built up also for larger spin systems. For N spins 1/2, the basis operators are given by

$$\hat{B}_s = 2^{(q-1)} \prod_{k=1}^{N} (I_{k\alpha})^{a_{ks}} \qquad [6.18]$$

where α=x, y, or z, and q is the number of operators in the product, and a_{ks} is 1 for the q spins whose operators appear in the product operator and $a_{ks} = 0$ for the remaining $N - q$ spins.

7 J-Coupled Spectra of Larger Spin Systems

7.1 Weakly-Coupled Spin Systems

As already seen for two spins, each transition in a weakly-coupled spin system can be assigned to a flip of a given spin. For N coupled spins 1/2

$$Z = N \cdot 2^{N-1} \qquad [7.1]$$

lines of equal intensity appear in the NMR spectrum. The subspectrum of each spin p is split into 2^{N-1} lines by the additional shift of $\pm\pi J$ from the coupling term to the $N-1$ other nuclei. Figure 7.1a shows the level diagram and the spectrum of a two-spin AX spin system.

N	Z
1	1
2	4
3	12
4	32

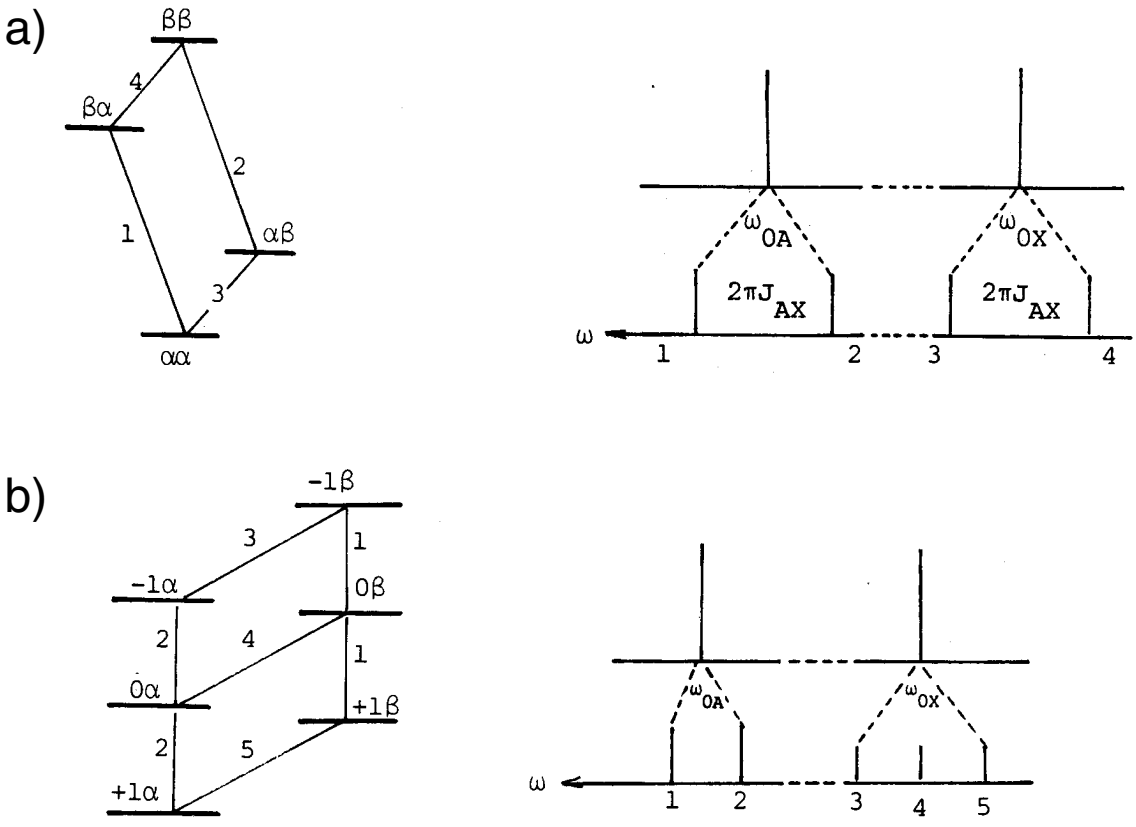

Figure 7.1: Two-Spin System AX
a) two spin-1/2 nuclei, b) spin-1/2 and spin-1 nuclei.

If nuclei with spin-quantum numbers $I \neq 1/2$ are involved, the number of transitions increases as can be seen in Fig. 7.1b for a AX spin system with one I = 1/2 and one I = 1 spin.

From weakly-coupled spectra, the chemical shifts and the J couplings can be directly read off. We use the following notation:

- Nuclei with different chemical shift have a different letter.
- The farther the letters are from each other in the alphabet, the weaker the coupling. (AB: strongly coupled, AX: weakly coupled).

Figure 7.2 shows the level diagram and the spectrum of a weakly-coupled three-spin AMX system.

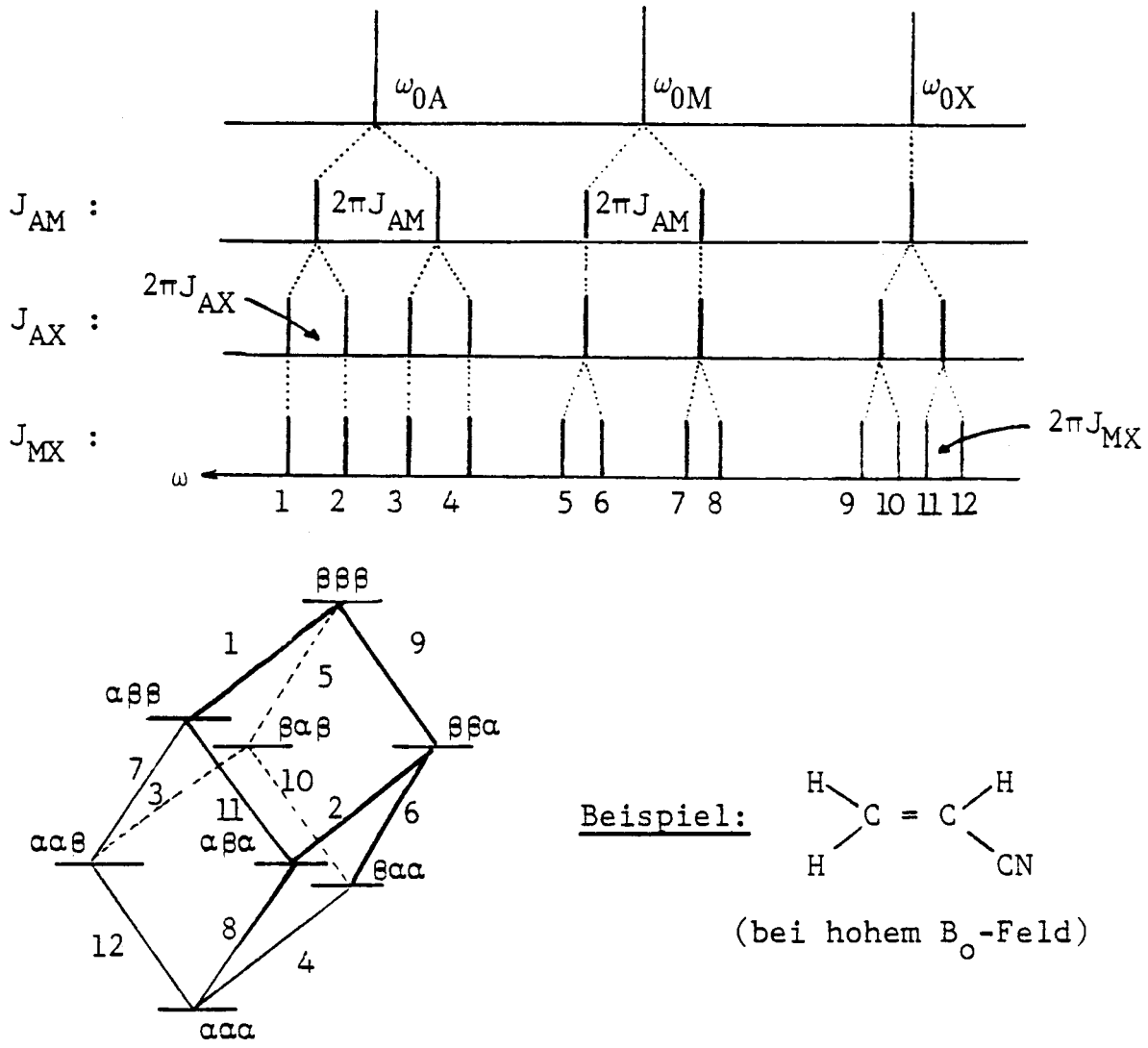

Figure 7.2: Three-Spin AMX System (Spin 1/2)

7.2 Strongly-Coupled Spin Systems

In strongly coupled spin systems the observed transitions cannot be assigned to a transition of a single spin anymore. Without degeneracies, the NMR spectrum consists of

$$Z = \binom{2N}{N-1} \qquad [7.2]$$

N	Z
1	1
2	4
3	15
4	56
5	216

lines of sometimes vastly different intensity. The chemical shifts and the J-coupling constants cannot be read off the spectrum anymore.

Spectra of systems with 3 and more nuclei can not be solved analytically either. To obtain the numerical values of the chemical shifts and the J-coupling constants, one has to simulate the spectrum of the spin system as a function of the parameters. On a personal computer, spin systems with up to about 12 nuclei can easily be simulated numerically.

7.3 Systems With Equivalent Spins

While strong coupling complicates the NMR spectra, symmetry elements simplify them. Simple spectra arise for *magnetically equivalent nuclei*, while *chemically equivalent nuclei* or *crystallographic equivalent nuclei* still lead to complicated spectra with strong coupling.

7.3.1 Definitions

Magnetic equivalence:

Magnetic equivalence of a group of spins is a property of the *Hamiltonian*. It may depend on the phase (oriented vs. isotropic) and on the experiment if two nuclei can be considered magnetically equivalent. A group of spins is magnetically equivalent, if the system Hamiltonian is invariant under a permutation P of these nuclei:

$$P\hat{\mathcal{H}} = \hat{\mathcal{H}} \qquad [7.3]$$

e.g. if $\hat{\mathcal{H}} = \hat{\mathcal{H}}\left(\hat{\vec{I}}_1, \hat{\vec{I}}_2, \hat{\vec{I}}_3, ..., \hat{\vec{I}}_N\right)$ then $P\hat{\mathcal{H}} = \hat{\mathcal{H}}\left(\hat{\vec{I}}_2, \hat{\vec{I}}_1, \hat{\vec{I}}_3, ..., \hat{\vec{I}}_N\right)$. We just change the labels in the Hamiltonian and see if it remained invariant. Magnetically equivalent nuclei are denoted as, e.g. A_2, A_3, A_2X_3 etc.

Chemical equivalence:

This definition is only useful in isotropic liquid phase. There, chemically equivalent nuclei are the ones that are related to each other by molecular symmetry operations. Magnetically equivalent nuclei are always chemically equivalent, the opposite is not true. Chemically equivalent nuclei have the same chemical shift and identical chemical properties but different J-coupling patterns. They are denoted by, e.g., AA′, AA′A′′, AA′XX′X′′.

Crystallographic equivalence:

This is the equivalent of chemical equivalent in a crystalline compound. Crystallographic equivalent nuclei are related by a symmetry element of the crystal. Crystallographic equivalent nuclei have the same chemical properties and the same principal values of the chemical-shielding tensor. The principal axis, however, may differ and therefore, crystallographic equivalent nuclei can give rise to different resonance lines (because of different chemical shifts) in a single-crystal spectrum. Under magic-angle spinning conditions (see later) where only the isotropic chemical shift is measured, their chemical shifts do coincide.

It can be shown that the J-coupling between magnetically equivalent nuclei does not influence the spectrum because it commutes with the rest of the Hamiltonian as well as with the observable operator. The spectrum and the level diagram of an AX_n spin system is shown in Fig. 7.3a. The X-spectrum is a doublet, the A-spectrum consists of n+1 lines with intensities $\binom{n}{0}, \binom{n}{1}, \binom{n}{2}, ...$. These intensities are given by the binomial coefficients which can be visualized in the Pascal triangle (see Fig. 7.4). As a second example the spectrum and the level diagram for an A_2X_2 spin

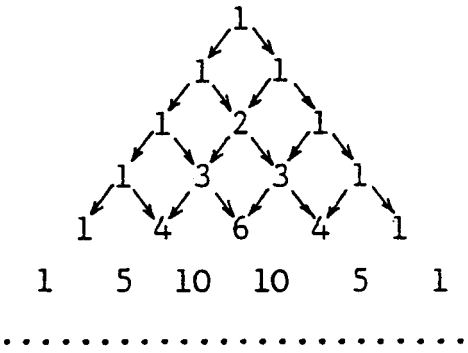

Figure 7.4: Pascal Triangle

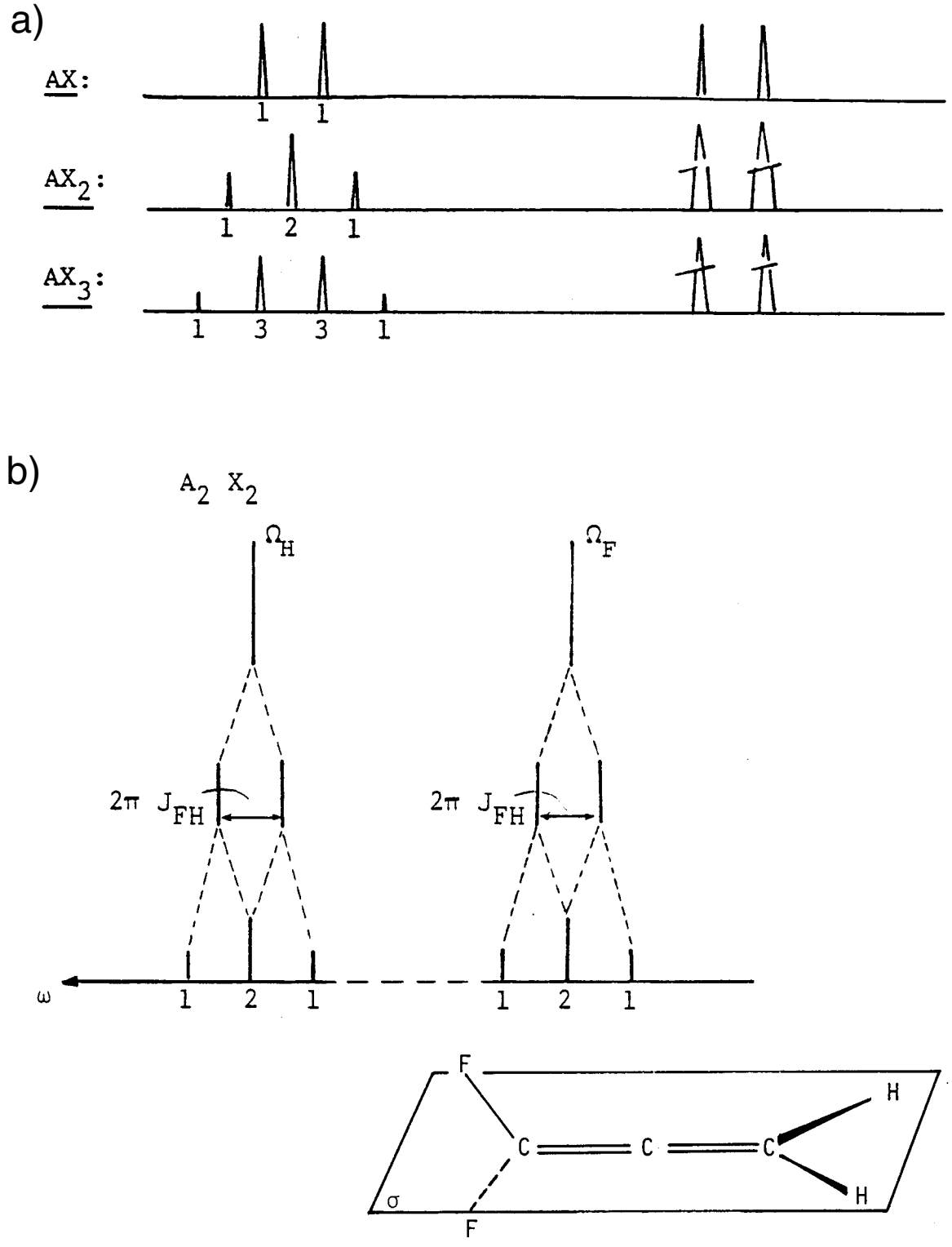

Figure 7.3: Spectra A_mX_n Spin System

system are shown in Figure 7.3b. In these spectra only the J couplings between the A and the X spins are visible in the spectrum and each line is split into a triplet.

Note that the proton spectrum of an A_2X_2 spin system is considerably simpler than the one of difluorethylen, an AA'XX' spin system (Fig. 7.5) which must be calculated numerically.

Rules for the localization of magnetically equivalent nuclei in isotropic phase:

- Magnetically equivalent nuclei are connected by a symmetry operation of the molecule which leaves the positions of all other magnetic nuclei in the molecule invariant.

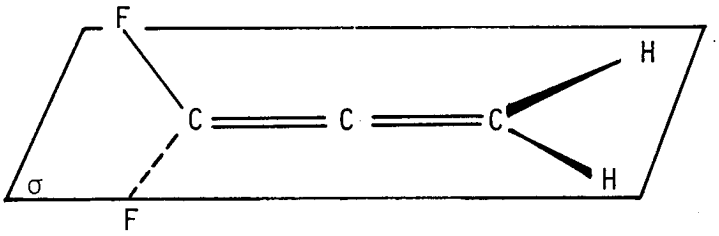

- The coupling constants to all other nuclei must be identical.

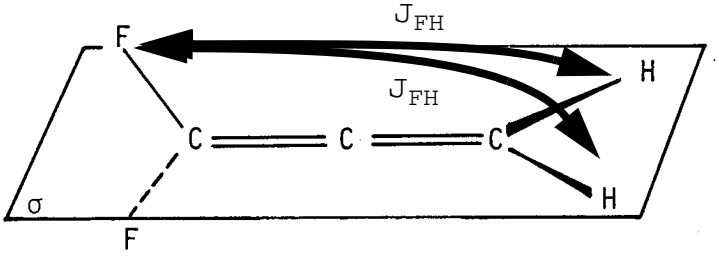

More examples for systems with magnetically or chemically equivalent nuclei can be found in Fig. 7.6. Magnetic equivalence can also be generated by dynamic

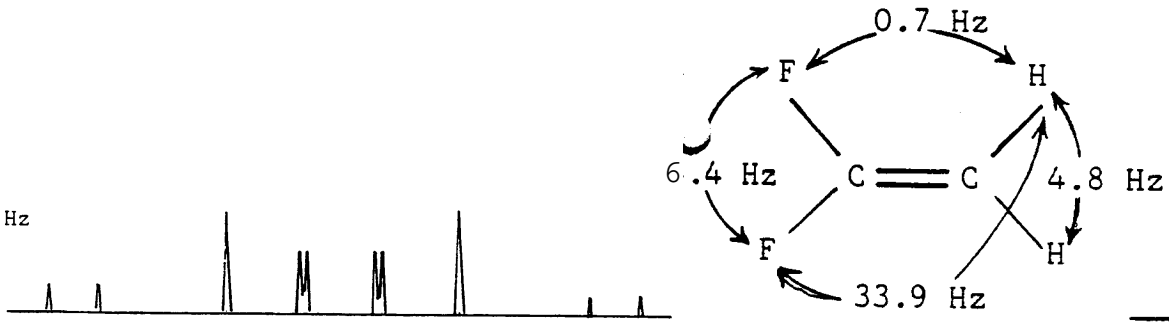

Figure 7.5: Spectrum of a AA'XX' Spin System

processes that are fast on the NMR time scale. The three protons of a methyl group are always magnetically equivalent if the methyl group rotates fast with respect to the rest of the molecule.

1. Magnetische Aequivalenz:

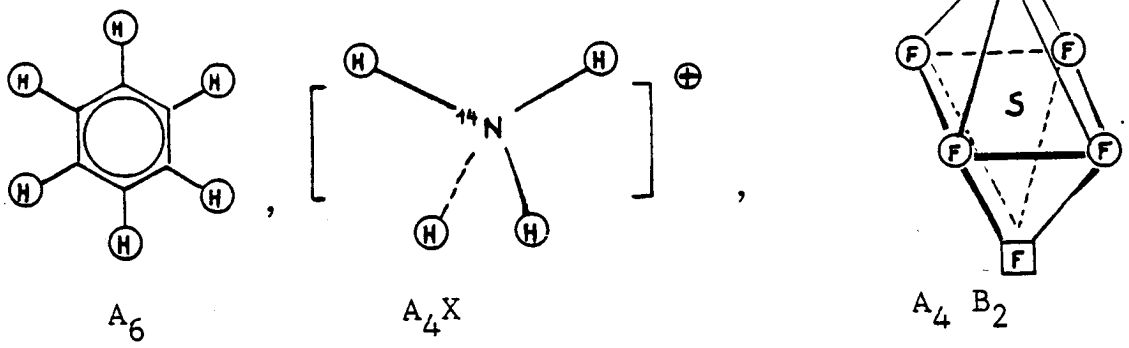

2. Chemische Aequivalenz:

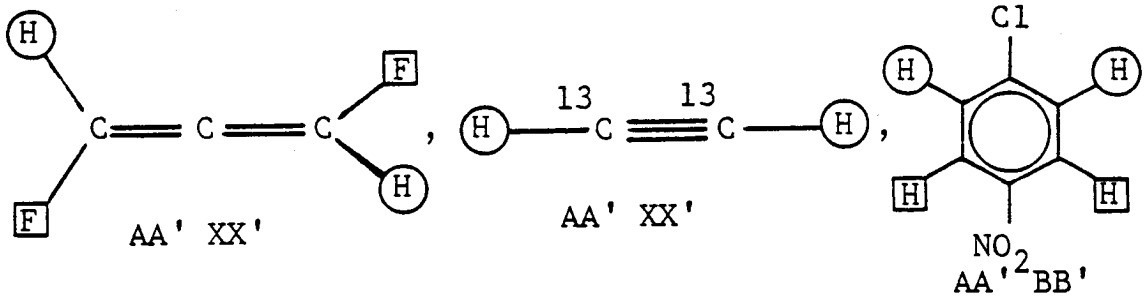

Figure 7.6: Examples For Magnetic And Chemical Equivalence

8 Pulse Techniques in NMR

In NMR spectroscopy, experiments are often build up from a few basic building blocks which are combined in different ways. These building blocks serve a certain function and can be analyzed independent from the details of how they are combined. In this Chapter we will discuss some of these building blocks and look at a few simple one-dimensional experiments which make use of them.

Many NMR experiments operate simultaneously on two different spin species, e.g., ^{13}C and ^{1}H. To make a clear distinction whether two spins are homonuclear, i.e., the same isotope with the same Larmor frequency, or heteronuclear, i.e., different isotopes with different Larmor frequencies, we will use different symbols, $\hat{I}_\kappa$ and $\hat{S}_\kappa$ for the spin operators of heteronuclear spins.

8.1 The Role of 180° Pulses

We have already seen in Chapter 2.8.1 that 180° pulses can be used to refocus the dephasing of signals due to a distribution of chemical shifts. In this Chapter we will analyze in more detail the role of 180° pulses in homonuclear and heteronuclear two-spin systems. Figure 8.1 shows the basic pulse sequence for homonuclear and

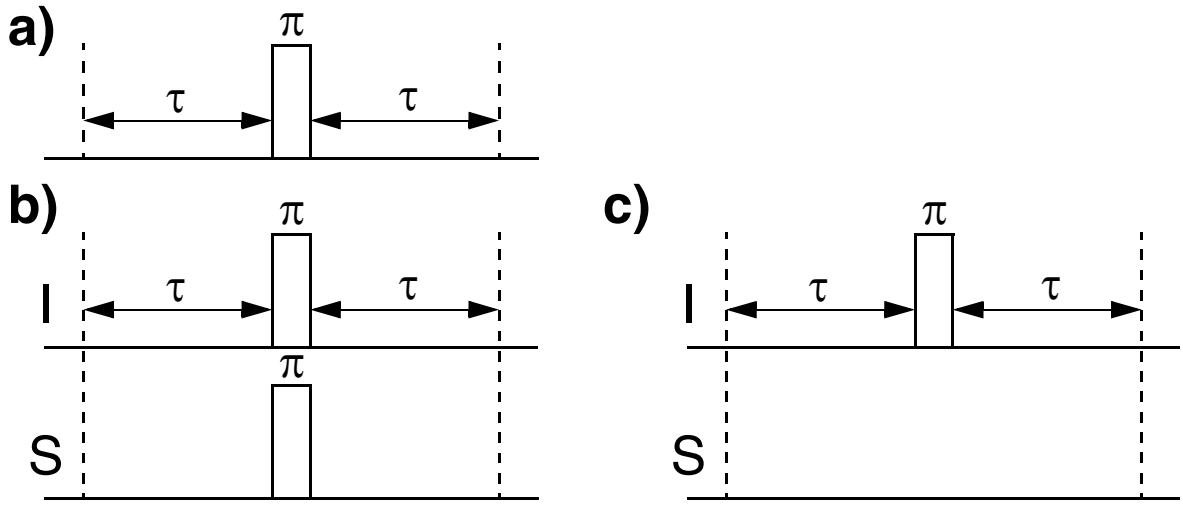

Figure 8.1: Spin-Echo Pulse Sequence
in a) homonuclear spin systems and b) and c) in heteronuclear spin systems.

heteronuclear spin systems. There are different sequences possible for the heteronuclear case because we can include a 180° pulse on only one of the two spin species or on both spin species simultaneously.

8.1.1 Spin Echoes in Homonuclear Spin Systems

The Hamiltonian of a homonuclear two-spin systems in liquids assuming weak coupling is given in the rotating frame by

$$\hat{\mathcal{H}}'' = \Omega_1 \cdot \hat{I}_{1z} + \Omega_2 \cdot \hat{I}_{2z} + 2\pi J_{12} \hat{I}_{1z} \hat{I}_{2z} \ . \qquad [8.1]$$

We now have to calculate the time evolution of the density operator under the pulse sequence shown in Fig. 8.1a. Starting from an initial density operator

$$\hat{\sigma}(0) = \hat{I}_{1x} \qquad [8.2]$$

we obtain before the 180° pulse the evolution during the delay τ under the chemical-shift and the J-coupling Hamiltonian. Since the different parts of the Hamiltonian commute, we can calculate the time evolution sequential:

$$\begin{aligned} \hat{\sigma}(\tau^-) = {} & \hat{I}_{1x} \cos(\Omega_1 \tau) \cos(\pi J_{12} \tau) + 2\hat{I}_{1y} \hat{I}_{2z} \cos(\Omega_1 \tau) \sin(\pi J_{12} \tau) \\ & + \hat{I}_{1y} \sin(\Omega_1 \tau) \cos(\pi J_{12} \tau) - 2\hat{I}_{1x} \hat{I}_{2z} \sin(\Omega_1 \tau) \sin(\pi J_{12} \tau) \end{aligned} \ . \qquad [8.3]$$

The 180° pulse will invert the sign of some of the spin operators. The phase of the pulse is not important and we will arbitrarily assume it to be a $(180°)_x$ pulse:

$$\begin{aligned} \hat{\sigma}(\tau^+) = {} & \hat{I}_{1x} \cos(\Omega_1 \tau) \cos(\pi J_{12} \tau) + 2\hat{I}_{1y} \hat{I}_{2z} \cos(\Omega_1 \tau) \sin(\pi J_{12} \tau) \\ & - \hat{I}_{1y} \sin(\Omega_1 \tau) \cos(\pi J_{12} \tau) + 2\hat{I}_{1x} \hat{I}_{2z} \sin(\Omega_1 \tau) \sin(\pi J_{12} \tau) \end{aligned} \ . \qquad [8.4]$$

The time evolution during the second delay τ will lead to 16 (4x4) terms which can be simplified to

$$\hat{\sigma}(2\tau) = \hat{I}_{1x} \cos(\pi J_{12} 2\tau) + 2\hat{I}_{1y} \hat{I}_{2z} \sin(\pi J_{12} 2\tau) \qquad [8.5]$$

using trigonometric transformations. The equivalent result will be obtained starting from an initial density operator $\hat{I}_{2x}$ with the indices 1 and 2 interchanged.

Exercise: Write down all the terms that are generated by the time evolution under the second delay τ and show that one gets indeed the result given in Eq. [8.5].

The result given in Eq. [8.5] shows that the spin-echo sequence refocuses the chemical shifts even in the presence of homonuclear dipolar couplings but leaves the time evolution under the weak homonuclear J coupling unaffected.

The calculation for the strong coupling case is more complicated due to the fact that the J-coupling and the chemical-shift Hamiltonian do not commute and there is no simple general analytical solution.

8.1.2 Spin Echoes in Heteronuclear Spin Systems

The Hamiltonian of a heteronuclear spin system is always a weak-coupling Hamiltonian

$$\hat{\mathcal{H}}'' = \Omega_I \cdot \hat{I}_z + \Omega_S \cdot \hat{S}_z + 2\pi J_{IS} \hat{I}_z \hat{S}_z \qquad [8.6]$$

and the only difference to the homonuclear case is that one can easily apply selective pulses on the two nuclei. Figure 8.1 shows the two possible cases: b) shows a spin-echo sequence with 180° pulses are applied simultaneously on both spins while in c) a spin-echo sequence is shown where the 180° pulse is only applied to the I spin.

The first case with pulses on both spins is fully equivalent to the homonuclear case and starting from

$$\hat{\sigma}(0) = \hat{I}_x \qquad [8.7]$$

we obtain a final density operator

$$\hat{\sigma}(2\tau) = \hat{I}_x \cos(\pi J_{IS} 2\tau) + 2\hat{I}_y \hat{S}_z \sin(\pi J_{IS} 2\tau) \; . \qquad [8.8]$$

Again, we obtain the equivalent result when starting from $\hat{S}_x$ with the I-spin and S-spin operators interchanged.

In the case of a single 180° pulse, we obtain the same intermediate density operator

$$\hat{\sigma}(\tau^-) = \hat{I}_x \cos(\Omega_I \tau)\cos(\pi J_{IS}\tau) + 2\hat{I}_y\hat{S}_z \cos(\Omega_I \tau)\sin(\pi J_{IS}\tau)$$
$$+ \hat{I}_y \sin(\Omega_I \tau)\cos(\pi J_{IS}\tau) - 2\hat{I}_x\hat{S}_z \sin(\Omega_I \tau)\sin(\pi J_{IS}\tau) \quad . \qquad [8.9]$$

We now apply only a 180° pulse on the I spins leading to the density operator

$$\hat{\sigma}(\tau^+) = \hat{I}_x \cos(\Omega_I \tau)\cos(\pi J_{IS}\tau) - 2\hat{I}_y\hat{S}_z \cos(\Omega_I \tau)\sin(\pi J_{IS}\tau)$$
$$- \hat{I}_y \sin(\Omega_I \tau)\cos(\pi J_{IS}\tau) - 2\hat{I}_x\hat{S}_z \sin(\Omega_I \tau)\sin(\pi J_{IS}\tau) \quad . \qquad [8.10]$$

The time evolution during the second delay τ will again lead to 16 terms which can be simplified using trigonometric expressions to

$$\hat{\sigma}(2\tau) = \hat{I}_x \quad . \qquad [8.11]$$

In this case the chemical shift of the I spin as well as the heteronuclear J coupling is refocused by the 180° pulses.

Starting from the S spin with

$$\hat{\sigma}(0) = \hat{S}_x \qquad [8.12]$$

leads to a final density operator of

$$\hat{\sigma}(2\tau) = \hat{S}_x \cos(\Omega_S 2\tau) + \hat{S}_y \sin(\Omega_S 2\tau) \quad . \qquad [8.13]$$

The role of 180° pulses in homonuclear and heteronuclear weakly-coupled spin systems is summarized in Box X.

Box X: The Role of 180° Pulses in Weakly-Coupled Spin Systems

- A 180° pulse refocuses the chemical shifts.
- A 180° pulse leaves the homonuclear J coupling unaffected.
- A 180° pulse on a *single* channel refocuses the heteronuclear J coupling.
- A 180° pulse on *both* channels leaves the heteronuclear J coupling unaffected.

8.2 Heteronuclear Spin Decoupling

We have seen in the Chapter discussing the Hamiltonians that couplings between different spin species leads to a splitting of the lines. These couplings can either be isotropic J couplings (in liquid and solid samples) or dipolar couplings which are orientation dependent (only in solids).

We consider a heteronuclear two-spin system where the irradiation frequencies of both spins are set on resonance with a coupling that can be described in the rotating frame by the Hamiltonian

$$\hat{\mathcal{H}}'' = b_{IS} 2\hat{I}_z\hat{S}_z \ . \qquad [8.14]$$

Such a Hamiltonian will lead to a splitting in the I-spin and the S-spin spectrum of magnitude b_{IS} as illustrated in Fig. 8.2a. Often these splittings are unwanted because they lead to more lines in the spectrum and make the spectrum more crowded and

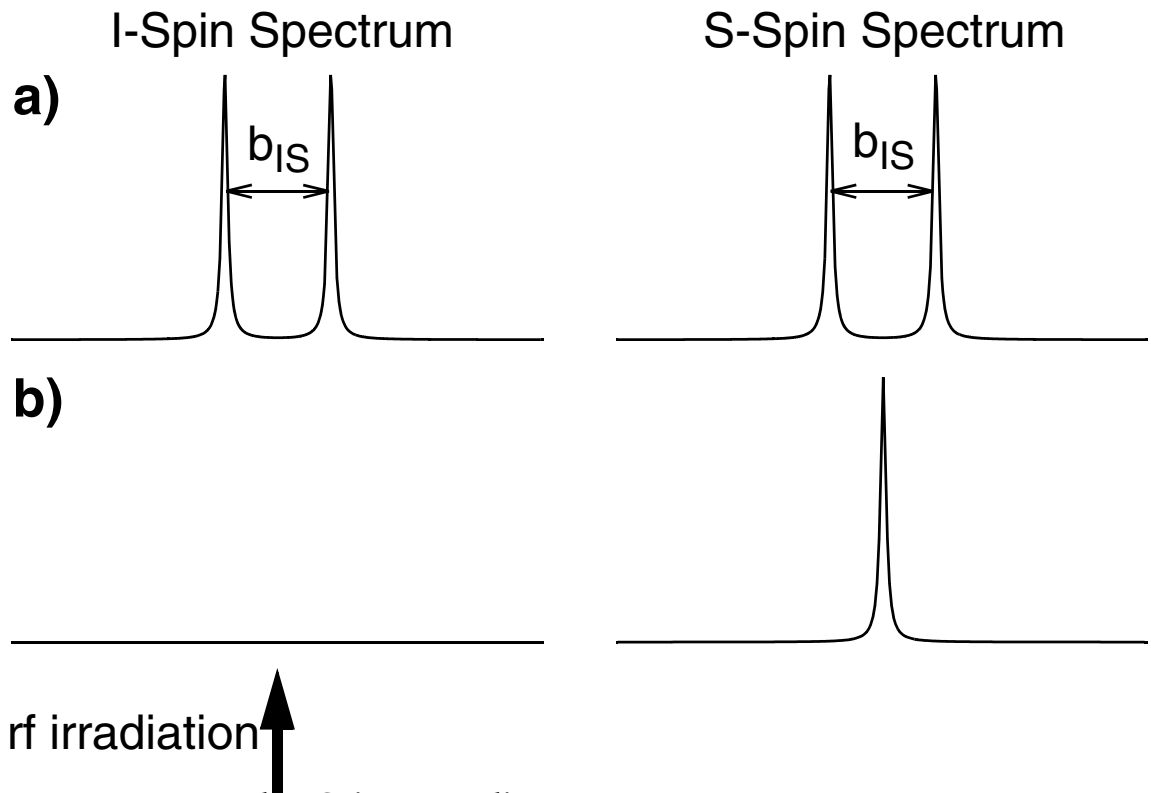

Figure 8.2: Heteronuclear Spin Decoupling
Spectra of a heteronuclear two-spin system a) without decoupling and b) with rf irradiation on the I spins.

complicated. Such splittings can be removed by irradiating the spin that is not observed with either cw irradiation ore more complicated multiple-pulse sequences. The schematic representation of the pulse sequence for acquiring an S-spin spectrum with I-spin decoupling is shown in Fig. 8.3. After the 90° pulse on the S-spin channel, the signal is detected on the S-spin channel while the I-spin channel is irradiated with an rf-field of amplitude ω_{1I}.

To explain the working of the decoupling sequence we can imagine that we replace the cw irradiation of Fig. 8.3 by many closely spaced 180° pulses. We have seen in Chapter 8.1 that 180° pulses lead to a refocusing of the heteronuclear couplings. Therefore, we expect to see a spectrum without the splitting if we sample the spectrum in the center of the delays between the 180° pulses as illustrated in Fig. 8.4. If we make the I-spin pulses in Fig. 8.4 weaker, the pulses get broader and broader until they start to touch each other. Then we end up with continuous wave (cw) irradiation on the "decoupler (I-spin) channel". It also turns out that the condition of "synchronous sampling" is not needed as long as $\omega_{1I} = |\gamma_I B_{1I}| \gg b_{IS}$.

Homonuclear couplings will, however, remain unaffected by the rf irradiation. In the practically important case of ^{13}C spectroscopy, the ^{13}C-^{13}C homonuclear couplings are negligible, because of the low natural abundance of ^{13}C: only about 1% of the carbons are magnetic and each given ^{13}C has most probably only ^{12}C neighbors.

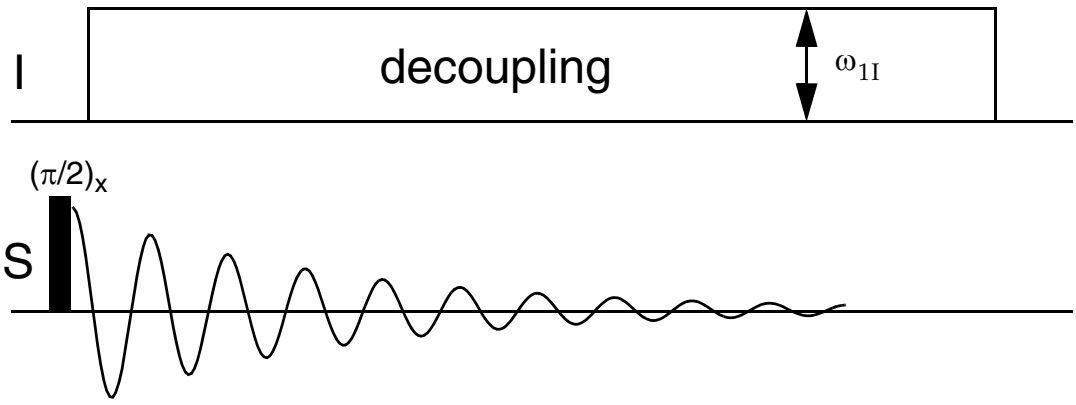

Figure 8.3: Decoupling Pulse Sequence
Schematic pulse sequence for acquiring the S-spin spectrum under I-spin decoupling.

So far, we have assumed that the irradiation on the I spin is performed "on resonance". In general, this will not be possible for all spins because of the chemical-shift dispersion. In the case of off-resonance cw irradiation where a chemical-shift term $\Omega_I I_z$ appears in the Hamiltonian, the coupling is not averaged to zero but scaled to:

$$b_{IS,\,eff} \approx \frac{\Omega_I}{\omega_{1I}} b_{IS} \qquad [8.15]$$

where ω_{1I} is the decoupler field amplitude.

To render the dependence on chemical-shift offset smaller than given by Eq. [8.15], broadbanded decoupling schemes have been invented (MLEV, WALTZ, DIPSI, GARP, WURST). The MLEV sequence, for example, uses composite pulses (see Chapter 2.8.2) of the type R=(90^0_x, 180^0_y, 90^0_x) and combines them into a "supercycle" according to:

$$\text{MLEV16} = R\bar{R}\bar{R}R\ \bar{R}R\bar{R}R\ R\bar{R}\bar{R}R\ \bar{R}R\bar{R}R \qquad [8.16]$$

where $\bar{R}$ is the phase-inverted composite pulse given by (90^0_{-x}, 180^0_{-y}, 90^0_{-x}).

These broadbanded pulse schemes are very effective for liquid state spectroscopy. In solids where the I-spins are usually strongly coupled amongst themselves (note that the spin systems are essentially infinitely large because the

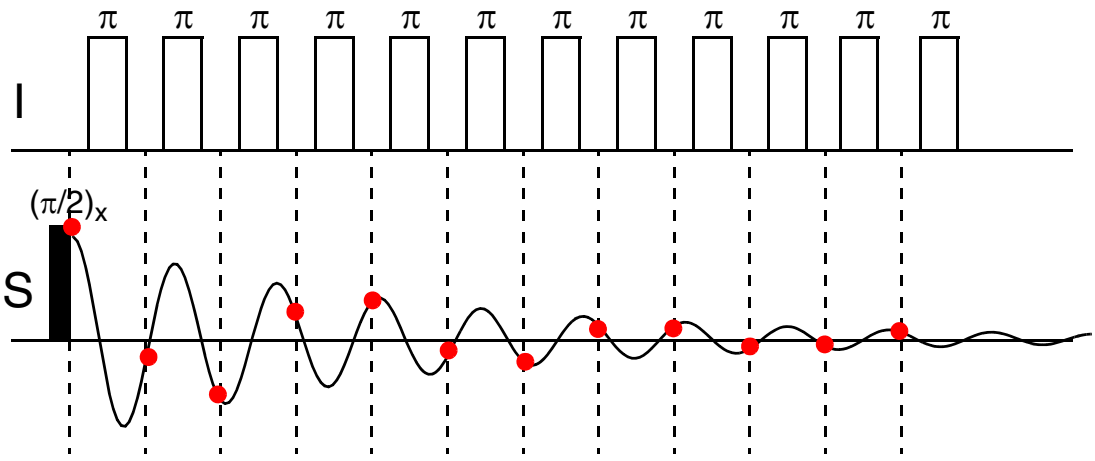

Figure 8.4: Decoupling Pulse Sequence
Schematic pulse sequence for acquiring the S-spin spectrum under I-spin decoupling.

dipolar through-space interaction couples all spins in a solid) other design principles must be applied.

8.3 Pulsed Polarization-Transfer Experiments

Polarization-transfer pulse sequences cause the transformation $\hat{I}_z \rightarrow \hat{S}_z$. Obviously, the two spins must be coupled to make such a transfer possible.There are several reasons why such a polarization transfer is desirable:

- To enhance the polarization of spins with a low gyromagnetic ratio γ_S. The equilibrium polarization of a nucleus is proportional to its gyromagnetic ratio. Almost all spectroscopically important nuclei have a lower gyromagnetic ratio than protons, e.g. ^{13}C with $\gamma_H/\gamma_C \approx 4$, ^{15}N with $\gamma_H/\gamma_N \approx 10$ and ^{2}D with $\gamma_H/\gamma_D \approx 6$. If we can transfer the polarization from the protons to these low-γ spins, we can improve the signal-to-noise on these nuclei by a factor of 4, 10 and 6 respectively. In terms of the measurement time needed to record a spectrum of a given target signal-to-noise ratio, this means a time saving of a factor 16, 100 and 36, respectively.
- The T_1-relaxation times of protons are often considerably shorter than the T_1-relaxation times of low-γ nuclei. If we use the equilibrium polarization of the protons, then we can chose a repetition rate of the experiment based on the build up of the equilibrium polarization of the protons.
- Polarization-transfer experiments can be used to correlate the chemical shifts of two spin species to elucidate the coupling network and the bonds that connect the spins. This will be discussed in more details in the next Chapter.

8.3.1 Principles of Polarization Transfer

If we consider the matrix representation of the $\hat{I}_z$ and the $\hat{S}_z$ operator in the default two-spin basis ($|\alpha\alpha\rangle$, $|\alpha\beta\rangle$, $|\beta\alpha\rangle$ and $|\beta\beta\rangle$) we find

$$(\hat{I}_z) = \begin{bmatrix} 1/2 & 0 & 0 & 0 \\ 0 & 1/2 & 0 & 0 \\ 0 & 0 & -1/2 & 0 \\ 0 & 0 & 0 & -1/2 \end{bmatrix} \qquad (\hat{S}_z) = \begin{bmatrix} 1/2 & 0 & 0 & 0 \\ 0 & -1/2 & 0 & 0 \\ 0 & 0 & 1/2 & 0 \\ 0 & 0 & 0 & -1/2 \end{bmatrix} . \qquad [8.17]$$

The energy level scheme for the such a two-spin system is given by

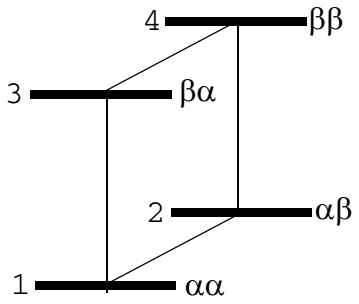

. [8.18]

From the matrix representation, we can immediately see that our desired transformation $\hat{I}_z \rightarrow \hat{S}_z$ could be realized by a population exchange between the levels 2 and 3. This could be realized by a selective 180° pulse applied to the (23) transition, except that this is a forbidden zero-quantum transition that cannot be excited by a radio-frequency field. Using rf fields we can only irradiate the four one-quantum transitions shown by solid lines in Eq. [8.18].

It is also immediately verified from the matrix representation that another way to achieve our goal is a pair of selective 180° pulses applied to the one-quantum transitions (24) and (34). Note that the one-quantum transitions (13) and (12) must remain untouched by the pulses. If there is no coupling between the two spins, the transitions (13)/(24) and (12)/(34) are degenerate and selective pulses on a single transition are impossible. From the matrix representation we can deduce the density operator after the first and second selective pulse

$$\hat{I}_z \xrightarrow{\pi^{(24)}} 2\hat{I}_z\hat{S}_z \xrightarrow{\pi^{(34)}} \hat{S}_z \qquad [8.19]$$

Such a pulse sequence can be realized but requires a precise knowledge of the transition frequencies and very selective pulses that invert only one line of the J-

coupled multiplet. In practice a pulse sequence that uses pulses and free evolution during delays is used that leads to the same result.

8.3.2 The INEPT Experiment

The refocused INEPT (Insensitive Nuclei Enhanced by Polarization Transfer) pulse sequence is schematically shown in Fig. 8.5. We assume again a heteronuclear two-spin system with the weak-coupling Hamiltonian

$$\hat{\mathcal{H}}'' = \Omega_I \cdot \hat{I}_z + \Omega_S \cdot \hat{S}_z + 2\pi J_{IS} \hat{I}_z \hat{S}_z \ . \qquad [8.20]$$

The initial density operator after the first 90° pulse is given by

$$\hat{\sigma}(0^+) = c_I \hat{I}_x \qquad [8.21]$$

and evolves during the first interval τ according to Chapter 8.1.2 to

$$\hat{\sigma}(\tau^-) = c_I \hat{I}_x \cos(\pi J_{IS}\tau) + c_I 2\hat{I}_y \hat{S}_z \sin(\pi J_{IS}\tau) \ . \qquad [8.22]$$

Setting $\tau = 1/(2J_{IS})$ leads to

$$\hat{\sigma}(\tau^-) = c_I \hat{I}_x \cos(\pi/2) + c_I 2\hat{I}_y \hat{S}_z \sin(\pi/2) = c_I 2\hat{I}_y \hat{S}_z \qquad [8.23]$$

a pure anti-phase term on the I spin. The two 90° pulses on the I-spin and S-spin channel lead to

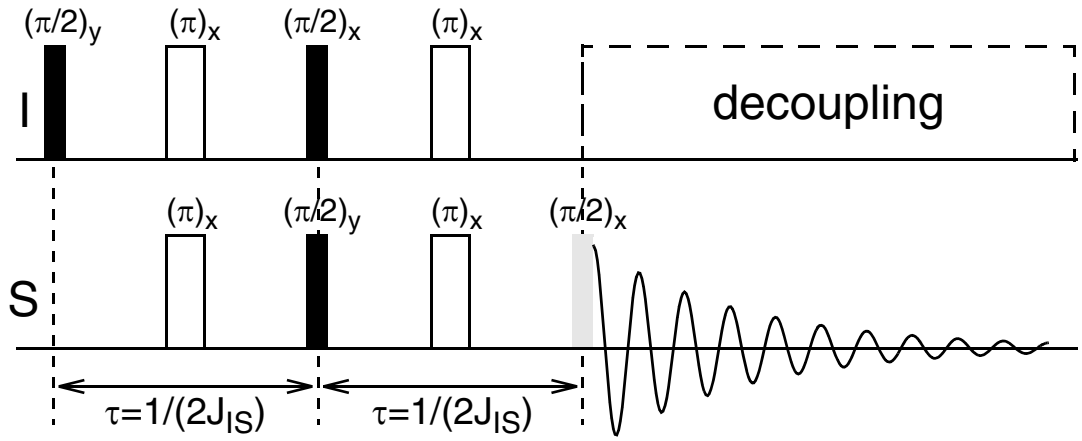

Figure 8.5: Refocused INEPT Pulse Sequence
Schematic pulse sequence for the refocused INEPT experiment.

$$\hat{\sigma}(\tau^+) = c_I 2\hat{I}_z\hat{S}_x \qquad [8.24]$$

pure anti-phase magnetization on the S spin. This term evolves now during the second interval τ under the heteronuclear spin-echo sequence to

$$\hat{\sigma}(2\tau) = c_I 2\hat{I}_z\hat{S}_x\cos(\pi J_{IS}\tau) + c_I\hat{S}_y\sin(\pi J_{IS}\tau)\ . \qquad [8.25]$$

Setting again $\tau = 1/(2J_{IS})$ leads to

$$\hat{\sigma}(2\tau) = c_I\hat{S}_y \qquad [8.26]$$

If we now apply the last 90° pulse (the gray pulse in Fig. 8.5) we have achieved the desired polarization transfer $\hat{I}_z \rightarrow \hat{S}_z$. Without the last 90° pulse we can directly detect the $\hat{S}_y$ magnetization with or without proton decoupling as shown on Fig. 8.5.

Using the INEPT pulse sequence we have achieved the same result as using the two selective pulses by using only hard unselective pulses and delays. Since most one-bond J couplings are of similar magnitude (130-150 Hz) we can adjust the delay τ simultaneously for all spin pairs.

The efficiency of the polarization transfer is 1 for a two-spin system if $\tau = 1/(2J_{IS})$. If this is not fulfilled, the efficiency is $\sin^2(\pi J_{IS}\tau)$ (the square comes from the two sine factors for the two periods of the experiment). For I_2S and I_3S spin systems modified conditions hold:

$$\begin{aligned} &CH: && \sin^2(\pi J_{IS}\tau) \\ &CH_2: && 2\sin^2(\pi J_{IS}\tau)\cos(\pi J_{IS}\tau) \\ &CH_3: && 3\sin^2(\pi J_{IS}\tau)\cos^2(\pi J_{IS}\tau) \end{aligned} \qquad [8.27]$$

As mentioned above, we can gain a factor of four in signal for the case of carbons and protons. Note that the gain in S/N can even be bigger than expected from our arguments because the relevant relaxation time (T_1) is the one of the protons, instead of the one of the carbons in direct excitation. Usually, the proton relaxation times are shorter than the ones of low-γ nuclei and more experiments per time unit can be performed, resulting in a further improved S/N of the averaged signal.

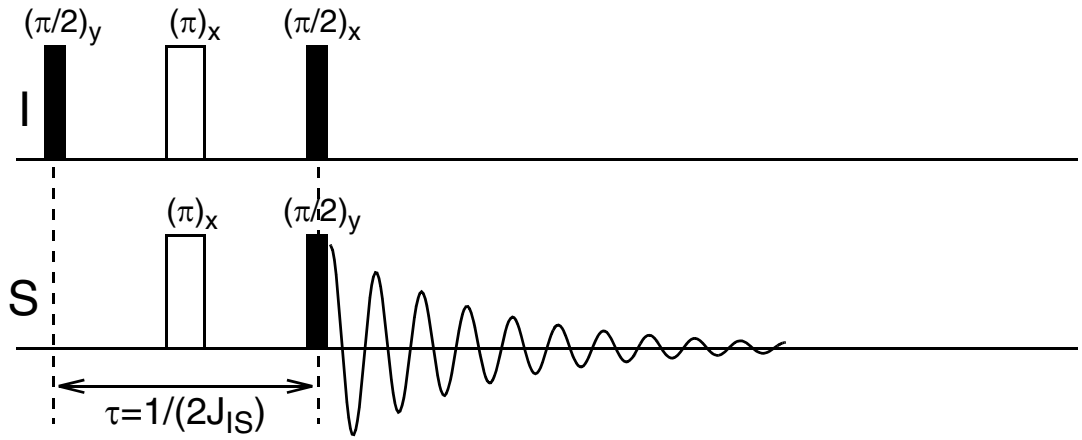

Figure 8.6: INEPT Pulse Sequence
Schematic pulse sequence for the INEPT experiment.

It should be noted that the experiment described above is the so called "refocused INEPT" experiment. An enhanced signal can also be obtained if one starts to detect after the first $\frac{\pi}{2}$ pulse on the S channel as shown in Fig.8.6. All pulses during the second τ period are left away. In this case, the FID starts with no intensity, because the state $2\hat{I}_z\hat{S}_x$ is not observable. Under the action of the J-coupling, observable magnetization develops during the FID. In such a spectrum, the S-spin multiplets are in antiphase and not in phase as in the refocused INEPT experiment as shown in Fig. 8.7. No decoupling can be used in this experiment since the heteronuclear coupling is needed during the acquisition time to generate detectable magnetization.

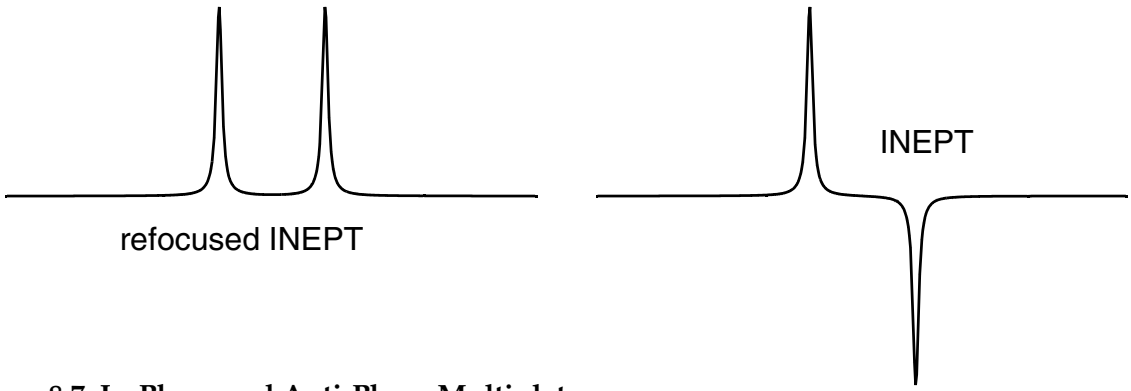

Figure 8.7: In-Phase and Anti-Phase Multiplet
Multiplet structure in an IS spin system for the refocused INEPT and the INEPT experiment.

8.3.3 Other Pulsed Polarization-Transfer Experiments

There are quite a few other experiments which implement polarization-transfer schemes in a similar way to the INEPT experiment. They are all based on the $\tau - \pi - \tau$ motif that is also used as the basis of the INEPT experiments. One example for such a sequence is the DEPT experiment (Fig. 8.8) leading to intensities that are modulated by the length of final θ-angle pulse on the I channel

$$\begin{aligned} &CH: && \sin(\theta) \\ &CH_2: && 2\sin(\theta)\cos(\theta) \\ &CH_3: && 4\sin(\theta)\cos^2(\theta) \end{aligned} \qquad [8.28]$$

and not by the size of the coupling as in the INEPt experiement.

Another example for such experiments is the APT sequence which is used to determine the number of directly bound protons on a ^{13}C atom. All these sequences can be incorporated as building blocks into more complicated one-dimensional or two-dimensional experiments.

8.4 Cross Polarization

An alternative way for heteronuclear polarization transfer is the so-called cross-polarization experiment (Fig. 8.9). This experiment is particularly important in

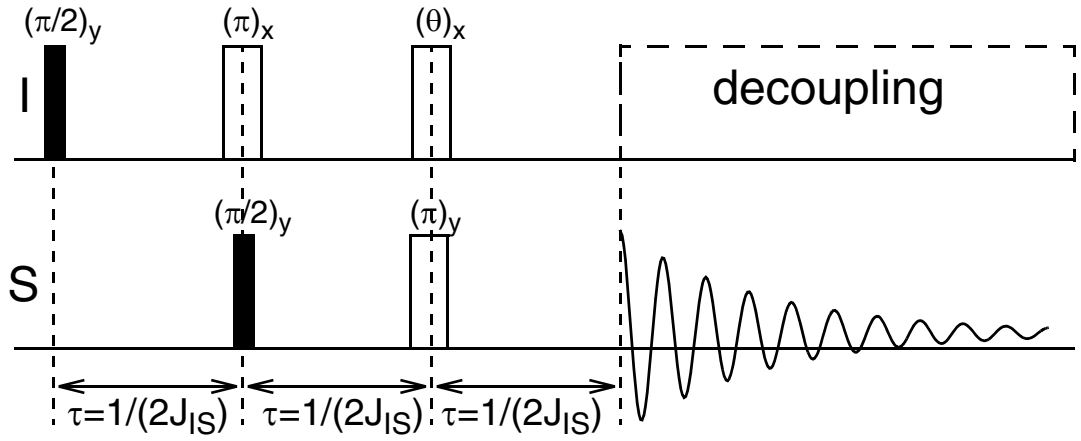

Figure 8.8: DEPT Pulse Sequence
Schematic pulse sequence for the DEPT experiment.

solid-state NMR where INEPT-based polarization transfer is difficult to achieve due to the strong homonuclear dipolar couplings.

For an isolated heteronuclear two-spin system the Hamiltonian neglecting chemical-shift terms is given by:

$$\hat{\mathcal{H}}'' = \omega_{1I}\hat{I}_x + \omega_{1S}\hat{S}_x + 2\omega_{IS}\hat{I}_z\hat{S}_z \qquad [8.29]$$

or if we tilt the coordinate system such that the new z-axis is along the old x axis:

$$\hat{\mathcal{H}}'' = \omega_{1I}\hat{I}_z + \omega_{1S}\hat{S}_z + 2\omega_{IS}\hat{I}_x\hat{S}_x \qquad [8.30]$$

The matrix representation of this Hamiltonian in the tilted frame is given by

$$(\hat{\mathcal{H}}'') = \frac{1}{2}\begin{bmatrix} \Sigma & 0 & 0 & \omega_{IS} \\ 0 & \Delta & \omega_{IS} & 0 \\ 0 & \omega_{IS} & -\Delta & 0 \\ \omega_{IS} & 0 & 0 & -\Sigma \end{bmatrix} \qquad [8.31]$$

with $\Sigma = \omega_{1I} + \omega_{1S}$ and $\Delta = \omega_{1I} - \omega_{1S}$.

Such a Hamiltonian can be decomposed into two non-interacting 2x2 blocks, or pictorially speaking, into two fictitious spin-1/2 systems, known as double-quantum (Σ) and zero-quantum (Δ) subspaces. The double-quantum subspace Σ contains the

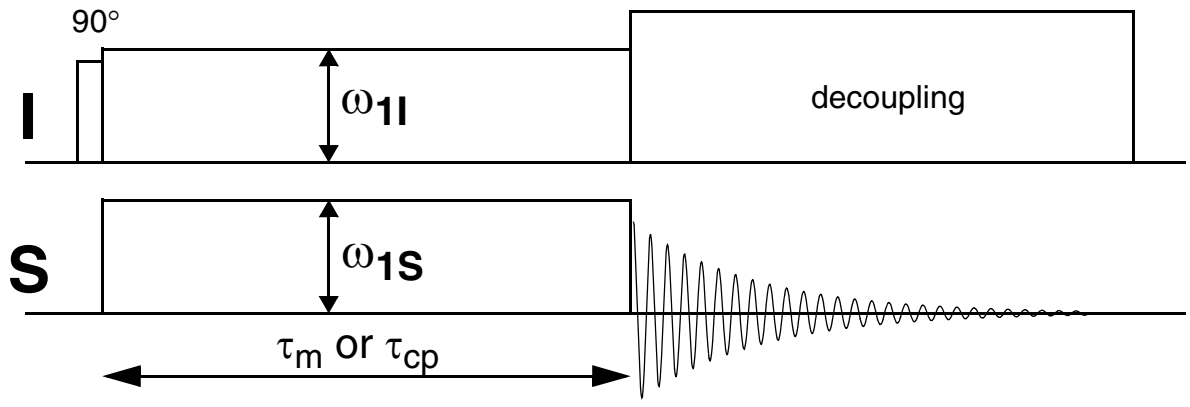

Figure 8.9: Pulse Sequence for Cross Polarization
In a cross-polarization experiment the rf-field amplitudes ω_{1I} and ω_{1S} are matched in order to allow polarization transfer from the I spins to the S spins.

energy levels 1, 4 and coherences between these two, the zero-quantum subspace Δ the energy levels 2, 3 and the coherences between them. We can write the Hamiltonian in these two subspaces in operator form as

$$\begin{aligned} \hat{\mathcal{H}}^{\Sigma} &= \Sigma\hat{I}_z^{\Sigma} + \omega_{IS}\hat{I}_x^{\Sigma} \\ \hat{\mathcal{H}}^{\Delta} &= \Delta\hat{I}_z^{\Delta} + \omega_{IS}\hat{I}_x^{\Delta} \end{aligned} \quad . \qquad [8.32]$$

Inspection of the Hamiltonian of Eq. [8.31] shows that for $\Delta = \omega_{1I} - \omega_{1S} = 0$ the dipolar coupling can lead to an inversion of the population of the energy levels 2 and 3. The condition $\Delta = 0$ is the so-called *Hartmann-Hahn condition*:

$$|\omega_{1I}| = |\gamma_I B_{1I}| = |\gamma_S B_{1S}| = |\omega_{1S}| \qquad [8.33]$$

The operator in the fictitious spin-1/2 subspace is then I_x^{Δ} and this can be used to apply a selective π pulse to the (23) transition. As mentioned earlier, such a pulse causes a complete transfer of polarization

$$\hat{I}_z \longrightarrow \hat{S}_z \qquad [8.34]$$

The "pulse length" is given by $\omega_{IS}\tau_{mix}$ and as function of τ_{mix} the magnetization oscillates back and forth between the I and the S spin. For a powdered solid sample, where b_{Is} is the dipolar interaction, the superposition of different cosine functions due to the orientation dependence of the dipolar coupling, gives rise to a damped oscillation as depicted in Fig. 8.10.

The cross-polarization experiments can also be performed in the liquid state, with the J-coupling as the transfer mechanism. It is, however, much more sensitive to the precise setting of the Hartmann-Hahn matching condition due to the smaller magnitude of the J coupling.

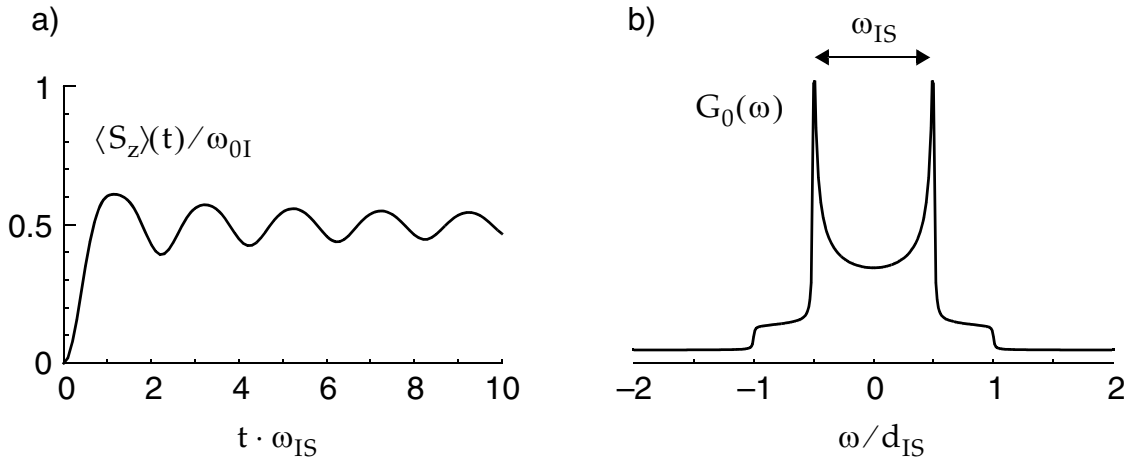

Figure 8.10: Cross Polarization
a) Evolution in a powder of the S-spin polarization for an isolated two-spin system IS with the initial condition $\sigma(0) = \omega_{0I} I_z$. The time is given in units of the dipolar coupling period $1/\omega_{IS}$. b) Pake doublet obtained from the Fourier transform of the oscillation $g_0(t)$. The frequency scale is in units of the dipolar coupling constant.

9 Two-Dimensional NMR Spectroscopy

We have briefly discussed the principles of two-dimensional NMR spectroscopy in Chapter 3.3 in the context of the longitudinal chemical-exchange experiment. Schematically, we can represent a 2D experiment as shown in Figure 9.1with four different time periods. The preparation period generates the initial state of the spin system for the time evolution during t_1. It can be a simple 90° pulse or a more complicated pulse sequence that generates the desired initial density operator. The state evolves then during the evolution time which is not a fixed time but incremented by an interval Δt_1 after each experiment. The mixing time converts the coherences which evolved during the evolution time into observable one-quantum coherences. These one-quantum coherences are then detected during the detection time t_2.

A typical example for the mixing time are either a change in the coherence order, i.e., the conversion of multiple-quantum coherences that evolved during the time t_1 into observable single-quantum coherences during t_2. A second important example is the transfer of magnetization from one spin to another spin during the mixing time to obtain correlation spectra that correlate the chemical shifts of different spins. The mixing period is a very important part of the pulse sequence because it determines the information content of the spectrum.

Such an experiment leads to a two-dimensional data set which can be described in the time domain by the signal $s(t_1, t_2)$. After Fourier transformation of both dimensions, one obtains a two-dimensional frequency-domain spectrum

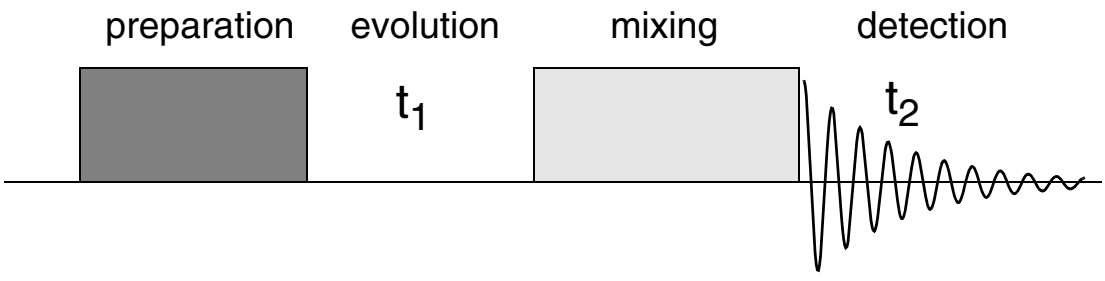

Figure 9.1: Two-Dimensional NMR Experiment
Schematic design of a two-dimensional NMR experiment.

$S(\omega_1, \omega_2)$. The details of the data-acquisition scheme and of the processing are not so important in the context of the present course and will not be discussed here. This topic can be found in detail in the textbooks about modern multi-dimensional NMR spectroscopy.

In the following we will discuss the pulse sequences and the resulting spectra of some important two-dimensional NMR experiments and their information content. In addition, important applications of the experiments will be shown.

9.1 Homonuclear 2D Correlation Spectroscopy (COSY)

One-dimensional NMR spectra cannot always be analyzed unambiguously. The spectrum shown in Fig. 9.2, for example, could be the one of a weakly coupled two-spin system but it could also be the spectrum of 4 uncoupled spins with different chemical shifts. To remove this ambiguity, homonuclear two-dimensional correlation spectroscopy can be employed. In such a spectrum, we can detect two-spin and multi-spin correlations as they appear between coupled spins where the Hamiltonian contains two-spin terms, e.g., the isotropic J-coupling Hamiltonian $2\pi J_{12}\hat{I}_{1z}\hat{I}_{2z}$.

Spins belonging to a coupled spin system can be identified by polarization-transfer or coherence-transfer experiments. Several examples for heteronuclear polarization transfer have been discussed in the preceding chapter. The corresponding 2D-spectra will have cross-peaks between correlated spins, while single spins appear only on the diagonal of the spectrum.

In the following, we discuss the example of the COSY experiment: The general principles of 2D spectroscopy as discussed in Chapter 3.3 also apply to this

Figure 9.2: One-Dimensional Spectrum

experiment. As already discussed in the previous section, the signal is detected as a function of the time t_2 while the time t_1 is varied systematically to generate a two-dimensional time-domain data set $s(t_1, t_2)$. After double Fourier transform, the 2D spectrum, $S(\omega_1, \omega_2)$, is obtained.

For the COSY experiment we consider two spins with chemical shifts and a weak J coupling. The Hamiltonian and the main features of the different time periods are:

- The preparation period consists of a relaxation delay where equilibrium magnetization $\hat{F}_z = \sum \hat{I}_{kz}$ is established and a 90° pulse that creates x magnetization. In the calculation here, we will only look at magnetization originating from spin 1 to simplify the discussion. Of course, magnetization of spin 2 must be considered the same way:

$$\hat{I}_{1z} \xrightarrow{\hat{I}_y\left(\frac{\pi}{2}\right)} \hat{I}_{1x} \qquad [9.1]$$

- In the evolution period, the magnetization evolves under the chemical shift and the scalar coupling (weak-coupling case) with the Hamiltonian:

$$\hat{\mathcal{H}}'' = \Omega_1 \cdot \hat{I}_{1z} + \Omega_2 \cdot \hat{I}_{2z} + 2\pi J_{12} \hat{I}_{1z} \hat{I}_{2z} \ . \qquad [9.2]$$

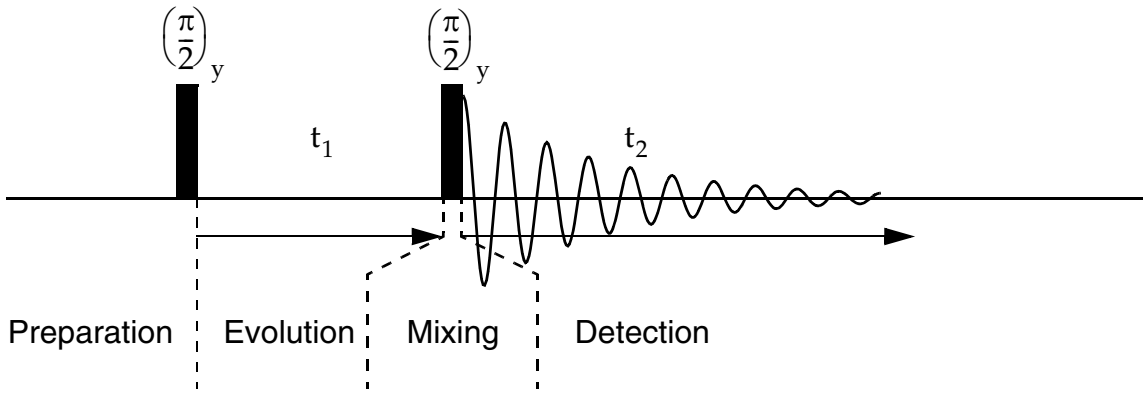

Figure 9.3: COSY Pulse Sequence
Schematic drawing of the COSY pulse sequence with two 90° pulses and the evolution time t_1 and the detection time t_2.

$$\hat{I}_{1x} \xrightarrow{\hat{I}_{1z}(\Omega_1 t_1)} \begin{cases} \hat{I}_{1x} \xrightarrow{2\hat{I}_{1z}\hat{I}_{2z}(\pi J t_1)} \begin{cases} \hat{I}_{1x} \\ 2\hat{I}_{1y}\hat{I}_{2z} \end{cases} \\ \hat{I}_{1y} \xrightarrow{2\hat{I}_{1z}\hat{I}_{2z}(\pi J t_1)} \begin{cases} \hat{I}_{1y} \\ -2\hat{I}_{1x}\hat{I}_{2z} \end{cases} \end{cases} \qquad [9.3]$$

- The mixing time consists of a single 90° pulse that interconverts coherences. Note that we have converted anti-phase coherence of spin 1 to anti-phase coherence on spin 2.

$$\begin{aligned} \hat{I}_{1x} &\xrightarrow{\hat{I}_y\left(\frac{\pi}{2}\right)} -\hat{I}_{1z} \\ 2\hat{I}_{1y}I_{2z} &\longrightarrow 2\hat{I}_{1y}\hat{I}_{2x} \\ \hat{I}_{1y} &\longrightarrow \hat{I}_{1y} \\ 2\hat{I}_{1x}\hat{I}_{2z} &\longrightarrow 2\hat{I}_{1z}\hat{I}_{2x} \end{aligned} \qquad [9.4]$$

- During the detection period, the system evolves under the influence of chemical-shift and J coupling. We detect $\langle M_x \rangle = \gamma(\hat{I}_{1x} + \hat{I}_{2x})$. Only the third and fourth term listed above contribute to the final signal. The fourth term does only contribute at times t_2>0 because it can evolve into observable magnetization:

$$\hat{I}_{1y} \xrightarrow{\hat{I}_{1z}(\Omega_1 t_2)} \begin{cases} \hat{I}_{1y} \xrightarrow{2\hat{I}_{1z}\hat{I}_{2z}(\pi J t_1)} \begin{cases} \hat{I}_{1y} \\ -2\hat{I}_{1x}\hat{I}_{2z} \end{cases} \\ -\hat{I}_{1x} \xrightarrow{2\hat{I}_{1z}\hat{I}_{2z}(\pi J t_1)} \begin{cases} -\hat{I}_{1x} \\ -2\hat{I}_{1y}\hat{I}_{2z} \end{cases} \end{cases} \qquad [9.5]$$

$$2\hat{I}_{1z}\hat{I}_{2x} \xrightarrow{\hat{I}_{2z}(\Omega_2 t_2)} \begin{cases} 2\hat{I}_{1z}\hat{I}_{2x} \xrightarrow{2\hat{I}_{1z}\hat{I}_{2z}(\pi J t_1)} \begin{cases} 2\hat{I}_{1z}\hat{I}_{2x} \\ \hat{I}_{2y} \end{cases} \\ 2\hat{I}_{1z}\hat{I}_{2y} \xrightarrow{2\hat{I}_{1z}\hat{I}_{2z}(\pi J t_1)} \begin{cases} 2\hat{I}_{1z}\hat{I}_{1y} \\ -\hat{I}_{2x} \end{cases} \end{cases} \qquad [9.6]$$

The total signal is then given by:

$$\begin{aligned} -s(t_1, t_2) = {} & \cos(\pi J t_1)\cos(\pi J t_2)\sin(\Omega_1 t_1)\sin(\Omega_1 t_2) \\ & + \cos(\pi J t_1)\cos(\pi J t_2)\sin(\Omega_2 t_1)\sin(\Omega_2 t_2) \\ & + \sin(\pi J t_1)\sin(\pi J t_2)\sin(\Omega_2 t_1)\sin(\Omega_1 t_2) \\ & + \sin(\pi J t_1)\sin(\pi J t_2)\sin(\Omega_1 t_1)\sin(\Omega_2 t_2) \end{aligned} \qquad [9.7]$$

and looks, after Fourier transform, as plotted in Fig. 9.4. The cross-peaks are in anti-phase absorption mode, i.e., each of the lines in the multiplet is an absorption line but the different lines in the multiplet have different signs. The diagonal peaks are in-phase dispersion mode, i.e., each of the multiplet lines is dispersive but all the lines in the multiplet have the same sign.

The cross peaks in a COSY spectrum appear only between spins that are directly coupled by a J coupling and they identify, therefore, neighbors. No relay peaks can be found. In an AMX spin systems with $J_{AX} = 0$, no cross peaks will appear between the resonances of spins A and X. Figure 9.5 shows an example of a COSY spectrum of a smaller protein. The magnitude and the relative sign of the J couplings can be extracted from the cross-peak patterns. There are, however, better experiments available to obtain this information.

There are many variations of the basic COSY experiment that are, nowadays, used more often than the original COSY sequence. The most important variation is the double-quantum-filtered COSY (DQF COSY) experiment. Figure 9.6 shows the pulse sequence which differs from the basic COSY sequence in an additional 90° pulse. The third pulse in combination with an appropriate phase cycle is used to select double quantum coherence and convert it into antiphase magnetization. This is the

second term in Eq. [9.4]. Through the phase cycle all the other terms are eliminated and the strong anti-phase diagonal peaks in the COSY spectrum are eliminated. The resulting spectrum has anti-phase absorption-mode lines for the diagonal and the cross peaks as shown in Fig. 9.7.

Other variations of the COSY experiment include the E.COSY experiment which has a simplified multiplet structure that allows better extraction of coupling constants.

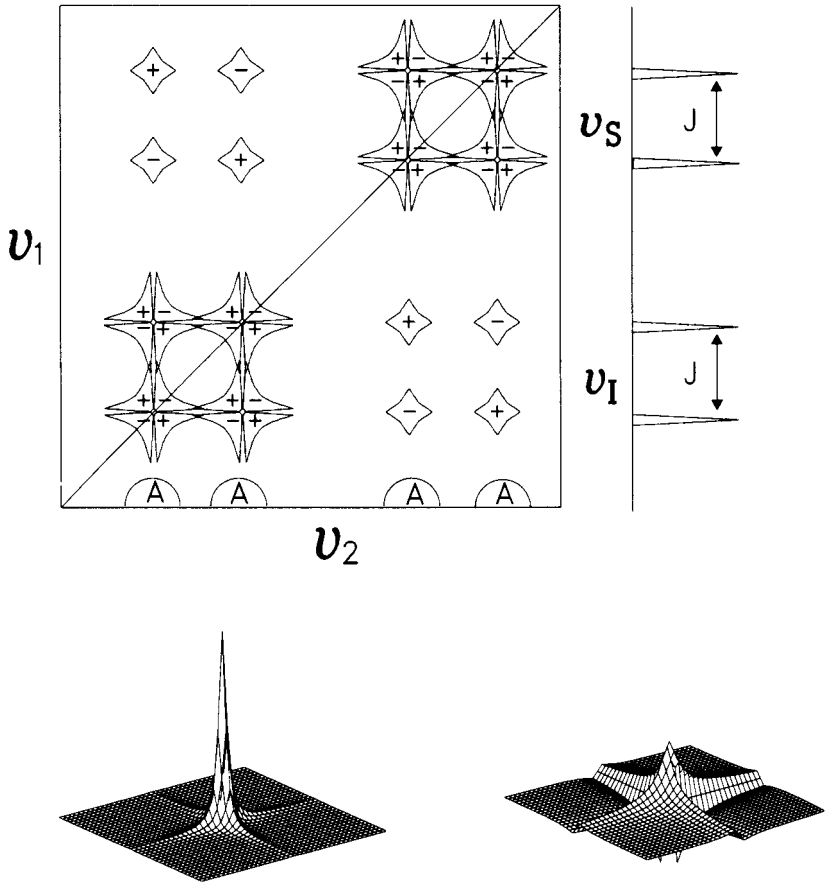

Line shapes of 2D peaks in absorption mode (left) and dispersion mode (right).

Figure 9.4: Peak Line Shapes in a COSY Spectrum
from F.J.M. van de Ven: Multidimensional NMR in Liquids, VCH Publishers

9.2 Nuclear Overhauser Effect Spectroscopy (2D NOESY)

Relaxation in spin systems is caused by fluctuations in the local magnetic field. Such fluctuations can be produced by a change in the anisotropic interactions (dipolar coupling, chemical shift, or quadrupolar coupling) due to molecular tumbling. Relaxation leads to a damping of the coherences (T_2 relaxation) and to an

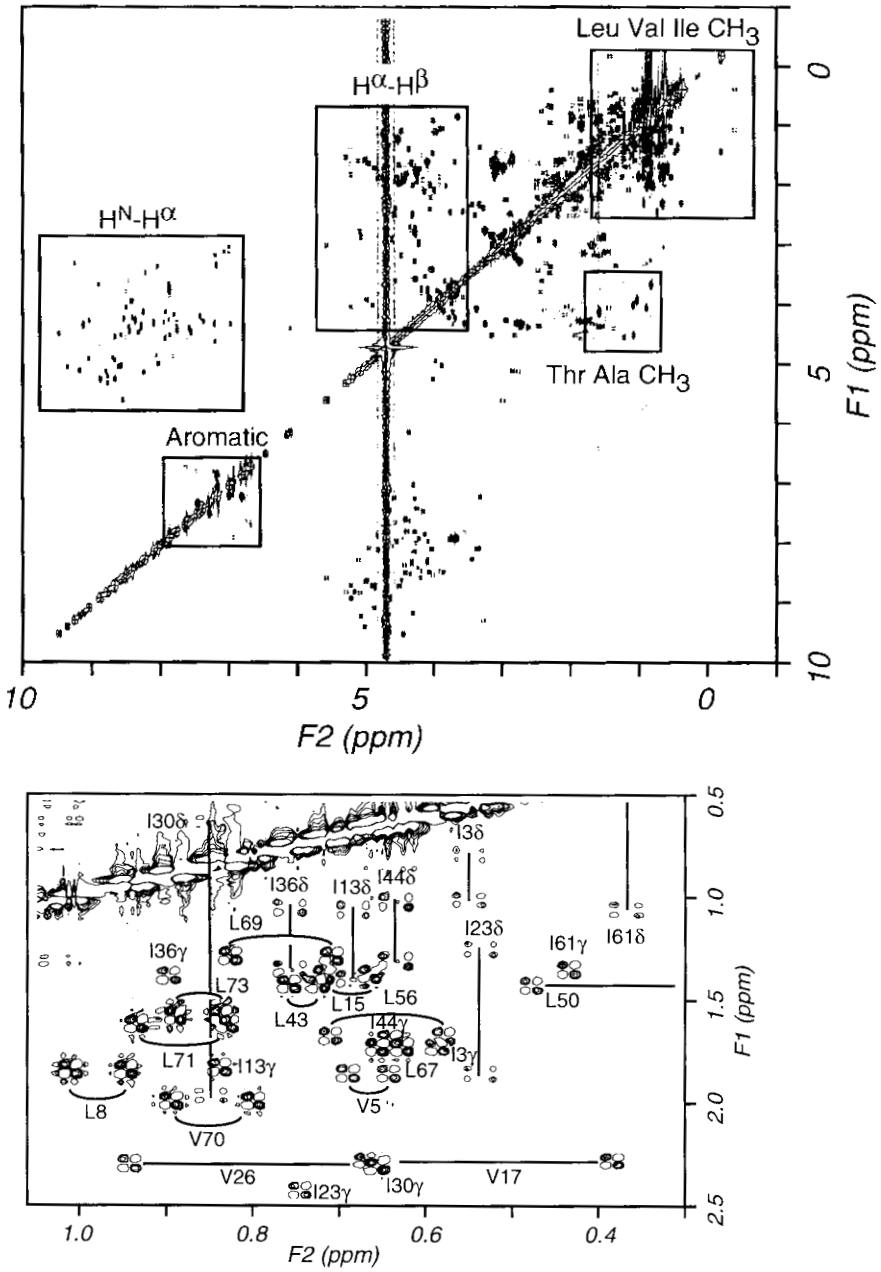

Figure 9.5: Example of an COSY Spectrum
^{1}H COSY spectrum of the small protein ubiquitin.

equilibration of the populations towards the equilibrium density operator (T_1 relaxation) as was already discussed in the classical description using the Bloch equations. Besides such a decay of the magnetization towards the thermal equilibrium, relaxation can also lead to polarization and coherence transfer between different nuclei. A detailed quantum-mechanical description of these phenomena is

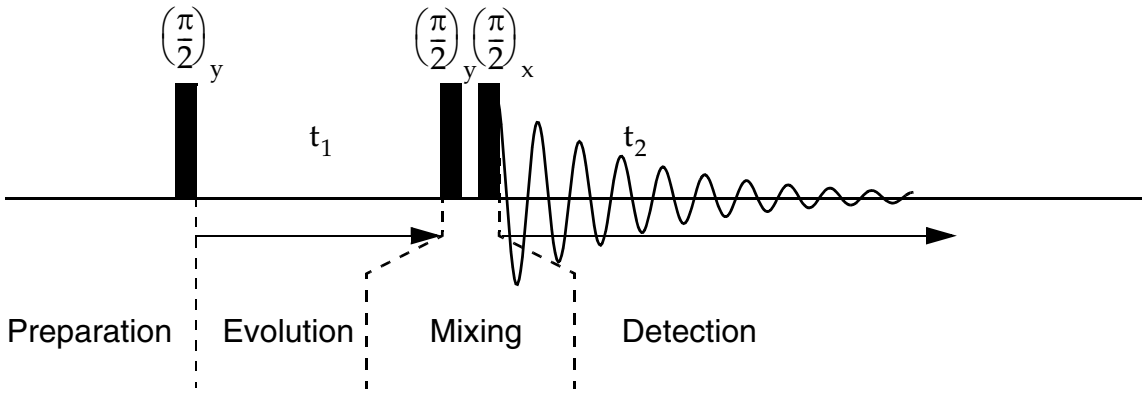

Figure 9.6: DQF COSY Pulse Sequence
Schematic drawing of the DQF COSY pulse sequence with three 90° pulses and the evolution time t_1 and the detection time t_2.

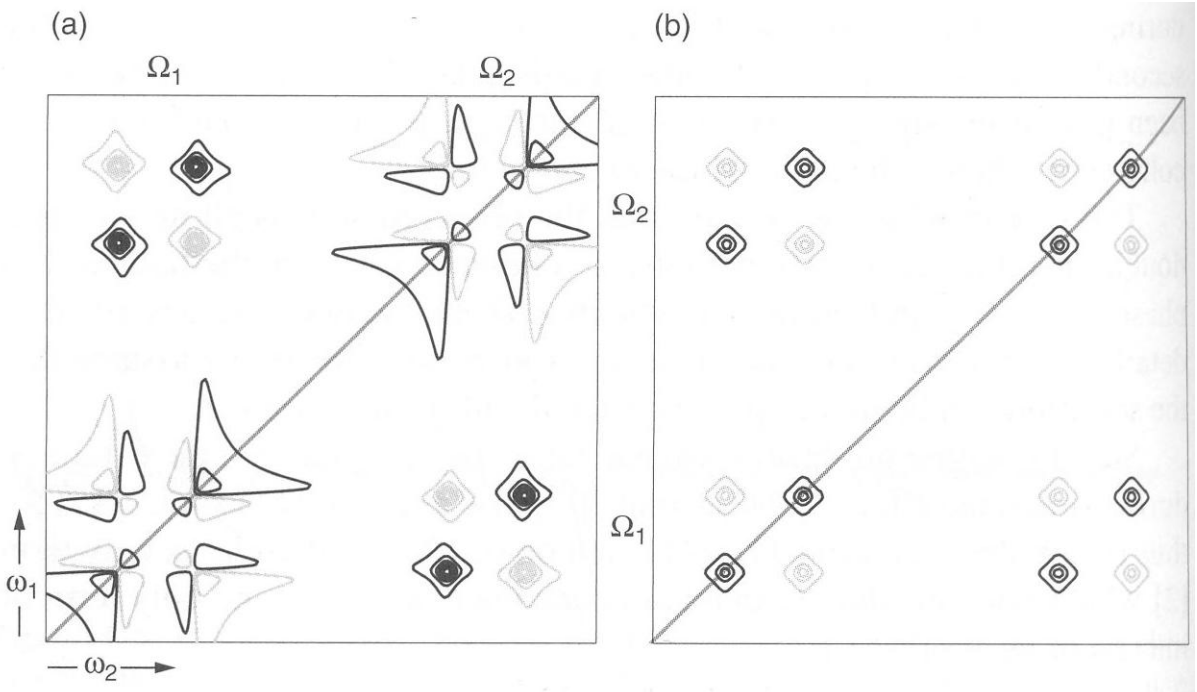

Figure 9.7: COSY Line Shapes
Line shapes of the diagonal and cross peaks in a) the COSY and b) the DQF COSY experiment. (From J. Keeler, Understanding NMR Spectroscopy)

beyond the scope of this lecture and we will only discuss them on a phenomenological level. For a two-spin system in a classical picture, we can write the following system of coupled differential equations for the z magnetization:

$$\frac{d}{dt}\begin{pmatrix} M_A \\ M_B \end{pmatrix} = \begin{pmatrix} \frac{-1}{T_1^{(A)}} & \sigma_{AB} \\ \sigma_{AB} & \frac{-1}{T_1^{(B)}} \end{pmatrix}\begin{pmatrix} M_A \\ M_B \end{pmatrix} = \begin{pmatrix} R_1^{(A)} & \sigma_{AB} \\ \sigma_{AB} & R_1^{(B)} \end{pmatrix}\begin{pmatrix} M_A \\ M_B \end{pmatrix} . \qquad [9.8]$$

Note the formal identity of Eq. [9.8] with the equations describing the 2D chemical exchange process (see Chapter 3.3). The auto-relaxation rate constant $1/T_1^{(i)}$ and the cross-relaxation rate constant σ_{AB} can be expressed in terms of the transition probabilities in the four energy levels of a two-spin 1/2 system (see Fig. 9.8). In a perturbation approach (Fermi's Golden Rule), the transition probabilities are given by:

$$W_{kl} = \left|\langle k|\hat{\mathcal{H}}_D|l\rangle\right|^2 J(\omega_{kl}) \qquad [9.9]$$

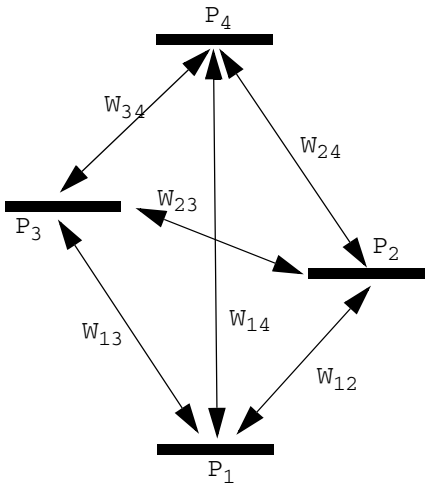

Figure 9.8: Transition Probabilities

where $\hat{\mathcal{H}}_D$ is the time-dependent dipolar Hamiltonian and $J(\omega_{kl})$ (Fig. 9.9) is the spectral-density function of the random process that modulates $\hat{\mathcal{H}}_D$ evaluated at the frequency ω_{kl}. For isotropic tumbling with a correlation time τ_c, we obtain

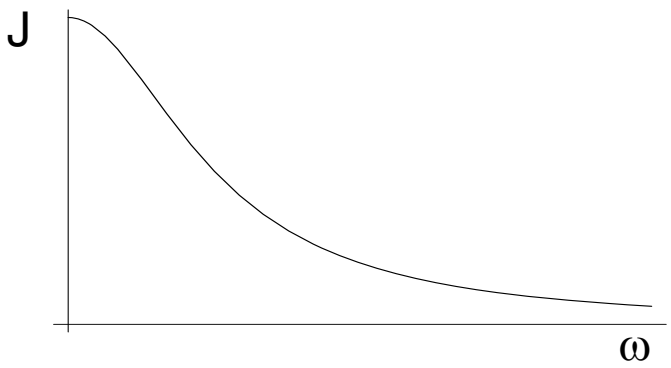

Figure 9.9: Spectral-Density Function J(ω)

$$J(\omega) = \frac{2\tau_c}{1 + (\omega\tau_c)^2} \qquad [9.10]$$

For the homonuclear case (two identical nuclei), the transition probabilities simplify to:

$$\begin{aligned} W_1 &= W_{13} = W_{24} = W_{12} = W_{34} = \frac{3}{2} q_{AB} J(\omega_0) \\ W_0 &= W_{23} = q_{AB} J(0) \\ W_2 &= W_{14} = 6 q_{AB} J(2\omega_0) \end{aligned} \qquad [9.11]$$

with

$$q_{AB} = \frac{1}{20}\left(\frac{\mu_0}{4\pi}\right)^2 \hbar^2 \gamma^4 \frac{1}{r_{AB}^6}. \qquad [9.12]$$

For the relaxation-rate constants, we obtain:

$$\begin{aligned} R_1 &= -(2W_1 + W_2 + W_0) = -q_{AB}(J(0) + 3J(\omega_0) + 6J(2\omega_0)) \\ \sigma_{AB} &= W_0 - W_2 = q_{AB}(J(0) - 6J(2\omega_0)) \end{aligned} \qquad [9.13]$$

Note, that the cross-relaxation rate constant σ_{AB} is proportional to $1/r_{AB}^6$. It allows, therefore, to measure internuclear distances. This is the basis for NMR structure determination. The correlation time τ_c is often unknown and no absolute distances can be determined. However, a known distance in the structure can be used for a calibration of the data.

Cross-relaxation rates are usually determined by 2D spectroscopy. The pulse sequence used is exactly the same as for 2D chemical exchange (Fig. 9.10). For $\tau_c\omega_0 > 1.12$, σ_{AB} is positive and the 2D spectrum looks the same as for chemical exchange (see Chapter 3.3) with positive cross peaks. For $\tau_c\omega_0 < 1.12$, the cross peaks have a negative intensity, but still a pure absorption line shape. For $\tau_c\omega_0 = 1.12$, cross relaxation is quenched. The intensities of diagonal and cross peaks for different correlation times are plotted in Fig. 9.11. At 500 MHz the zero-crossing of the cross-relaxation rate constants appears at a correlation time of $\tau_c = 3.6$ ns.

9.3 Double-Quantum Filtered Spectroscopy: INADEQUATE

The homonuclear methods described so far apply mostly to ^{1}H spectroscopy where we have a high abundance (100%) of the nuclei. The methods do not work for ^{13}C or ^{15}N where we have a natural abundance of only 1.1% and 0.4%, respectively. There is a very low probability that we have two magnetically active nuclei close to each other and the spectra (COSY and NOESY) will be dominated by the isolated nuclei and have, therefore, little information content. The DQF COSY spectrum eliminates the contributions from isolated spins and could in principle be applied to diluted spin systems.

In practice, however, a different experiment is used which is a double-quantum single-quantum correlation experiment named INADEQUATE (Incredible Natural Abundance DoublE QUAntum Transfer Experiment). The basic pulse sequence is shown in Fig. 9.12. A typical spectrum shows peaks at the sum chemical-shift frequency in t_1 and the chemical shifts in t_2 if two spins have a one-bond J coupling as is shown for the example of ethyl benzene in Fig. 9.13. Such a spectrum allows the tracing out of the coupling network and, therefore, the connectivity of the carbon atoms. Such a spectrum is very useful for the assignment of the ^{13}C resonances.

The pulse sequence generates double-quantum coherence during the preparation period where only the J coupling and no chemical shifts are active (see

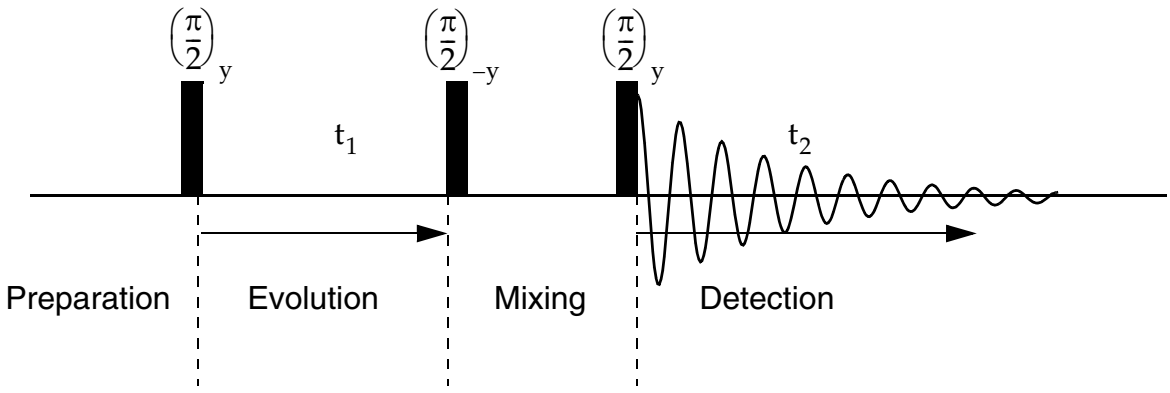

Figure 9.10: NOESY Pulse Sequence
Schematic drawing of the NOESY pulse sequence with three 90° pulses and the evolution time t_1 and the detection time t_2.

Chapter 8.1). The double-quantum coherence then evolves during t_1 at a frequency which is the sum of the chemical shifts. It is then converted to observable one-quantum coherence by the mixing pulse. The advantage of the INADEQUATE experiment over the DQF COSY experiment is the improved suppression of the isolated spins due to the absence of diagonal peaks.

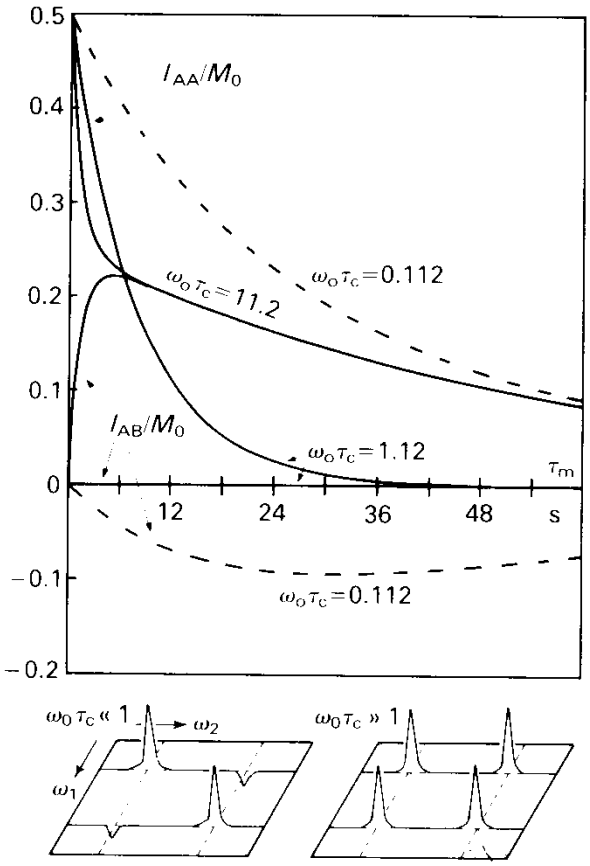

FIG. 9.7.2. Dependence of the diagonal and cross-peak intensities $I_{AA} = I_{BB}$ and $I_{AB} = I_{BA}$ on the mixing time τ_m for cross-relaxation in an AB spin system. Three typical correlation times τ_c have been assumed: $\omega_0\tau_c = 0.112$ corresponds to a short correlation time (extreme narrowing, negative cross-peaks), while $\omega_0\tau_c = 11.2$ represents a case of long correlation time (slow motion, positive cross-peaks). The critical case $\omega_0\tau_c = 1.12$ leads to vanishing cross-peaks irrespective of the mixing time τ_m. The indicated time-scale assumes a Larmor frequency $\omega_0/2\pi = 100$ MHz and $q = 3.33 \times 10^6\ s^{-2}$. (Reproduced from Ref. 9.5.)

Figure 9.11: Peak Intensities in NOESY Spectra

9.4 Heteronuclear Correlation Spectroscopy

We can also correlate the chemical shifts of different nuclei by including a polarization-transfer sequence (see Chapter 8) into the pulse sequence. The polarization transfer can either be based on the J coupling or a dipolar coupling between the two spins. Such experiments allow the assignment of the chemical shifts of the X nuclei if the proton chemical shifts are known. In addition, the chemical-shift range of the X nuclei is often larger and provides better resolution for crowded proton spectra.

To obtain the highest possible sensitivity, it is important to optimize the way the experiment is designed. There are three points to consider: (i) The initial Boltzmann population that determines the amount of polarization that can be used in the experiment is proportional to the Larmor frequency. It is, therefore, advantageous to start the experiment on the nucleus with the higher resonance frequency. Typically, this will be the protons. (ii) The detection frequency determines the voltage induced in the coil which is proportional to the square of the Larmor frequency while at the same time the noise goes up with the square root of the Larmor frequency. It is, therefore, advantageous to detect the magnetization at the highest possible frequency which is typically protons. (iii) The efficiency of the polarization-transfer process determines how much of the initial polarization can be detected. Important points to

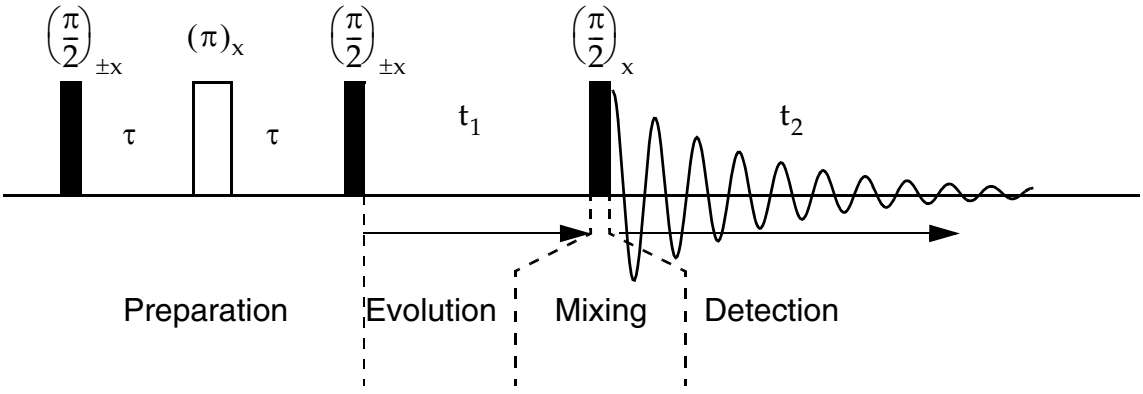

Figure 9.12: Pulse Sequence of the INADEQUATE Experiment
Pulse sequence of the 2D INADEQUATE experiment to detect the coupling network of diluted spin pairs. The delay is set to $\tau = 1/(4^1J_{CC})$.

consider here are the number of polarization-transfer steps, their length (relaxation) and the theoretical efficiency of the transfer.

In total we find for the signal-to-noise ratio of an experiment assuming a 100% efficient polarization transfer

$$\frac{S}{N} = \frac{\gamma_i(\gamma_f)^2}{(\gamma_f)^{1/2}} = \gamma_i(\gamma_f)^{3/2} \qquad [9.14]$$

where γ_i is the gyromagnetic ratio of the starting nucleus while γ_f is the gyromagnetic ratio of the detection nucleus.

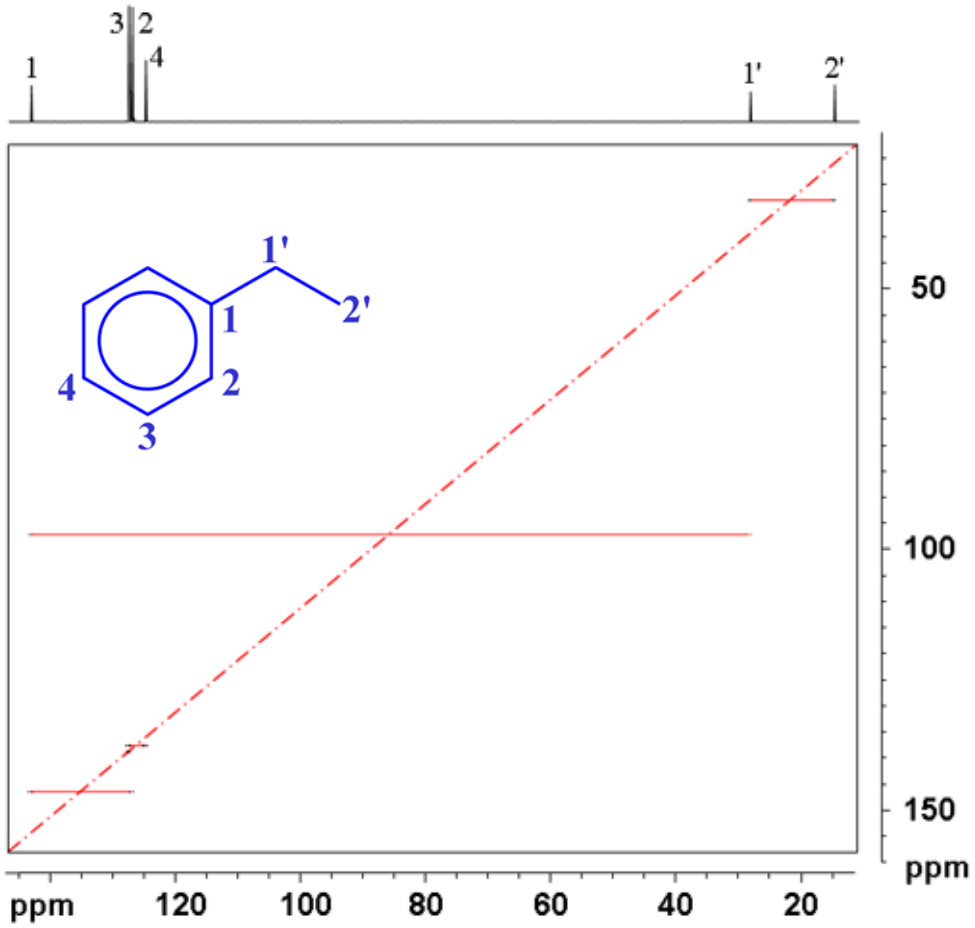

Figure 9.13: ^{13}C INADEQUATE Spectrum
2D INADEQUATE spectrum of ethyl benzene showing the connectivity of the carbon atoms. (copied from http://drx.ch.huji.ac.il/nmr/techniques/2d/inad/inad.html)

A good overview over the various heteronuclear experiments can be found at "http://www.chem.queensu.ca/FACILITIES/NMR/nmr/webcourse/".

9.4.1 X-Nucleus Detected Experiments

Experiments that start on protons and transfer the polarization to the X nucleus (^{13}C, ^{15}N, ...) where it is detected have not the highest possible sensitivity but they are very robust and easy to implement. The simplest experiment would use a refocused INEPT polarization-transfer (see Chapter 8.3) or a cross-polarization sequence as a mixing step (Fig. 9.14). Due to the low sensitivity of such experiments, they are not widely used in liquid-state NMR. In solid-state NMR, however, X-nuclei detection is still widely used due to the broad lines of the protons. There are more advanced implementations of this experiment which combine the evolution and the mixing time (constant-time experiments) and have better relaxation properties.

9.4.2 Proton-Detected Experiments

In liquid-state NMR, most heteronuclear correlation experiments are done using initial proton polarization and proton detection. They require, therefore, multiple polarization-transfer steps with high efficiency.

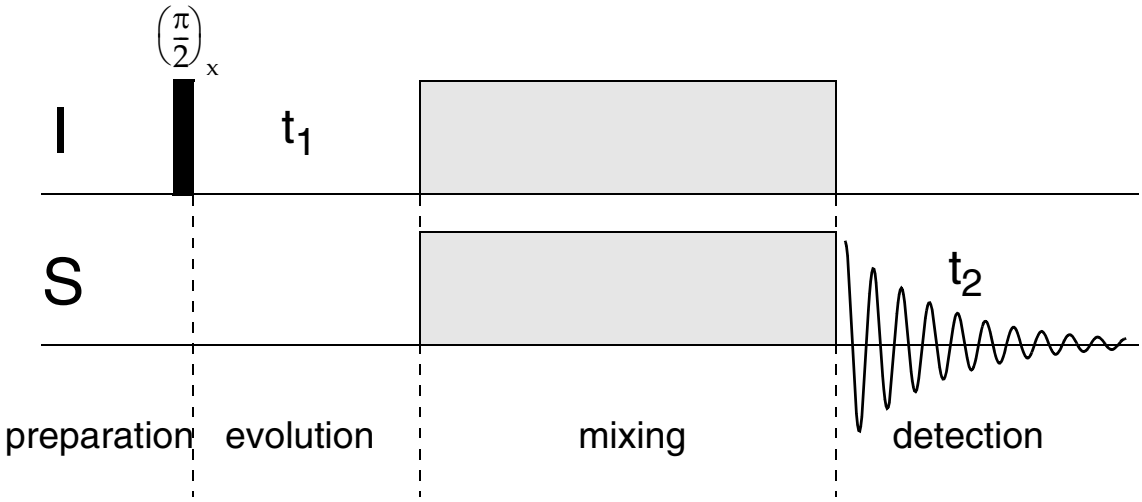

Figure 9.14: Heteronuclear Correlation Spectroscopy
Schematic heteronuclear correlation experiment with X-nucleus detection. The mixing sequence can be any heteronuclear polarization-transfer sequence.

The conceptually simplest proton-detected 2D chemical-shift correlation experiment is the HSQC (heteronuclear single-quantum correlation spectroscopy) experiment which is a double INEPT experiment (Fig. 9.15a). A more sensitive experiment is the HMQC (heteronuclear multiple-quantum correlation spectroscopy) experiment (Fig. 9.15b) which requires fewer pulses but has the same length of the mixing sequence. Both pulse sequences give the same type of spectra. The main difference is that in the HSQC spectrum we have single-quantum coherences during t_1 while in the HMQC spectrum we have multiple-quantum coherences during t_1 with the chemical shifts of the I spins refocused due to the π pulse in the center of t_1. This difference will lead to different behavior under relaxation leading to differences in sensitivity of

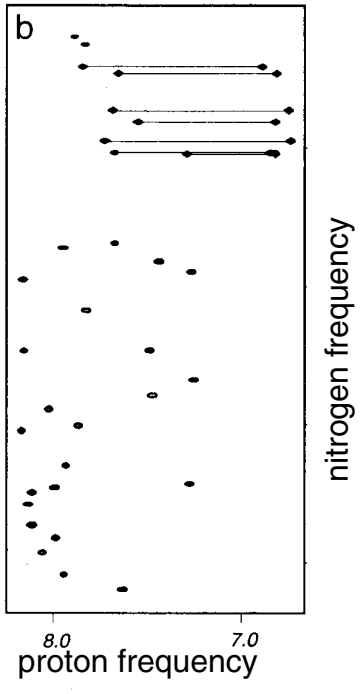

Figure 9.16: HSQC Spectrum
^{15}N-^{1}H HSQC spectrum of the protein ubiquitin.

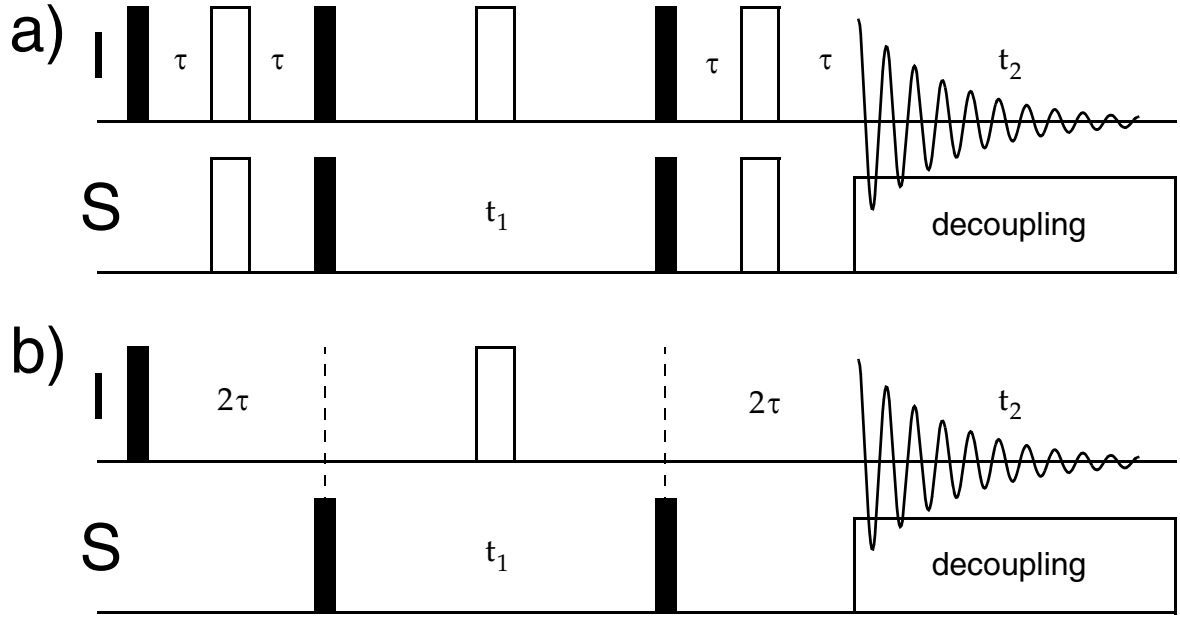

Figure 9.15: HSQC and HMQC Experiment
Schematic drawing of the a) HSQC and b) HMQC sequence for acquiring heteronuclear correlation spectra with I-spin detection. The delay is set to $\tau = 1/(4J_{IS})$.

the two experiments as a function of the molecular weight. An example of an ^{15}N-^{1}H HSQC spectrum of the protein ubiquitin is shown in Fig. 9.16.

Heteronuclear correlation spectra can be used to resolve a crowded proton 2D spectrum (NOESY, COSY, ...) into a third S-spin chemical-shift frequency dimension, i.e., the nitrogen frequency (heteronuclear-edited spectroscopy). This leads to three- or higher-dimensional (3D, ND) spectra (Fig. 9.17).

9.5 Structure Determination by Multidimensional NMR

One of the main application of multi-dimensional liquid-state NMR is the three-dimensional structure determination in biomolecules, especially proteins and RNA. A combination of the COSY and NOESY schemes allows for a three-

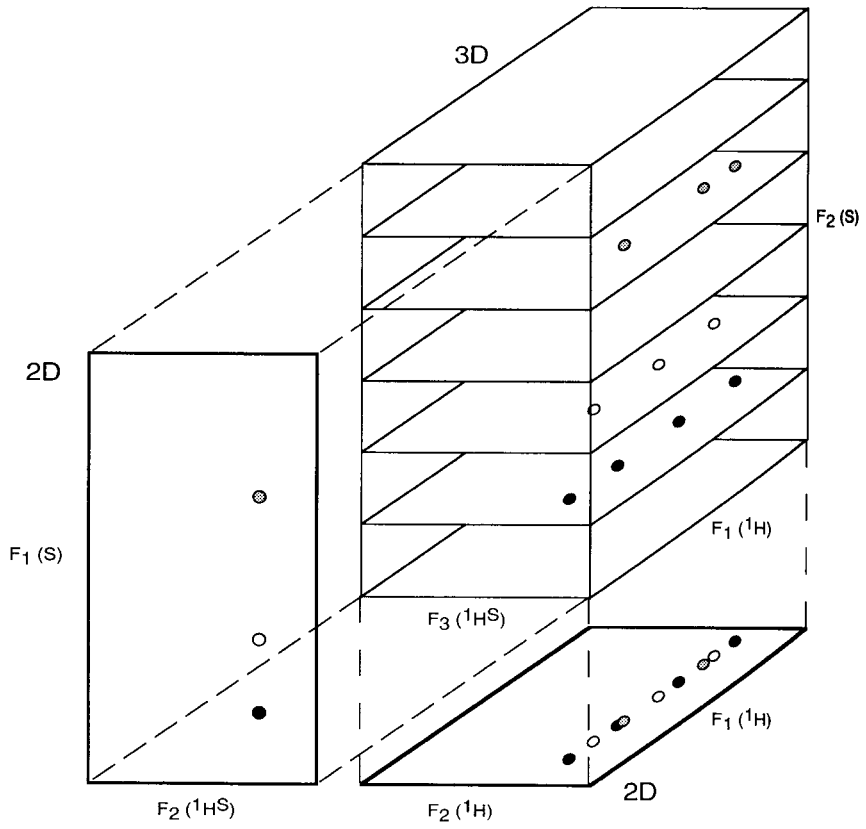

Figure 9.17: Three-Dimensional Spectra
Heteronuclear correlation spectra can be used to increase the resolution in crowded proton 2D spectra.

dimensional structure determination of dissolved molecules with a molecular weight smaller than about 50 kDa (Fig. 9.18).

The COSY experiment allows to identify protons that are J-coupled and, therefore, belong to the same amino acid. The NOESY experiment allows to determine distances of protons located on different amino acids (Fig. 9.19). These NOESY distances are used as constraints in structure determination programs. The two main procedures used are:

- Distance geometry algorithm
- Restrained molecular dynamics

For larger proteins, more advanced methods that involve heteronuclear multi-dimensional spectroscopy are used to increase the resolution of the spectra as described earlier.

It should be noted, that the NOESY intensities lead to rather imprecise distance constraints. The large number of such constraints makes up for this uncertainty and leads to very-well determined structure. Keep, however, the time scale of the NMR experiments in mind (see Chemical Exchange chapter). The NMR method determines,

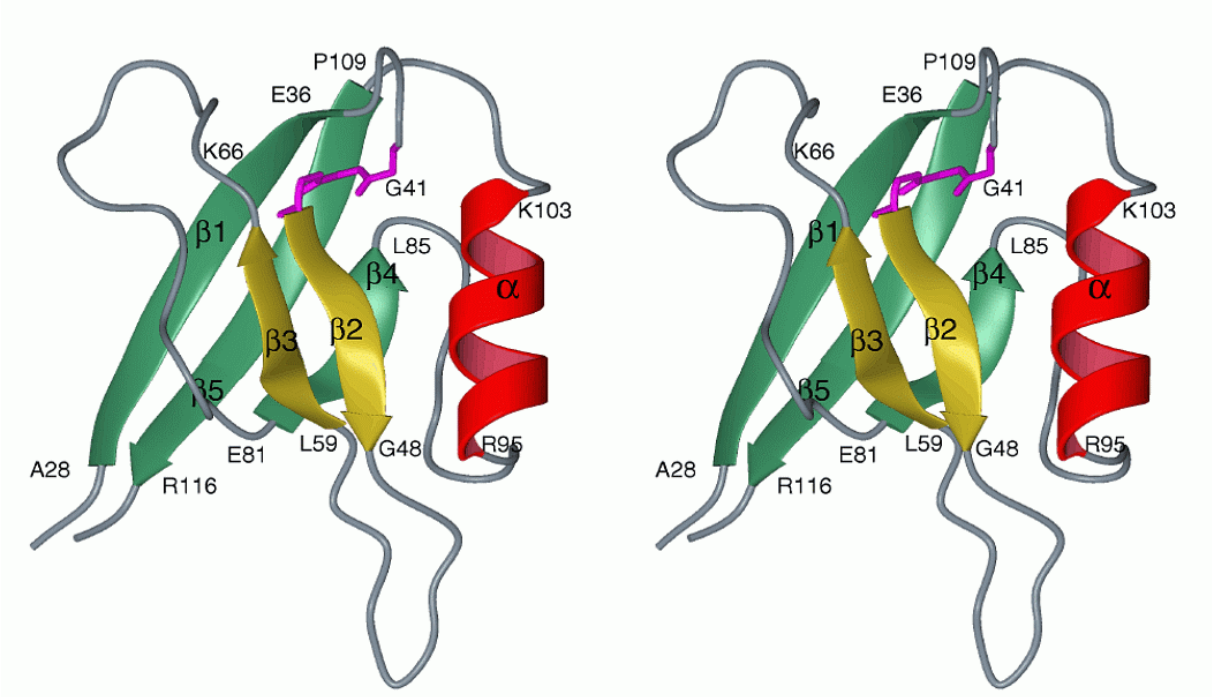

Figure 9.18: Protein Structure
Example: Stereo view of the 3D-NMR-structure of Interleukin-16 (Nat. Struct. Biol. 5, 682-686).

in case of fast dynamics, an “average” structure. Note the unusual averaging law, because the distance inter as the inverse sixth power.

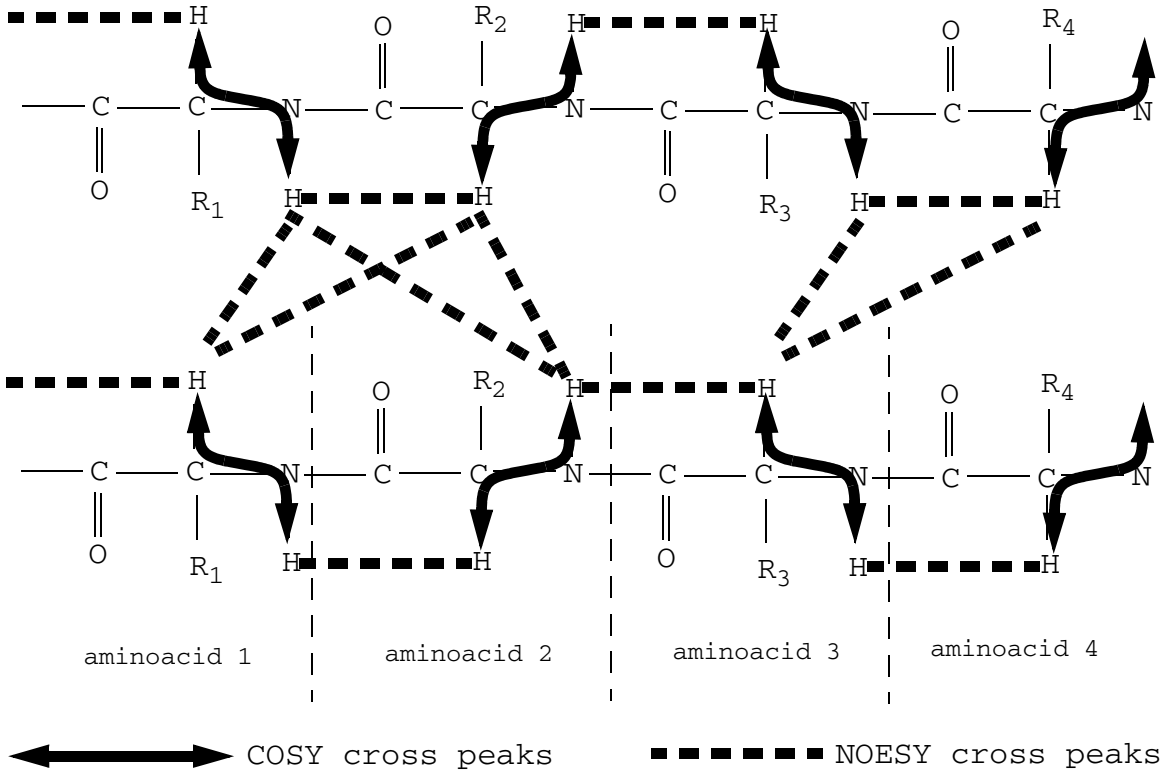

Figure 9.19: NOESY-COSY Scheme For Structure Determination